UNIVERSITAT DE BARCELONA

Dopaminergic neuromodulation: a novel targeted therapy for pancreatic cancer

Pablo Caruana Santiago

Doctoral Program in Biomedicine

Dopaminergic neuromodulation: a novel targeted therapy for pancreatic cancer.

Neuromodulació dopaminérgica: una nova teràpia dirigida per al càncer de pàncrees.

Thesis submitted by

Pablo Caruana Santiago

To qualify for the Doctorate degree by the Universitat de Barcelona

Dr. Marta Cascante Serratosa, Thesis Tutor

Dr. Mª Virtudes Céspedes Navarro, Thesis Director

Department of Biochemistry and Molecular Biomedicine 2025

UNIVERSITAT DE BARCELONA

UNIVERSITAT DE BARCELONA

This project was supported by the "Ayudas para contratos predoctorales de Formación en investigación en salud (PFIS) 2021" fellowship (**FI21/00146**) and project ***PI20/00623*** from the "Instituto de Salud Carlos III (ISCIII)" *co-funding from* the European Social Fund (investing in Your Future).

Agradecimientos

Esta tesis lleva mi nombre, pero no ha sido escrita por una sola persona. Aprovecho este espacio para agradecer sinceramente a aquellas personas que han hecho esto posible.

Gracias a la Dr. María Virtudes Céspedes por su tutelaje y su dedicación de principio a fin en este proyecto. Su gran entusiasmo y pasión por la ciencia son contagiosos y han construido poco a poco el científico que soy hoy en día.

Gracias a l'Institut de Recerca de Sant Pau por su participación y acompañamiento en este proyecto. Gracias Sandra, Mª Angels, Nía, Marta, Iris, Pau, Oriol, Laura, Sergi y sus equipos.

Gracias a mis amigos, porque sin ellos no hubiera tenido la fuerza necesaria para seguir adelante en los momentos más difíciles de mi tesis, por escucharme y aconsejarme y por hacer de la vida un lugar divertido y acogedor.

Gracias a mi pareja que, después de estar ahí en los peores días, se merece este mérito tanto como yo. Por amarme, por respetarme y por entenderme, gracias Rafa.

Por último, gracias a Yolanda y Juan Carlos, mis padres, y a mis 4 hermanos por ser mi eterno apoyo y compartir conmigo el orgullo de este día.

A todos, muchas gracias.

Summary

Pancreatic cancer (PC) is the third leading cause of cancer-related deaths worldwide, with many patients diagnosed at advanced stages due to the absence of early symptoms and effective screening methods. PC often progresses rapidly and is resistant to standard therapies, making it one of the most challenging to treat. Current options, including surgery and chemotherapy, provide only marginal benefits and can have significant side effects. There is a critical need for new therapeutic approaches, which could offer promising treatment advancements and address this unmet clinical need.

In this work, we explored a novel therapeutic approach for pancreatic ductal adenocarcinoma (PDAC), focusing on the role of dopamine receptor signaling in tumor growth and dissemination. Our studies demonstrated that dopamine (DA), but not norepinephrine (NE) or epinephrine (E), reduces tumor cell proliferation in PANC-1, MIA PaCa-2 and the patient-derived M2 pancreatic cell lines *in vitro*. This cytotoxic effect is mediated through activation of D1-like receptors, leading to apoptosis and autophagy across the three models. Importantly, the activation of dopaminergic signaling with selective agonists was able to inhibit tumor cell migration in PANC-1 and MIA PaCa-2 cells.

In vivo, selective activation of dopaminergic receptors proved effective in reducing tumor progression. Treatment with fenoldopam (a D1 receptor agonist) and bromocriptine, (a D2 receptor agonist) in subcutaneous mouse models decreased tumor burden, enhanced tumor cell death pathways and reduced angiogenesis without observable toxicity. Moreover, in an orthotopic metastatic model, both drugs—alone and in combination—significantly lowered the incidence of metastatic spread. Interestingly and complementary to these findings, inhibition of the D2-like pathway with domperidone (a D2 receptor blocker) reduced proliferation *in vitro* and impaired tumor progression *in vivo*, again without inducing toxicity.

Additionally, either the activation of D1 or the inhibition of D2 pathways in spheroids –a CSC-rich model– reduced in size and number of tumor spheroids

derived from all three pancreatic cell lines, and their combined use further enhanced antiproliferative activity.

In parallel, and in collaboration with Dr. J.L. Corchero's team, we began implementing nanoparticles as drug delivery vehicles, specifically nanovaults, to enhance the therapeutic potential of dopaminergic drugs. Nanovaults provide an excellent platform for encapsulating bioactive molecules, ensuring controlled release and protection from premature degradation. Concurrently, two nanobodies were designed to selectively target dopaminergic receptors, reducing the proliferative capacities of the three PC cell lines with doses up to 100 times lower than those required by conventional drug ligands. Ultimately, these approaches offer a translational advantage by bridging pharmacological efficacy with clinically relevant delivery methods.

Together, these findings provide preclinical evidence that dopaminergic modulation—via receptor-specific agonists, antagonists, or combination strategies—represents a promising avenue for targeted PDAC therapy. This work lays the groundwork for future studies aimed at improving outcomes in a disease that currently lacks effective treatments and has seen few advances in clinical management.

Keywords

Pancreatic cancer, Pharmacological targets, Dopamine, Animal experimentation, Nanomedicine

Resum

El càncer de pàncrees (CP) és la tercera causa de mort per càncer al món, amb molts pacients diagnosticats en estadis avançats a causa de l'absència de símptomes precoços i de mètodes de cribratge efectius. El CP sovint progressa ràpidament i mostra resistència a les teràpies estàndard, fet que el converteix en un dels més difícils de tractar. Les opcions actuals, incloent-hi la cirurgia i la quimioteràpia, ofereixen només beneficis marginals i poden comportar efectes adversos significatius. És, per tant, imprescindible desenvolupar noves estratègies terapèutiques que permetin avenços prometedors en el tractament i responguin a aquesta necessitat clínica no coberta.

En aquest treball, hem explorat un enfocament terapèutic innovador per a l'adenocarcinoma ductal de pàncrees (PDAC), centrant-nos en el paper de la senyalització dels receptors dopaminèrgics en el creixement i la disseminació tumoral. Els nostres estudis han demostrat que la dopamina (DA), però no la noradrenalina (NE) ni l'adrenalina (E), redueix la proliferació cel·lular tumoral *in vitro* en les línies PANC-1, MIA PaCa-2 i M2 derivada de pacient. Aquest efecte citotòxic es produeix mitjançant l'activació de receptors de tipus D1, la qual cosa indueix apoptosi i autofàgia en els tres models. Cal destacar que l'activació de la senyalització dopaminèrgica amb agonistes selectius va ser capaç d'inhibir la migració cel·lular tumoral en les línies PANC-1 i MIA PaCa-2.

In vivo, l'activació selectiva dels receptors dopaminèrgics es va mostrar eficaç en la reducció de la progressió tumoral. El tractament amb fenoldopam (agonista del receptor D1) i bromocriptina (agonista del receptor D2) en models murins subcutanis va disminuir la càrrega tumoral, va potenciar les vies de mort cel·lular i va reduir l'angiogènesi sense evidència de toxicitat. A més, en un model ortotòpic metastàtic, ambdós fàrmacs —administrats sols o en combinació— van reduir significativament la incidència de disseminació metastàtica. De manera interessant i complementària, la inhibició de la via D2-like amb domperidona (antagonista del receptor D2) va reduir la proliferació *in vitro* i va frenar la progressió tumoral *in vivo*, també sense induir toxicitat.

Addicionalment, tant l'activació de la via D1 com la inhibició de la via D2 en esferoides —un model ric en cèl·lules mare canceroses (CSC)— va disminuir la mida i el nombre d'esferoides derivats de les tres línies pancreàtiques, i la seva combinació va amplificar encara més l'activitat antiproliferativa.

En paral·lel, i en col·laboració amb l'equip del Dr. J.L. Corchero, vam iniciar la implementació de nanopartícules com a vehicles d'alliberament de fàrmacs, en concret nanovaults, per potenciar el valor terapèutic dels fàrmacs dopaminèrgics. Els nanovaults ofereixen una plataforma excel·lent per encapsular molècules bioactives, assegurant un alliberament controlat i protegint-les de la degradació prematura. Alhora, es van dissenyar dos nanocossos per dirigir-se selectivament als receptors dopaminèrgics, reduint la capacitat proliferativa de les tres línies cel·lulars pancreàtiques amb dosis fins a 100 vegades inferiors a les requerides pels lligands farmacològics convencionals. En conjunt, aquests enfocaments aporten un avantatge translacional en vincular l'eficàcia farmacològica amb mètodes d'administració clínicament rellevants.

En conjunt, aquests resultats proporcionen una sòlida evidència preclínica que la modulació dopaminèrgica —mitjançant agonistes, antagonistes o estratègies combinades específiques de receptors— representa una via prometedora per al tractament dirigit del PDAC. Aquest treball estableix les bases per a futurs estudis encaminats a millorar el pronòstic d'una malaltia que actualment manca de tractaments efectius i ha experimentat pocs avenços en la seva gestió clínica.

Paraules clau

Càncer de pàncrees, Dianes farmacològiques, Dopamina, Experimentació animal, Nanomedicina

INDEX

Abbreviations

5FU = Fluorouracil

AC = Adenylate cyclase

ADEX = aberrantly differentiated endocrine exocrine

ATCC = American Type Culture Collection

ATP = Adenosine triphosphate

BMI = Body mass index

BHP = N-nitroso-bis(2-hydroxypropyl)amine

BOP = N-nitroso-bis(2-oxopropyl)amine

BRO = Bromocriptine

CAFs = Cancer associated fibroblasts

Ca 19-9 = Carbohydrate antigen 19-9

cAMP = Cyclic adenosine monophosphate

CNS = Central nervous system

CSC = Cancer stem cell

CT = Computed tomography

DA = Dopamine

DMBA = 7,12 dimethylbenzanthracene

DMEM = Dulbecco's Modified Eagle Medium

dNTPs = Deoxynucleotide triphosphates

DOM = Domperidone

DR = Dopamine receptor

ECM = Extracellular matrix

EMA = European Medicines Agency

EPR = Enhanced permeability and retention

EUS = Endoscopy ultrasound

FBS = Fetal bovine serum

FE/FEN = Fenoldopam

FGFβ = Fetal growth factor B

FOLFORINOX = 5-Fluorouracil, Folinic acid, Irinotecan and Oxaliplatin

Gem-nabP = Gemcitabine with nab-paclitaxel

GFP = Green fluorescent protein

GIRK = Gated inwardly rectifying K+

H/E = Hematoxylin/eosin

IGF-1 = Insulin growth factor 1

IL = Interleukin

MDSCs = Myeloid-derived suppressor cells

MPP = Matrix metalloproteinases

MRI = Magnetic resonance imaging

mOS = Median Overall Survival

MVP = Major vault protein

NFkB = Necrotic factor kappa beta

OS = Overall survival

PanINs = Pancreatic intraepithelial neoplasias

PBS = Phosphate buffered saline

PC = Pancreatic Cancer

PCR = Polymerase chain reaction

PDAC = Pancreatic Ductal Adenocarcinoma

PDX = Patient derived xenograft

PKD = Proteinase K digestion buffer

PLGA = Poly(lactic-co-glycolic acid)

PSCs = Pancreatic stellate cells

PVDF = Polyvinylidene fluoride

ROS = Reactive oxygen species

RT = Radiotherapy

RT = Room temperature

RTPCR = Real-time PCR

SCID = Severe combined immunodeficiency

SPF = Specific pathogen free

TAMs = Tumor associated macrophages

TME = Tumor microenvironment

TPP = Tumor-penetrating peptide

WHO = World Health Organization

List of genes and proteins

Akt = Akt serine/threonine kinase

APC = Adenomatous polyposis coli

ATM = Ataxia telangiectasia mutated

BRCA1 = Breast cancer gene 1

BRCA2 = Breast cancer gene 2

BTK = Bruton's tyrosine kinase

cAMP = Cyclic adenosine monophosphate

cGMP = Cyclic guanosine monophosphate

CD45 = Cluster of differentiation 45

CDK4/6 = Cyclin-dependent kinase 4/6

CFTR = Cystic fibrosis transmembrane conductance regulator

CREB = cAMP-response element binding protein

CSC = Cancer stem cell

CTGF = Connective tissue growth factor

D1 = Dopamine Receptor 1

D2 = Dopamine Receptor 2

D3 = Dopamine Receptor 3

D4 = Dopamine Receptor 4

D5 = Dopamine Receptor 5

DC = Dendritic cell

EGFR = Epidermal growth factor receptor

ERK = Extracellular signal-regulated protein kinase

ERK1/2 = Extracellular signal-regulated kinase 1/2

GAPDH = Glyceraldehyde-3-phosphate dehydrogenase

HER2 = Human epidermal growth factor receptor 2

HGF = Hepatocyte growth factor

HIF-α = Hypoxia-inducible factor alpha

IGF-1R = Insulin-like growth factor receptor

iNOS = Inducible nitric oxide synthase

JAK = Janus kinase

KRAS = Kirsten rat sarcoma oncogene

LC3A/B II = LC3-phosphatidylethanolamine conjugate

MAPK = Mitogen-activated protein kinase

MCP-1 = Monocyte chemoattractant protein 1

MDM2 = Mouse double minute 2 homolog

MEK = Mitogen-activated protein kinase kinase

MLH1 = MutL homolog 1

MSH2 = MutS homolog 2

MMP = Matrix metalloproteinase

mTOR = Mammalian target of rapamycin

NAD(P)H = Nicotinamide adenine dinucleotide phosphate

NFATc1 = Nuclear factor of activated T cells, cytoplasmic 1

NFκB = Nuclear factor kappa-light-chain-enhancer of activated B cells

Notch = Notch receptor

nNOS = Neuronal nitric oxide synthase

NRG1 = Neuregulin 1

NTRK = Neurotrophic receptor tyrosine kinase

P16/CDKN2A = Cyclin-dependent kinase inhibitor 2A

PALB2 = Partner and localizer of BRCA2

PALLD = Palladin

PARP = Poly (ADP-ribose) polymerase

PDGF = Platelet-derived growth factor

PI3K = Phosphatidylinositol 3-kinase

PI3K/Akt = PI3K/Akt signaling pathway

PKA = Protein kinase A

PKG = Protein kinase G

PRSS1 = Protease serine 1 (cationic trypsinogen)

RAF = Rapidly accelerated fibrosarcoma

RANTES = Regulated upon activation, normal T cell expressed and secreted (CCL5)

RhoA/Rac = Ras homolog family member A / Ras-related C3 botulinum toxin substrate

sGC = Soluble guanylyl cyclase

SHH = Sonic hedgehog

SMAD4 = Mothers against decapentaplegic homolog 4

SMO = Smoothened

SPINK1 = Serine peptidase inhibitor, Kazal type 1

STAT = Signal transducer and activator of transcription

STAT3 = Signal transducer and activator of transcription 3

STK11 = Serine/threonine kinase 11 (LKB1)

TGF-β = Transforming growth factor beta

TP53 = Tumor protein p53

TRAP = Tartrate-resistant acid phosphatase

VEGF = Vascular endothelial growth factor

VEGFR = Vascular endothelial growth factor receptor

I. INTRODUCTION

1. Overview of pancreatic cancer

1.1. Epidemiology

Pancreatic cancer (PC) is the second most common digestive cancer and the third cause of cancer death in Europe [1] and pancreatic ductal adenocarcinoma (PDAC) is the most frequent histological subtypes representing over 85% of the pancreatic neoplasms. By the year 2030, the estimations say that PDAC will be the second most prevalent cancer death if we cannot find better tools for diagnosis and treatment (Fig. 1).

1.2. Etiology and Risk Factors of Pancreatic Cancer

Pancreatic cancer (PC) is a complex disease with unclear etiology, but several hereditary and non-hereditary risk factors have been identified. These factors vary in their impact and are associated with genetic, environmental, and medical influences. [2]

1.2.1. Hereditary Risk Factors

A family history of PC significantly increases the risk, particularly when multiple first-degree relatives are affected. Around 10% of PC cases are linked to hereditary syndromes, with several high-risk genetic mutations identified [3]. Notable examples include mutations in the *STK11* gene, associated with Peutz-Jeghers syndrome, and in *PRSS1* and *SPINK1*, implicated in hereditary pancreatitis. Mutations in *BRCA2*, *p16*, and *TP53* (associated with Li-Fraumeni syndrome) also elevate PC risk. Similarly, the *CFTR* gene, commonly mutated in cystic fibrosis, has been linked to early-onset PC.

Moderate-risk genetic alterations include mutations associated with Lynch syndrome (*MSH2* and *MLH1*) and variants in *ATM*, *APC*, and *PALLD*. [4] Additionally, studies suggest that genetic polymorphisms affecting DNA repair mechanisms may increase susceptibility to PC by reducing resistance to carcinogens such as tobacco.

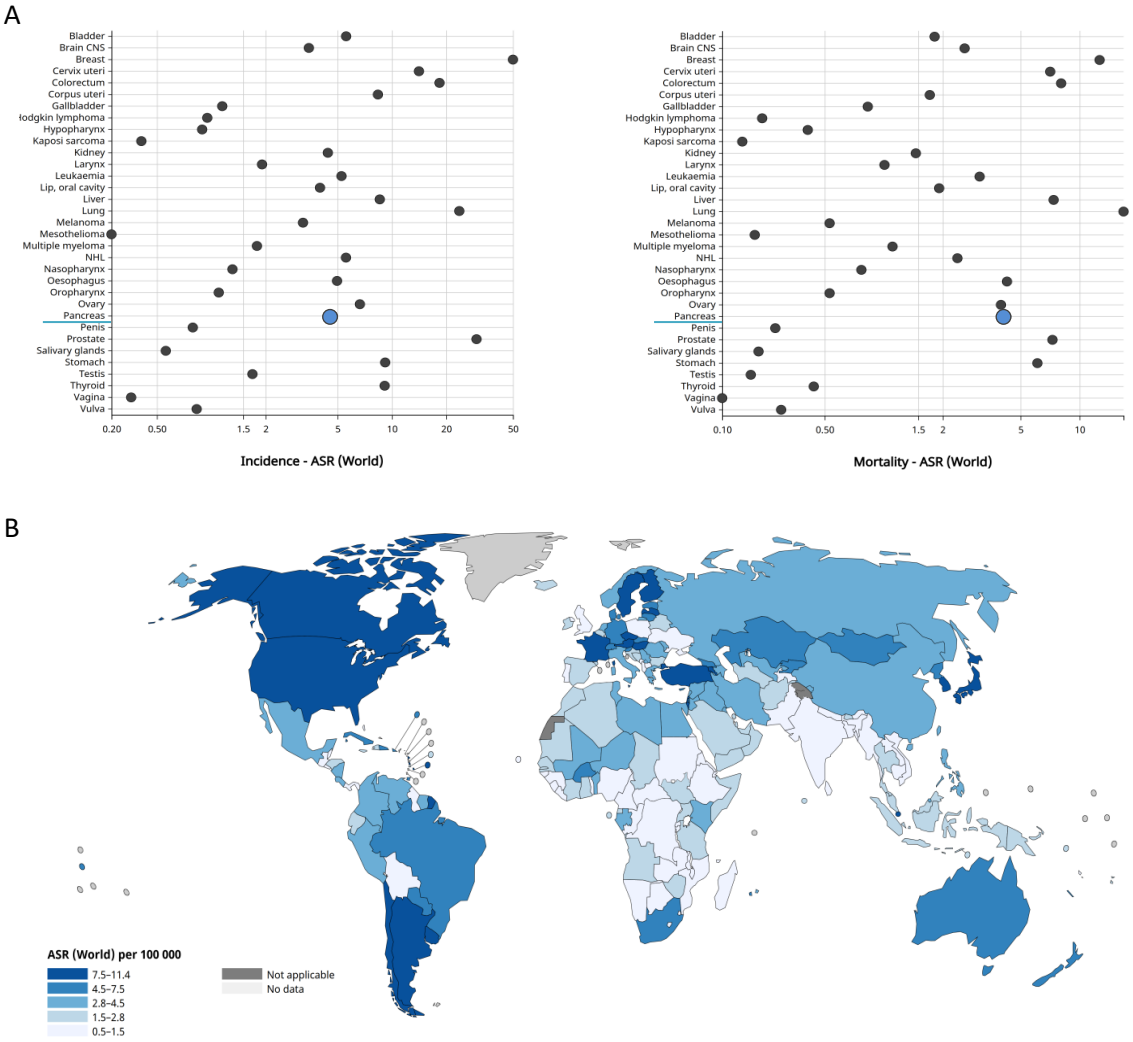

Figure 1. Epidemiology of PC. A) Cancer incidence and mortality for the most of the most prevalent cancers. **B) Incidence of pancreatic cancer per 100.000 people.** Data extracted from the International Agency for Research on Cancer (WHO) [5].

1.2.2. Non-Hereditary Risk Factors

Environmental, lifestyle, and medical factors contribute to PC development. Among these, smoking is the most significant modifiable risk factor, responsible for approximately 25% of all cases. Current smokers have a higher risk rate, while former smokers face a lower but persistent risk for at least a decade after quitting [6]. Smoking also doubles the risk of PC in patients with hereditary pancreatitis and is associated with earlier onset. Occupational exposures to substances such as chlorinated hydrocarbons and nickel compounds have been linked to PC in meta-analyses, although risks from other agents, including formaldehyde and polycyclic aromatic hydrocarbons, were small or insignificant. [7]

Nutritional factors play a role in PC risk, though findings are inconsistent. High-fat diets may elevate fasting insulin levels and increase PC risk, particularly in smokers. Although no strong association exists between total fruit or vegetable intake and PC, some evidence suggests that cabbage consumption may offer protection. Folate, essential for DNA synthesis and repair, is linked to a reduced PC risk. Conversely, obesity and associated metabolic changes increase PC risk. A meta-analysis found a 2% risk increase for every unit rise in body mass index (BMI), though the association is weaker in women. Physical activity may be protective; studies indicate that moderate exercise is linked to a 55% risk reduction. However, more research is needed to confirm these findings. [8]

1.2.3. Medical and Hormonal Factors

Several medical conditions are associated with PC. Diabetes mellitus is both an early symptom and potential cause of PC. A meta-analysis of 36 studies reported a modest association between type 2 diabetes and PC with risk highest in cases diagnosed within four years of PC onset [9]. Chronic pancreatitis is a well-established risk factor, with an observed/expected case ratio of 26.3 and a cumulative risk of 4% at 20 years post-diagnosis [10]. The severity and duration of pancreatitis influence the risk, independent of alcohol consumption.

Gallstones and cholecystectomy have been inconsistently associated with PC, possibly due to confounding factors like BMI and physical activity. Respiratory diseases also play a role; asthma has been linked to increased PC risk, while allergies appear protective. Infectious agents, including *Helicobacter pylori* and hepatitis B virus, may contribute to PC development, as indicated by epidemiological studies and the presence of bacterial DNA in pancreatic tissues. [2]

Hormonal factors, such as parity, have shown potential protective effects, with women having four or more pregnancies exhibiting a reduced PC risk. This may be linked to lower insulin-like growth factor levels and reduced iron stores during pregnancy. [11]

1.3. Diagnosis, staging and prognosis

PDAC is typically diagnosed later in the body and in the tail of the pancreas compared to the head of the pancreas [12]. This is due to the fact that smaller lesions in the head may present more noticeable and earlier symptoms. The diagnosis of PDAC must be confirmed through biopsy or surgical resection. This is especially important when differentiating between pancreatic masses caused by pancreatitis. In cases of dissemination or unresectability, confirming the diagnosis is crucial to assess operability and guide treatment decisions.

Computed tomography (CT) scans, MRI, and endoscopic ultrasound (EUS) are the main tools for diagnosing and staging PDAC [13]. Among these, contrast-enhanced CT is considered the most reliable for diagnosing the disease and assessing resectability, with an accuracy of up to 80% [14]. Additionally, EUS provides the advantage of enabling tumor biopsies with high effectiveness.

The survival rate of patients depends on the histological grade and the staging (the extent of the disease at diagnosis), which determines the management of PDAC.

The staging of PDAC considers three scenarios: resectable, locally advanced, and/or metastatic disease. Factors considered in preoperative staging include

tumor size, vascular involvement, patient age, and comorbidities. Based on these factors and considering resectable cases, surgical resection remains the only potentially curative treatment for PDAC. Local disease is described, accounting for 10-15% of cases, when there is not vascular involvement. In these cases tumors are resectable or borderline resectable. When tumors are borderline resectable, a combination of chemotherapy and/or radiotherapy prior to surgery might remove the tumor completely.

Locally advanced disease (25-30% of cases) is considered when vascular involvement occurs. In these cases surgery won't remove the tumor completely. Surgery to remove these tumors is unlikely to be beneficial and may cause significant side effects. However, less extensive procedures can still be performed to prevent or relieve symptoms, such as a blocked bile duct, rather than attempting to remove the pancreatic tumor. Finally, metastatic disease (50-60% of cases) occurs when the PDAC cells have been able to migrate to distant organs. Surgery is not capable of removing the tumor completely and only palliative chemotherapy is considered [12].

Only 15-20% of PDAC cases are resectable at diagnosis, with the tumor being localized and without distant metastasis. These patients generally have a good quality of life, as assessed by functional status scales (Performance Status). Unresectability, on the other hand, is often due to local or vascular invasion (locally advanced or borderline resectable disease) or the presence of distant metastases. [15]

The survival rate following R0 resection for resectable PDAC is approximately 24%, while it drops to 9% for locally advanced cases and 2% for metastatic PDAC. In resectable cases, the 5-year survival rate can reach up to 50% for tumors smaller than 2 cm, and nearly 100% for tumors smaller than 1 cm. However, the presence of lymph node involvement significantly reduces the survival rate, even in resectable cases, to about 7-8% at 5 years. [16]

Postoperative morbidity is high, exceeding 60% in most cases, though hospital mortality rates in experienced centers are generally less than 2%. Complications following surgery include gastric emptying disorders, wound infections, abdominal abscesses, and pancreatic fistulas. The implementation of fast-track protocols, which streamline the perioperative process, has contributed to reducing surgical stress, accelerating recovery, and improving safety for patients undergoing resection [17]. A complication-free postoperative course is associated with better long-term survival. [18], [16]

For monitoring PDAC, the most commonly used serum marker is Ca 19-9 (carbohydrate antigen 19-9), which has an 80% sensitivity and specificity at diagnosis. However, this marker can also be elevated in benign conditions, such as cholestasis or pancreatitis, and is therefore more useful as a prognostic marker rather than a diagnostic tool. Research is ongoing to identify more specific biomarkers to detect early-stage PDAC, though none have yet shown sufficient accuracy for routine use. [19]

The prognosis of PDAC is generally poor, primarily due to the nature of the disease: late-stage diagnosis, its aggressive character with early metastasis and neurovascular invasion, as well as resistance to chemotherapy and radiotherapy (RT). Furthermore, genetic and epigenetic alterations and changes in the tumor microenvironment contribute to its challenging prognosis. [20]

Improving patient survival in PDAC requires optimizing disease diagnosis and refining neoadjuvant and adjuvant treatment strategies. The aim should be to increase the number of resectable cases with curative intent and to target not only the tumor cells but also the surrounding stroma, in order to improve the prognosis following surgical resection.

1.4. Pathology and molecular biology

Pancreatic cancer development involves a series of histological and morphological changes, progressing from precursor lesions to invasive carcinoma. Pancreatic intraepithelial neoplasias (PanINs) are early microscopic lesions of the pancreas.

They are classified morphologically along a spectrum of progressively dysplastic features. These microscopic lesions are characterized by the gradual replacement of normal pancreatic ductal epithelium with atypical cells. Histologically, PanINs exhibit varying degrees of cellular atypia, nuclear enlargement, and mitotic activity. [21]

As these precursor lesions accumulate genetic mutations, they may progress to invasive pancreatic ductal adenocarcinoma. Histologically, PDAC is characterized by irregular, infiltrating glands lined by atypical cuboidal to columnar epithelial cells with enlarged, hyperchromatic nuclei. A prominent feature is the desmoplastic stroma, comprising dense fibrous tissue with myofibroblasts, macrophages, lymphocytes, and mast cells. This stroma contributes to the tumor's hypovascularity and hypoxia, creating a microenvironment that supports tumor growth and resistance to therapy. [22]

1.4.1. Genetic mutations

PDAC is marked by a high burden of somatic and germline mutations affecting oncogenes, tumor suppressor genes, and genes involved in genome maintenance. Key mutations include the activation of oncogenes, predominantly KRAS (found in 90% of patients), playing a critical role in tumor progression. However, these mutations have been seen in patients without PDAC, which implies that KRAS mutations might be necessary but insufficient for carcinogenesis, requiring additional genetic events to promote tumor progression. Furthermore, deletions and mutations in tumor suppressor genes have been found, causing the inactivation of TP53 (55%), CDKN2A/p16 (85-98%) and SMAD4 (31-38%) genes which contributes to genomic instability and progression to more aggressive phenotypes (Fig. 2). Moreover, several genes involved in genetic maintenance and DNA repair are altered in PDAC patients. Mutations in BRCA1, BRCA2, PALB2, MLH1, and MSH2 compromise homologous recombination repair (HRR) and mismatch repair pathways, leading to mutation accumulation. These pathways are disrupted in approximately 24% of patients, particularly in subtypes carrying genomic instability. [23].

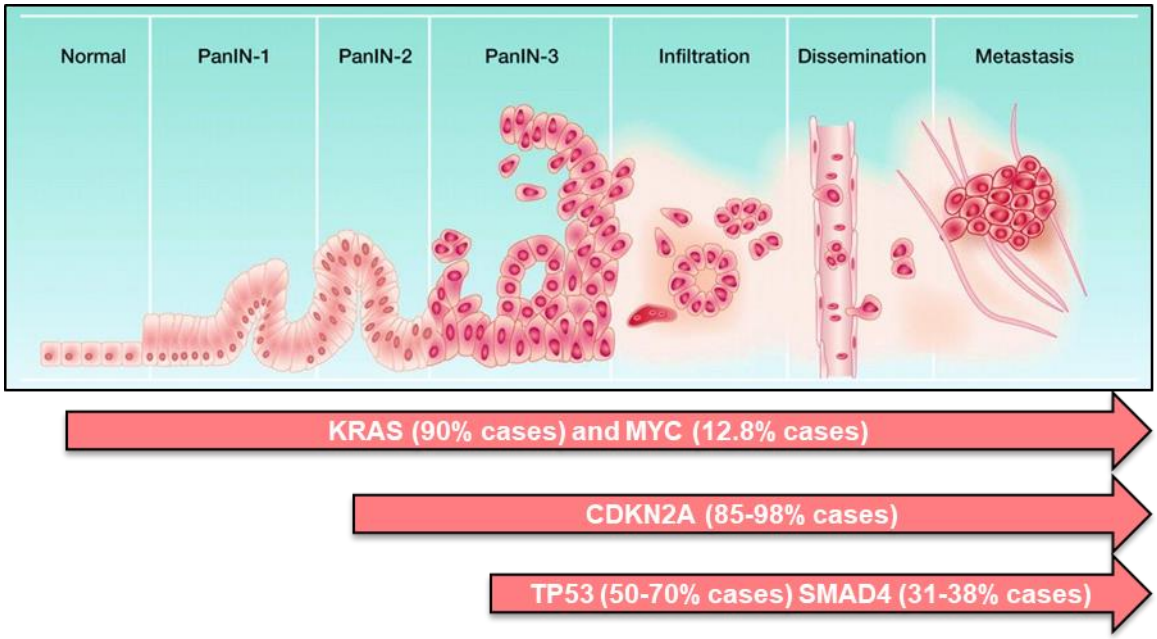

Figure 2. PanINs acquire genetic alterations during its development that allow them to progress into aggressive PDAC. Modified from American Cancer Association for Cancer Research (2012**)** Molecular studies have demonstrated that PanIN grading system corresponds to the sequential accumulation of genetic abnormalities in invasive ductal adenocarcinoma. Early alterations, such as telomere shortening and KRAS mutations, are present in low-grade lesions. p16/CDKN2A inactivation occurs at a later stage and is commonly found in intermediate lesions, whereas the inactivation of BRCA1, TP53, and DPC4/SMAD4 is typically observed only in PanIN-3 and invasive ductal adenocarcinoma. Adapted from Shacks et al. 2018 [24].

1.4.2. Molecular status and new classification

Advances in transcriptomic profiling have identified molecular and transcriptomic subtypes with clinical significance in pancreatic ductal adenocarcinoma (PDAC), as confirmed by the International Cancer Genome Consortium. These subtypes include the pancreatic progenitor (classical), squamous, aberrantly differentiated endocrine exocrine (ADEX), and immunogenic subtype (Fig. 3), which partially overlaps with the classical subtype and is influenced by immune cell interactions in the tumor microenvironment. The squamous subtype, characterized by poor

prognosis, chemotherapy resistance, and frequent mutations in TP53, is associated with higher tumor grade and metastatic disease. In contrast, the progenitor subtype tends to have a more favorable prognosis. [25]

Additionally, structural variations in chromosomes have been used to classify PDAC into four genomic subtypes: Stable, Locally Rearranged, Scattered, and Unstable [26]. The Unstable subtype is particularly notable for a high rate of DNA variations and significant defects in DNA damage repair, specifically within the HHR system. These molecular and genomic classifications offer valuable insights into the disease and can have potential clinical utility, guiding treatment strategies based on subtype-specific characteristics [12].

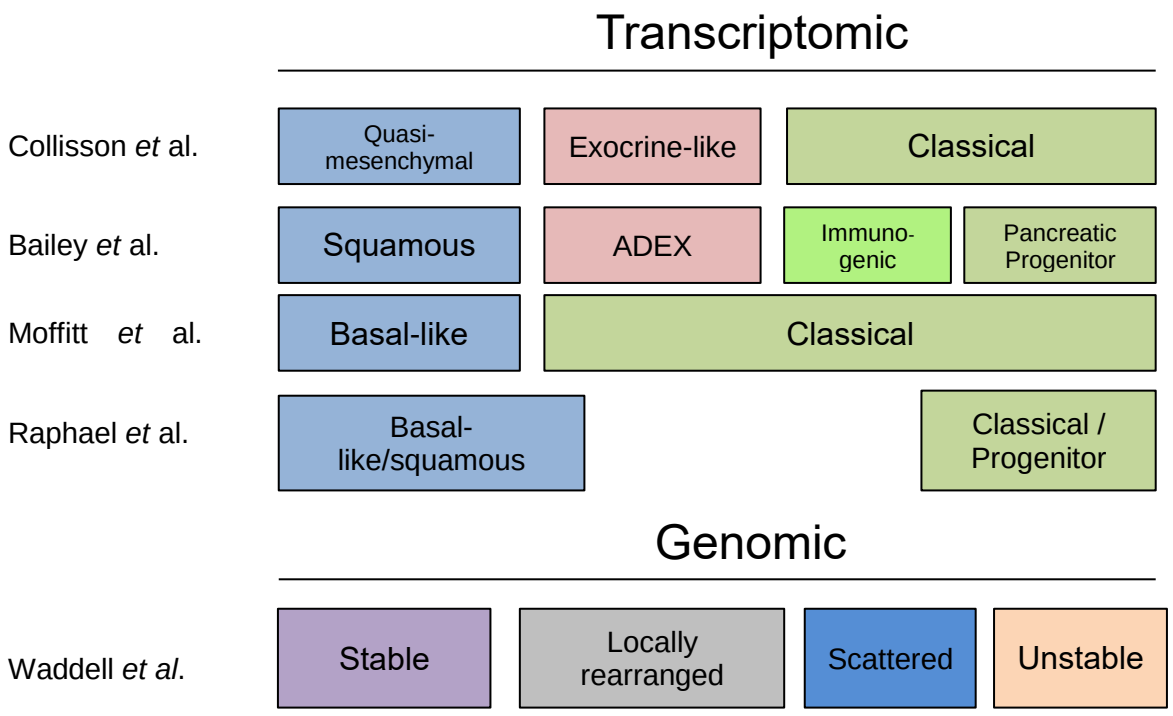

Figure 3. Subtyping in PDAC. Transcriptomics and genomic classifications. [26]–[30]

1.4.3. Tumor microenvironment

The stroma in pancreatic tumors accounts for 90% of the total tumor weight. It represents the tumor microenvironment (TME). Moreover, TME is highly

heterogeneous and can be divided by its cellular and acellular components (Fig. 4). Collectively, the cellular and acellular components of the TME create a complex, dynamic environment that significantly contributes to the malignancy of PDAC, influencing not only tumor growth but also its response to treatment.[31]

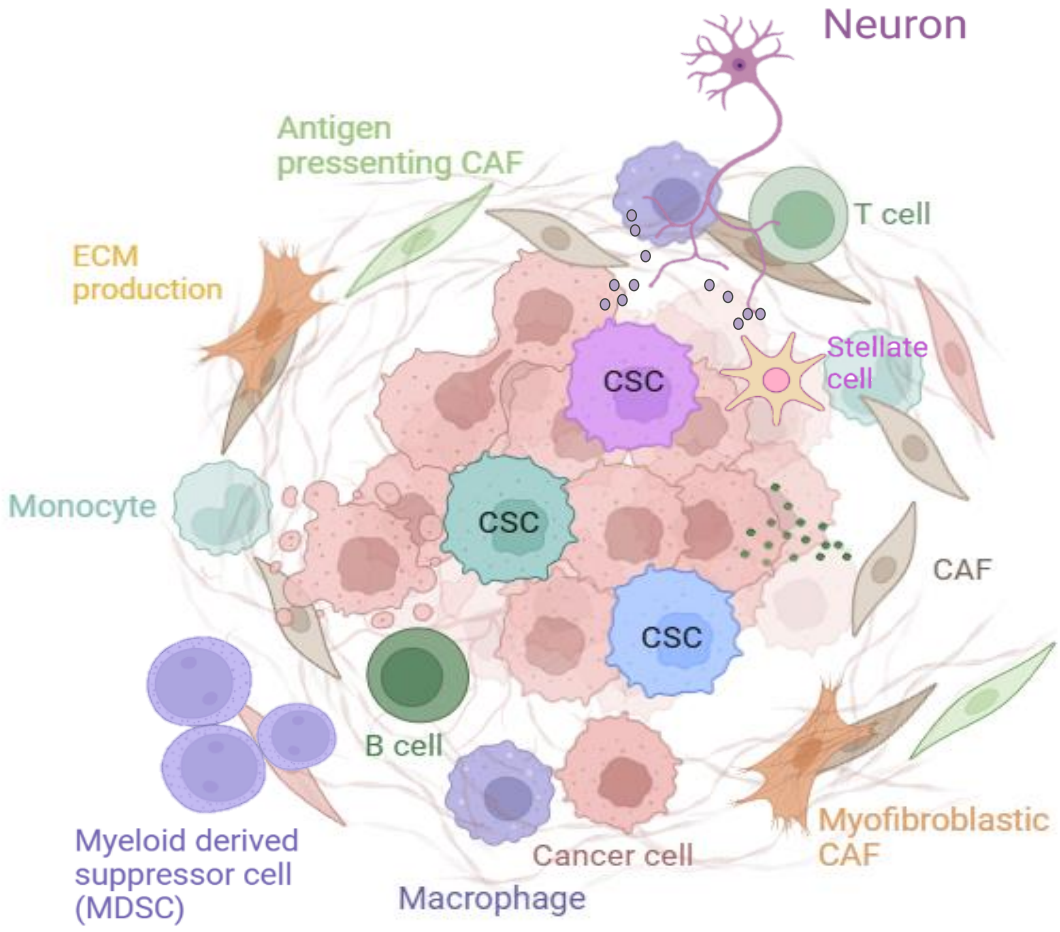

Figure 4. Tumor microenvironment of PDAC. Pancreatic cancer cell's crosstalk with the tumor microenvironment facilitates tumor growth, drug resistance and metastases. CSC: cancer stem cell.

1.4.3.1. Cellular components

The cellular components of the TME include pancreatic stellate cells (PSCs), cancer-associated fibroblasts (CAFs), myeloid-derived suppressor cells (MDSCs),

and tumor-associated macrophages (TAMs), all of which contribute to the complex interactions that support tumor growth. PSCs are the most abundant stromal cells, residing in the exocrine pancreas in a quiescent state. Upon activation by cytokines and growth factors secreted by tumor cells and other stromal cells, they transform into a fibroblastic state, proliferating and producing extracellular matrix (ECM) proteins, inflammatory cytokines like IL-8, chemokines (MCP-1 AND RANTES) and growth factors such as PDGF and TGF-β. This activation is essential for both the growth of the tumor and the promotion of metastasis [32]. Importantly, PSCs also secrete soluble factors that influence the phenotype of pancreatic tumor cells, rendering them more resistant to chemotherapy [33]. Similarly, CAFs, which arise from the activation of quiescent fibroblasts, support tumor progression by producing ECM proteins, growth factors, and cytokines. Their heterogeneity is shaped by interactions with tumor cells via paracrine signaling, facilitating cellular proliferation and invasion [34]. CAFs also promote the differentiation of monocytes into pro-tumor macrophages, further contributing to tumor progression. MDSCs are immature myeloid cells that play an immunosuppressive role in the TME. In PDAC, circulating MDSCs are associated with advanced tumor stages and exhibit increased recruitment to the tumor site under hypoxic conditions, mediated by HIF-α. These cells secrete reactive oxygen species (ROS), leading to immune cell dysfunction and inhibiting T cell proliferation. They also upregulate PD-L1, a protein that binds to PD-1 protein expressed by activated T cells and inactivates them, contributing to immune evasion. MDSCs can differentiate into macrophages in a hypoxic TME, through activation of CD45 and STAT3 inhibition [35]. TAMs, derived from the chemoattraction of immune cells to the tumor site or the polarization of M1-like pro-inflammatory macrophages into an M2-like phenotype, are abundant in advanced PDAC. Furthermore TAMs promote immune evasion and fibrosis by secreting IL-10 and TGF-β, with the latter inhibiting cellular growth in early stages but playing an immunosuppressive role as the disease progresses. Altogether, TAMs are associated with cancer invasion and early metastasis. [36], [37]

1.4.3.2. Acellular components

The acellular components of the TME are equally crucial in supporting PDAC progression. The ECM proteins, primarily produced by PSCs and CAFs, consist of collagen types I, III, IV, hyaluronic acid, fibronectin, and laminin. These ECM components facilitate interactions with tumor cells, enhancing their proliferation, migration, and survival [38]. Furthermore, the ECM proteins act as a physical barrier against chemotherapy and immune cell infiltration, thereby contributing to drug resistance. Fibronectin, laminin, and IGF-1 promote pancreatic tumor cell survival by interacting with integrin receptors on tumor cells, further protecting tumor cells from apoptosis and regulating cell adhesion and migration. Additionally, hyaluronic acid, a glycosaminoglycan secreted by tumor cells, forms a gel-like matrix between collagen fibers, trapping growth factors and cytokines within the stroma. This promotes water retention, elevating interstitial pressure and resulting in hypoperfusion, hypoxia, and vascular collapse, all of which hinder the effective delivery of chemotherapy to tumor cells [39]. Moreover, matrix metalloproteinases (MMPs) play a critical role in ECM degradation, promoting tumor invasion and metastasis. Overexpression of MMPs, such as MMP-9, has been observed in PDAC, highlighting their essential role in tumor dissemination. [36]

1.4.3.3. Neural components

In the last decade, neural elements were described as part of the TME being cancer cells and nerves dependent of each other for its function. The evidence suggests that the nervous system plays a key role in cancer progression and metastasis and the TME alters nervous system form and function [40]–[42]. Cancer and stromal cells express neuroreceptors that can promote several signaling cascades that can lead into a variety of effects, including cell proliferation, cell migration and invasion, and cell death.

Magnon (2013) was one of the first authors to describe the interactions between autonomic nerves and cancer within the TME [43]. In her work, Magnon explains that in early stages tumor growth can be inhibited by blocking neuroreceptors.

Peripheral neurogenesis, the process by which new neurons are formed in the peripheral nervous system, and axonogenesis, the process of axon generation and elongation, are crucial for the development, maintenance and repair of peripheral nerves. In this context Boilly et al. (2017) described that cancer cells are able to release soluble factors that promote neurogenesis (Fig. 5). Furthermore, cancer stem cells development is dependent on their innervation and the absence of nerves leads to reduction of the tumor progression [42].

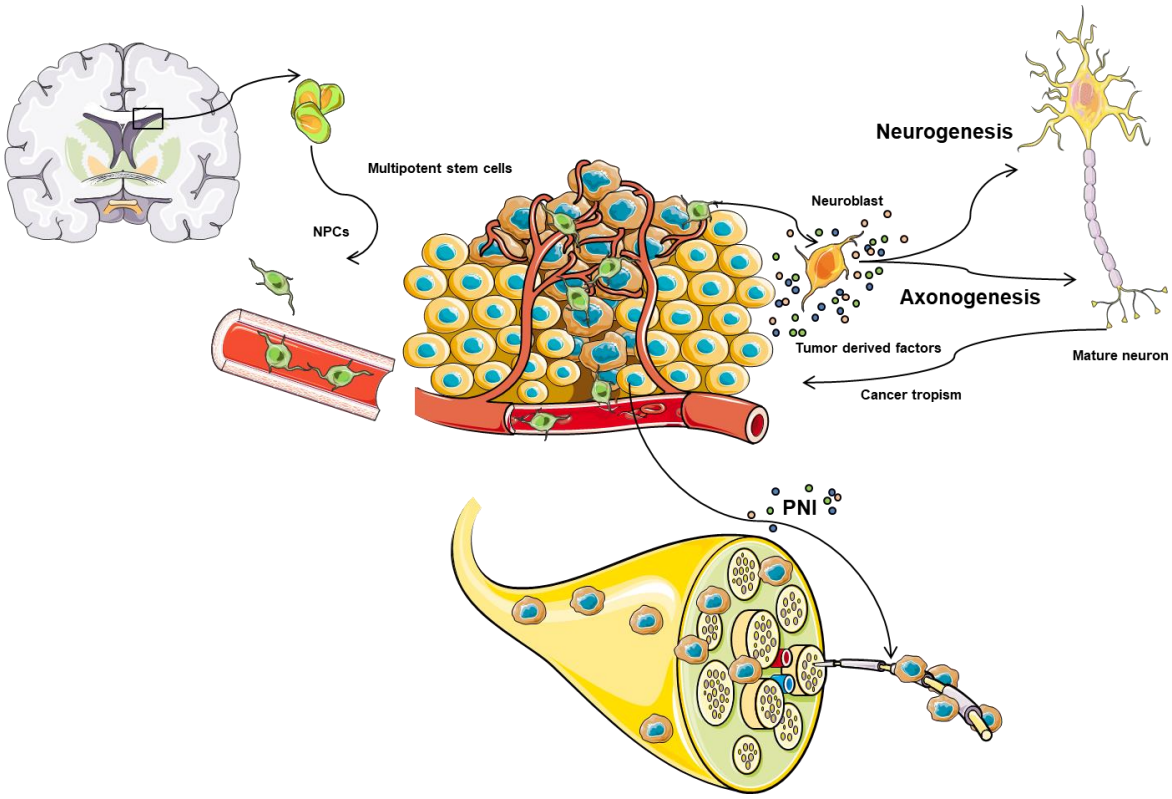

Figure 5. Nervous system and cancer crosstalk. Multipotent neural stem cells arrive to the TME. The TME releases soluble factors that promote neurogenesis and axonogenesis. The neurons have cancer tropism and promote tumorigenesis. Perineural invasion occurs when cancer cells are able to propagate through the nerves.

Recently Magnon et al. (2023) described that tumors can not only establish local networks with autonomic and sensory nerves but also engage in long-distance communication with the brain. This interaction is mediated by circulating

adipokines, inflammatory cytokines, neurotrophic factors, and afferent nerve inputs, all of which contribute to cancer initiation, progression, and dissemination [44].

Conversely, the central nervous system influences tumor development and metastasis by activating or dysregulating specific neural circuits, as well as by modulating neuroendocrine, neuroimmune, and neurovascular pathways (Fig. 6).

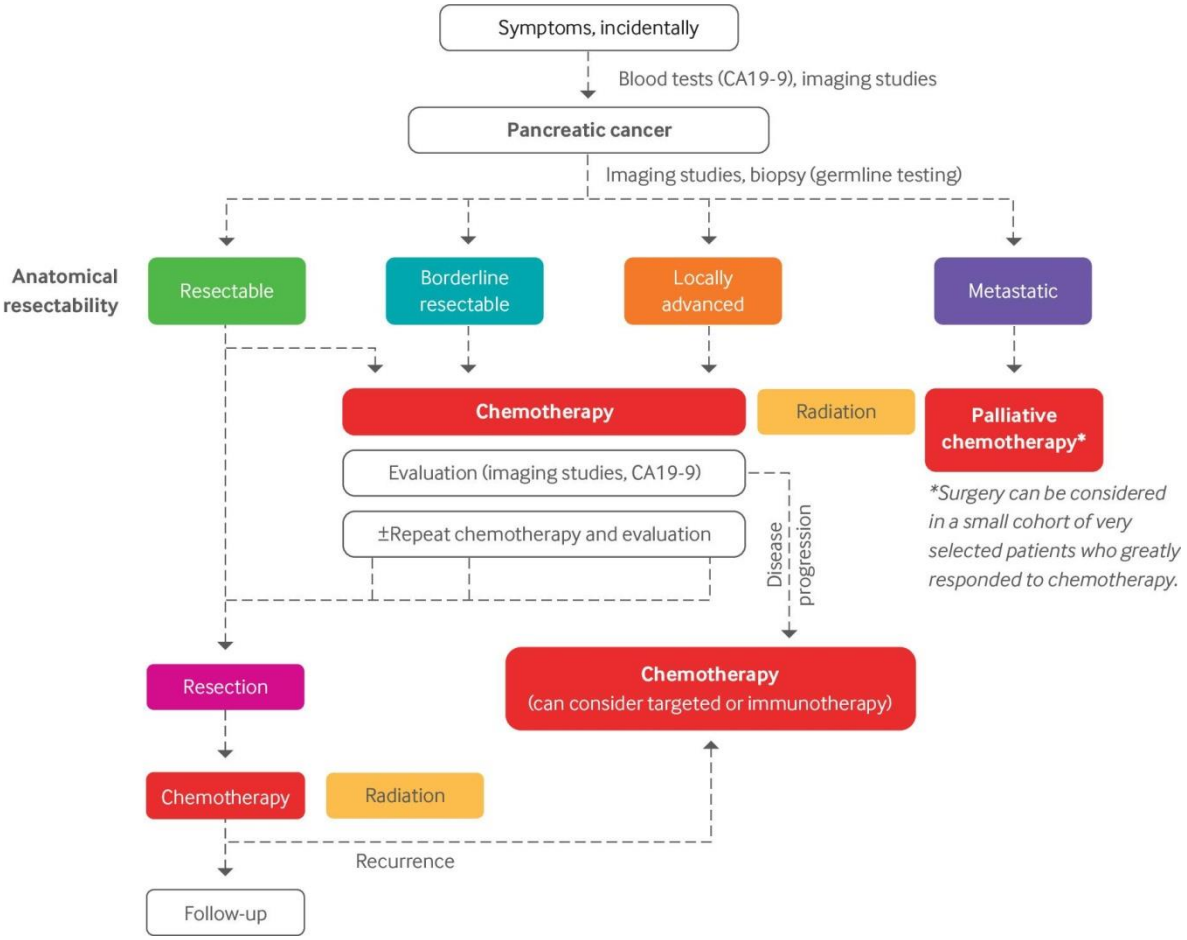

Figure 6. Current management for pancreatic cancer following the established guidelines. Extracted from Del Chiaro et al. [45].

1.5. Management and Treatment

Pancreatic cancer can be difficult to treat due to late diagnosis. The available treatments for pancreatic cancer are surgery, chemotherapy, radiotherapy and targeted therapy and the treatment choice will depend on the size and location of the tumor, the stage and the general health of the patient.

1.5.1. Surgery

The choice of surgical procedure—whether a Whipple procedure (cephalic pancreaticoduodenectomy), distal pancreatectomy, or total pancreatectomy—depends on the location of the tumor. The usual procedure is the pancreaticoduodenectomy, which consists in removing the distal segment (antrum) of the stomach, the first and second portions of the duodenum, the head of the pancreas, the common bile duct, and the gallbladder. Lymph nodes in the area are often removed during the operation as well (lymphadenectomy). [45] Surgery followed by chemotherapy is the only curative approach for patients nowadays.

1.5.2. Chemotherapy

1.5.2.1. Palliative chemotherapy

Patients diagnosed with locally advanced and/or metastatic PDAC are usually considered non-curative and are given chemotherapy to try to improve their life expectancy. Several clinical trials have shown that palliative chemotherapy improves the overall survival (OS) of the patients.

For long gemcitabine was the standard treatment given to PDAC patients, but recent studies have brought alternatives therapies that achieved better overall results. These therapies are FOLFIRINOX (5-Fluorouracil, Folinic acid, Irinotecan y Oxaliplatin) and gemcitabine with nab-paclitaxel (Gem-nabP) giving a benefit of 4.3 and 1.8 months benefit of survival compared to gemcitabine alone. No head-to-head study comparing FOLFIRINOX and Gem-nabP has been done and both are considered good options as first-line treatments for unresectable PDAC. FOLFORINOX causes more toxicity than its counterpart, and it's normally reserved for patients with a better health state. Gem-nabP is given to vulnerable population, those with mediocre performance, comorbidities or old age [46]–[48].

When first-line treatments fail to stop tumor progression the current second-line therapy is the combination with liposomal irinotecan with fluorouracil (5FU), which has a survival advantage over its predecessor, 5FU alone [49].

One of the latest studies showed that metastatic patients given Gem-nabP followed by modified FOLFOX (without irinotecan) showed a significantly higher 12 and 24 month survival vs Gem-nabP alone. This treatment can become a potential first-line option for metastatic patients [50].

1.5.2.2. Adjuvant chemotherapy

After surgery, chemotherapy is given to avoid relapse. The benefits are backed by several studies. Initially single agent adjuvant therapy with 5FU or Gemcitabine was given. Recent trials found that gemcitabine/capecitabine combination provides better overall survival compared to its monotherapy. On the other hand, mFOLFIRINOX improved the mOS even more compared to Gemcitabine, but more toxicity was found. Gemcitabine and its combination with capecitabine are still an option for those who can't tolerate mFOLFIRINOX [51] [52].

1.5.2.3. Neoadjuvant chemotherapy

Patients with borderline resectable tumors face a high rate of margin positivity after surgery (cancer cells are still present on the margins of the resectable site). Neoadjuvant chemotherapies studies have been conducted on patients with borderline resectable/ locally advanced PDAC to address this issue. Furthermore, distant metastases after surgery are the main mode of disease recurrence. Many believe that the high incidence of relapse in PDAC patients is due to micro-metastases present at time of surgery. In order to address this problem, neoadjuvant chemotherapy appears beneficial over adjuvant chemotherapy. In addition, completion rates compared to adjuvant chemotherapies are higher as patients have shown to tolerate neoadjuvant chemotherapy better.

Several ongoing phase II and III trials using Gemcitabine and its combination with nab-paclitaxel, oxaliplatin, FOLFIRINOX, mFOLFIRINOX and erlotinib are starting to bring more accurate information as to which are the best regimens and the benefit in each clinical setting [53]–[55].

1.5.3. Radiation

Radiation is widely used despite the evidence behind its efficacy remains inconsistent. Adjuvant radiation in combination with chemotherapy (chemoradiotherapy) has been studied with unclear results [56].

Neoadjuvant radiation appears to be a better option theoretically, but results have been modest. Patient OS treated with chemoradiotherapy with 5FU or gemcitabine as radiosensitizers have seen a slight improvement. In borderline resectable cases chemoradiotherapy has significantly increased resection rate, disease free survival and OS [57].

More evidence is needed to support the use of radiotherapy and chemoradiotherapy as a valid treatment for PDAC.

1.5.4. Targeted therapies

Radiotherapy and chemotherapy, although they improve outcomes to some extent, are still insufficient to ensure favorable patient survival rates. In this context, new strategies are emerging to address this issue. Targeted therapies focus on individualized treatment responses based on the specific characteristics of each tumor and follow three main approaches: inhibiting the overexpression of oncogenes, regulating the inactivation of tumor suppressor genes, and exploiting biological functional defects in specific genes.

With 60 mutations across 12 signaling pathways linked to PDAC, targeted therapies could enhance treatment efficacy. These genetic changes disrupt crucial signaling pathways affecting apoptosis and cell proliferation (Fig. 7).

1.5.4.1. KRAS pathway.

KRAS mutations are a hallmark of pancreatic ductal adenocarcinoma (PDAC), present in approximately 90-95% of cases. The most common mutations occur at codon 12, including G12D (42%), G12V (32%), G12R (15%), and G12C (1.5%), with G12D being the most prevalent. These mutations lead to the activation of

downstream signaling pathways that promote tumorigenesis, making KRAS a critical therapeutic target in PDAC [58].

Efforts to directly inhibit KRAS have faced significant challenges due to the complex signaling feedback loops and activation of compensatory pathways, such as PI3K/Akt, EGFR, and HER2 that diminish the effectiveness of KRAS inhibitors. Initial strategies targeted farnesylation through inhibitors like R115777, but clinical trials, such as SWOG 9924, showed no clinical benefit for metastatic PDAC patients.

The *KRAS G12C* mutation occurs in about 2% of PDAC cases. Targeted therapies for this mutation, including sotorasib and adagrasib, have shown encouraging results. The CRYSTAL-1 phase II trial with adagrasib demonstrated a 50% response rate and 6.6 months mPFS in *KRAS G12C*-mutated PDAC patients. Similarly, sotorasib in heavily pretreated patients showed 21.1% Overall response rate, 84.2% disease control rate, and median progression free survival of 4 months with mOS of 7 months. These results underscore the potential of targeted therapies for KRASG12C mutations in PDAC. Ongoing trials (NCT03785249 and NCT04330664) continue to explore the full clinical potential of these therapies [59] [60]**.**

For *KRAS G12D* mutations, which are present in a significant portion of PDAC cases, efforts are also underway to develop targeted therapies. A phase I/II trial investigated the use of RNAi targeting *KRAS G12D* through a biodegradable tumor implant, showing promising results with a median OS of 15 months. Additionally, innovative therapies using genetically engineered T-cells that target KRASG12D have demonstrated significant clinical responses, including a 72% reduction in tumor size in a single patient, with the response lasting more than 6 months. These approaches suggest that KRASG12D may be amenable to targeted immunotherapies and other novel treatments [60]**.**

Given the difficulty in directly targeting KRAS, therapies targeting downstream signaling pathways such as the RAF/MEK/ERK MAPK pathway and PI3K/Akt are

in development. MEK inhibitors (e.g., selumetinib, trametinib) have shown limited success as monotherapies due to feedback activation and pathway crosstalk, which often leads to the activation of compensatory pathways like PI3K/mTOR/Akt [61]–[63]. Combination strategies, such as combining MEK inhibitors with EGFR inhibitors, are being investigated to improve efficacy. Some early-phase trials have shown that combining MEK inhibitors with other agents may improve responses, though toxicity remains a concern [64].

In a small subset of KRAS wild-type (WT) PDAC cases, other genetic alterations such as NTRK fusions and NRG1 fusions drive tumorigenesis and may be targeted with specific therapies. NTRK fusions, though rare (0.3% of PDAC cases), can be targeted with larotrectinib and entrectinib, which have shown durable antitumor activity in PDAC patients with these fusions [65]. A pooled analysis from clinical trials demonstrated a 79% response rate for larotrectinib and 57% for entrectinib in solid tumors with NTRK fusions, including PDAC. For NRG1 fusions, the monoclonal antibody seribantumab has shown promising preclinical results, and ongoing trials such as CRESTONE (NCT04383210) are evaluating its efficacy in patients with metastatic or locally advanced solid tumors [66].

1.5.4.2. Tyrosine Kinase Receptor Pathway

This pathway involves several key proteins that regulate critical processes such as cell proliferation, survival, angiogenesis, and tumor progression. The main receptors targeted in PDAC treatment include EGFR (epidermal growth factor receptor), VEGF (vascular endothelial growth factor), and IGF-1R (insulin-like growth factor receptor 1).

EGFR is overexpressed in 30-50% of PDAC cases, contributing to tumor growth and resistance to apoptosis [67]. EGFR signaling is critical even in the presence of an oncogenic KRAS mutation. EGFR activation can promote downstream signaling through the MAPK and PI3K/Akt pathways, leading to uncontrolled cell division and survival. Targeting EGFR with inhibitors such as erlotinib and nimotuzumab has shown some clinical benefit, particularly in combination with chemotherapy like

gemcitabine. Erlotinib is currently approved by the European Medicines Agency (EMA) for the treatment of metastatic pancreatic cancer in combination with gemcitabine. However, the efficacy of EGFR inhibitors remains limited, and newer treatments are being explored to improve outcomes [68].

VEGF is a key regulator of angiogenesis, the formation of new blood vessels, which is essential for tumor growth and metastasis. In PDAC, overexpression of VEGF leads to tumor vascularization, facilitating the supply of nutrients and oxygen to the tumor. [69]. However, the dense stromal tissue surrounding PDAC tumors creates a barrier to effective drug delivery, limiting the success of antiangiogenic therapies. Despite this, agents like bevacizumab (an anti-VEGF antibody) have been tested in clinical trials, often in combination with chemotherapy. These studies have shown some improvement in progression-free survival but no significant benefit in OS [70]. Newer agents, such as anlotinib, are being explored for their potential to improve clinical outcomes by targeting VEGF and other growth factor receptors [71].

IGF-1R is overexpressed in PDAC and is associated with reduced apoptosis, increased cell proliferation, and enhanced tumor survival [72]. IGF-1R signaling is linked to the constitutive activation of the PI3K/Akt pathway and MAPK signaling, which contributes to cancer cell resistance to therapy. Despite its significance, targeting IGF-1R alone has not yielded substantial improvements in PDAC treatment. Clinical trials with ganitumab (an IGF-1R monoclonal antibody) have shown no significant survival benefit. However, combining IGF-1R inhibitors with EGFR inhibitors has been proposed as a strategy to overcome resistance mechanisms, with some studies showing improved OS in combination with chemotherapy [73].

1.5.4.3. PI3K/Akt/mTOR pathway

Akt is overexpressed in more than 40% of PDAC tumors. The upregulation of PI3K/Akt/mTOR pathway is involved as a key driver of PDAC progression and therapy resistance, regulating cell growth, survival, metabolism and apoptosis. The inhibition of this pathway has been proven to reduce tumor growth and induce apoptosis [74].

The current clinical trials are using Akt inhibitors such as perifosine which, in combination with gemcitabine, is achieving synergistic effects in PDAC. Other approaches include mTOR inhibitors and P13K inhibitors [75]. Monotherapies targeting this pathway have shown limited efficacy, but combination approaches with chemotherapy or multitarget inhibitors appear more promising [76].

1.5.4.4. Tumor suppressor pathway

Another strategy is to target the tumor suppressor genes, which have a contrary role to oncogenes. These genes are mutated in PDAC patients and therefore, their roles as growth inhibitors, proliferation, apoptosis and genomic stability is disrupted. Targeted therapies not only aim to reactivate tumor suppressor genes but to inhibit its antagonizers The most promising approaches target tumor suppressor genes TP53, SMAD4, CDKN2A and its respective antagonizers MDM2, TGF-β and CDK4/6. Some treatments have shown encouraging results, but it's the combination regimens the ones that appear to be the most efficient approach for tumor suppression in PDAC [77]–[80].

1.5.4.5. NF-κβ pathway.

The nuclear factor kappa β is a protein complex that regulates cell proliferation and apoptosis and appears overexpressed in 70% of pancreatic cancers. Targeted inhibitors such as curcumin have demonstrated good preclinical results [81]. Another inhibitor, nafamostat mesilate, when combined with gemcitabine, has shown promising results in phase I and II studies [82].

1.5.4.6. Stroma

The stroma is involved in numerous processes regarding growth and spreading of cancer cells. Furthermore, PDAC stroma is dense and fibrous, representing 90% of tumor volume, providing a protumorigenic environment. Some targeted therapies that focus on the stroma are being developed, targeting the extracellular matrix directly or pathways that promote the development of the tumor stroma. Most of the studies have failed to achieve satisfactory results, and the general belief is that a combination strategy targeting SHH and previously mentioned pathways such as P13K may improve outcomes [83]. Treatments inhibiting MPPs involved in tumor invasion and angiogenesis, in combination with gemcitabine and nabP, for example andecaliximab, have demonstrated clinical activity and safety [84]. Targeting the connective tissue growth factor with pamrevlumab or using c-MET/HGF inhibitor tivantinib is a potential treatment that is being evaluated in clinical trials [85], [86].

1.5.4.7. Cancer stem cells

Whiting the tumor there is a subpopulation of cells able to self-renew and differentiate known as cancer stem cells. CSCs play a key role in carcinogenesis, progression, metastasis and drug resistance. Therapies targeting important pathways in CSCs development such as WNT, Notch and activating of JAK/STAT pathways are being studied in clinical assays. Specifically, WNT inhibitors vantictumab and ipafricept in combination with chemotherapy have shown moderate efficacy [87], [88]. Unfortunately targeting notch and JAK/STAT pathways are yet to improve outcomes.

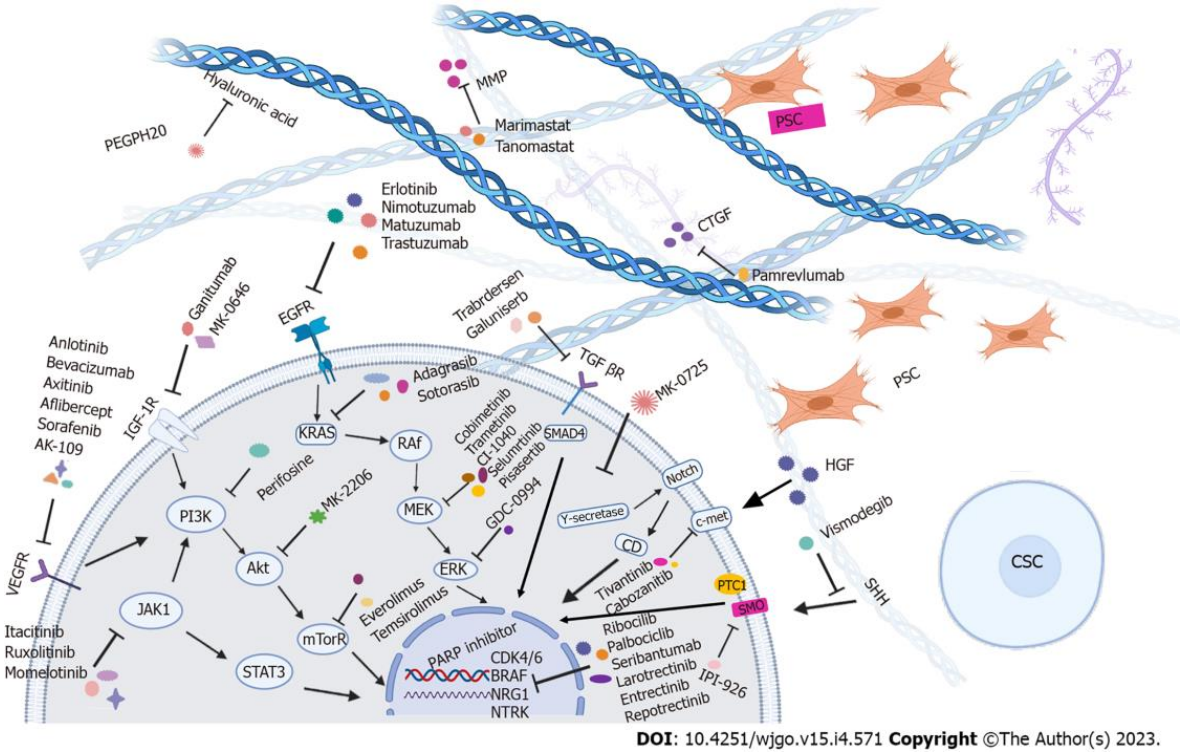

DOI: 10.4251/wjgo.v15.i4.571

Figure 7. Overview of targeted therapy strategies for pancreatic adenocarcinoma. The figure summarizes the systemic therapeutic targets and corresponding drugs for pancreatic cancer, including treatment strategies for many aspects such as signaling pathways and gene mutations in tumor cells, and molecules in the extracellular environment, and extracellular matrix. "—|" indicates "targeting", Figure from Fang YT et al. 2023 [89].

2. Peripheral Dopamine and cancer.

2.1. Dopamine synthesis and molecular signaling

Dopamine (DA) is a catecholamine neurotransmitter primarily discovered in the central nervous system (CNS), where it plays a crucial role in regulating movement, cognition, motivation, and reward-related behavior. Dopamine is traditionally recognized as a precursor to norepinephrine and epinephrine in the periphery [90]. However, emerging evidence highlights distinct peripheral functions as an autocrine or paracrine signaling molecule rather than a neurotransmitter or circulating hormone.

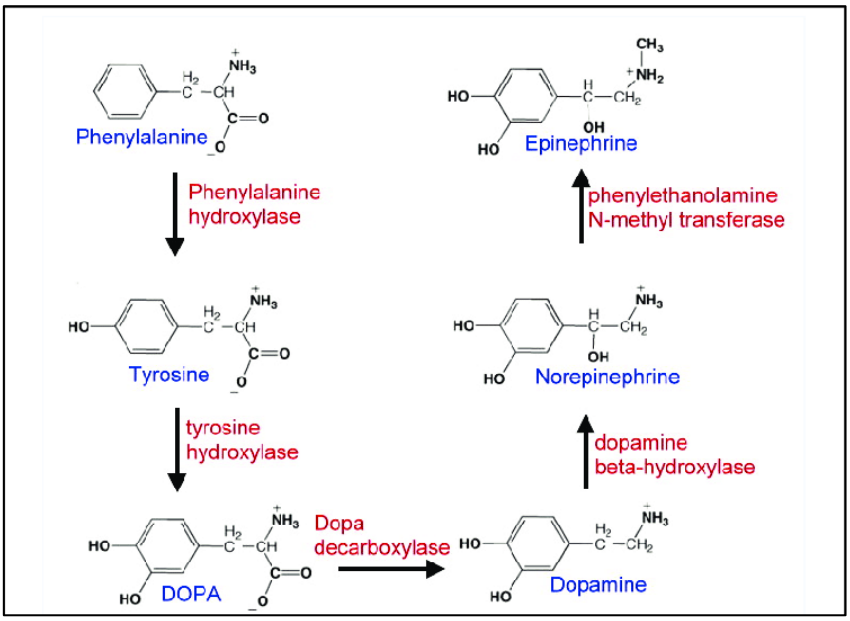

Figure 8. The biosynthetic pathway of dopamine. From Yang PP et al 2020 [91]**.**

The biosynthesis of dopamine begins with the amino acid tyrosine, which is converted into L-DOPA by tyrosine hydroxylase, followed by the decarboxylation of L-DOPA by aromatic L-amino acid decarboxylase to form dopamine (Fig. 8). Dopamine exerts its effects through five G protein-coupled receptor subtypes: D1–D5 [90]. All dopamine receptors are metabotropic, meaning they produce second

messengers that either activate or inhibit certain cell signaling pathways. These receptors belong to members of the G protein-coupled receptor family, which are divided into two large subclasses: D1R-like (D1, D5) and D2R-like (D2, D3, D4) receptors. Their functions are described to be different and/or opposite. D1R-like stimulate the adenylate cyclase (AC) resulting in the production of cyclic adenosine monophosphate (cAMP) through the hydrolysis of adenosine triphosphate (ATP). This cascade will end in the activation of CREB-binding protein in the nucleus, promoting the transcription of genes. Furthermore, they are described to activate ion channels such as Ca^{2+}, K^{+} and Na^{+} channels and G-protein gated inwardly rectifying K^{+} (GIRK) channel [92]. On the other hand, D2R-like family bind through coupling proteins that result in the suppression of the AC, activating GIRK and closing voltage activated Ca^{2+} channel. Moreover, DA receptors can be found as monomers, dimeric and/or oligomeric complexes, which affect their pharmacological and functional traits [92].

Dopamine receptors are distributed not only in the CNS but also in various peripheral organs, including the gastrointestinal tract, kidneys, adrenal glands, pancreas, and immune cells, where their function also varies; pointing dopamine as a modulator in diverse physiological processes.

In the periphery, dopamine plays a key role in metabolic regulation, cardiovascular function, and immune modulation. In the kidneys, dopamine modulates sodium excretion and blood pressure by acting on renal dopamine receptors, particularly D1R-like receptors, which promote natriuresis and diuresis.

The gastrointestinal tract is a major site of dopamine production and metabolism, accounting for nearly half of the body's dopamine outside the nervous system. Dopamine in the gut modulates gastric acid production, and local blood flow, with D2R-like receptor activation exerting inhibitory effects on intestinal motility. In the pancreas, dopamine may modulate secretion of digestive enzymes and is involved in the regulation of glucose metabolism, as it influences insulin secretion from pancreatic β-cells and bicarbonate. Additionally, mesenteric organs significantly

contribute to the production of dopamine sulfate, a major circulating dopamine metabolite [93].

Dopamine also interacts with the immune system, where it modulates the activity of T cells, B cells, and macrophages. Peripheral dopamine has been shown to exert immunosuppressive effects by inhibiting pro-inflammatory cytokine production and promoting regulatory T cell activity [94].

2.2. Dopamine in cancer.

In this context, the dopaminergic pathway has been explored as prognostic and therapeutic target [41].

Epidemiological studies, suggests that patients with schizophrenia treated with antipsychotic drugs (mainly dopamine receptor antagonists and dopamine receptor blockers) have a lower incidence of certain cancers, including gastrointestinal and brain malignancies, compared to the general population. Initial observations that cancer patients receiving antipsychotics alongside their standard oncologic treatment exhibited improved clinical outcomes further supported the hypothesis that dopamine receptors (DRs) might influence tumor progression [95].

With growing evidence that dopamine signaling is disrupted in peripheral tissues during cancer development, research into repurposing dopaminergic drugs for oncology has gained momentum. Given the challenges of developing new cancer therapies, repurposing existing neuropharmacological drugs offers a promising, cost-effective strategy that could benefit both patients and drug developers [96].

In this context, dopamine interaction with cancer cells and tumor microenvironment has been studied. DRs are expressed in a variety of cancers, and several authors have reported different expression patterns depending on the tumor type and genetic background [95]. Furthermore, changes in DRs expression have been found not only in cancer cells but in cells interacting with the tumor, and these changes alter cell functions, affecting the tumor biology. The described effects of the DRs in cancer are described in figure 9.

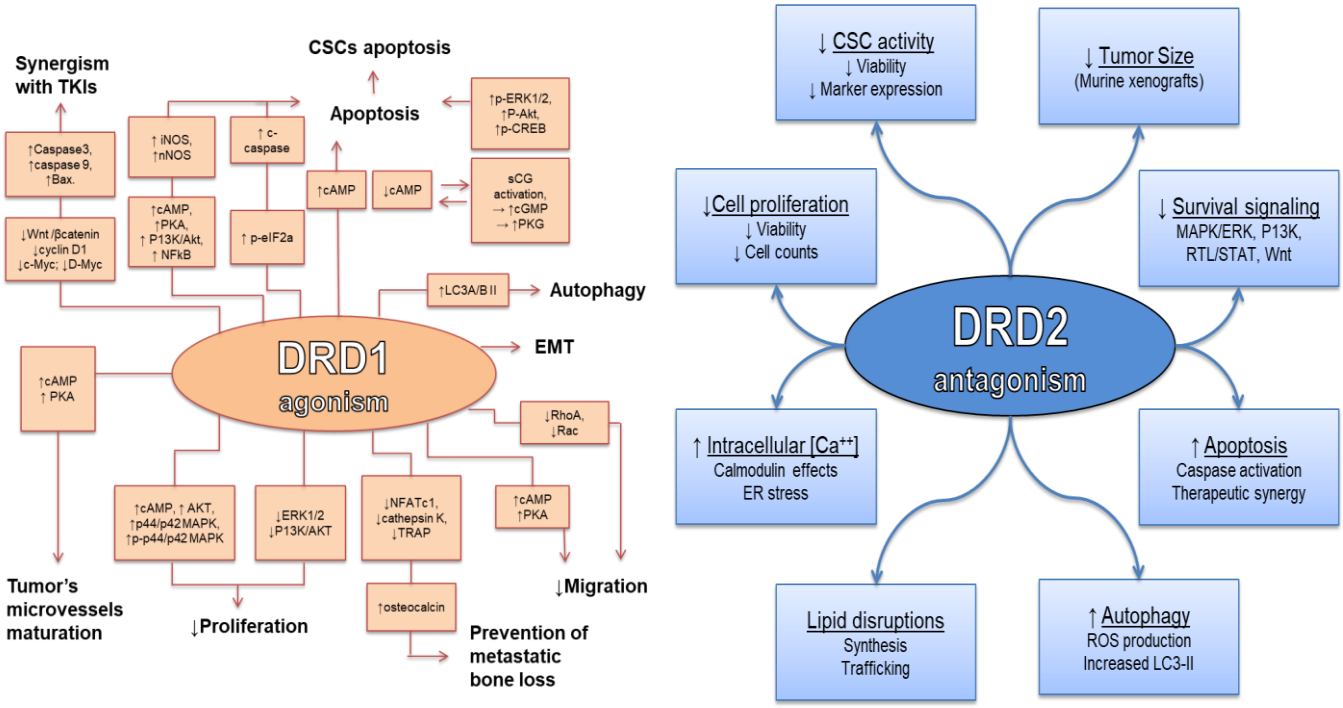

Figure 9. Dopaminergic receptors' role in cancer. A) The dopamine D1 receptor plays a crucial role in cancer biology by influencing various cellular and tumor-related processes. **B)** Treatment with D2 antagonists disrupts essential metabolic processes in cancer cells and tumors.

The effects of dopamine in cancer are contradictory, depending on the tumor type and the DR family that is being targeted. On one hand, D1-like receptor agonism has suppressed viability in triple-negative breast cancer cell lines both *in vivo* and *in vitro*. The agonism also inhibited cell growth in some nervous system neoplasms (meningioma and neuroblastomas) while significantly promoting cell proliferation and migration in U87 glioma cell line. Some studies on lung and gastrointestinal cancers show that the agonism might reduce the number of CSCs.

On the other hand, studies centered on the D2R family have shown that the modulation D2-like receptors in pancreatic cancer reduces tumor growth [97].

Several authors have been able to acknowledge dopamine's role in TME modulation. Dopamine is able to regulate immune cell activity, angiogenesis and cell proliferation. Amongst the functions, dopamine can influence macrophages and T-cells, has implications in fibrosis, and inhibits angiogenesis suppressing VEGF [98], [99].

DRD1 agonism in neoplasms affects cell proliferation, apoptosis, autophagy induction, and migration potential reduction. On a larger scale, DRD1 impacts tumor vessel maturation, drug distribution within the tumor, and bone metastasis formation. These effects are mediated through several key signaling pathways, including the cAMP/PKA/CREB axis, which regulates gene transcription and cell survival; the PI3K/Akt pathway, which controls cell growth and apoptosis; and the ERK1/2 cascade, which influences proliferation and differentiation. Additionally, D1R activation affects immune response and inflammation via NFκB and NFATc1, modulates nitric oxide production through iNOS and nNOS, and influences cytoskeletal rearrangement and motility via RhoA/Rac proteins. Other pathways, such as sGC/cGMP/PKG, contribute to vascular function and tumor signaling.

On the other hand DRD2 antagonism reduces cancer stem cell-like activity, survival signaling, and proliferation while increasing intracellular calcium levels, autophagy, and apoptosis.

Initially, D2-like receptors are more attractive for targeted therapies. Some dopaminergic drugs have been investigated for repurposing in oncology. Bromocriptine (DRD2 agonist) has been investigated in acute myeloid leukemia, where it induces apoptosis and differentiation of stem cells. Caripazine (D2R-like partial agonist) is able to modulate multidrug resistance in cancer therapy.

In PDAC zuclopenthixol, a D1 and D2 receptor antagonist, inhibited PSC activation and reduced tumor growth in an *in vivo* experiment [100]. ONC201 (DRD2 antagonist) has shown some effect inducing cancer cell death in PDAC and other cancer types [101].

Furthermore, dopamine improves the chemotherapeutic efficacy in PDAC by modulating TAMs both *in vitro* and *in vivo* studies [102].

3. Animal models in cancer research.

Animal models have been instrumental in advancing our understanding of cancer biology, enabling researchers to investigate the mechanisms underlying tumor development, progression, and metastasis. These models serve as essential tools for identifying diagnostic, prognostic, and therapeutic targets, as well as for evaluating the efficacy of experimental treatments before clinical application in humans.

Among the various animal models employed in cancer research, murine models—encompassing both rats and mice—are particularly valued. Their genetic similarity to humans, sharing approximately 95% of genes, coupled with their affordability, ease of maintenance, and rapid reproductive cycles, make them ideal for translational studies. Notably, the lifetime risk of developing cancer is comparable between rodents and humans, with about 30% of laboratory mice developing cancer toward the end of their lifespan, mirroring the incidence in humans aged 70-80 years.

However, it is important to recognize the limitations inherent in these models. Certain antineoplastic mechanisms are specific to humans, leading to potential discrepancies in responses to carcinogenesis and chemopreventive agents. Differences in body size and lifespan result in humans experiencing more cell divisions than rodents, which can influence tumor development and evolution. Additionally, variations in drug metabolism and efficacy between species can affect the translational applicability of findings from murine models to human clinical settings.

To enhance the clinical relevance of animal models in cancer research, efforts have been made to develop models that closely replicate human tumor characteristics. An ideal model should exhibit the histopathological features of

human tumors, progress through similar stages, involve the same genetic and signaling pathways, and reflect human responses to specific therapies. Such models are invaluable for understanding the alterations leading to tumor formation, identifying prevention and treatment targets, and elucidating mechanisms of drug resistance.

3.1. Chemically induced PDAC animal models

One of the earliest strategies used to generate animal models of pancreatic ductal adenocarcinoma was exposure to carcinogenic chemicals. The DNA-alkylating carcinogen azaserine and the surgical implantation of 7,12-dimethylbenzanthracene (DMBA) have been employed to induce pancreatic carcinogenesis and metastasis in rats. However, in these models, tumor cells do not exhibit the oncogenic KRAS mutation, thus, limiting their ability to accurately represent human PDAC and reducing their translational relevance.

In contrast, the DNA-alkylating agents N-nitroso-bis (2-oxopropyl) amine (BOP) and N-nitroso-bis(2-hydroxypropyl)amine (BHP) in hamsters promote guanine methylation, leading to nucleotide mutations and inducing KRAS gene mutations. Consequently, these models exhibit greater morphological similarity to human pancreatic cancer, making them more relevant for studying PDAC pathogenesis.

3.2. Genetically engineered mouse models (GEMMs) for PDAC

In the context of PDAC, GEMMs have been particularly informative. For instance, the K-Ras^{LSLG12D}; Pdx1-Cre (pancreatic duodenal homeobox-1) model involves the expression of an endogenous K-Ras^{G12D} oncogene in all epithelial pancreatic lineages during early embryonic development. These mice develop the full spectrum of PanIN lesions and PDAC tumors histologically indistinguishable from those present in human patients. However, the incidence of PDAC tumors in these strains is relatively low at 1 year of age. Introducing additional mutations, such as inactivation of tumor suppressors like p53 (resulting in KPC strains), accelerates the progression of PanIN lesions to invasive PDAC and induces metastasis in a significant percentage of cases [103].

These GEMMs faithfully reproduce the histological lesions characteristic of human pancreatic tumors. Incorporating additional mutations, primarily involving tumor suppressor genes known to be mutated in human PDAC tumors, results in accelerated tumor progression and the induction of invasive and metastatic malignancies. This model has the advantage that their immune system remains intact, displaying a desmoplastic stroma and inflammatory responses that closely resemble those observed in human patients.

3.3. Xenograft Models of PDAC

Xenograft models of pancreatic ductal adenocarcinoma (PDAC) are developed using immunodeficient mice, allowing the implantation of human tumor cells or tumor tissue. The most commonly used mouse strains for these models include athymic nude mice, which lack T cells, and NOD-SCID mice, which exhibit severe combined immunodeficiency (SCID) due to the absence of both T and B lymphocytes [104].

These models can be generated through the surgical implantation of tumor tissue fragments or the injection of established tumor cell lines into immunodeficient mice. To enhance engraftment efficiency and improve tumor growth rates, the use of extracellular matrix components, such as Matrigel, is often employed [104]. However, subcutaneous xenograft models typically do not metastasize and fail to accurately replicate the intrapancreatic neoplastic progression observed in human PDAC. These limitations can be addressed using orthotopic xenograft models, where tumor cells or tissue fragments are implanted directly into the pancreas. Orthotopic models not only recapitulate pancreatic tumor growth but also enable metastasis, allowing the study of tumor progression and metastatic mechanisms. Advanced imaging techniques, including bioluminescence, fluorescence, ultrasound, CT, and magnetic resonance imaging (MRI), can be utilized to monitor tumor development and dissemination *in vivo* [103].

Orthotopic xenograft models can be established either by direct intrapancreatic injection of isolated tumor cells or by surgical implantation of tumor tissue

fragments into the pancreas. The latter approach enhances engraftment rates, reduces variability in primary tumor size, and minimizes the risk of peritoneal leakage [105].

3.4. Patient-Derived Xenografts (PDX)

Xenografts generated from commercially available tumor cell lines often exhibit genetic and epigenetic alterations that do not fully represent the heterogeneity of human tumors. These models primarily consist of neoplastic tumor cells, comprising approximately 10% of the total tumor mass, without accounting for the influence of the stromal microenvironment or infiltrating immune cells [106].

To overcome these limitations, patient-derived xenografts (PDX) have been developed. PDX models involve the implantation of freshly resected patient tumor tissue into immunodeficient mice, either subcutaneously or orthotopically. These models maintain the genomic integrity, histopathological characteristics, and, in the case of orthotopic models, metastatic potential of the original patient tumors [106], [107]. PDX models also provide a valuable tool for assessing therapeutic responses, with implantation success rates varying from 10% to 100% depending on tumor type and host conditions. The summary of this section is represented in figure 10.

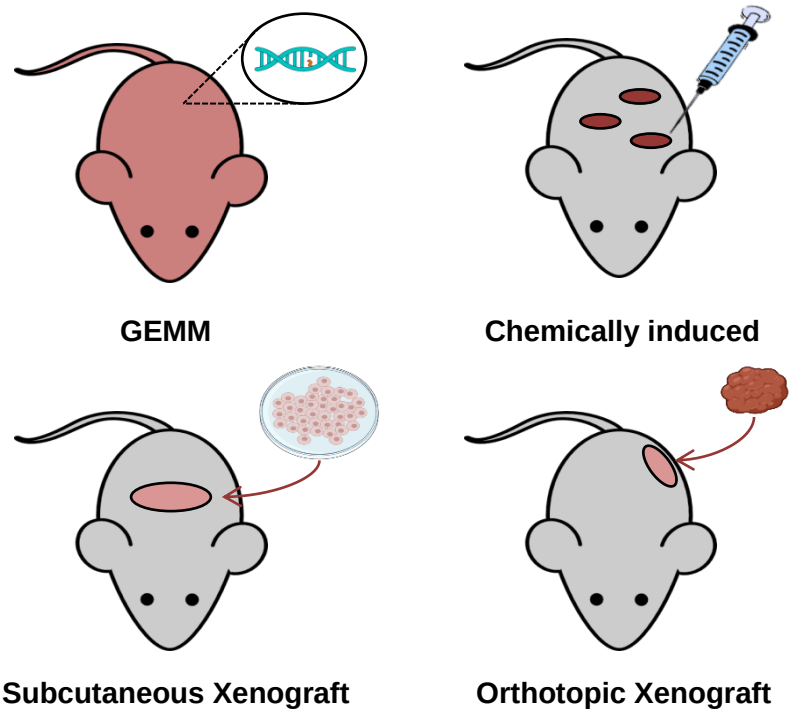

Figure 10. Murine models in PDAC.

3.5. Humanized Xenograft Models

One of the main limitations of PDX models is the requirement for immunodeficient mice, which prevents the evaluation of immune system interactions and immunotherapy responses. To address this issue, humanized xenograft models have been developed, incorporating components of the human immune system to better replicate innate immune responses and tumor-immune interactions.

Examples of humanized xenograft models include mice engrafted with CD34+ hematopoietic stem cells derived from umbilical cord blood, allowing intrahepatic immune cell development, and mice transplanted with human peripheral blood mononuclear cells into athymic nude mice. These models provide a platform for studying immune-tumor interactions and evaluating novel immunotherapeutic approaches in a more clinically relevant context [108].

4. Nanotherapy in PDAC.

In recent years, nanomedicine has emerged as a promising approach, enhancing drug delivery, improving therapeutic efficacy, and overcoming biological barriers within the tumor microenvironment [109].

One of the primary obstacles in PDAC treatment is the tumor's highly fibrotic and hypovascularized microenvironment, which restricts the perfusion of therapeutic agents. Unlike other cancers where systemic chemotherapy can achieve relatively efficient tumor penetration, PDAC features a thick extracellular matrix composed of collagen, hyaluronic acid, and activated stromal cells that create a physical and biochemical barrier. This unique tumor biology contributes to inadequate drug accumulation, making it difficult to achieve cytotoxic concentrations within cancer cells. Furthermore, PDAC tumors are characterized by the overexpression of efflux transporters, which actively pump chemotherapeutic agents out of the cells, further reducing drug efficacy [110].

4.1. Liposomes

Nanotechnology-based drug delivery systems have been developed to overcome these challenges by enhancing drug stability, increasing circulation time, and enabling controlled release at the tumor site. Lipid-based nanoparticles, such as liposomes and solid lipid nanoparticles, have gained significant attention due to their ability to encapsulate hydrophobic drugs, protect them from degradation, and facilitate passive targeting through the enhanced permeability and retention (EPR) effect. One notable example of this approach is pegylated liposomal irinotecan (nal-IRI), which has been approved (2024) [111] for use in combination with 5-fluorouracil and leucovorin for metastatic PDAC. Nal-IRI enhances irinotecan delivery to the tumor while reducing systemic toxicity, leading to improved patient outcomes compared to conventional irinotecan formulations.

Table 1. Ongoing and completed clinical trials for liposome-based drug delivery for PDAC.

Trial Identifier	Treatment	Intervention	Treatment Type	Clinical Phase	Trial Status	References
NCT04083235 (NAPOLI 3)	Irinotecan liposome injection, oxaliplatin, 5-fluorouracil/leucovorin	Metastatic pancreatic cancer	First-line therapy	III	Active	Wainberg et al. (2023)
NCT03468335 (PREDICT)	Irinotecan liposome	Locally advanced or metastatic pancreatic cancer	Second-line therapy	III	Active	Frampton (2020); Katayama et al. (2020)
NCT05074589	Irinotecan liposome/5-fluorouracil/leucovorin	Gemcitabine-refractory pancreatic cancer	Second-line therapy	III	Completed	L. Wang et al. (2022)
NCT04217096	Paclitaxel liposome/S-1	Advanced pancreatic cancer	First-line therapy	IV	Unknown	Raza et al. (2023)
NCT05100329	Mitoxantrone hydrochloride liposome	Advanced pancreatic cancer	Second-line therapy	II	Active	Yang et al. (2023)
NCT04852367 (PanDox)	Thermosensitive liposomal doxorubicin (ThermoDox/Focused Ultrasound)	Non-resectable primary pancreatic tumors (stage IV)	—	I	Withdrawn	Spiers et al. (2023)
NCT04083235 (NAPOLI 3)	Irinotecan liposome injection, oxaliplatin, 5-fluorouracil/leucovorin	Metastatic pancreatic cancer	First-line therapy	III	Active	Wainberg et al. (2023)
NCT03468335 (PREDICT)	Irinotecan liposome	Locally advanced or metastatic pancreatic cancer	Second-line therapy	III	Active	Frampton (2020); Katayama et al. (2020)

NCT05074589	Irinotecan liposome/5-fluorouracil/leucovorin	Gemcitabine-refractory pancreatic cancer	Second-line therapy	III	Completed	L. Wang et al. (2022)
NCT04217096	Paclitaxel liposome/S-1	Advanced pancreatic cancer	First-line therapy	IV	Unknown	Raza et al. (2023)
NCT05100329	Mitoxantrone hydrochloride liposome	Advanced pancreatic cancer	Second-line therapy	II	Active	Yang et al. (2023)
NCT04852367 (PanDox)	Thermosensitive liposomal doxorubicin (ThermoDox/Focused Ultrasound)	Non-resectable primary pancreatic tumors (stage IV)	—	I	Withdrawn	Spiers et al. (2023)

Beyond liposomes, polymeric nanoparticles have been explored as versatile platforms for PDAC therapy. These nanoparticles can be engineered to provide sustained drug release, allowing for prolonged therapeutic exposure while minimizing off-target effects. Poly(lactic-co-glycolic acid) (PLGA) nanoparticles, for instance, have been widely studied for the controlled release of gemcitabine, one of the standard chemotherapeutic agents for PDAC. Encapsulation of gemcitabine in polymeric nanoparticles improves its half-life, reduces premature degradation, and enhances intracellular uptake [112]. Moreover, polymeric nanoparticles can be functionalized with targeting ligands, such as antibodies or peptides, to facilitate active targeting of PDAC cells expressing specific surface markers, such as epidermal growth factor receptor (EGFR) or mesothelin [113].

Another emerging class of nanomaterials in PDAC treatment is inorganic nanoparticles, including gold nanoparticles, silica-based nanoparticles, and quantum dots. Gold nanoparticles, in particular, have shown promise as both therapeutic and diagnostic agents due to their unique optical and photothermal properties. Functionalized gold nanoparticles can be designed to selectively accumulate in PDAC cells, where they can serve as contrast agents for imaging or

be used for photothermal therapy, a technique that utilizes laser-induced hyperthermia to ablate cancer cells. Silica-based nanoparticles have also been explored for the co-delivery of multiple therapeutic agents, enabling combination therapy approaches that simultaneously target different aspects of tumor biology [114].

Another promising avenue in PDAC nanomedicine is the use of stimuli-responsive nanoparticles, which release their payload in response to specific tumor-associated triggers such as pH, enzyme activity, or redox conditions. These “smart” nanoparticles can be designed to remain stable in circulation but rapidly disassemble upon reaching the tumor microenvironment, ensuring precise drug delivery while minimizing exposure to healthy tissues [115]. pH-sensitive liposomes, for example, have been engineered to release gemcitabine in the acidic microenvironment of PDAC tumors, leading to enhanced cytotoxicity compared to conventional formulations [116]. Similarly, enzyme-responsive nanoparticles have been developed to degrade upon interaction with tumor-associated enzymes such as matrix metalloproteinases, thereby facilitating deeper tumor penetration and improved therapeutic efficacy [117]. The ongoing research on liposomes in PDAC is described in table 1.

4.2. Nanovaults

Among the various nanoparticles explored for PDAC treatment, vault nanoparticles have attracted significant attention due to their unique structure and ability to encapsulate and deliver molecular cargo. Vaults are naturally occurring ribonucleoprotein particles that possess a large internal cavity capable of carrying therapeutic agents. Its structure is defined by 78 copies of the major vault protein (MVP), each approximately 97 kDa, which assemble into two symmetrical, cup-shaped halves to form a barrel-like structure measuring roughly $72.5 \times 41 \times 41$ nm. These particles, exhibit a highly stable yet dynamic architecture that allows them to encapsulate chemotherapeutic drugs, nucleic acids, and even immunomodulatory molecules. The MVP is composed of twelve domains: nine repeat domains at the

N-terminus (R1 to R9), and α/β shoulder domain, a cap-helix and a cap-ring domain at the C-terminus (Fig. 11) [118].

In the context of cancer treatment, vault nanoparticles offer a versatile platform for drug delivery. Their large internal cavity can be exploited to encapsulate a variety of compounds, thereby protecting them from premature degradation in the biological milieu. Moreover, the surface of the nanoparticle can be chemically or genetically modified to display targeting ligands, which enhances the selective delivery to tumor cells and minimizes off-target toxicity. This targeted approach is especially valuable in cancer, where precise delivery of drugs can overcome challenges such as multidrug resistance—a phenomenon in which vault components themselves have been implicated due to their roles in intracellular trafficking and the nuclear export of drugs [119]. Additionally, by engaging with cellular signaling pathways (for example, those involved in survival and apoptosis), the engineered vault nanoparticle may not only serve as a passive carrier but also actively modulate the tumor microenvironment to favor therapeutic outcomes [120]. Their versatility has led to significant interest in their use as nanocarriers for targeted therapy where drug resistance and poor bioavailability are major challenges.

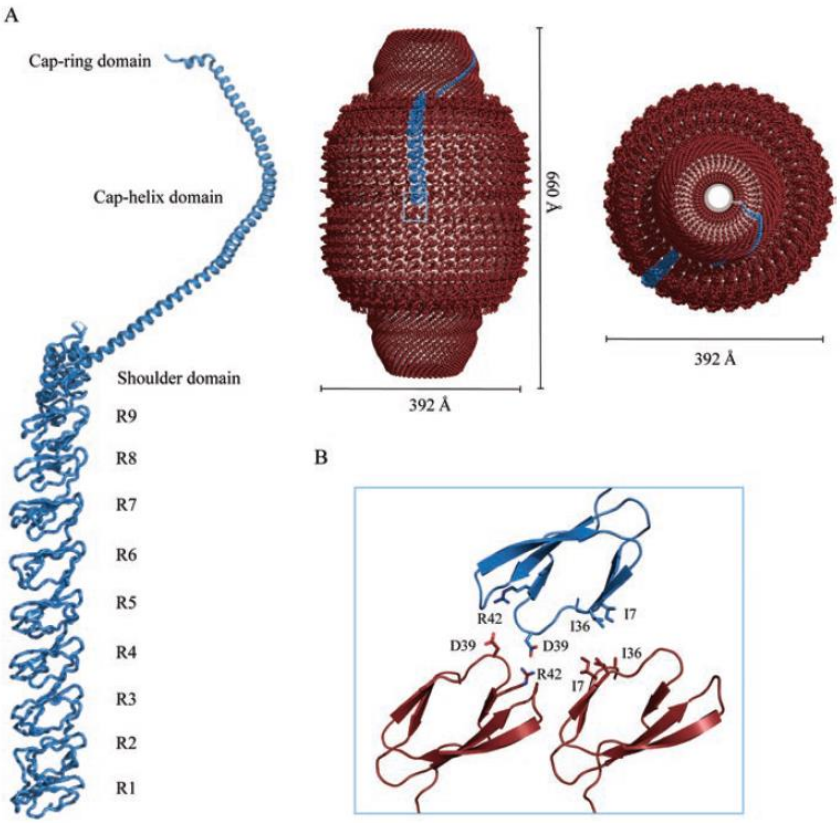

Figure 11. Overall structure of the vault complex and MVP domain organization. A) Side and top views of the vault shell, colored in maroon with one of the 78 MVP copies forming the particle shown in blue (PDB ID: 4HL8; Casañas et al. 2013). B) Detailed view of the R1-R1 contacts at the half vault interface. The reference R1 domain (blues) contacts two consecutive R1 molecules (maroon) through the molecular two-fold axis. Interacting residues are shown in sticks and labelled. From González-Álamos et al 2024 [118].

II. AIMS AND OBJECTIVES

Pancreatic ductal adenocarcinoma (PDAC), the most common subtype of pancreatic cancer, is one of the most aggressive and lethal malignancies, with a 5-year survival rate of approximately 5-7% worldwide. It is the third leading cause of cancer-related deaths globally, largely due to its asymptomatic nature in early stages, resulting in late-stage diagnoses with loco-regionally advanced or metastatic disease. These factors, coupled with limited effective systemic therapies and resistance to treatments, contribute to the poor prognosis, highlighting the urgent need for innovative therapeutic strategies.

The emerging field of neural-tumor interactions offers a promising avenue for novel treatments. Within this context, dopamine signaling has gained attention as a potential therapeutic target. Dopamine and its receptors are extensively involved in physiological and pathological processes, including tumor progression, angiogenesis and immune modulation. While studies in other cancers suggest that dopamine signaling can influence tumor biology, its specific role in PC, particularly with regard to its therapeutic potential, remains poorly explored. Further research is needed to better understand the role of dopamine signaling in PC and to assess its viability as an innovative therapeutic strategy.

Therefore, the general aim of this Ph.D. project was to investigate dopaminergic neuromodulation as a novel therapeutic approach for PDAC, integrating molecular, cellular, and *in vivo* models to assess its antitumor and antimetastatic potential, and to develop nanotechnology-based drug delivery systems to enhance the therapeutic efficacy of dopaminergic drugs for PC therapy.

To achieve this goal, the following specific objectives were pursued:

1) Characterize dopaminergic receptor expression profiles in pancreatic cancer cell lines (PANC-1, MIA PaCa-2, and patient-derived M2) to study the impact of its activation on tumor cell proliferation and migration responses and explore the underlying mechanisms and pathways involved in these antitumor effects.

2) Evaluate the therapeutic potential of dopaminergic modulation in subcutaneous and orthotopic PDAC mouse models, with particular focus on tumor progression and metastasis.

3) Assess the effects of D2 receptor blockage both *in vitro* and *in vivo*, studying the potential inhibitory effects on cell proliferation and tumor growth.

4) Conduct a drug screening study of available D1 receptor agonists and D2 receptor antagonists, both individually and in combination, to identify synergistic strategies that enhance antitumor efficacy and investigate their effect in three-dimensional spheroid models enriched with pancreatic cancer stem cell-like populations to evaluate the therapeutic responses.

5) Develop of a nanovault-based drug delivery system and newly design nanobodies with high selectivity for dopaminergic receptors, aiming to enhance therapeutic efficacy while minimizing systemic toxicity.

II. MATERIALS & METHODS

1. In vitro experiments in pancreatic cell lines.

1.1. PC cell lines.

PANC-1 and MIA PaCa-2 cell lines were purchased from the American Type Culture collection (ATCC) and were cultured under standard conditions using *Dulbecco's Modified Eagle Medium* (DMEM, GIBCO) supplemented with 10% fetal bovine serum (FBS, GIBCO), penicillin/streptomycin at 100 µg/ml, 2 mM of glutamine and 1 µg/ml of amphotericin (Life Technologies) and incubated at 37ºC in a 5% CO2 atmosphere.

- **PANC-1** cell line is a human cell line established from a ductal-origin pancreatic carcinoma isolated from a 56-year-old Caucasian male [121]. This cell line undergoes neuroendocrine differentiation, which makes them suitable for neuroendocrine chemotherapy [122] .

- **MIA PaCa-2** was derived from a pancreatic tumor tissue from a 65-year-old Caucasian male [123]. This cell line also undergoes neurocrine differentiation [122].

- **SPM2 (M2)** tumor cell line was established from a primary culture of a pancreatic ductal adenocarcinoma patient that underwent surgery in our Hospital. The sample was extracted directly from the tumor, cleaning the necrotic areas and discarding the non-viable tissue. The viable tissue was disintegrated for cellular suspension. In order to do so, 300 mg of viable tissue was submerged in a solution made with 3ml of 0.005% trypsin and 3µl of DNase (final concentration 100µg/ml). After manual disintegration by pipetting the resulting product was incubated 20min at 37ºC under agitation. Then it was filtered using a 40µm sterile mesh to exclude the non-digested tumor pieces and the resulting product was filtered at 2400 rpm for 10 min. The pellet was resuspended in 10 ml of culture media, *Dulbecco's Modified Eagle Medium* (DMEM, GIBCO) high glucose (4.5 g/l) supplemented

additionally with FGFβ (1µg/µl, Sigma-Aldrich) and B27 (50:1, Sigma Aldrich) and the cells were placed in a low-attachment flask (GIBCO) to culture them in suspension conditions. After one month in culture, cells were seeded in adhesion conditions. Cells were characterized previously in the laboratory using flow cytometry; the epithelial and human pancreatic origin was determined using the EPCAM antibody (BV421 mouse anti-human CD326, BD Bioscience) and its corresponding isotype (BV mouse IgG1, K isotype control, BD Bioscience).

The characteristics and the specific conditions of each cell line are outlined below (Table 2):

Table 2. Pancreatic cancer cell lines' characteristics.

Cell Line	Age	Gender	Derivation	Metastasis	Proliferation (doubling time, Td)	Histological Differentiation	K-ras	P53	p16	SMAD4
MIA PaCa-2	65	Male	Primary tumor	nd	40 h	Poor	mt	mt	mt	wt
PANC-1	56	Female	Primary tumor	Yes	52 h	Poor	mt	mt	wt	wt

nd= not determined
mt= mutated
wt= wild type.

1.2. Luciferase reporter expression in PC cell lines.

In order to monitor tumor growth for *in vivo* orthotopic experiments the pancreatic cell lines PANC-1 and MIA PaCa-2 needed to be transfected with the reporter gene luciferase. Luciferin is a compound that can undergo an enzyme-catalyzed reaction (by luciferase) producing an intermediate that emits light upon decaying into its final form. Using this mechanism a mouse can be given luciferin and only the cells expressing luciferase will produce the reacting and emit light.

For the transfection protocol 200.000 cells of each cell line were seeded in 2ml of growing media in 6 well plates' format (TPP). 24H after the media was washed and changed to Optimem media (GIBCO) for 2h. Then, different tubes were prepared

containing Optimen (control tube), 48µl/ml of lipofectamine (Thermofisher scientific) in Optimem (lipofectamine tube) and 16µl/ml of luciferase plasmid (PGL3, Promega) and incubated during 5 min at room temperature (RT) (Fig. 12). Afterwards, 250 µl of the control was mixed with 250 µl of lipofectamine tube and was incubated for 20m at RT. The same procedure was performed using the luciferase containing plasmid tubes. Then, 100 µl of the tubes were added to the plate with the pancreatic cell lines and were left in the incubator for 24H. The media was changed and geneticine (G-418, Sigma Aldrich) 800µg/ml was added so only the transfected cell population survived. To confirm that the cells expressed luciferase, one million of cells per well were seeded in 6 well plates and after 24h, luciferin (Perkin Elmer) was added to each well and fluorescence was read in IVIS Spectrum 2000 (Perkin Elmer) at 508 nm wavelength.

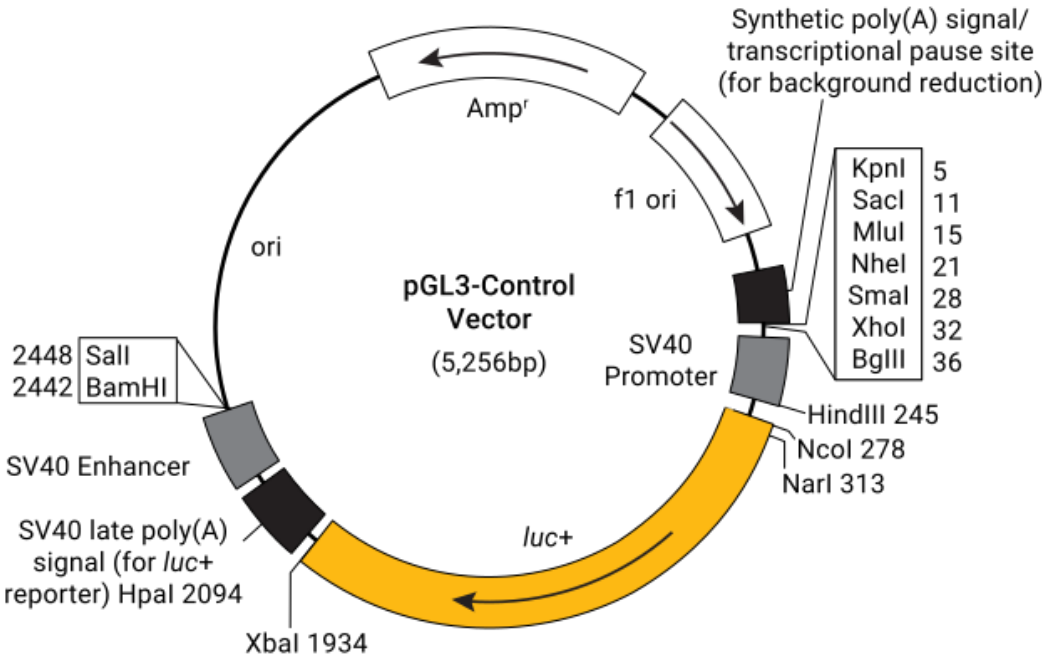

Figure 12. Plasmid vector used for luciferase transfection.

1.3. Cell proliferation assay:

To evaluate the effect of the dopaminergic agonists and antagonists (Table 3) cell proliferation 48h after administration was evaluated through measuring the metabolic capacity using the XTT kit (Sigma-Aldrich). The assay is based on the conversion of tetrazolium salt XTT to soluble formazan salt. This reaction only occurs in viable cells because is tied to the production of NAD(P)H during glycolysis. When cells reached 70-80% of confluence they were detached used trypsin 0.05%-EDTA and centrifuged (1500 rpm, 5 min). Cell concentration was measured using BIORAD / TC Automated Cell Counter 2058 equipment (Life Science). Pancreatic cells were seeded in a 96-well plate (5.000 cells per well) and drugs added 24h after the seeding at the indicated concentrations (1, 10, 25, 50, 75 or 100 µM). Then, the metabolic activity of viable cells was quantified 48h later following the XTT kit's protocol, which consists in the incubation of the 96 well plates with 50 µL of the mixture of XTT reagents (5ml of labelling reagent and 0.1 ml of electro coupling reagent) for 2-4h and then measuring the absorbance signals of each well at 450nm using the Infinite M200 Pro plate reader (TECAN). The absorbance value is directly related to the number of viable cells.

Table 3. Dopaminergic receptor agonists and antagonists.

Agonist/Antagonist	Receptor Affinity	Reference	Molecular weight (g/mol)
Pergolide	D2 agonist	Y0000010 Merck	410.59
Fenoldopam	Selective D1-like agonist	1269458 USP	401.86
SKF-83822	Selective D1-like agonist	2075 TOCRIS	424.76
SKF-82958	D1/D5 receptor full agonist (Selective), ERα agonist.	5719 TOCRIS	410.73
SKF-83959	Selective D1 (partial) agonist Sigma 1 receptor alpha2-adrenoceptor antagonist	S2816 Merck	398.72
Domperidone	Peripherally selective antagonist D2 & D3	18875 Cayman	425.9
Butaclamol	D2 blocker high affinity	D033 Merck	397.96
L-741,626	High affinity D2 antagonist	1003 TOCRIS	340.85
SCH 23390	Selective D1 antagonist	D054 Merck	324.24

1.4. Cell viability assay

Cell viability assay was performed similarly to the proliferation protocol, but with a few modifications: 200.000 cells were seeded per well and the growth medium was changed to 1% of FBS 24h prior to the seeding and remained at this concentration until the end of the experiment.

1.5. Wound healing assay

To evaluate cell migration *in vitro*, 200,000 cells per well were seeded in 24-well plates and incubated for 5h to establish a uniform monolayer at approximately 80% confluence. The culture medium was then replaced with medium containing 1% FBS and maintained for 24h prior to the initiation of the migration assay. A 10 µL pipette tip was used to generate a linear artificial wound (“scratch”) in the cell monolayer. Following the scratch, cells were washed three times with PBS to remove non-adherent cells. Subsequently, 1 mL of medium supplemented with 10 µM catecholamine agonists was added to each well.

Cell migration was monitored using an inverted phase-contrast microscope (BX15, Olympus, Japan) equipped with an integrated camera (B45). Images were captured 48h post-scratch. Morphometric analysis was performed at 100× magnification using the automated morphometry toolbox in the Olympus Cell D Imaging 3.3 software (Olympus Corporation, Tokyo). The extent of wound closure for each cell line was quantified and expressed as a percentage relative to the control condition. All experiments were conducted three times, with each condition tested in duplicate.

1.6. Real time quantitative PCR for gene expression

In order to check the expressed dopaminergic receptors in the cells the polymerase chain reaction assay (PCR) was performed using specific primers: DRD1 (Hs00265248_s1), DRD2 (Hs00241436_m1), DRD3 (H00364455_m1), DRD4 (Hs00609526_m1) and DRD5 (Hs00361234_s1). All primers were supplied by ThermoFisher Scientific. Expression of the genes was calculated using the 2-ΔCt method, referring to the constitutive gene GAPDH (Hs02786624_g1). The technique amplifies a sequence of our choice exponentially, allowing us to detect it. In this case Real Time quantitative RT-PCR was run, which uses cDNA (synthesized from 1 µg total RNA from the sample) and allows us to measure the accumulative fluorescent signal that occurs during the exponential phase of the reaction.

First, RNA was extracted from pancreatic cancer cell lines. The procedure was done when cells reached a confluency of 80-85% following the RNeasy Mini Kit (QIAGEN) following protocol specifications. RNA was quantified in a Nanodrop (Thermo Scientific) and then stored at -80ºC.

Second, Real time quantitative RT-PCR was carried out in two steps. To start, a retrotranscription was performed using High-Capacity cDNA Reverse Transcription Kit (applied Biosystems) and cDNA was stored at -20ºC until use. Later, RT-PCR was run with SensiFAST™ Probe Hi-ROX Kit (Bioline) using the 7900HT Fast Real-Time PCR System (Thermofisher scientific).

1.7. Protein extraction and quantification

The cell lines were seeded in a 6 well plate with its growing medium at 1% FBS instead to avoid cell growth. Control with phosphate buffered saline (PBS), dopamine and fenoldopam were added to each well at different times (0.5, 1, 3, 6 and 24h). Then, wells were washed with cooled PBS and cells were lysed with a cell scrapper and RIPA buffer combined with activated sodium orthovanadate and a protease inhibitor (Sigma-Aldrich). Following a 15 min cooling in ice, the extracts were centrifuged 10 min at 12.000rpm at 4ºC. The supernatants were stored in a -80ºC freezer until use.

For the quantification we performed the colorimetric Bradford assay based on an absorbance shift of the dye Coomassie brilliant blue G-250 (BIORAD) The Coomassie brilliant blue G-250 dye exists in three forms: anionic (blue), neutral (green), and cationic (red). Under acidic conditions, the red form of the dye is converted into its blue form, binding to the protein being assayed; else the solution will remain brown. In order to do so, a calibration curve with known concentration of albumin (0, 20, 15, 10, 5 µg/mL) was prepared. Then, a 96 well plate is loaded with this curve and 2 different concentrations of samples, diluted 200 and 400 times. Finally the dye reagent was added to each well, the plate was shacked and incubated 15 min at 37ºC. Afterwards, the absorbance was measured at 595 nm and the final concentration was calculated using the calibration curve considering the previous dilution.

1.8. Western blot for protein expression

Western Blotting is based on the electrophoretic transfer of proteins from sodium dodecyl sulfate polyacrylamide gels to sheets of polyvinylidene fluoride (PVDF) or nitrocellulose membrane, followed by immunodetection of proteins using antibodies with fluorescent or chemiluminescent detection. This allows us to detect the amount of protein expressed by PC cells at a given time in a semi-quantitative way, in comparison to a housekeeping protein (GAPDH).

First, protein samples were prepared adding H2O and sample buffer 3x to the protein extracts previously obtained, and after, the samples were heated at 100ºC for 5 min. Acrylamide gels (12% for higher KDa proteins and 15% for low KDa proteins) were loaded with 15-30 µg depending on the sample and electrophoresis was conducted (BIO-RAD ; Mini-PROTEAN®) for 90 min and 100mV at RT followed by a wet transfer for 70 min and 100mV at 4ºC using PVDF membranes (Thermo Scientific; 88520) previously activated with methanol. Membranes were blocked using TBS-Tween 0.2% with 5% of BSA. Primary antibodies were incubated overnight at 4ºC following secondary antibodies during 1h at RT (antibodies used are listed in Table 4). Membranes were revealed using Molecular Imager® ChemiDoc™ XRS+ with Image Lab™ software (BIO-RAD). We used antibodies for cell death pathways markers; p62 and LC3B for autophagy, cleaved Caspase-3 and c-PARP for apoptosis. Also GADPH was used as a housekeeping protein.

Table 4. Antibodies used for Western Blot.

Antibody	Dilution	Distributor / Reference
Ascites Mouse Anti-PARP	1:3000	BD Biosciences/ 556362
Cleaved Caspase-3	1:2000	Cell Signaling/ 9661
SQSTM1/p62	1:1000	Cell Signaling/ 5114
Anti-LC3B	1:1000	Sigma-Aldrich/ L7543
DRD1	1:1000	Bio-techne (R&D system)
DRD2	1:1000	Santa Cruz Biotechnology INC (sc-5303)
DRD5	1.1000	MyBiosource (Mb176794)
Recombinant Anti-GAPDH	1:500	Abcam/ EPR16891
Goat anti-Rabbit	1:10000	ThermoFisher 31460
Goat anti-Mouse	1:10000	ThermoFisher 31430

For the analysis of the membranes they were incubated for 1 minute with the mix of Clarity Western Blot ECL substrates (BIORAD) peroxide and Luminol/enhancer solutions, and then, the membrane is covered with a film and placed in the Chemidoc MP system. Imagelab software was programed to take 1 picture per second. A good quality image was often acquired between seconds 2 to 20, but for some results times of 40s to 1 minute were necessary. Images were then saved for the analysis with ImageJ software. The intensity and size of each band was measured individually and quantified. Every measurement is then normalized by the internal control (GAPDH) for each well.

1.9. Spheroid processing and proliferation assays

Spheroids were obtained by plating PANC-1, MIA PaCa-2 and M2 cells at low density (500-5.000 cells/well) on 24 well plates ultralow attachment surface (Corning, 3473, Madrid, Spain). They were grown in their growth media but at 1% FBS supplemented with 1% penicillin/streptomycin, 1% glutamine, 0.2% fungizone, bFGF (1 µl/ml, Sigma-aldrich, Madrid, Spain) and B27 (20µl/ml, Life-technologies, Madrid, Spain). For the initial test, spheroids were left in culture from 96h, taking pictures every 24h.

For the proliferation assays, spheroids were left in culture 72h and then the treatment (Table 3) was added (fenoldopam at 87 µM, domperidone at 30 µM, SKF83822 at 40 µM, fenoldopam + domperidone at 87/30 µM and SKF83822 + domperidone at 40/30 µM)). After an incubation of 48h the cells were photographed using a microscope.

The images were then analyzed using ImageJ. The script designed is described in figure 14.

```
run("Set Measurements...", "area display redirect=None decimal=3");
requires("1.33s");
dir = getDirectory("Choose a Directory ");
setBatchMode(true);
count = 0;
countFiles(dir);
n = 0;
processFiles(dir);
print(count + " files processed");
function countFiles(dir) {
   list = getFileList(dir);
   for (i = 0; i < list.length; i++) {
      if (endsWith(list[i], "/") || endsWith(list[i], "\\")) {
         countFiles(dir + list[i]);
      } else {
         count++;
      }
   }
}
function processFiles(dir) {
   list = getFileList(dir);
   for (i = 0; i < list.length; i++) {
      if (endsWith(list[i], "/") || endsWith(list[i], "\\")) {
         processFiles(dir + list[i]);
      } else {
         showProgress(n++, count);
         path = dir + list[i];
         processFile(path);
      }
   }
}
function processFile(path) {
    if (endsWith(path, ".tif")) {
       setBatchMode(false);
       open(path);
       run("Subtract Background...", "rolling=50 light separate");
       run("8-bit");
       setThreshold(0, 235, "raw");
       run("Convert to Mask");
       waitForUser("Select an Oval ROI, then click OK to continue");
       run("Clear Outside");
       run("Analyze Particles...", "size=0.004-4 circularity=0.10-1.00 show=Outlines display exclude clear summarize composite");
       title = getTitle();
       dotIndex = lastIndexOf(title, ".");
       if (dotIndex != -1)
           baseName = substring(title, 0, dotIndex);
       else
           baseName = title;
       sep = "/";
       if (indexOf(path, "\\") != -1) {
         sep = "\\";
       }
       folder = substring(path, 0, lastIndexOf(path, sep) + 1);
       selectWindow("Results");
       saveAs("Results", folder + baseName + "_Results.txt");
       run("Close All");
   }
}
```

Figure 14. ImageJ script used to analyze the number and size of the spheroids in our 24 well plates. The script allows you to pick a folder and process every image removing the background, setting a threshold and measuring the area of every particle. The threshold is selected depending on the experiment. The script can be modified to analyze jpg or TIF files.

1.10. Production of vault-based nanoparticles

The sequence of the human major vault protein (MVP, UniProt Q14764, MVP_HUMAN) was used to design the recombinant MVP-H6 gene, but adding extra triplets encoding a six-histidine tag (6xHis) for purification purposes. The sequence was then cloned into pTriEx1.1-Hygro vector (Novagen, cat. n° 70928-3, 6951 bp) between *NcoI* and *Eco*RI restriction sites. The INT domain of the protein can be fused at the 3' end of valuable genes, such as the reporter gene GFP or cytotoxic compounds such as TNR as prototype.

Afterwards this vector was transfected into a suspension of human embryonic kidney (HEK) cells FreeStyle 293F (Invitrogen, Life Technologies) by polyethylenimine-mediated transfection, producing the proteins by transient gene expression. Transfection conditions for this cell line had been previously set and optimized [22] at 1 μg DNA ml−1 of culture and a ratio DNA:PEI of 1:3 (w/w). Valproic acid (VPA) was added to cells (at 4 mM final concentration) 4 h post-transfection in order to improve recombinant protein expression. In co-expression experiments, both plasmids pTriEx1.1-MVP-H6 and pTriEx1.1-GFP-INT were mixed at different ratios (before their mixing with PEI), always maintaining the final amount of 1 μg plasmid DNA ml−1 and a ratio DNA: PEI of 1:3 (w/w).

The MVP-H6 protein was purified using magnetic particles (MPs), with the soluble fractions from transfected HEK 293F cells serving as the starting material. A total of 30 μg of MVP-H6 from the soluble fraction was incubated with 5 mg of MPs. Samples collected throughout the process, including the initial, flow-through, wash, and elution fractions, were analyzed by SDS-PAGE and western blot.

1.11. Nanoparticle characterization and functional assay.

1.11.1. Internalization assay.

In the characterization assays of functional nanoparticles (Table 5) the capacity of the GFP-fluorescent nanoparticles to internalize in PANC-1 and MIA PaCa-2 cell lines was tested. A total of 500.000 cells were seeded in 6 well plates. 48h after

seeding a negative control (PBS) and the nanoparticles MVP-H6-GFP-INT and MVP-H6-TPP-GFP-INT were added to the wells at 5 and -10 nM. After 2h of exposure the cells were washed, detached and centrifuged 5 min at 400g, discarding the supernatant. Afterwards, they were washed with PBS and incubated at 37ºC with diluted trypsin (1 mg/mL) to remove non-specific binding of the nanoparticles to cell membranes. After a couple washes the pellet was then resuspended in a final volume of 200-500 µL in cytometry tubes. Then, a FACSCalibur cytometer (BD Biosciences) was used to measure the fluorescence emitted by the GFP protein at 509 nm, and the results were expressed in the percentage of fluorescent cells using the CellQuest Pro program (BD Biosciences). Every measurement was done by duplicate and was replicated at least 3 times.

Table 5. Nanoparticles used in *in vitro* and *in vivo* experiments.

Nanoparticle	Concentration (mg/ml)
MVP-H6	1.171
MVP-H6-TPP	1.077
MVP-H6-GFP-INT	1.286
MVP-H6-TNR-INT	1.021
MVP-H6-TPP-TNR-INT	1.485
MVP-H6-TPP-GFP-INT	1.565

1.11.2. Cytotoxicity Evaluation of the vaults-based nanoparticles

To check the effect of vaults loaded with TPP and TNR on cell proliferation, the cells were exposed to different concentration of nanoparticles (0, 0.1, 10, 20 and 40 nM) and then a proliferation assay was performed as described in section 1.3.

1.11.3. Production of selective nanobodies targeting the dopaminergic receptor D1

A nanobody phage display library was screened to identify binders specific to the dopamine receptor D1. To reduce nonspecific interactions, the phage library was first exposed to HEK293 cells, allowing depletion of phages binding irrelevant cell surface components. After two rounds of negative selection, the remaining phage population was incubated with NOMAD-D1 cells (a D1 overexpressing tumor cell line, Innoprot), a cell line engineered to express human D1. Phages binding specifically to the receptor were recovered and subsequently amplified. To enable propagation, selected phages were incubated with E. coli TG1 cells, and infected bacteria were cultured in LB medium supplemented with ampicillin, as the phagemid vector carried a resistance marker. Phagemid DNA was extracted from bacterial cultures using a QIAwave Plasmid Miniprep Kit (Qiagen).

Phagemids obtained from this selection were transformed into E. coli ER2738 cells, which were plated on selective agar to isolate individual colonies. Colonies were expanded in liquid culture, and phage particles were rescued by infection with M13KO7 helper phage (Invitrogen™). Following overnight incubation at 37 °C with shaking, bacterial cells and debris were removed by centrifugation, and phages in the supernatant were precipitated by addition of a PEG6000 (30%)/NaCl (1 M) solution. After incubation at 4 °C for 1 h, samples were centrifuged and the resulting phage pellet was resuspended in storage buffer supplemented with 20% glycerol before being stored at –80 °C until further use.

The specificity of individual phage clones was then evaluated in binding assays using HEK293 cells as a negative control and NOMAD-D1 cells for positive selection. Cells were incubated with phages, washed extensively, and stained with an anti-M13 antibody conjugated to Alexa Fluor 488 (M13 Major Coat Protein Antibody, RL-ph1, sc-53004, Santa Cruz Biotechnology). Binding was quantified by fluorescence microscopy and flow cytometry, and clones that demonstrated

significantly higher fluorescence in NOMAD-D1 compared to HEK293 cells were considered specific D1 binders and selected for downstream analyses.

1.11.4. Cytotoxic evaluation of nanobodies.

In the previous section two clones were selected: Nanobody 2 and Nanobody 8. PANC-1, MIA PaCa-2 and M2 cell lines were seeded in 96 well plates and the cells were administered Nanobody 2 or Nanobody 8 following the protocol in section 1.4. The doses used were 0.01, 0.1, 0.25, 0.5, 0.75 and 1µM.

2. *In vivo* experiments in human pancreatic cancer xenograft models.

2.1. Mice strain

For the further study of the therapeutic effectivity of dopamine ligands, murine (*mus musculus*) xenografted models were generated bearing human pancreatic tumors. 5 week old females mice (between 17 -20g weight) obtained in Inotiv laboratories (ENVIGO, Barcelona) were utilized. The mouse strain was *athymic* Foxn1nu mice, which are partially immunodepressed without mature T lymphocytes and this leads into a dysfunctional adaptive response but a complete innate response.

Mice were housed in racks with controlled ventilation in an SPF (Specific Pathogen Free) area, being fed *ad libitum* with food and water, at a controlled temperature of 21 ± 2.9 °C, a relative humidity of 45 ± 15% and a 12-hour light cycle. All the *in vivo* procedures were previously approved by the Ethics Committee of the Sant Pau Research Institute and the Government of Catalonia (Protocol number 10234 ANNEX 2).

2.2. Generation of human pancreatic cancer xenografts

2.2.1. Subcutaneous implanted xenografts.

For generating murine xenografted models of human pancreatic cancer it was necessary to stablish the pancreatic human tumor line for PANC-1 and MIA PaCa2. For that athymic mice were utilized. First, they were anesthetized using a

combination of ketamine and xylazine (Ketamidor 100mg/ml Ritcher pharma; Rompun 20mg/ml, Bayer). For each mouse 150-200 µL (depending on mice body weigh) of anesthesia was injected intraperitoneally (0.1g/kg of Ketamidor and 0.01 g/kg of Rompun). After a few min the plantar reflex of the mouse was evaluated and then, mouse was placed on a thermic sheet to avoid a possible hypothermia during the procedure.

After sanitizing the skin with povidone-iodine (Meda Pharma) two dorsal flanks were inoculated with 20 million of PANC-1 cells in 200 µL of DMEM medium 4.5 g/l glucose with no supplements using a 29G insulin syringe (BD) (Fig. 15).

Tumors were monitored weekly using a caliper until they reached a volume of 100-150 mm^3. The mouse was then euthanized and the tumor was cut into 3 mm^3 pieces and re-implanted in a new mouse using a trocar system (Cadence Science). For that purpose, a small incision was done in the back skin and the trocar, loaded with a tumor piece and some media, was introduced in the cavity. Afterwards the tumor piece was released in the cavity and the trocar removed, sanitizing the skin with povidone-iodine. The wound is small enough so no staples are necessary. When that was not the case the wound was sutured using a surgical 6-0 needle, (Prolene).

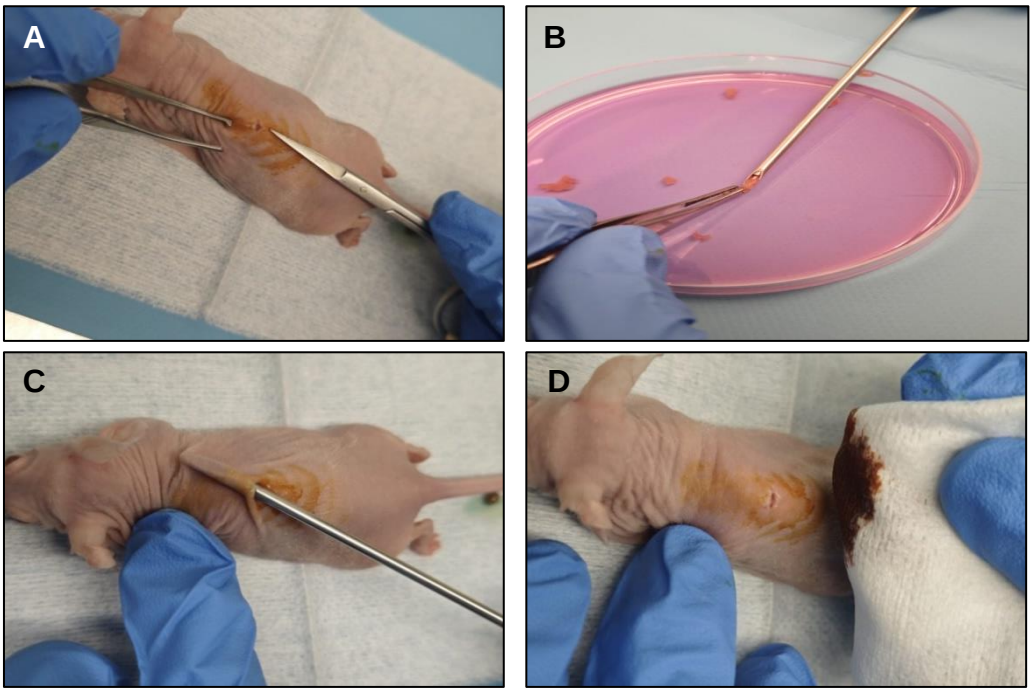

Figure 15. Subcutaneous implantation of pancreatic tumors. A) Dorsal incision. **B)** Collecting the tumor piece in the trocar. **C)** Introduction of the tumor piece in the subcutaneous area. **D)** Sanitation of the skin with povidone-iodine.

2.2.2. Orthotopic metastatic human pancreatic model

For the generation of orthotopic xenografted models of human pancreatic cancer a grown subcutaneous tumor was used. For that purpose, the tumor was sliced in 4-5mm^3 pieces. The mice were anesthetized using a combination of ketamine and xylazine (0.1 and 0.01g/kg each). For each mouse 150-200 µL (depending on mice body weigh) of anesthesia was injected intraperitoneally. We evaluated the plantar reflex of the mice and then, the mice were placed on a thermic sheet to avoid a possible hypothermia during the procedure.

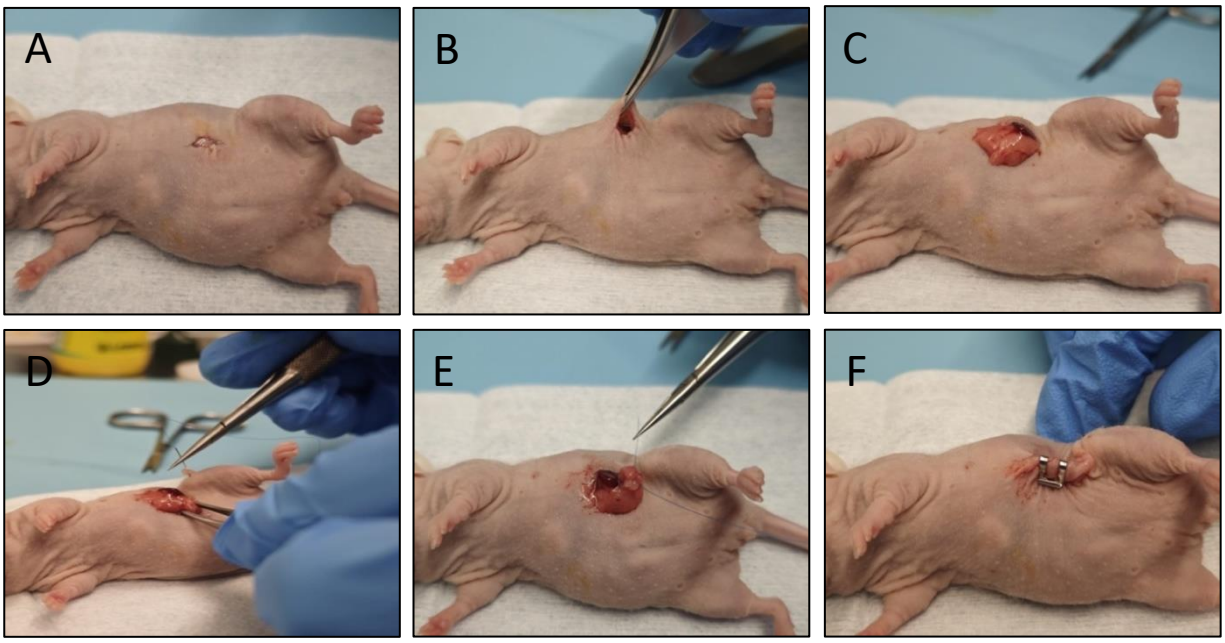

Figure 16. Orthotopic implantation of pancreatic cancer tumors. A) Ventral incision. **B & C)** Exposure of the pancreas. **D & E)** Sewing of the tumor piece to the pancreas. **F)** Sealing with a surgical staple.

Following, the left peritoneal zone was sanitized with povidone-iodine and a small incision was performed, cutting first the skin and then the muscle. With a pair of tweezers the pancreas was exposed and laid on the ventral zone. The tumor piece was then attached to the pancreas using a non-absorbable surgical suture (6/0 Optilene, Braun). Afterwards, the pancreas was introduced in the peritoneum and the incision was sealed using surgical 7mm staples (Braun) (Fig. 16).

2.3. Monitoring the tumor progression.

2.3.1. Subcutaneous xenografts.

The monitoring has to be done to evaluate the tumor progression and to stablish an experimental endpoint. After the subcutaneous implantation, tumors grow on the back on the mice and its volume can be easily measured immobilizing the mouse and using a caliper. When possible this procedure was performed with

another group member so one holds the mouse properly and the other measures with the caliper. Tumors were measured twice a week using this method. The tumor volume was estimated using the ellipse formula by measuring the small and the big diameters of the tumor.

$$Tumor\ volume = \frac{Big\ diameter\ \times Small\ diameter^2}{2}$$

The subcutaneous tumor monitoring schematics are described in figures 18 and 21.

2.3.2. Orthotopic model monitoring

For the monitoring of the tumor progression in the orthotopic model, pancreatic cell lines were previously transfected with a luciferase reporter, to express luciferase. Tumor growth and dissemination were evaluated *in vivo* by measuring the bioluminescent emission of the tumors and metastatic nodes 5 min after 150 µl intraperitoneal injection of D-luciferin (Caliper LifeSciences) at 15mg/ml. Mice were monitored using the IVIS Spectrum 2000 (Perkin Elmer) twice a week. Results were analyzed using Living Image® software (Perkin Elmer). Abdominal palpation was performed as another indicator of tumor progression. Tumor progression was labeled then with numbers, being 0.5= presence of small tumor, 1= tumor presence (starting point), 2= Moderate to big tumor, 3= Big tumor with some abdominal distension. The orthotopic tumor monitoring schematics are described in figure 19.

2.4. Randomization

For subcutaneous tumors, once the tumors reached an average size of 61.5 mm3 the experiment began. Mice were divided in groups (control, bromocriptine and fenoldopam) depending on tumor volume so every group had a similar average size and the standard deviation was the lowest. For the orthotopic experiments, as there is not a way to directly measure tumor volume, mice were sorted by both abdominal palpation score and bioluminescence. The experiment started once the average tumor bioluminescence was 5 *10^{10} (p/s) and a palpation score of 1.

2.5. Drug administration

Fenoldopam administration was 400ng/kg/min diluted in physiological saline either intravenously (for subcutaneous model) or released by micro-osmotic pumps (Alzet ®, model 1002) implanted subcutaneously on anesthetized mice the first day of administration (for the orthotopic model). Bromocriptine administration was 15mg/Kg/d diluted in physiological saline intragastrically. Domperidone was given at 20mg/Kg intragastrically 5 times a week. Control group was administered with physiological saline in the same administration pattern as the experimental groups. The administration regime is described in Figure 17.

For the micro-osmotic pump implantation, the day of randomization the treated mice were anesthetized and a medium size incision was made in the back of the animal. The pumps were filled with fenoldopam so it released 400ng/kg/min and with water for the controls. Then the pump was introduced in the cavity and the cut was sealed using a surgical 6-0 needle (Prolene).

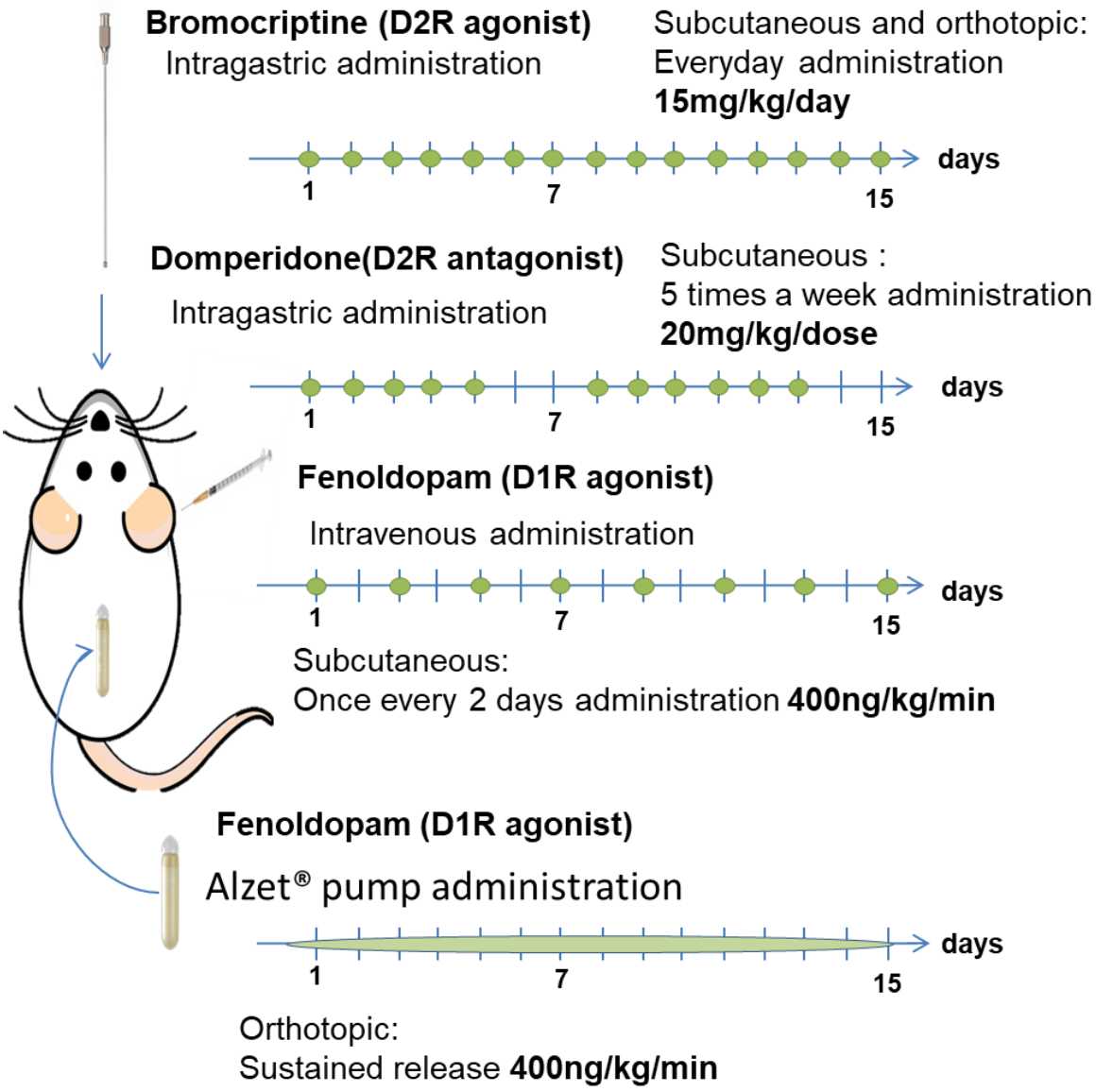

Figure 17. Administration regimes for the dopaminergic agonist and antagonist assays. Mice bearing pancreatic xenografts were divided in 3 groups; one group was administered bromocriptine intragastrically once a day, another group fenoldopam, either intraperitoneally (subcutaneous assays) or by osmotic release (orthotopic) and the third group was administered saline serum using the most aggressive administration regime In the antagonism assay mice were divided in 2 groups; one group was administered domperidone intragastrically 5 times a week and the other group was given saline serum intragastrically.

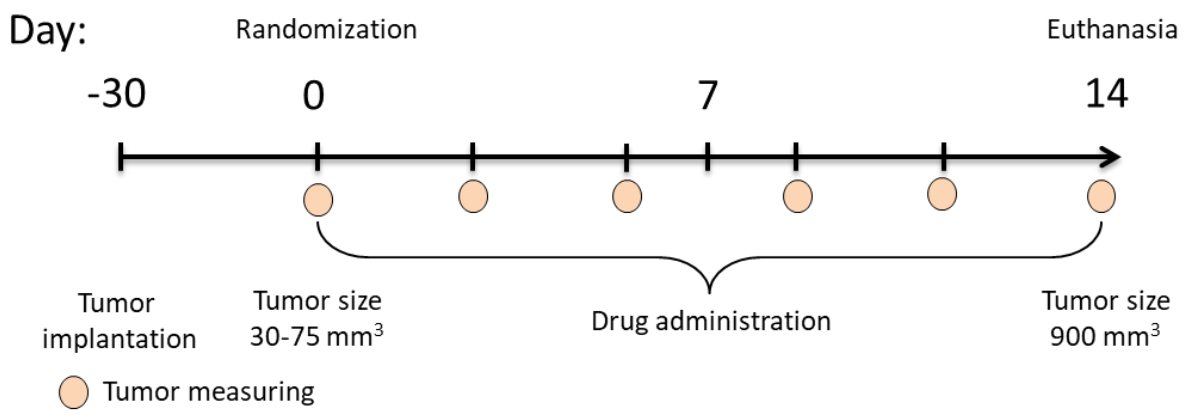

Figure 18. Tumor monitoring regime for the subcutaneous agonist assays. Experiments began once tumors reached 30-75 mm^3. Subcutaneous tumors were measured 3 times a week until the volume was over 900 mm^3.

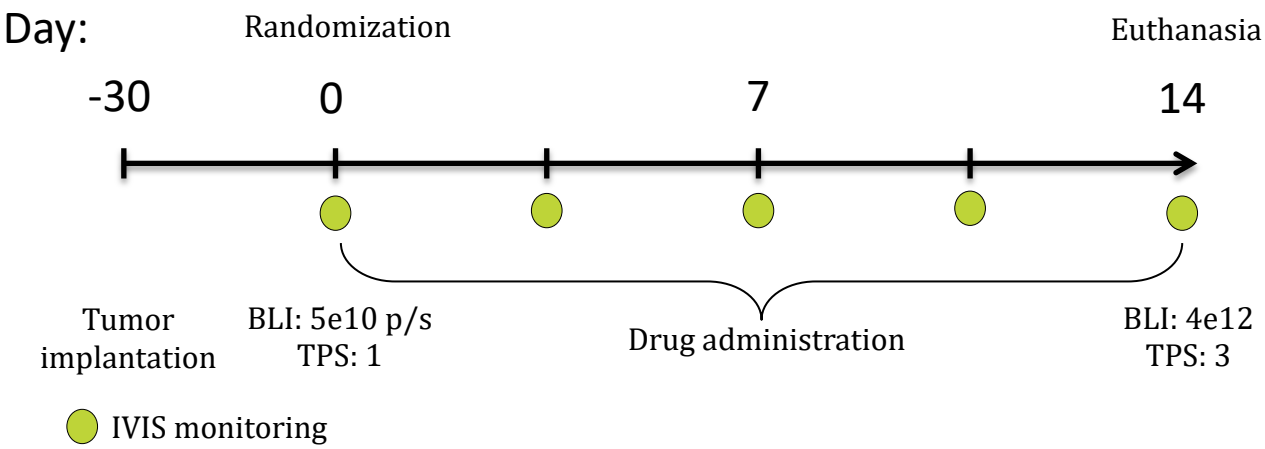

Figure 19. Tumor monitoring regime for the orthotopic agonist assays. Experiments began once tumors reached a palpation score of 1. Subcutaneous tumors were monitored 2 times a week using the IVIS Spectrum 2000 until the first mice reached a palpation score of 3.

2.6. Necropsy and tissue processing

After every experiment reaches the final point, the mice were euthanized by cervical dislocation, which consists in applying pressure to the neck and dislocating the spinal column from the skull or brain. The endpoint criteria varied in each experiment depending on the objective. In experiments with mice carrying subcutaneous tumors, they were euthanized when the tumors reached a maximum size of 800 mm^3. For the orthotopic experiments, when the first mice reached an abdominal palpation of 3 they were imaged using IVIS Spectrum Imaging System before a complete necropsy procedure was performed.

In all cases the organs (pancreas, spleen, kidneys, liver, lungs, heart, brain and diaphragm) and tumor were collected in cassettes (Thermo Fisher) and submerged in formaldehyde 3.7%.

2.7. Sample processing

After necropsy, the collected and fixed tumor and organs were embedded in paraffin, cut and then stained with hematoxylin-eosin or used for immunohistochemistry.

2.7.1 Sample dehydration: at least 24h after fixating the tissue in 3.7% formaldehyde samples were dehydrated. This is necessary since most fixing solutions are aqueous and the following step requires embedding the samples in paraffin, which is hydrophobic. For that purpose, the samples were washed in distilled water to remove the previous fixing solution and then the water is slowly replaced with ethanol. This is achieved by immersing the samples in vessels with increasing concentrations of ethanol (70, 80, 90 and 100%) followed by 10 minute incubations in 3 solutions of xylene 100% to dissolve the alcohol.

2.7.2 Paraffin embedding: after the dehydration, the sample is ready for a suitable histological wax. In this case we used paraffin, which is the most

common one. Paraffin infiltrates into tissue on its liquid state, at 60ºC and solidifies at 20ºC. This allows us to easily cut the embedded tissue into thin slices in which we can perform immunohistochemistry assays. Samples were then infiltrated with paraffin for 1 hour 3 times. 3h after, the samples were placed in a mold on a cassette, filled with paraffin and placed in a cold play for it to solidify.

2.7.3 Sectioning: the solidified paraffin embedded samples where then cut into 3-5 µm sections using a microtome. The sections were then mounted in in glass microscope slides.

2.7.4 Rehydration: in order to perform immunohistochemistry, paraffin must be removed from the tissues and samples rehydrated. Thus, slides were incubated at 60ºC for 1h and immersed in xylene 100% twice. Then, a progressive rehydration using decreasing ethanol concentrations (100, 96, 80 and 50%) was done.

2.7.5 Hematoxylin-eosin staining: samples were washed with distilled water for 5 min and then stained with the Mayer-hematoxylin solution for 5-10 min. After washing for 15 min with distilled water and some structures start to be recognizable, samples were washes a couple times more and stained with 0.2% eosin for 0.5-2 min. Samples where then dehydrated again and covered with mounting media (Toluene-Free Mounting Medium, Dako) and covered with a coverslip.

2.8. Immunohistochemistry staining analysis

The samples were then characterized using immunohistochemistry staining for different molecular markers. Immunohistochemistry allow us to identify proteins of interest present in our sample and where they are located within the tumor's morphology, selectively targeting antigens using manufactured antibodies. This

technique was performed to characterize cell death using markers such as c-Caspase-3 (apoptosis) and p62 (autophagy), proliferation using Ki67 marker and the blood vessel marker CD31.

Table 6. Antibodies used for IHC studies

Antibody	Dilution	Reference
Cleaved Caspase-3	1:300	BD Biosciences/
CD31	1:200	Cell signalling/ 85873
Ki67	1:200	Abcam 16667

The sections were placed in positively coated slides (*FLEX IHC* Microscope Slides, Dako) to make sure the samples adhere and do not fall during the immunohistochemistry process. Afterwards, samples were incubated during 1h at 60ºC and rehydrated as explained in section **2.7**. Then, a heat-induced antigen retrieval using the *PT Link* system (Dako) was programmed, consisting of an incubation for 10 min at 95ºC, followed by a 45 min incubation at 65ºC in a Tris/EDTA buffer at pH 9 (Dako). The immunostaining was performed by the automated system *Autostainer Link 48* (Dako), using the reagents from *EnVision Flex, High pH* kit (Dako) as it follows: 1 minute washing with *rinse buffer*, 5 min incubation with *Peroxidase-Blocking Reagent*, 1 minute washing with *rinse buffer*, 30 min with the primary antibody of our choice (Table 6) diluted in *rinse buffer*, 1minute washing with *rinse buffer*, 2 min with *EnVision/HRP*, 1 minute washing with *rinse buffer*, an incubation with the chromogenic solution (DAB+ *Chromogen and Substrate Buffer*), 1 minute washing with *rinse buffer*, 5 min incubation with hematoxylin for counterstaining and a final 1 minute wash with *rinse buffer*.

Blood vessels (positive for CD31) were counted manually at the microscope Olympus. Ki67 and c-Caspase 3 areas of positive cells were counted using the script detailed in Figure 20. Values of 10 different images per tumor of 200x magnification (for p62 and Ki67) and 400x (c-Caspase 3) were measured. The values given correspond to the percentage of the positive area relative to the whole

tumor area. Cell death bodies were counted manually in 10 different images at 400x magnification on H/E stained slides. Necrosis area was then measured on pictures of the whole tumor. The values given correspond to the percentage of the necrotic area relative to the whole tumor area.

All images used for the analysis of the markers in tumor were taken outside of the necrosis area, only taking into account viable tissue. ImageJ software was required for the treatment and analysis of the images.

```
run("Set Measurements...", "area display redirect=None decimal=3");
   requires("1.33s");
   dir = getDirectory("Choose a Directory ");
   setBatchMode(true);
   count = 0;
   countFiles(dir);
   n = 0;
   processFiles(dir);

   function countFiles(dir) {
      list = getFileList(dir);
      for (i=0; i<list.length; i++) {
          if (endsWith(list[i], "/"))
              countFiles(""+dir+list[i]);
          else
              count++;
      }
  }

   function processFiles(dir) {
      list = getFileList(dir);
      for (i=0; i<list.length; i++) {
          if (endsWith(list[i], "/"))
              processFiles(""+dir+list[i]);
          else {
             showProgress(n++, count);
             path = dir+list[i];
             processFile(path);
          }
      }
  }

  function processFile(path) {
       if (endsWith(path, ".jpg")) {
           open(path);
run("Subtract Background...", "rolling=50 light separate");
       run("Colour Deconvolution", "vectors=[H DAB]");
close();

setThreshold(0, 223);
setOption("BlackBackground", false);
run("Convert to Mask");
run("Create Selection");

run("Measure");
getValue("Area")
           close();
      }
  }

```

Figure 20. ImageJ script used to analyze and quantify immunohistochemistry images with DAB. The script allows you to pick a folder and process every image removing the background, applying a color deconvolution the colors and selecting the area above a given threshold. The threshold is selected depending on the staining. The script can be modified to analyze jpg or TIF files.

2.9. Drug toxicity evaluation

To analyze the toxicity of the treatments the H/E stained organs were studied with the help of a pathologist. Damage in brain, kidneys, liver, pancreas, spleen, lungs, and heart was evaluated and compared to those of the control group.

2.10. Transcriptomic microarray analysis of tumors

RNA was automatically extracted using the Qiacube system (Qiagen). For this, two sections of 7 µm were cut from each sample. Paraffin was removed with xylene, and subsequently, the xylene was washed off using absolute ethanol. The resulting pellet was left to dry for about 10 min until the ethanol evaporated completely. The remaining sample was treated with PKD buffer (proteinase K digestion buffer) and Proteinase K for one hour at 56°C with agitation. The samples were then incubated at 80°C for 15 min. After this process, the samples were centrifuged, the supernatant was collected, and total RNA was extracted using the Qiacube system with the RNEasy FFPE kit (Qiagen). The quality and integrity of the RNA samples, as well as the potential presence of contaminants, were assessed by measuring the absorbance ratio at 260 and 280 nm using a spectrophotometer. An Abs260/Abs280 ratio of 1.8 or higher indicated that the sample was pure. To assess the degree of degradation or the integrity of the RNA, the 2100 Bioanalyzer (Agilent Technologies) was used.

For gene expression and microRNA analysis, microarray technology was employed, allowing the measurement of thousands of messenger RNA (mRNA) transcripts to obtain a global view of gene expression patterns in the tumor sample. For mRNA analysis, the ClariomS-Human microarray (Applied Biosystems™) was used, evaluating approximately 22,000 genes per sample. For miRNA analysis, the GeneChip 4.1 (Applied Biosystems™) was used, analyzing around 350 miRNAs. Since the initial concentration of mRNA is usually too low for hybridization, mRNA amplification was performed first.

Once the total RNA was purified and amplified, the first strand of cDNA was synthesized using the traditional reverse transcription method. For this, the isolated RNA served as a template, along with the reverse transcriptase enzyme, DNA primers, RNAase enzyme, dNTPs (deoxynucleotide triphosphates), and a buffer to ensure optimal conditions. The resulting material was then hybridized onto a microarray, or GeneChip, composed of an inert matrix of 1.28 cm^2, subdivided into multiple 50 μm^2 cells, and a set of probes (probe-sets) representing oligonucleotides of the genes included in the GeneChip. During hybridization, the RNA binds to its complementary sequences immobilized on the chip, allowing for the identification and quantification of the DNA present in the sample. The level of hybridization was measured by determining the wavelength emitted by each cDNA fragment using a laser scanner, the Affymetrix GeneChip Scanner 3000 7G, at the Genomics and Transcriptomics platform of IR-HSCSP.

2.11. Metastatic foci evaluation (BLI y AP)

Orthotopic implantation allows us to study the metastatic pattern of the tumor progression. Therefore, the cellular dissemination of the tumor or distant organs and the peritoneal carcinomatosis was studied in hematoxylin-eosin stained samples of the target organs. Pancreatic cancer often metastasizes to the lymph nodes, liver, lungs, and retroperitoneum. These organs were analyzed and the presence of foci was counted. Diaphragm often presented bigger secondary tumors and was divided in micro (0.2-2mm) or macro (>2mm) metastasis depending on the size.

2.12. Effect of domperidone in tumor progression

In order to analyze the effect of domperidone *in vivo* we generated 20 PANC-1 subcutaneous xenografts following the section 2.1 of this thesis. For the experiment only tumors within 60-160 mm^3 were selected. At the time of the experiment, 11 tumors met the inclusion criteria. Mice were divided in 2 groups, a group treated with 20 mg/kg/day 5 days a week and a control group which was given vehicle. Tumors and mice weight were measured at least 3 times a week.

After 2 weeks (12 days) the experiment reached the endpoint because some control tumors reached 2000 mm^3. Tumors were weighted ex-vivo and in order to analyze toxicity, pancreas/spleen, brain, kidneys, heart/lungs and liver were weighted too. The scheme of the administration regime is the following (Fig. 21):

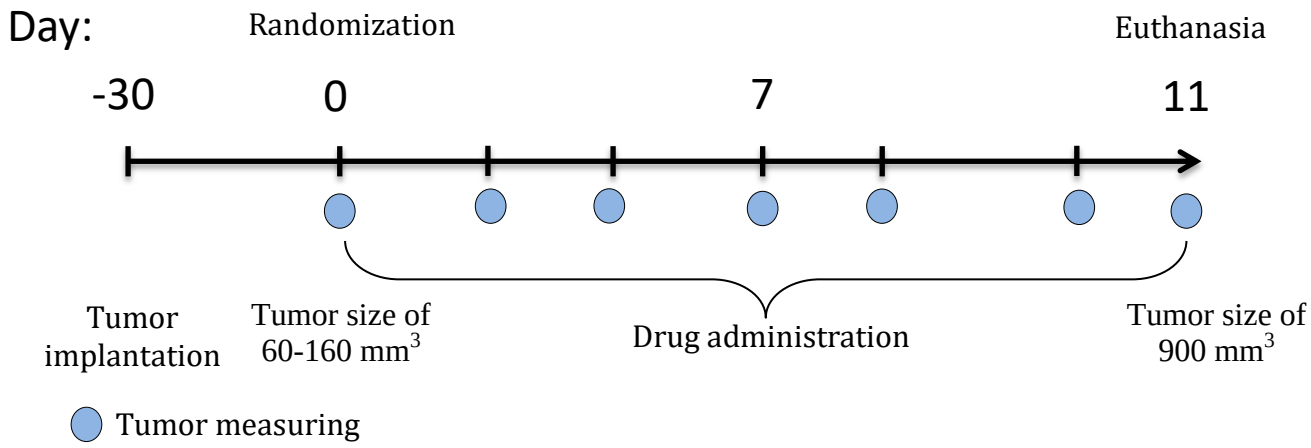

Figure 21. Tumor monitoring regime for the subcutaneous antagonist assay. Experiment began once tumors reached 60-160 mm^3. Subcutaneous tumors were measured 3-4 times a week until the volume was over 900 mm^3.

2.13. Vault-based nanoparticle biodistribution in pancreatic subcutaneous xenografts

The biodistribution of the nanoparticles loaded with the fluorescent marker GFP (MVP-H6-GFP-INT) and also with tumor penetrating peptide (MVP-H6-TPP-GFP-INT) was evaluated using stablished PANC-1 subcutaneous xenograft. PANC-1 tumors were subcutaneously implanted following the section 2.1.1. Once they reached a volume of 400 mm^3 the mice were divided in groups (Control, MVP-H6-GFP-INT 5h and 24h, MVP-H6-TPP-GFP-INT 5h and 24h) so the average volume of the tumors was similar and the standard deviation was the smallest. After randomization the tubes with the nanoparticle dilutions were measured at 508 nm wavelength using IVIS Spectrum 2000 and then the controls and the 24h groups were administered 400 µg of nanoparticles in 150 µl intravenously. The next day,

5h before the end of the experiment, the two remaining groups were administered with the same dose. Afterwards the necropsy was performed and organs (kidney, liver, lungs & heart, pancreas & spleen and brain) and tumor were registered using IVIS Spectrum 2000 in order to evaluate the fluorescent nanoparticle biodistribution.

Furthermore, we analyzed the antitumor activity of these nanoparticles when loaded with TNR, a cytotoxic compound, instead of GFP. The protocol was the same but the organs were collected and processed as explained in sections 2.6 and 2.7.

3. Statistical analysis

In order to test the normal distribution of the results we used the Shapiro-Wilk test. Either Student-t test or Anova was performed with results following the normal distribution. The results that were not normally distributed we used the Mann-Whitney U test. For the *in vivo* metastatic analysis Fisher's exact test was used. The values were obtained in duplicate and the data was expressed as mean ± standard error of the mean (s.e.m.). Statistics were calculated using GraphPad Prism 8. Statistically different value's threshold was set at $p<0.05$.

IV. RESULTS

1. In vitro evaluation of the impact of dopaminergic pathways in pancreatic cancer

1.1. Analysis of catecholamine's effect in proliferation in pancreatic cancer cell lines.

In this study, our objective was to investigate how the sympathetic signaling influences cell proliferation and to determine whether its signaling pathways can be harnessed to develop therapeutic strategies against pancreatic cancer. We began our investigation by conducting a proliferation assay on three different human pancreatic cancer cell lines: PANC-1, MIA PaCa-2, and M2. These cells were exposed to catecholaminergic neurotransmitters for 48 hours to assess their potential impact on cellular proliferation. The dose-curve was 0.1, 1, 10 and 100 µM.

Among the neurotransmitters tested, dopamine exhibited a notable antiproliferative effect. When administered at a concentration of 100 µM, dopamine reduced cell proliferation to 58±3% of control levels in PANC-1($p= 0.045$), 53±4% in MIA PaCa-2 ($p= 0.042$) and 68±7% in M2 ($p= 0.039$) cell lines, indicating a consistent inhibitory effect. In contrast, epinephrine at 100 µM significantly induced proliferation in the M2 ($p= 0.041$) cell line, whereas norepinephrine, at a lower concentration of 10 µM, led to a 20% increase in proliferation in the PANC-1 cell line ($p= 0.031$). Epinephrine, at 100 µM, induced a significant 50% increase in pro changes were observed. No other catecholamines showed a significant impact (Fig. 22).

Given the consistent antiproliferative response to dopamine, we next sought characterize pharmacologically the involvement of specific dopaminergic receptor pathways. To this end, we utilized fenoldopam, a selective agonist of dopamine

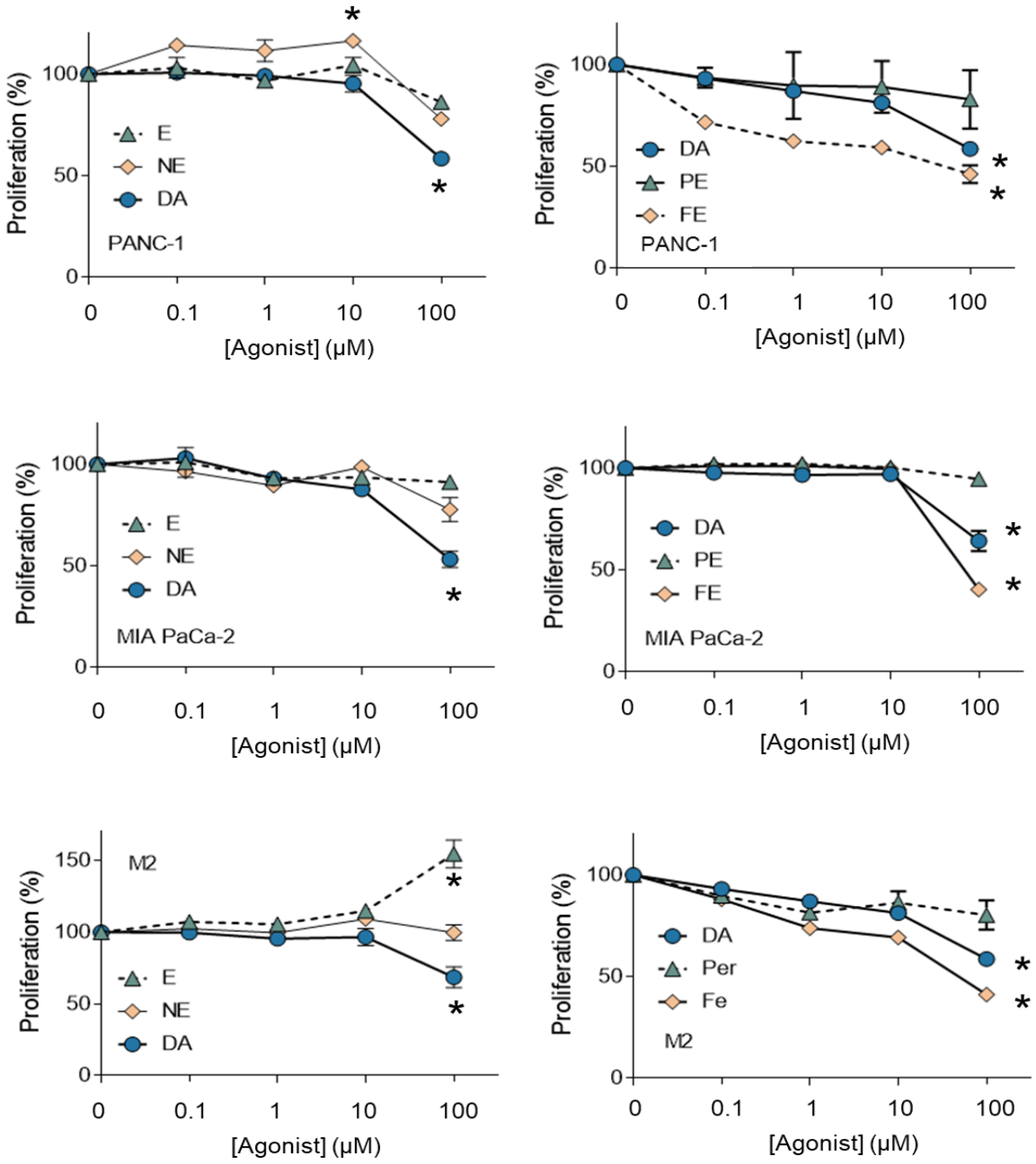

Figure 22. Impact of catecholamines on cell proliferation in PANC-1, MIA PaCa-2, and M2 pancreatic cell lines. A) Effects of epinephrine (E), norepinephrine (NE), and dopamine (DA) on cell proliferation. B) Effects of fenoldopam (FE), a D1 dopaminergic receptor agonist, and pergolide (PE), a D2 dopaminergic receptor agonist, on cell proliferation. Data are presented as mean ± SEM (% compared to drug absence). Statistical significance:*p<0.05.

receptor D1, and pergolide, a dopamine receptor D2 agonist. A similar 48-hour proliferation assay was conducted with these receptor-specific compounds. The dose-curve used was also 0.1, 1, 10 and 100 µM. The results strongly suggested that the observed effects of dopamine were mediated predominantly through the DRD1 pathway. Treatment with fenoldopam led to a significant reduction in proliferation across all three cell lines, bringing levels down to 46±4% in PANC-1 ($p= 0.042$), 40±4% in MIA PaCa-2 ($p= 0.037$) and 41±2% in M2 ($p= 0.049$) compared to control values. In contrast, pergolide produced only minor and statistically non-significant changes.

1.2. Dopamine receptor's presence in pancreatic cancer cell lines

With these results, the next step was to check for the gene expression of the dopaminergic receptors in all three lines in order to confirm the presence of the receptors in the cells. To achieve this objective, we performed a qRT-PCR using probes for each specific dopamine receptor gene (Materials and methods section 1.5). DRD1 was expressed in PANC-1, MIA PaCa-2 and M2 cell lines and the other family member, DRD5, was expressed to a lesser extent. Surprisingly, the DRD2 family was only present in M2 cell line. Since the protein exerts the function, DRD1 and DRD2 protein expression were also evaluated using the western-blot technique. The results showed that both dopaminergic receptor families are expressed in these cell lines, being de D1 family the one with better expression in all three cell lines (Fig. 23).

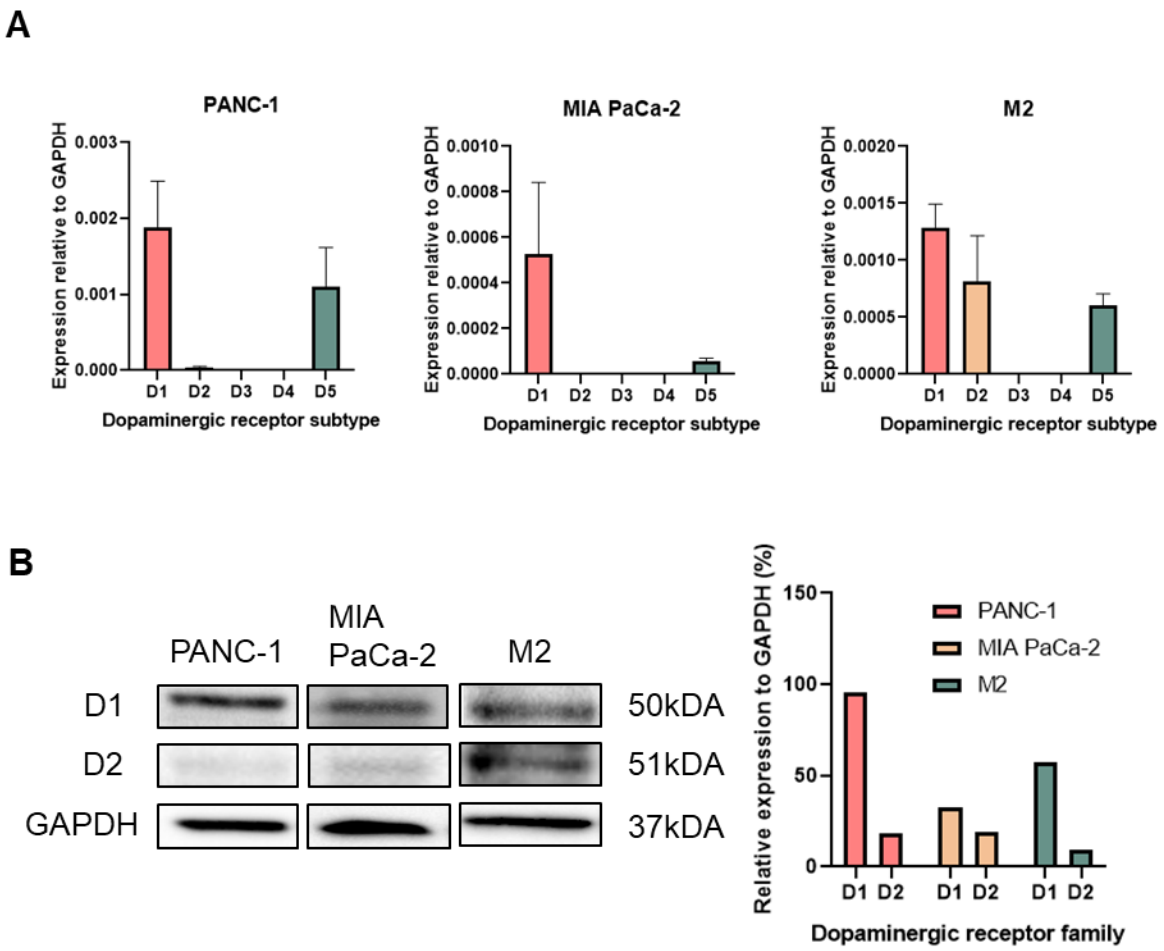

Figure 23. Expression of dopaminergic receptors (D1-D5) in PANC-1, MIA PaCa-2 and M2 cells. A) mRNA expression of each receptor subtype. B). Protein expression values of D1 and D2 receptor families. Data is presented as mean ± SEM.

1.3. Effect of DRD1 agonism in cell death and autophagy.

To investigate the mechanisms underlying cell death induced by dopaminergic agonists, we analyzed the expression of key apoptotic and autophagy proteins in PANC-, MIA PaCa-2 and M2 pancreatic cancer cell lines. Cells were treated with dopamine or fenoldopam (87 µM) and harvested at 0, 0.5, 1, 3, 6, and 24 hours for protein extraction. Western blot analysis was performed to evaluate markers of

apoptosis (cleaved caspase-3 and cleaved PARP) and autophagy (LC3-I, LC3-II, and p62).

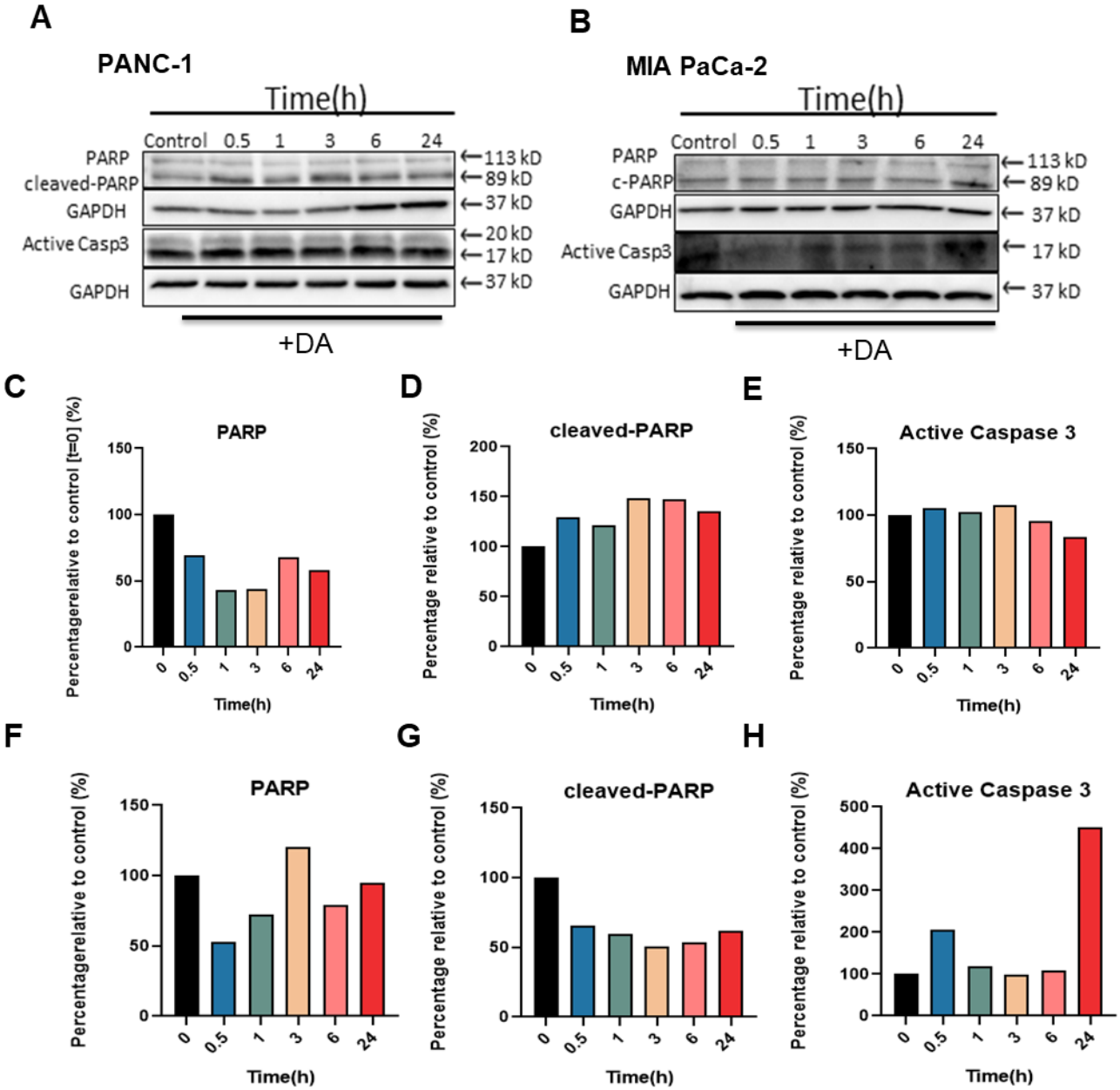

Figure 24. Impact of Dopamine (DA) on cell death in PANC-1 and MIA PaCa-2 Cells. (A-B) Western blot images showing levels of PARP, cleaved PARP, and Caspase-3 proteins at 0, 0.5, 1, 3, 6, and 24 hours post-dopamine treatment (87 µM) in PANC-1 and MIA PaCa-2 cells. **(C-E)** Quantification of PARP, cleaved PARP, and active Caspase-3 levels in PANC-1 cells following dopamine treatment. **(F-H)** Quantification of PARP, cleaved PARP, and active Caspase-3 levels in MIA PaCa-2 cells after dopamine treatment. Results are normalized to the GAPDH control gene. Data is presented as a percentage versus t=0.

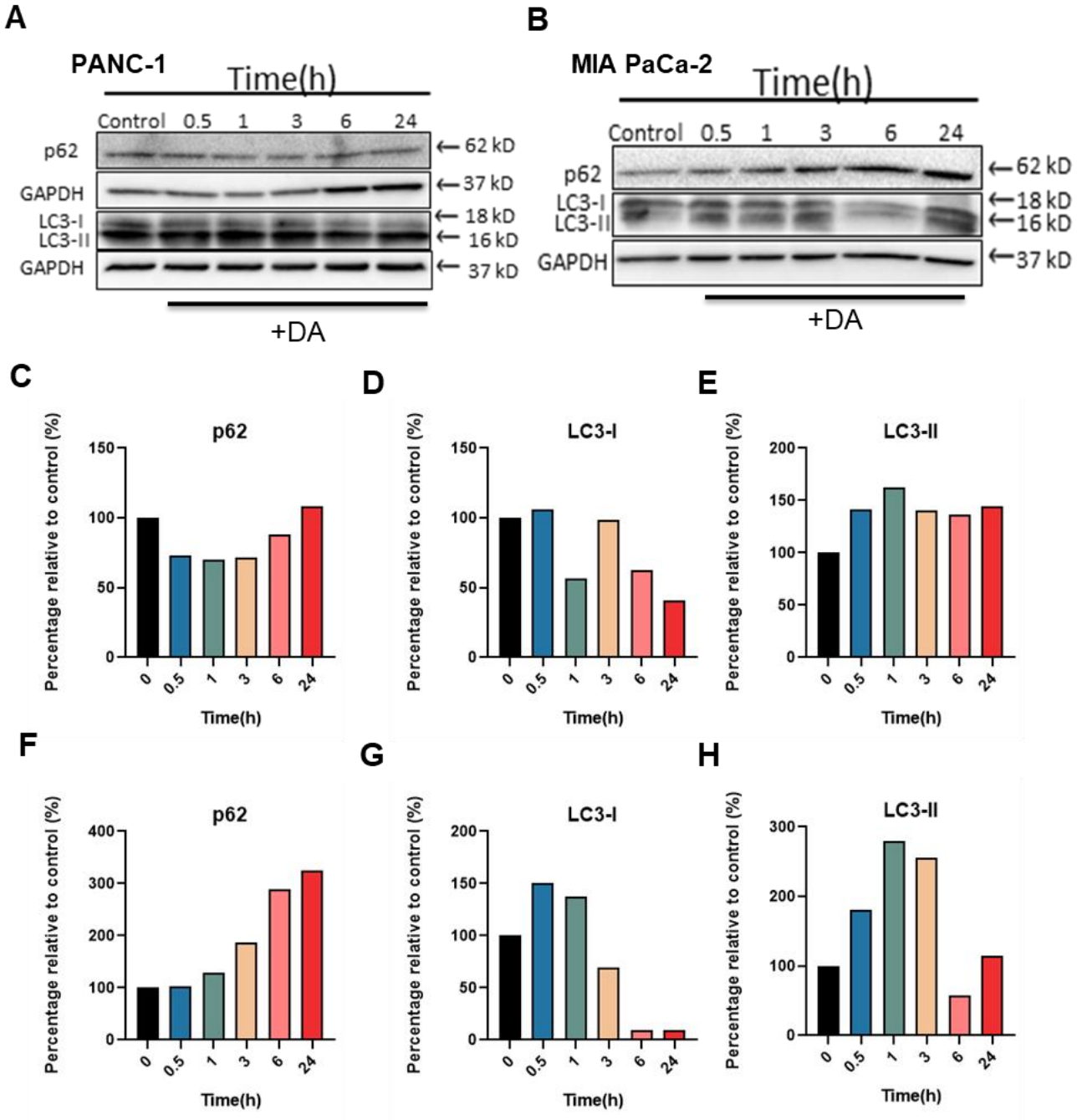

Figure 25. Induction of autophagy cell death by Dopamine (DA) in PANC-1 and MIA PaCa-2 Cells. (A-B) Western blotting images showing levels of p62 , LC3-I and LC3-II proteins involved in autophagy cell death induction at 0, 0.5, 1, 3, 6, and 24 hours post-dopamine treatment (87 µM) in PANC-1 and MIA PaCa-2 cells. **(C-E)** p62, LC3-I and LC3-II level quantification in PANC-1 cells after dopamine treatment. **(F-H)** p62, LC3-I and LC3-II level quantification in MIA PaCa-2 cells after dopamine treatment. Results are normalized to the GAPDH control gene. Data is presented as a percentage versus t=0.

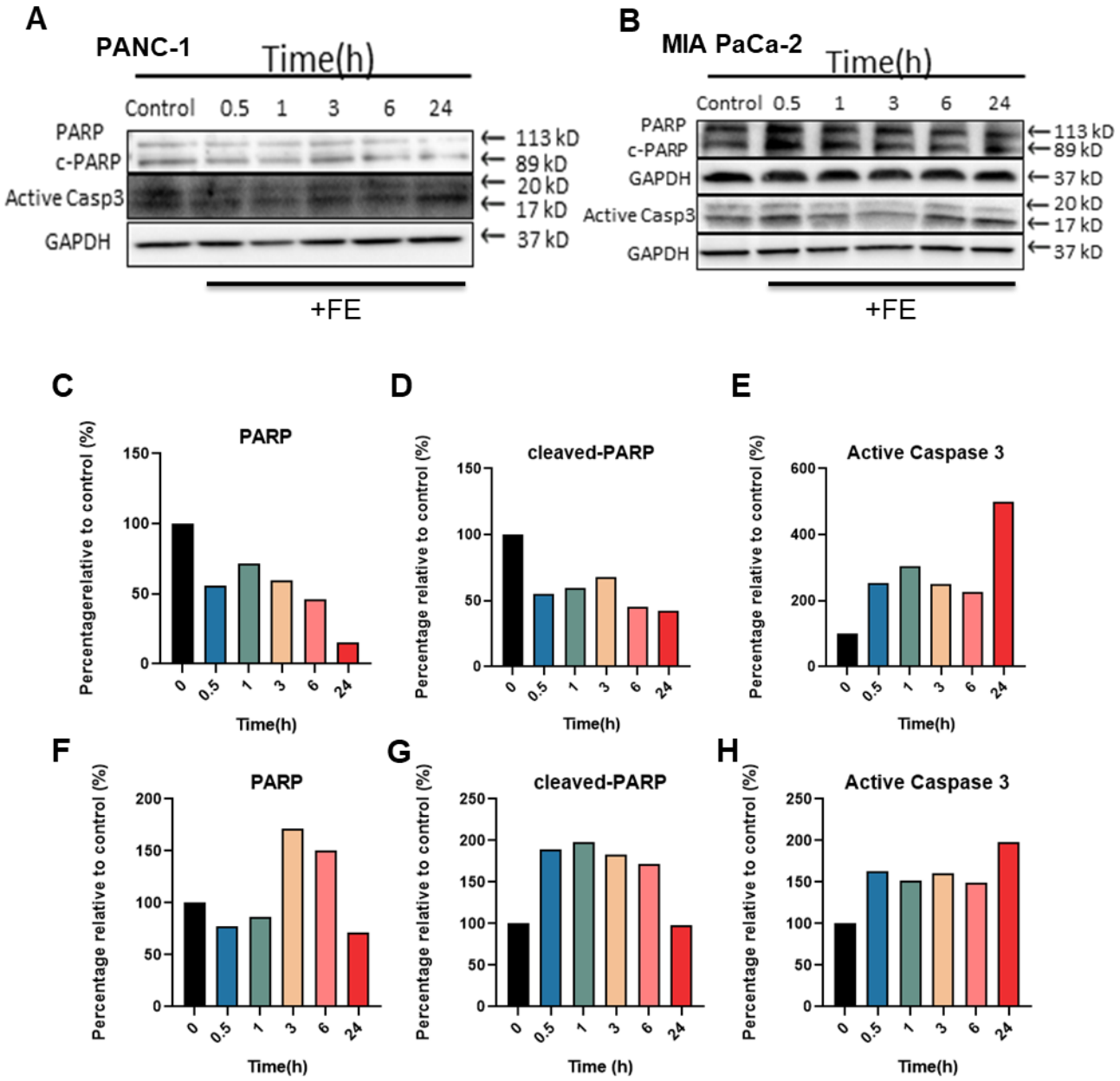

Figure 26. Impact of Fenoldopam (FE) on cell death in PANC-1 and MIA PaCa-2 Cells. (A-B) Western blot images showing levels of PARP, cleaved PARP, and Caspase-3 proteins at 0, 0.5, 1, 3, 6, and 24 hours post-treatment (87 µM) in PANC-1 and MIA PaCa-2 cells. **(C-E)** Quantification of PARP, cleaved PARP, and active Caspase-3 levels in PANC-1 cells following treatment. **(F-H)** Quantification of PARP, cleaved PARP, and active Caspase-3 levels in MIA PaCa-2 cells after fenoldopam treatment. Results are normalized to the GAPDH control gene. Data is presented as a percentage versus t=0.

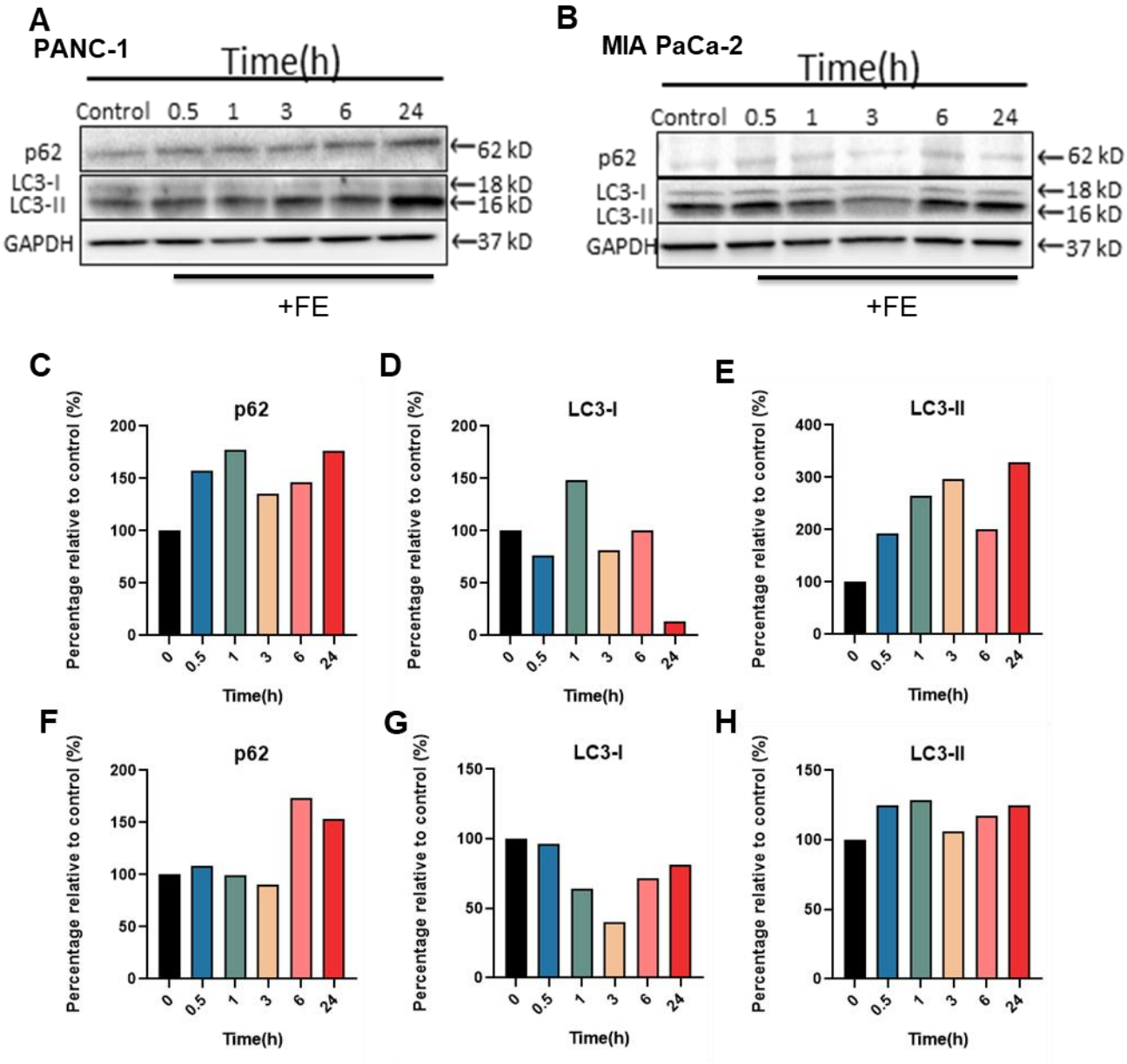

Figure 27. Induction of autophagy cell death by Fenoldopam (FE) in PANC-1 and MIA PaCa-2 Cells. (A-B) Western blotting images showing levels of p62 , LC3-I and LC3-II proteins involved in autophagy cell death induction at 0, 0.5, 1, 3, 6, and 24 hours post-treatment (87 µM) in PANC-1 and MIA PaCa-2 cells. **(C-E)** p62, LC3-I and LC3-II level quantification in PANC-1 cells after treatment. **(F-H)** p62, LC3-I and LC3-II level quantification in MIA PaCa-2 cells after fenoldopam treatment. Results are normalized to the GAPDH control gene. Data is presented as a percentage versus t=0.

In PANC-1 cells (Fig. 24), dopamine treatment led to a decrease in full-length PARP to 42% at 1 hour, followed by a slight recovery to 58% at 24 hours. Correspondingly, levels of cleaved PARP, indicative of apoptosis, increased to148% at 3 hours and remained elevated at 24 hours. Cleaved caspase-3 showed

a mild reduction to 83% of basal levels. In terms of autophagy (Fig. 25), dopamine reduced p62 expression to 70% at 1 hour, with levels recovering by 24 hours. LC3-I decreased progressively, reaching 41% at 24 hours, while LC3-II levels rose to 163% at 1 hour and remained elevated thereafter.

Fenoldopam treatment induced more pronounced apoptotic effects in PANC-1 cells (Fig. 26). PARP levels declined sharply to 15% of basal expression by 24 hours, while cleaved PARP was reduced to 42%. Notably, cleaved caspase-3 levels increased significantly, peaking at 498% at 24 hours. Autophagy-associated changes (Fig. 27) included an early increase in p62 to 177% at 1 hour, sustained through 24 hours. LC3-I initially rose to 148% at 1 hour but subsequently decreased to 13% at 24 hours. LC3-II levels increased steadily, reaching a maximum of 329% at 24 hours.

A similar trend was observed in MIA PaCa-2 cells (Fig. 24). Dopamine led to a reduction in cleaved PARP to 51% of basal levels, which persisted through 24 hours, while cleaved caspase-3 surged to 451% at 24 hours. Autophagy markers were also affected (Fig. 25); p62 expression increased as early as 1 hour and peaked at 325% at 24 hours. LC3-I showed an early rise to 150% at 0.5 hours, followed by a decline to 10% at 24 hours. LC3-II levels peaked at 279% at 1 hour before returning to its baseline.

Fenoldopam treatment in MIA PaCa-2 (Fig. 26) cells induced a transient increase in total PARP to 171% at 3 hours, which declined to 71% by 24 hours. Cleaved PARP rose to 198% at 0.5 hours before normalizing. Cleaved caspase-3 showed a progressive increase, peaking at 198% at 24 hours. Autophagy was again altered (Fig. 27) with p62 rising to 174% at 6 hours and maintaining that level through 24 hours. LC3-I declined to 40% at 3 hours, recovering to 81% at 24 hours. LC3-II expression increased to 128% at 0.5 hours and remained elevated thereafter.

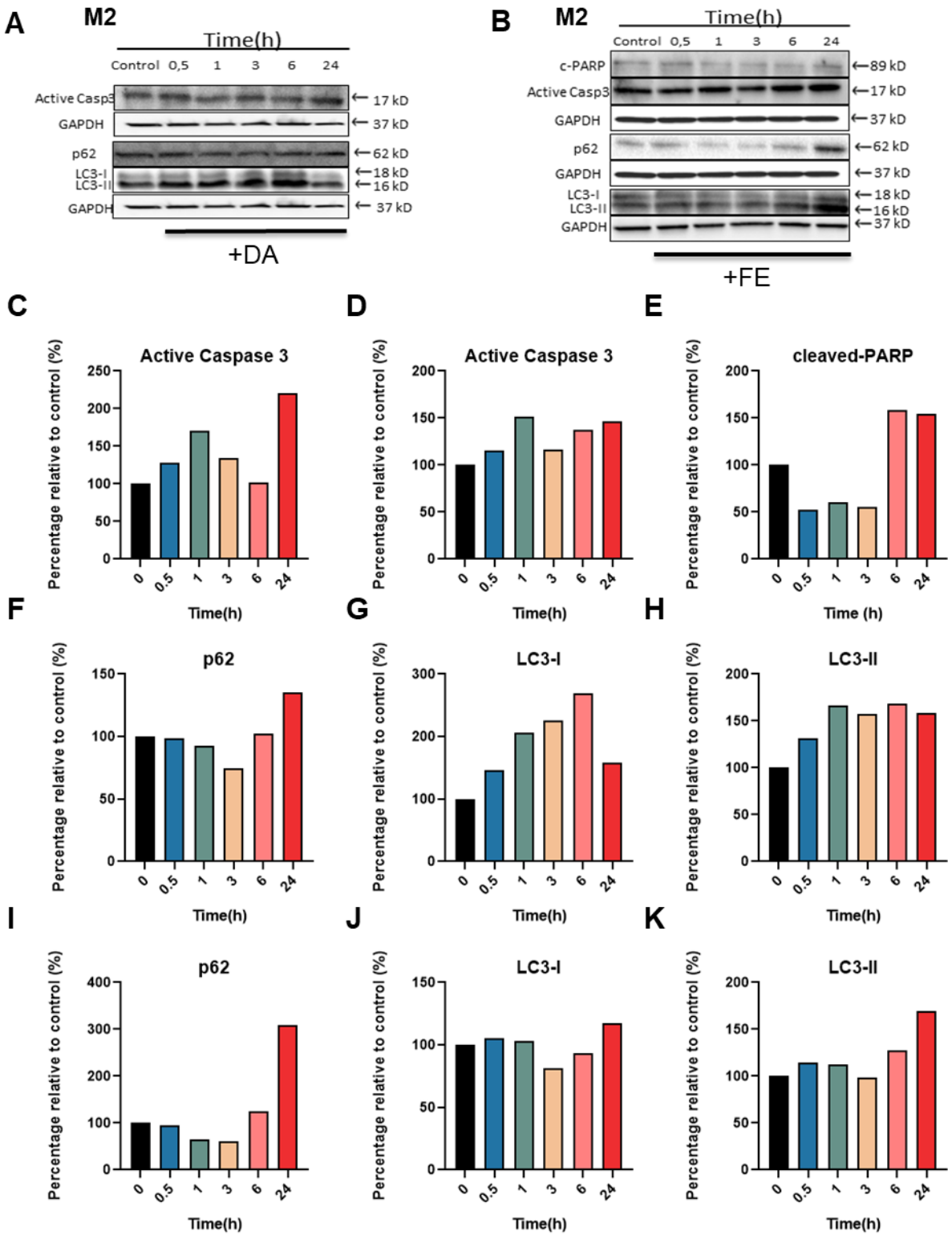

Figure 28. Effect of Dopamine (DA) and Fenoldopam (FE) on cell death in M2 cells. (A-B) Western blotting images showing levels of p62, LC3-I and LC3-II proteins involved in autophagic cell death induction and PARP, cleaved-PARP, Caspase 3 proteins involved in apoptotic cell death induction at 0, 0.5, 1, 3, 6, and 24 hours post-treatment of DA (87 µM) and FE (87 µM). **(C-K)** Protein level quantification of the above cell death markers. Results are normalized to the GAPDH control gene. Data is presented as a percentage versus t=0.

In M2 cell line dopamine fenoldopam seem to increase apoptosis (Fig. 28). Dopamine is able to increase cleaved caspase 3 by 220% at 24h, whereas fenoldopam gets a 140% increase at the same time, but also increased cleaved-PARP by 150% at 6h and maintained the increase at 24h. When it comes to autophagy (Fig.28) dopamine increases p62 at 24h by 35%, also increasing LC3-I by 170% at 6h, which falls to a 58% increase at 24h. LC3-II protein levels get to 166% of the basal levels 1h after treatment and maintain this increase at 24h. Fenoldopam, on the other hand, is able to produce autophagy by increasing p62 protein levels until 309% of the basal levels; this is further reflected in a 20% reduction of LC3-I at 3h followed by a 70% increase of LC3-II at 24h after treatment.

1.4. Effect of catecholamines on the migration capacity of PC cell lines.

To investigate whether catecholamines influence cell migration, a wound healing assay was performed, measuring migration regression 48 hours after treatment (Fig. 29). While Norepinephrine reduced migration only in PANC-1 (66%, $p = 0.0053$), and epinephrine showed no effect, the results indicate that 10 µM dopamine significantly inhibited migration in PDAC cell lines. Migration in PANC-1 and MIA PaCa-2 cells was reduced by 50% ($p = 0.0091$, $p = 0.082$, respectively), while the patient-derived cell line M2 showed no response.

To pharmacologically characterize the dopamine receptor involved, treatments with dopamine, the selective D1 agonist fenoldopam (FE), and the D2 agonist pergolide (Per) were tested. All three treatments reduced migration in PANC-1 and MIA PaCa-2 cells. Fenoldopam reduced migration by 50% in PANC-1 ($p = 0.0098$) and by 66% in MIA PaCa-2 ($p = 0.0047$). Pergolide exhibited a stronger inhibitory effect, reducing migration by 90% in both cell lines ($p = 0.0025$ and $p = 0.0012$, respectively). M2 cell line remained unresponsive to all treatments.

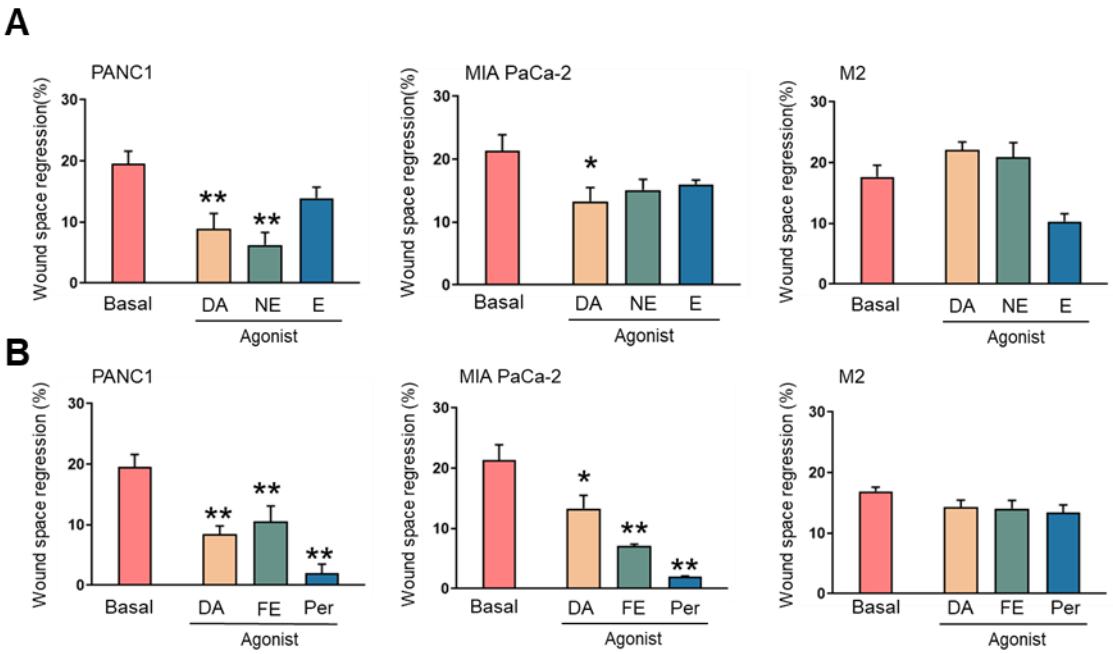

Figure 29. Impact of catecholamines on cell migration capacity in PANC-1, MIA PaCa-2, and M2 cells. A) Effects of dopamine (DA), norepinephrine (NE) and epinephrine (E) at 10μM for 48 hours on migration **B)** Effects of 10μM DA, FE and PE for 48h on cell migration capacity. Cell migration was determined by the wound healing assay. Data are presented as mean ± SEM. Statistical significance: *p<0.05; **p=<0.01

2. Evaluation of the therapeutic effect of dopamine agonists *in vivo*

In parallel with *in vitro* studies, the therapeutic potential of dopamine agonists was assessed *in vivo*. On one hand, fenoldopam was chosen as a selective D1-like due to its established use in lowering blood pressure and the fact that it does not cross the blood-brain barrier, making it a strong candidate for a drug repurposing strategy. Similarly, bromocriptine was selected as a DRD2 agonist because is accessible and has already been used in patients to fight Parkinson's disease and to reduce blood sugar levels in patients with type 2 diabetes [124].

To check the therapeutic effectiveness of the agonisms we stablished CDX models using two pancreatic cell lines (PANC-1 and MIA PaCa-2).

Both cell lines are used by many authors in literature and they are well established and representative of PDAC. As shown in previous experiments, they express the receptors and responded to the drugs *in vitro*.

2.1. Determination of the antitumor activity of fenoldopam and bromocriptine in tumor progression in PANC-1 subcutaneous pancreatic cancer xenografts.

Afterwards, *Athymic* mice were implanted subcutaneously with PANC-1 tumors. Tumor volumes were measured weekly until they reached a starting volume between 76 mm^3. This allowed us to follow the tumor progression after the administration of the drugs, up until the endpoint of the experiment.

The results of the PANC-1 experiment are shown in Figure 30. In PANC-1 tumor bearing mice, the treatment with fenoldopam reduced tumor volume reaching a 62% decrease of at day 14 of administration compared to controls (p= 0.009).

The final tumor volume was reduced from 647±91 mm^3 in the controls to 403±100 mm^3 (p= 0.05) in bromocriptine treated tumors and 248±85 mm^3 (p= 0.0018) in fenoldopam treated mice. Tumor weight was also affected, diminishing from 0.5 ± 0.08g in the control group to 0.31 ±0.08g in the bromocriptine group (p= 0.0489) and to 0.25±0.11(p=0.00493) in the fenoldopam treated group. The treatments did not affect mouse body weight during 14 days of administration.

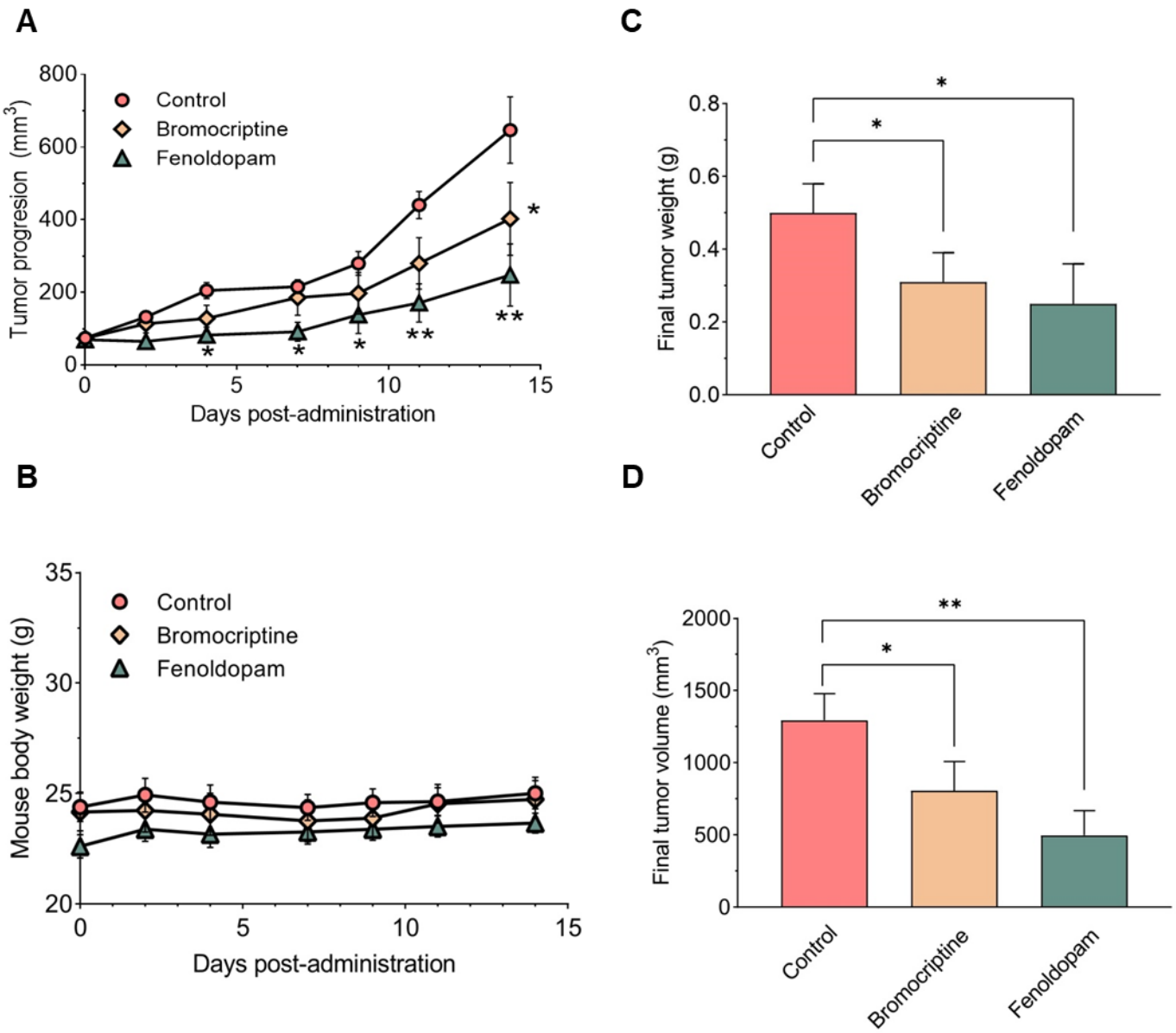

Figure 30. Analysis of the therapeutic effect of the dopaminergic agonists bromocriptine and fenoldopam in a pancreatic mouse cancer model. The mice strain *Swiss nude* was implanted with PANC-1 derived tumor pieces so we could evaluate **A) The tumor volume progression** of each group during 14 days of treatment, measured using an electronic caliper. **B) The mice body weight progression** during 14 days of treatment. **C) The final tumor weight** right after euthanasia. **D) The final tumor volume** right after euthanasia. Dose used: Fenoldopam 12.5mg/kg 3 times a week; bromocriptine 2mg/kg/day. Data is presented as mean ± SEM. Statistical significance:*p<0.05; **p=<0.01

2.2. Determination of the antitumor and antimetastatic activity of fenoldopam and bromocriptine in MIA PACA-2 subcutaneous xenografts.

Simultaneously, the same experiment was performed with MIA PaCa-2 tumors. The results (Figure 31) show a reduction in tumor progression, reaching a 50% ($p<0.001$) decrease after 14 days of fenoldopam administration regime. Bromocriptine reduced tumor progression by 40% ($p= 0.004$). The final tumor volume were also reduced after fenoldopam treatment from 1383±218 mm^3 to 707±198 ($p= 0.0096$) and final tumor weight from 1.00±0.20g to 0.41±0.09g ($p=0.041$). Bromocriptine reduced final tumor volume from 1383±218 mm^3 to 780±175 mm^3 ($p=0.0098$) and final tumor weight from 1.00±0.20g to 0.68±0.20g ($p= 0.05$).

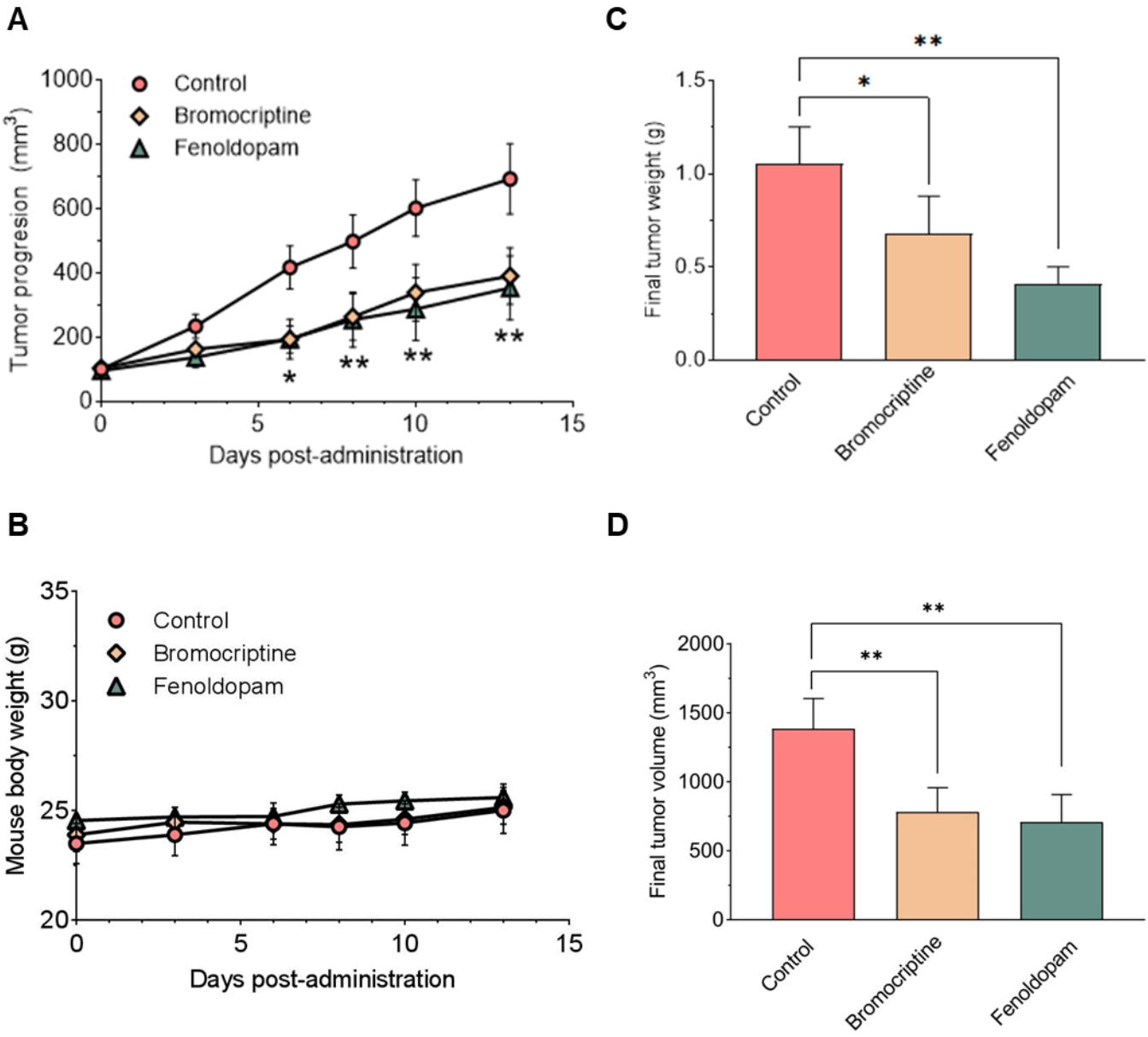

Figure 31. Analysis of the therapeutic effect of the dopaminergic agonists bromocriptine and fenoldopam in a pancreatic mouse cancer model. The mice strain *Swiss nude* was implanted with MIA PaCa-2 derived tumor pieces so we could evaluate **A) The tumor volume progression** of each group during 14 days of treatment, measured using an electronic caliper. **B.) The mice body weight progression** during 14 days of treatment. **C) The final tumor weight** right after euthanasia **D)The final tumor volume** right after euthanasia. Dose used: Fenoldopam 12.5mg/kg 3 times a week; bromocriptine 2mg/kg/day. Data is presented as mean ± SEM. Statistical significance:*p<0.05; **p=<0.01

2.3. Effect of fenoldopam and bromocriptine in tumor progression and metastasis in a highly metastatic orthotopic pancreatic cancer model.

The next objective was to evaluate the antitumor and antimetastatic effect of dopaminergic agonists in the pancreatic cancer orthotopic mouse model. To do so, athymic mice were implanted orthotopically with passage 3 PANC-1-luc tumors. In this case, the tumors were not accessible for measurement, so the tumor progression was monitored by measuring the bioluminescence of the tumor after a luciferin injection. The tumor cells were previously transfected with luciferase, an enzyme able to oxide the luciferin, releasing a measurable bioluminescent signal in the process. The bigger the tumor, the more cells can metabolize the luciferin, and a higher signal will be measured. The mice were randomized in 4 groups: Control, Fenoldopam (400ng/kg/min), Bromocriptine (15mg/kg/day) and Fenoldopam + Bromocriptine (same doses as previously described).

The endpoint of the experiment was reached at 14 days. After the necropsy, the tumors were removed, weighed, and measured.

In the PANC-1 orthotopic model, the results followed a similar tendency (Fig. 32). Bromocriptine-treated tumors had a bioluminescence emission progression similar to controls with a final increase of 64059% of its initial value when control increase was 88642%. Fenoldopam treated tumor bioluminescence emission progression; on the other hand, it diminished. After 14 days of fenoldopam treatment, the tumors emitted 5256% of their initial value. The combination of both fenoldopam and bromocriptine treatments highly decreased the bioluminescence emission progression was 1361% at day 14 compared to day 0. After necropsy, tumors were weighed and measured *ex vivo*. The size and weight of fenoldopam-treated tumors were not significantly different from controls. Bromocriptine-treated tumors were bigger and heavier than the control group, but the differences were not statistically significant. The mice's weight remained stable for all conditions during the experiment. The control group the one with the biggest decrease, a difference of 1 gram compared to day 0.

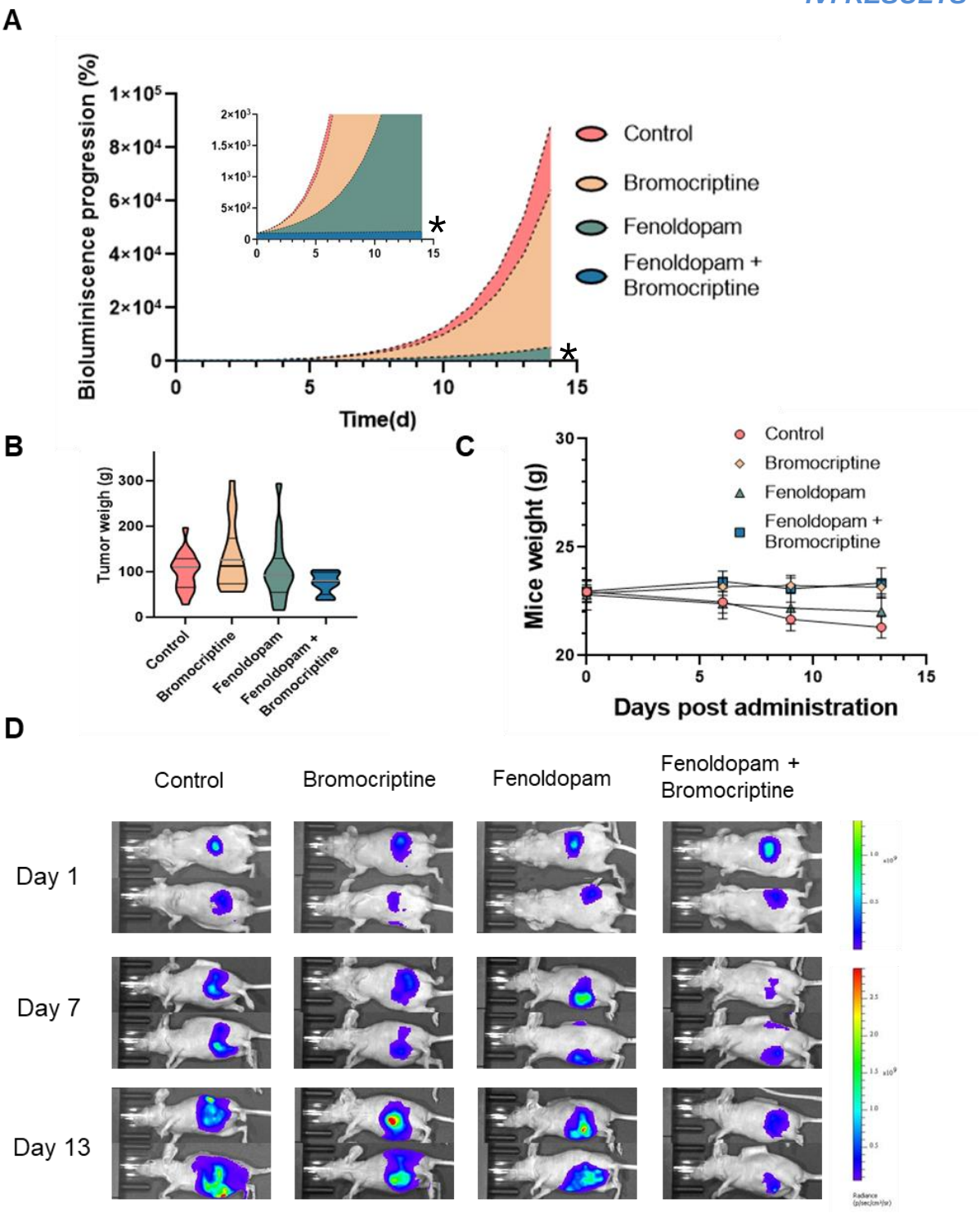

Figure 32. Effect of dopamine agonist treatments and its combination in PANC-1 **orthotopic xenografts. (A)** Bioluminescence levels of PANC-1 orthotopic xenografts during dopamine agonist treatments. **(B)** Final tumor weigh after dopamine agonist treatments. **(C)** Mice body weigh during dopamine agonist treatments **(D)**. Bioluminescence imaging of the mice at different days of the treatment. Data is presented as mean ± SEM. Statistical significance: p=0.004

2.3.1. Evaluation of metastatic foci.

First we analyzed the number of mice where metastasis occurred and the location of the foci (Table 8). The results showed an overall decrease in the number of mice with metastases, especially in peripancreatic lymph node metastases (75% reduction in all groups compared to controls, $p<0.05$ in Fenoldopam + Bromocriptine group) and in the mesenteric lymph nodes (25% for bromocriptine treated mice and 50% for both groups treated with fenoldopam).

After this orthotopic experiment reached the endpoint, a molecular characterization of the antitumor mechanism was performed.

Table 8. Number of mice with metastatic foci.

		Metastasis findings in tumor-bearing mice [*n* (%)]					
Group	**No. of mice bearing tumor**	**General**	**Peripancreatic lymph nodes**	**Mesenteric lymph nodes**	**Carcinomatosis peritoneal (micrometastais)**	**Carcinomatosis peritoneal (macrometastais)**	**Hematogenic metastasis**
Control	10	8 (80)	8 (80)	8 (80)	4 (40)	7 (70)	3 (30)
Bromocriptine	10	7 (70)	2 (20)*	6 (60)	4 (40)	4 (40)	0 (0)
Fenolodopam	10	7 (70)	2 (20)*	4 (44.4)	3 (33.3)	2 (22.2)	1 (10)
Fenolodopam + Bromocriptine	11	6 (54.5)	2 (18.2)*	4 (36.4)	2 (18.2)	3 (27.3)	0 (0)

*=p<0.05

2.3.2. Molecular analysis of the anti-tumor activity of fenoldopam and bromocriptine treatments.

Next, we wanted to evaluate the impact of dopaminergic agonists in cell death (Fig. 33). For that, we measured the percentage of the total area of the tumor slices that were necrotic. The results show that tumors treated with fenoldopam had a 10% increase compared to controls ($p<0.0090$). There were no differences in the necrotic area in bromocriptine-treated tumors compared to controls. Moreover, fenoldopam tumors was also 10% more necrotic than its combination with bromocriptine ($p=0.0484$). Furthermore, when we analyzed the number of cells in the process of dying, we observed statistical significances in all 3 groups. The percentage of cells in the process of dying was 65% higher in bromocriptine-

treated tumors (p = 0.0020) and almost 170% higher in both the fenoldopam and the combination groups when compared to the control values (p= 0.0006, p <0.0001 respectively). We evaluated the molecular mechanism underneath this effect and analyzed the apoptosis (Fig.34 A) by checking the presence of the active caspase-3, and this marker was found to be more present in fenoldopam-treated tumors, almost a 2.5-fold increase (p=0.0361). The combination treatment led to an 8 fold increase in the percentage of active caspase-3 positive area compared to control (p<0.0001) and the difference was also significant vs fenoldopam and bromocriptine groups (p<0.0001). Additionally, we studied the area of proliferative cells using Ki67 (Fig. 34 B), a common marker of proliferation index. Treatments showed no statistically significant differences compared to control.

When analyzing the number of blood vessels using the marker CD31 (Fig. 35), bromocriptine, fenoldopam, and its combination were able to reduce the number of blood vessels by almost 50% (p=0.0062, p=0.030 and p= 0.023 respectively).

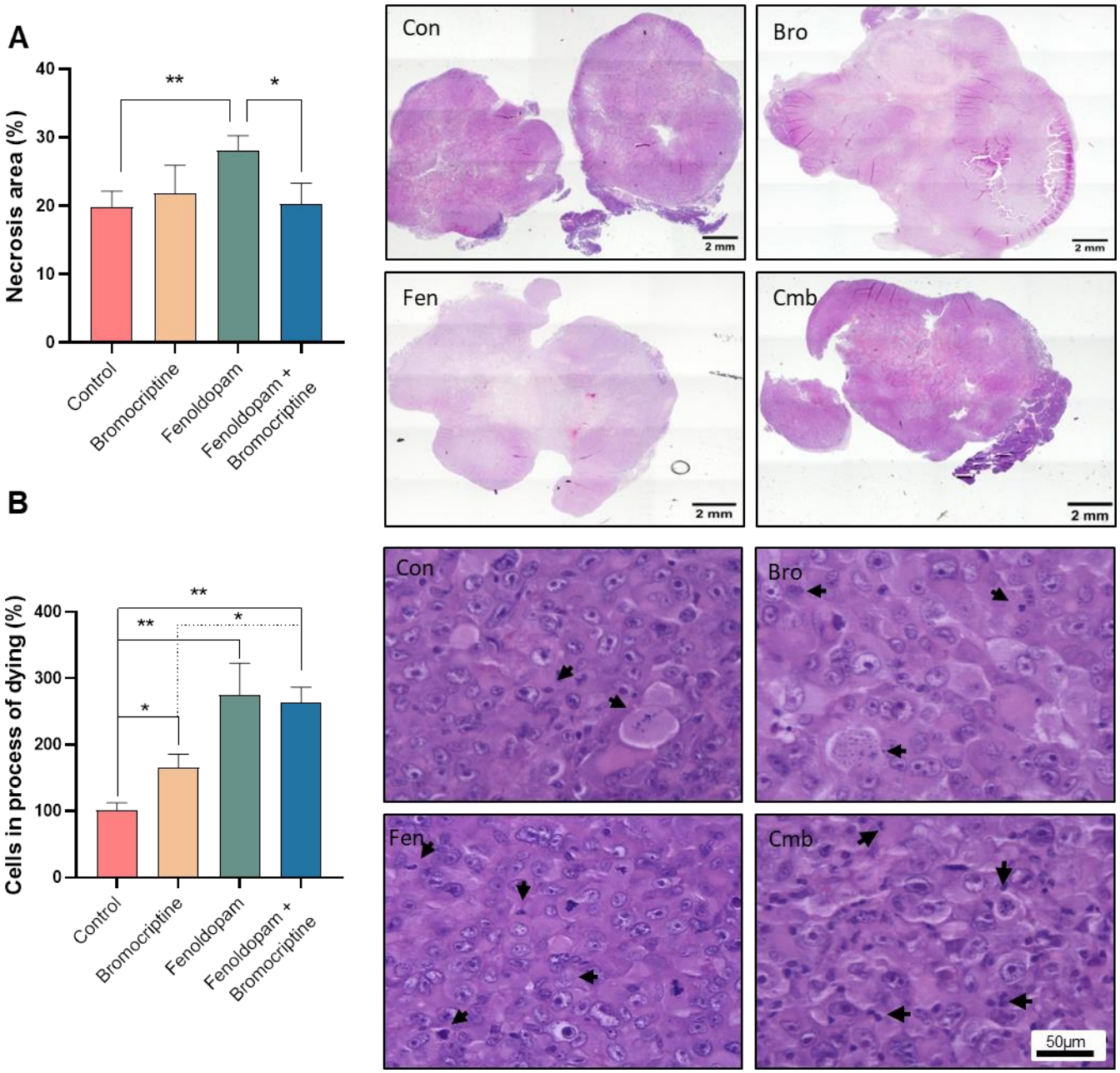

Fig 33. Histopathological analysis of the effect of dopamine agonist treatments and its combination in PANC-1 **orthotopic xenografts**. **A)** Representative hematoxylin-eosin figures and quantification of tumor necrosis after dopamine agonist treatments. Images were taken at 20x magnification. Scale bar = 2mm **. B)** Representative hematoxylin-eosin figures and quantification of cells in process of dying after dopamine agonist treatments. Images were taken at 400x magnification. Black arrow = cells in process of dying. Scale bar = 50µm. Data is presented as mean ± SEM. Statistical significance:*p<0.05; **p=<0.01. Con= Control, Bro= Bromocriptine, Fen= Fenoldopam, Cmb = Fenoldopam + Bromocriptine.

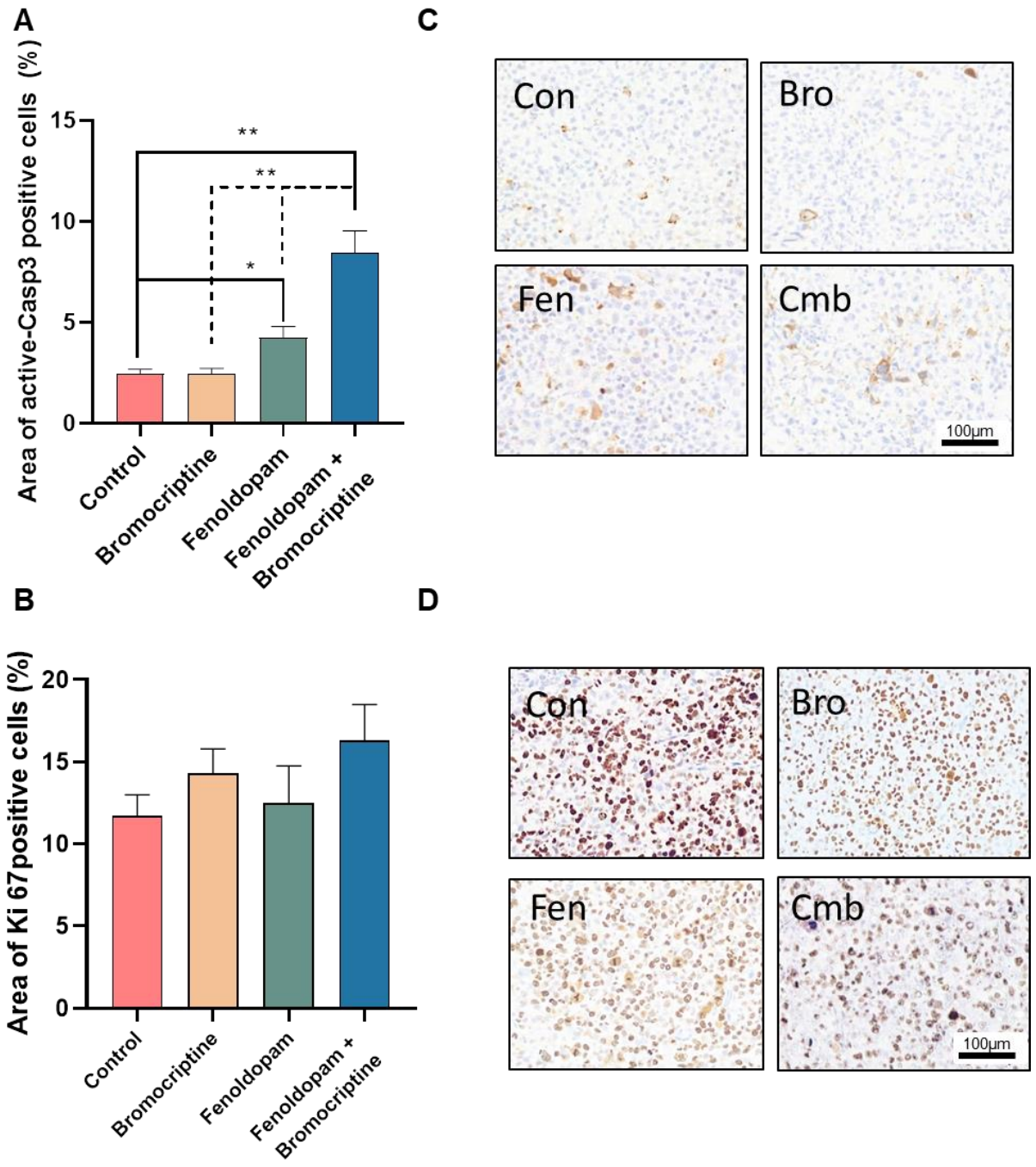

Figure 34. Molecular analysis of the effect of dopamine agonism treatments and its combination in PANC-1 orthotopic xenografts. A) Graphical representation of the area of Casp3 positive cells after dopamine agonist treatments. **B)** Immunohistochemistry images of c-Caspase 3 positive areas in PANC-1 orthotopic tumors after dopamine agonist treatments at 200x magnification. Scale bar = 100µm. **C)** Quantification of the area of Ki67 positive cells after dopamine agonist treatments. **D)** Representative Immunohistochemistry images of Ki67 positive areas in PANC-1 orthotopic tumors after dopamine agonist treatments at 200x magnification. Scale bar = 100µm. Data is presented as mean ± SEM. Statistical significance:*p<0.05; **p=<0.01. Con= Control, Bro= Bromocriptine, Fen= Fenoldopam, Cmb = Fenoldopam + Bromocriptine.

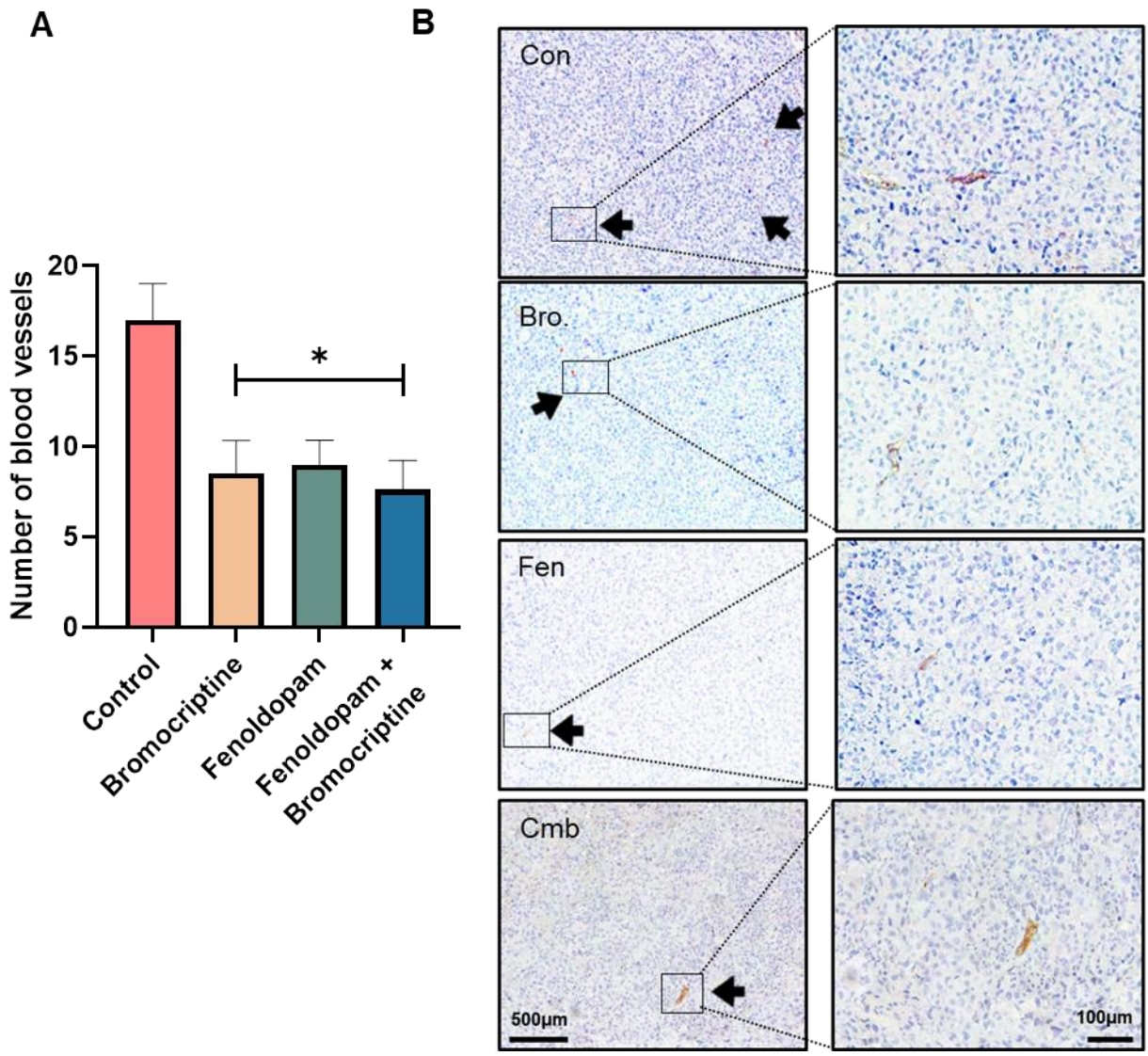

Fig 35. Antiangiogenic effect of the dopaminergic agonism. A) Quantification of number of blood vessels in PANC-1 orthotopic xenograft tumors after dopamine agonist treatments. **B)** Immunohistochemistry images of CD31 stained blood vessels. Scale bar = 500µm. Scale bar of insert = 100µm. Black arrow = blood vessel. Data is presented as mean ± SEM. Statistical significance:*p<0.05. Con= Control, Bro= Bromocriptine, Fen= Fenoldopam, Cmb = Fenoldopam + Bromocriptine.

2.3.3. Evaluation toxicity of fenoldopam and bromocriptine treatments

To analyze the toxicity of fenoldopam and bromocriptine, we performed hematoxylin-eosin staining of the organs of each experimental mouse. With the help of a pathologist, the liver, lungs, kidneys, pancreas, spleen, and brain were evaluated and compared to the control group. No toxic side effects were found in

any organ, after neither fenoldopam or bromocriptine treatments, nor its combination treatment. Furthermore, no significant differences were observed in the mouse body weight between the groups (Fig. 36).

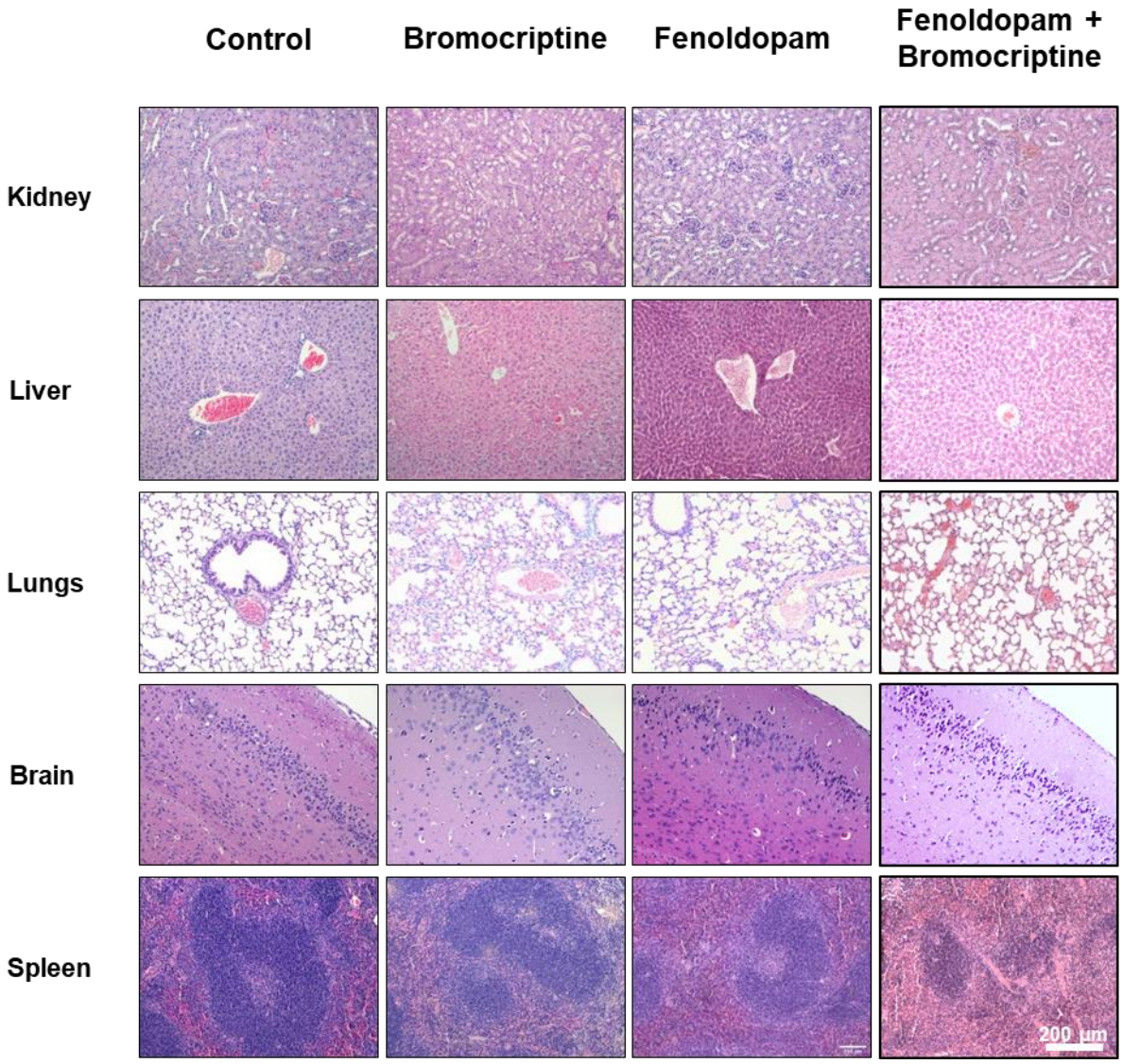

Figure 36. Histological samples of the kidneys, livers. lungs, brains and spleens of mice after 14 days of dopaminergic agonist treatments stained with hematoxylin/eosin.

2.3.4. Identification of potential oncogenes and tumor suppressor genes using microarrays of tumor tissue.

To further characterize the molecular signaling under dopaminergic activation in PANC-1 tumors, we conducted microarray technology to analyze the differential expression of 22,000 genes per sample. After a deep analysis we selected a few genes that have the biggest fold versus control tumors with the highest p value. (Fig. 37, 38 & Annex1). We studied the pathways in which these genes were involved and sought for cell death, cell proliferation and cell migration processes. Our most important findings were CDC42EP3 which is downregulated in bromocriptine treated mice and is a gene that many authors indicate as an oncogene, involved in the cell proliferation and migration processes. Fenoldopam treated tumors had MRPS23, PAICS, SLC38A1, REEP3, RPGRIP1L and HSDL2 downregulated compared to the control group. All these genes are described as oncogenes in literature. Furthermore USP10, a described tumor suppressor gene was upregulated. Finally, the combination of bromocriptine and fenoldopam treated tumors had CCDC58, an oncogene, downregulated, whereas TRIM13, a tumor suppressor gene was upregulated. This analysis is preliminary and this differential expression must be confirmed by RT-PCR in the future for validation.

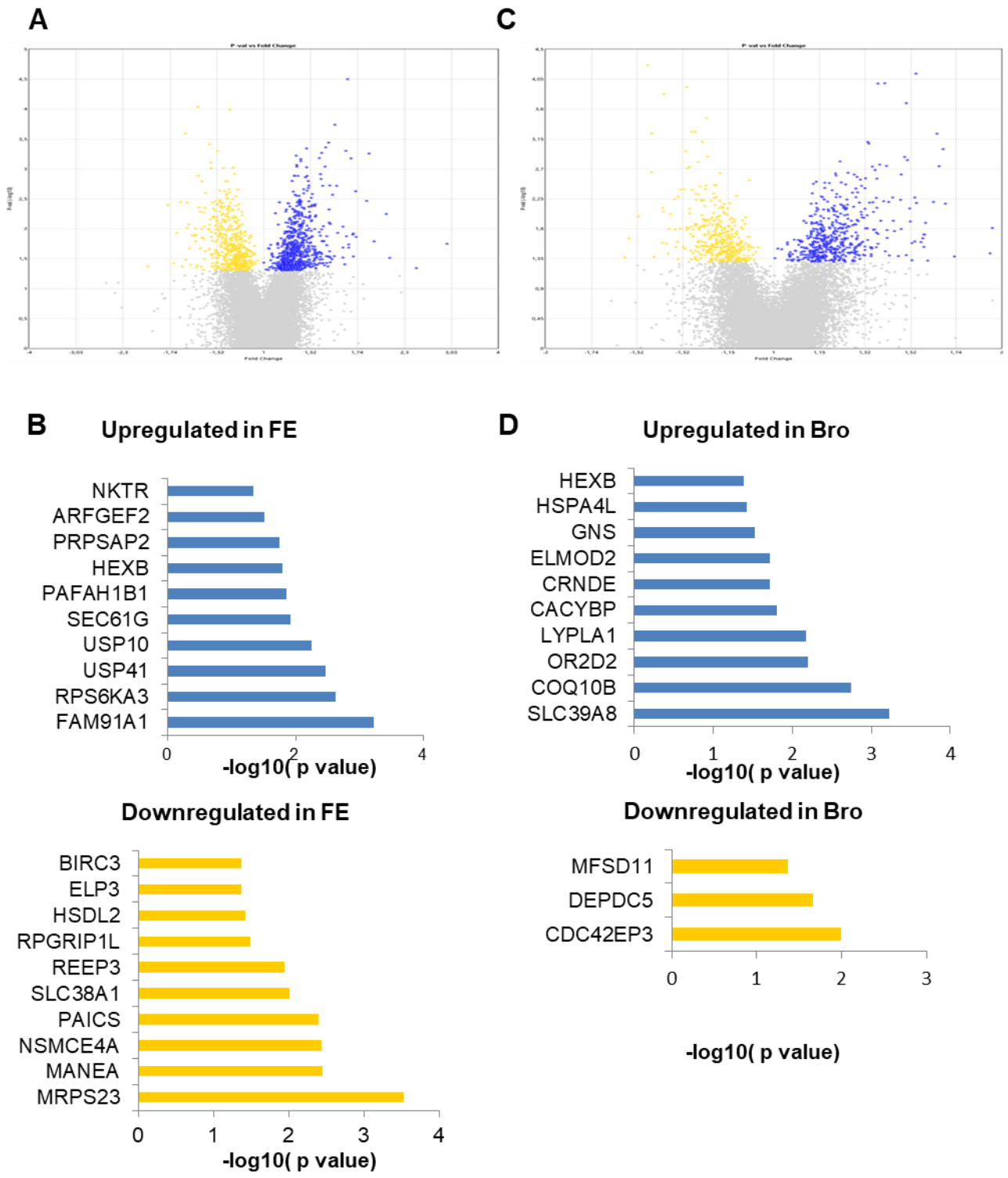

Figure 37. Transcriptomic analysis of the differential expression of 22.000 genes in treated PANC-1 orthotopic xenografts activation compared to controls. **A)** Volcano plot of the upregulated (blue) and downregulated (yellow) genes after fenoldopam treatment. **B)** Upregulated (blue) and downregulated (yellow) genes after fenoldopam treatment over 1.5 fold with the highest significance. **C)** Volcano plot of the upregulated (blue) and downregulated (yellow) genes after bromocriptine treatment. **D)** Upregulated (blue) and downregulated (yellow) genes after bromocriptine treatment over 1.5 fold with the highest significance. FE= fenoldopam, Bro= bromocriptine.

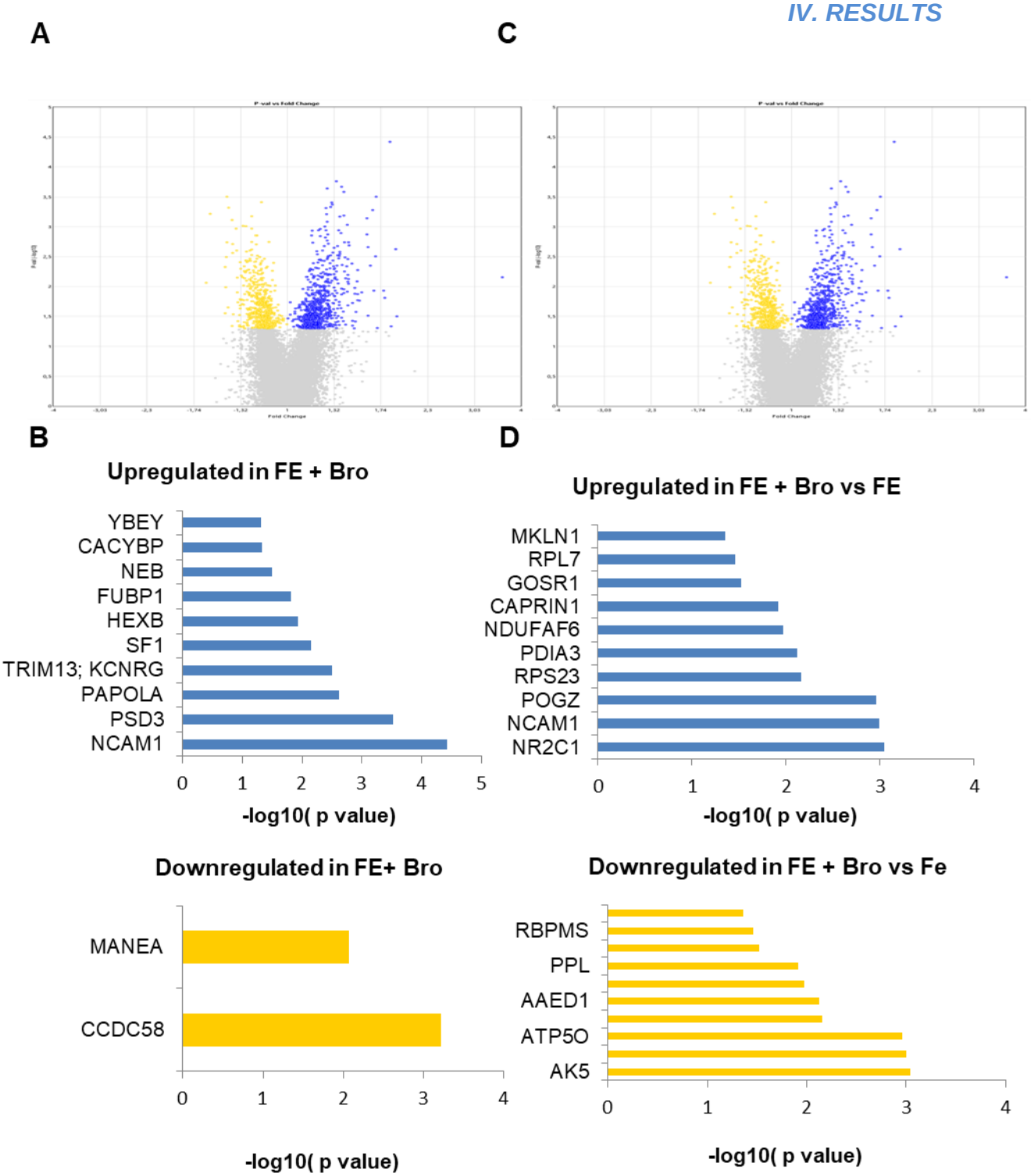

Fig 38. Transcriptomic analysis of the differential expression of 22.000 genes in treated PANC-1 orthotopic xenografts. **A)** Volcano plot of the upregulated (blue) and downregulated (yellow) genes after fenoldopam + bromocriptine treatment compared to controls. **B)** Upregulated (blue) and downregulated (yellow) genes after fenoldopam + bromocriptine treatment over 1.5 fold with the highest significance compared to control. **C)** Volcano plot of the upregulated (blue) and downregulated (yellow) genes after fenoldopam + bromocriptine treatment compared to fenoldopam. **D)** Upregulated (blue) and downregulated (yellow) genes after fenoldopam + bromocriptine treatment over 1.5 fold with the highest significance compared to fenoldopam. FE= fenoldopam, Bro= bromocriptine.

3. Evaluation of the therapeutic effect of dopamine inhibition.

3.1. Effect of dopaminergic signaling inhibition in pancreatic cancer cells.

We next examined pharmacology the effects of four selective dopaminergic receptor antagonists: SCH23390 (dopamine D1 receptor subtype) and butaclamol, L741,626 and domperidone (dopamine D2 receptor subtype). To this end, proliferation assays were performed in PANC-1, MIA PaCa-2, and M2 cells across a concentration range of 1-100 µM (Fig. 39).

SCH23390 (also known as halobenzazepine) produced only mild, non-significant changes in both proliferation and viability at all tested doses in the three cell lines.

In contrast, D2 antagonism elicited a pronounced inhibitory effect. In PANC-1 cells, butaclamol decreased proliferation by 36% at 75 µM ($p < 0.001$) and by 64% at 100 µM. Domperidone demonstrated a dose-dependent reduction in proliferation. A modest, non-significant 15% decrease was observed at 75 µM, while treatment with 100 µM resulted in a statistically significant 43% reduction compared to control ($p = 0.0030$), indicating potential antiproliferative effects at higher doses. L-741,626 was tested in a single experiment, limiting statistical interpretation. However, preliminary analysis suggested an IC_{50} of approximately 29.92 µM.

In MIA PaCa-2 cells, butaclamol reduced proliferation by 36% at 50 µM and fully suppressed it at 100 µM ($p < 0.0001$). Domperidone demonstrated a robust dose-dependent inhibition of proliferation. A non-significant 15% reduction was seen at 25 µM, followed by statistically significant reductions of 45% at 50 µM ($p=0.0001$), 88% at 75 µM ($p=0.0001$), and 85% at 100 µM ($p=0.0001$). L-741,626 produced a statistically significant 33% reduction in proliferation beginning at 25 µM ($p=0.0001$). The effect intensified at 50 µM with near-complete inhibition (100% reduction, $p=0.0001$) and remained significant at 75 and 100 µM ($p = 0.0001$).

Finally, in M2 cells, butaclamol decreased proliferation by 32% at 75 µM ($p = 0.0042$) and by 56% at 100 µM ($p < 0.0001$). Domperidone exhibited a dose-dependent antiproliferative effect, reaching in a statistically significant 50% reduction in proliferation at 100 µM ($p= 0.0123$), indicating strong inhibitory activity at high concentrations. L-741,626 displayed a pronounced inhibitory effect starting at 50 µM, with a statistically significant 87% reduction in proliferation observed at 100 µM ($p= 0.0224$), suggesting potent antiproliferative activity in M2 cells.

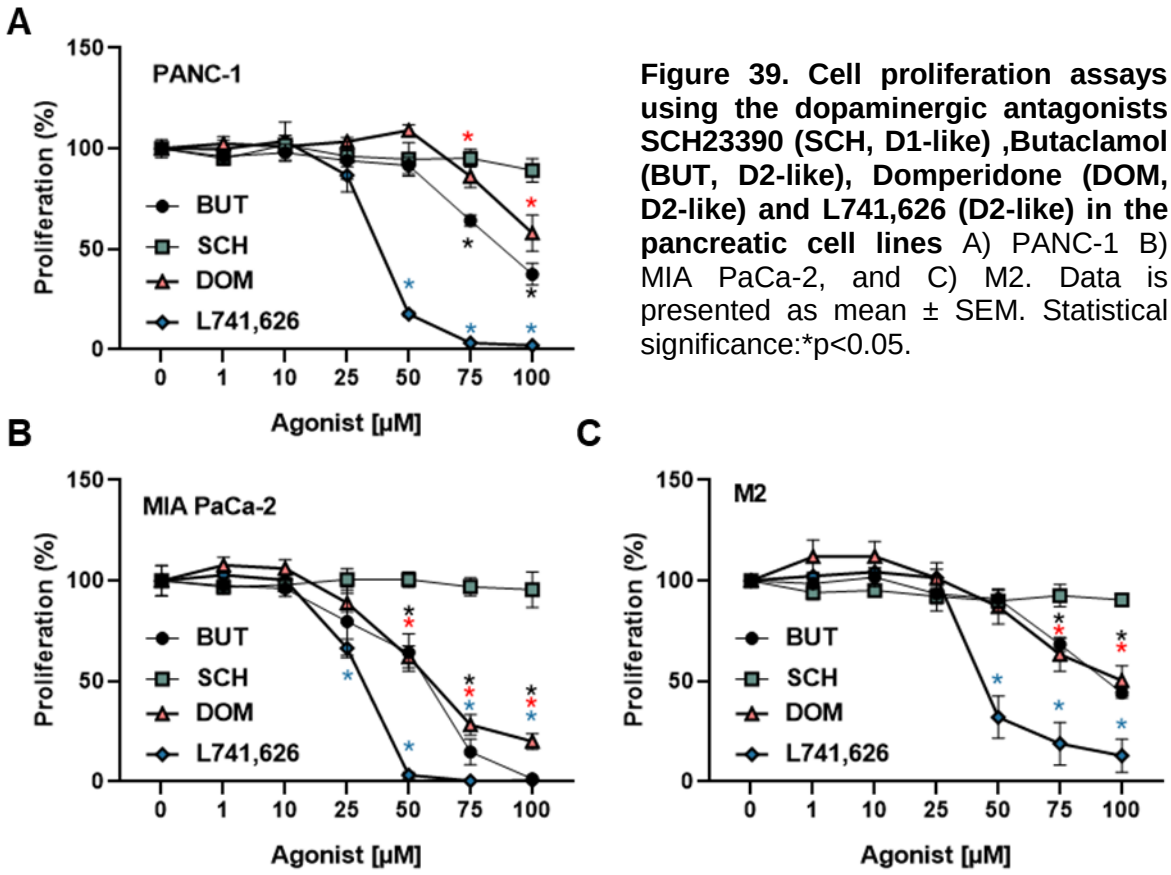

Figure 39. Cell proliferation assays using the dopaminergic antagonists SCH23390 (SCH, D1-like) ,Butaclamol (BUT, D2-like), Domperidone (DOM, D2-like) and L741,626 (D2-like) in the pancreatic cell lines A) PANC-1 B) MIA PaCa-2, and C) M2. Data is presented as mean ± SEM. Statistical significance:*p<0.05.

3.2. Evaluation of the antitumor effect of domperidone in a PANC-1 subcutaneous xenograft model.

To assess the therapeutic effectiveness of domperidone we established a subcutaneous CDX model using PANC-1 cells as described in materials & methods section 2.2.1. After 11 days of daily intragastric treatment, the results

showed that control tumors reached an average of 7.16 times of their initial size, whereas domperidone treated tumors reached a 3.09 times of their initial size (Fig. 40). This difference was statistically significant (p=0.0313).

At necropsy, day 12, we measured tumor weight and volume. The data indicated that control mice's tumors weighed an average of 0.5g and domperidone mice's tumors 0.25g (p=0.0485) (Fig 40 D). Regarding tumor volume, control tumors' average volume was 626 mm^3 and domperidone treated tumor's average volume was 338 mm^3 (Fig 40 C) but results were close to significant (p=0.052).

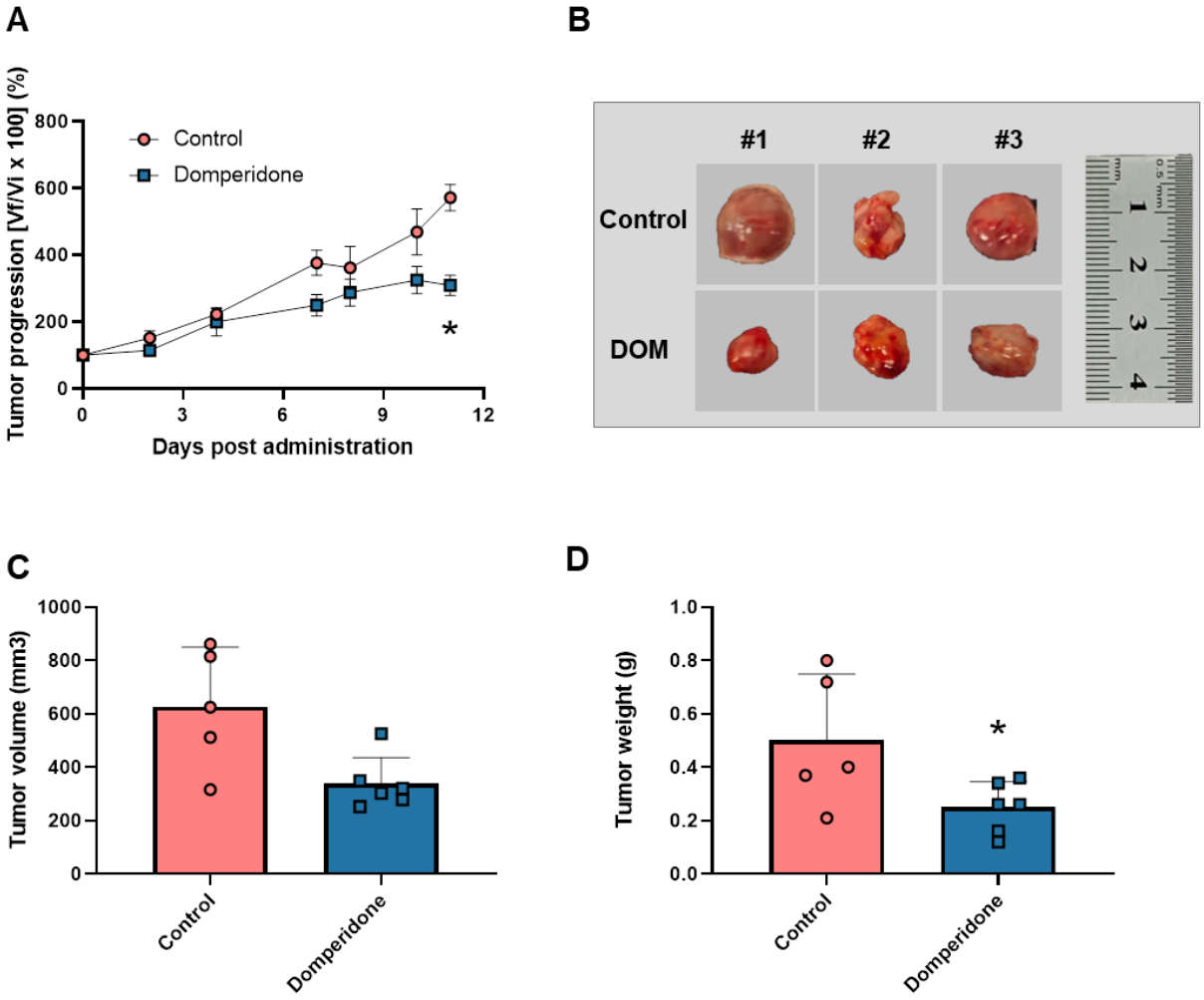

Figure 40. Evaluation of the effect of domperidone (DOM) 20mg/kg/dose on tumor growth in PANC-1 subcutaneous xenografts. (A) Tumor progression curve expressed as percentage of their initial size over 11 days in control and domperidone-treated groups. **(B)** Representative images of excised tumors from both groups, showing macroscopic size differences. **(C)** Average tumor volume (mm^3) and **(D)** tumor weight (g) in each experimental group. Data are presented as mean ± standard error of the mean (SEM). Statistical significance:*p<0.05.

3.2.1. Evaluation of the toxicity of domperidone treatment in a PANC-1 xenograft model.

With the objective of analyzing the toxic impact of domperidone in mice we also weighed mouse body weight 3 to 4 times a week until the end of the experiment. The results showed no statistically significant differences between control and domperidone treated groups over the experiment (Fig. 41 A). Moreover, at the endpoint we weighed brain, heart/lungs liver, kidneys, and pancreas, ex vivo and no statistical significances were found between groups (Fig. 41 B).

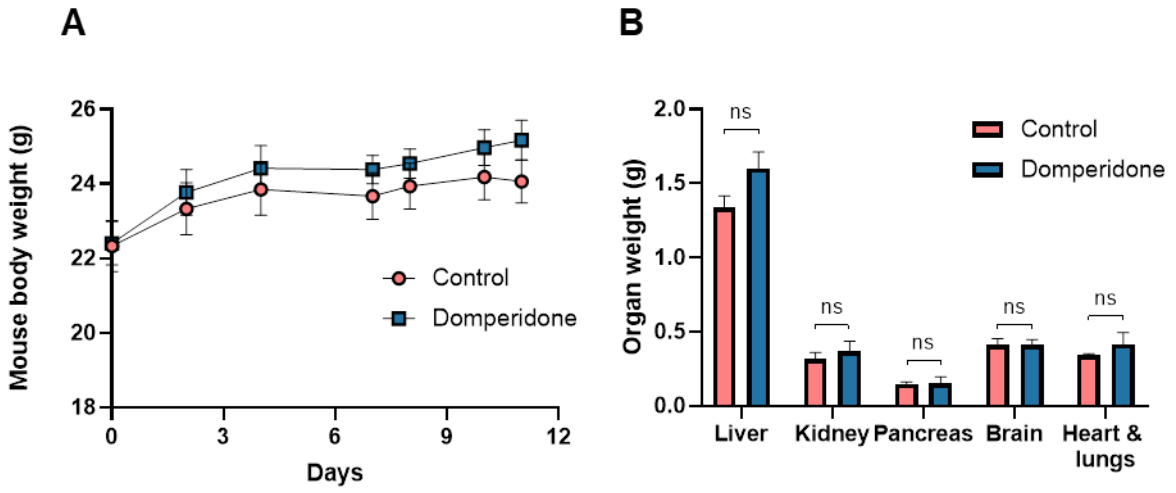

Figure 41. Evaluation of the toxicity of domperidone (DOM) in PANC-1 subcutaneous xenografts. (A) Mice weight progression (g) over 11 days in control and domperidone-treated groups. **(B)** Final weight of the liver, kidneys, pancreas, brain and heart & lungs in control and domperidone-treated groups. Data are presented as mean ± standard error of the mean (SEM). ns= no statistical differences.

4. Evaluation of the combination of D1 activation and D2 inhibition *in vitro*.

4.1. In depth analysis of the activation of dopamine signaling by other available dopamine agonists on proliferation in pancreatic cancer cells.

After these results, we aimed to characterize and improve the effect we observed after activating the DRD1 family. In order to do so we performed a screening of more specific dopamine agonists for the DRD1 families.

For the experiments we used a dose-curve ranging of 10, 25, 50, 75 and 100 µM for 48 hours of fenoldopam and the more selective ligands SKF83822 and SKF82958 in all three lines and SKF83959 in M2 and MIA PaCa-2, which were responding better to the treatments.

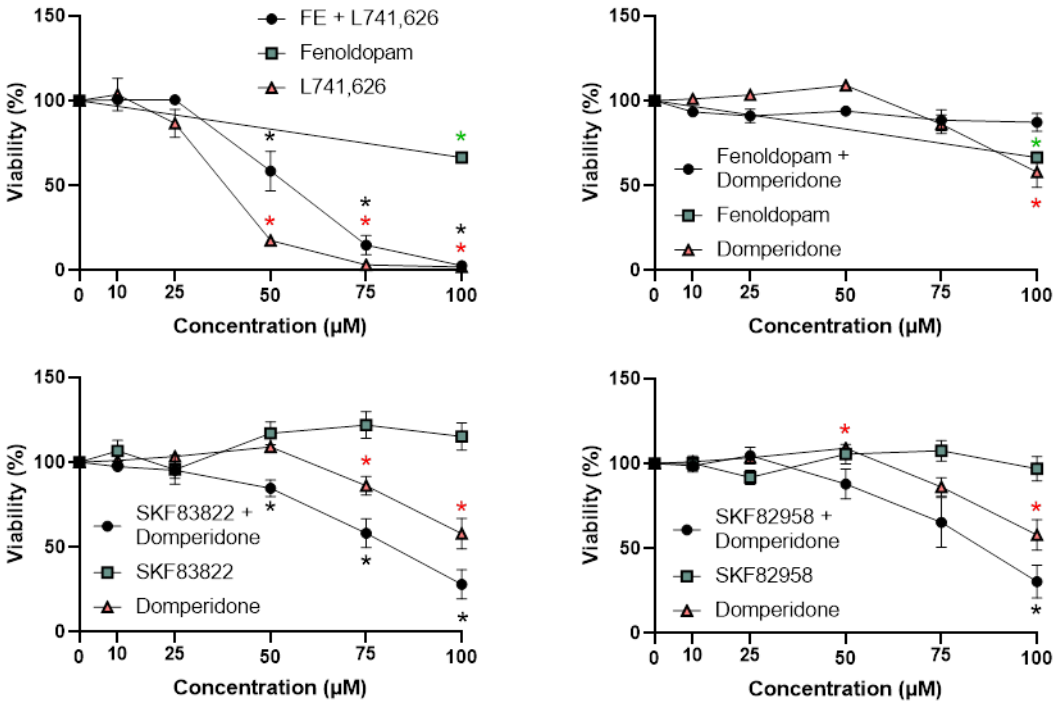

Figure 42. Effect of dopaminergic agonists and antagonists and its combinations in PANC-1 cell viability. Data is presented as mean ± SEM. Statistical significance:*p<0.05.

In PANC-1 cell line (Fig. 42) the cell proliferation reduction after fenoldopam treatment was significant (p=0.029), but SKF83822 and SKF82958 did not produce statistically significant changes in cell proliferation at any tested concentration, suggesting limited or no effect on PANC-1 cell viability under these conditions.

MIA PaCa-2 cell line (Fig, 43) responded better to the dopaminergic treatments. The DRD1 agonist fenoldopam significantly reduced cell proliferation at higher concentrations, with a 22% reduction at 75 μM ($p = 0.0264$) and a pronounced 35% reduction at 100 μM ($p = 0.0001$). SKF83822 elicited a consistent and statistically significant antiproliferative effect, beginning with a 27% reduction at 10 μM ($p = 0.0023$). This effect remained significant across 25 μM ($p = 0.0039$), 50 μM ($p = 0.0004$), 75 μM ($p = 0.0001$), and 100 μM ($p = 0.0001$), with the highest dose resulting in a 58% reduction. SKF82958 also reduced proliferation in a dose-dependent manner, starting with an 18% reduction at 10 mM. Statistically significant effects were observed from 50 μM ($p = 0.0070$) onward, including 75 μM ($p = 0.0002$) and 100 μM ($p = 0.0001$), where a 49% reduction was achieved. SKF83959 induced a strong antiproliferative response, with an 86% reduction observed at 100 μM. However, as the experiment was only performed twice, no statistical analysis was conducted, and the result should be interpreted with caution.

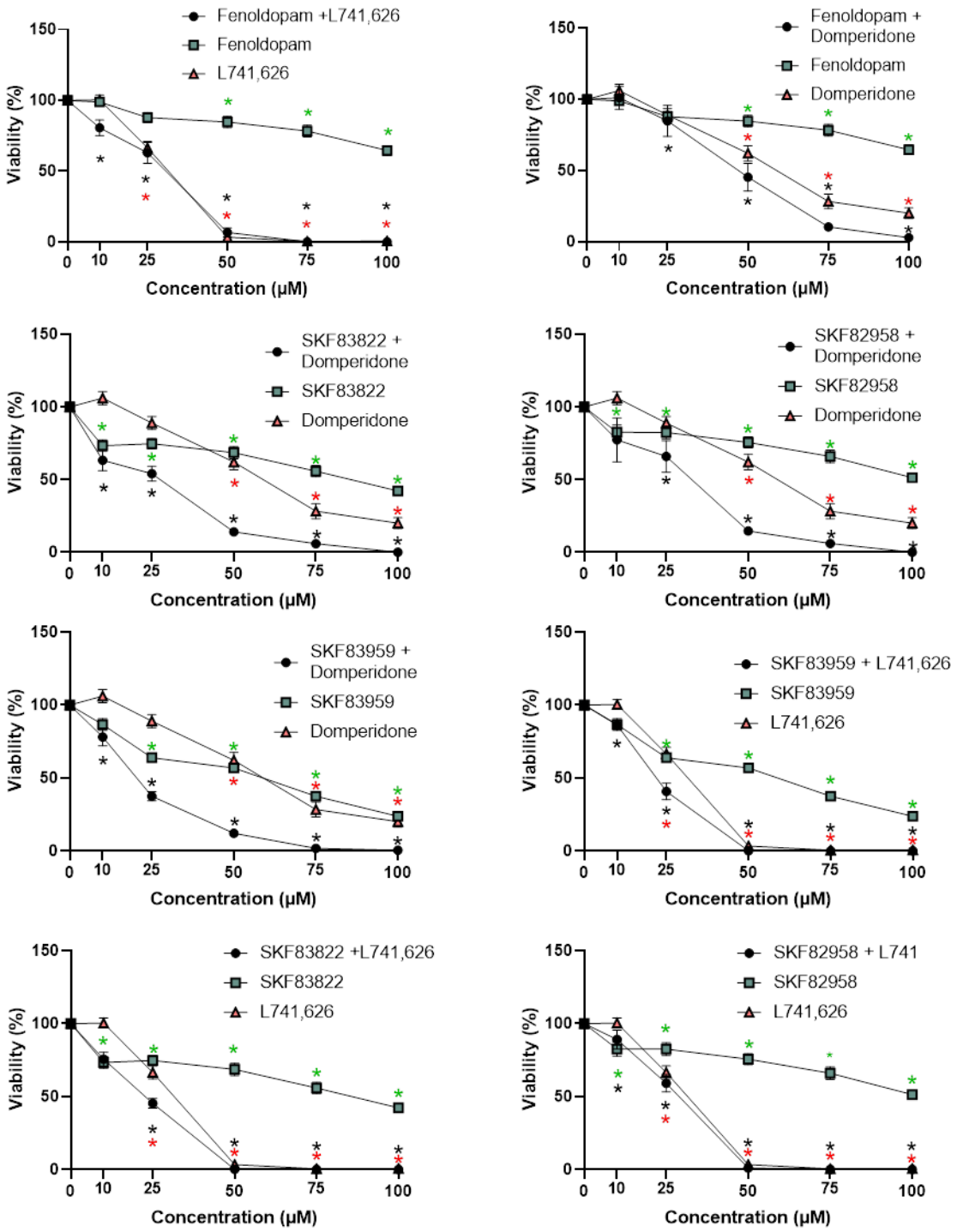

Figure 43. Effect of dopaminergic agonists and antagonists and its combinations in MIA PaCa-2 cell viability. Data is presented as mean ± SEM. Statistical significance:*p<0.05.

The proliferation assays in M2 (Fig. 44) showed that 48 hours after fenoldopam treatment cell proliferation was 42% lower compared to controls ($p=0.023$), SKF83822, and SKF82958 induced minor reductions in cell proliferation at the highest tested dose (100 µM), showing a 6-8% decrease. However, none of these reductions were statistically significant across the tested concentrations. SKF83959 reduced cell proliferation by up to 45% at 100 µM. However, due to the limited number of replicates ($n=2$), no statistical analysis was performed, and these findings should be interpreted as preliminary.

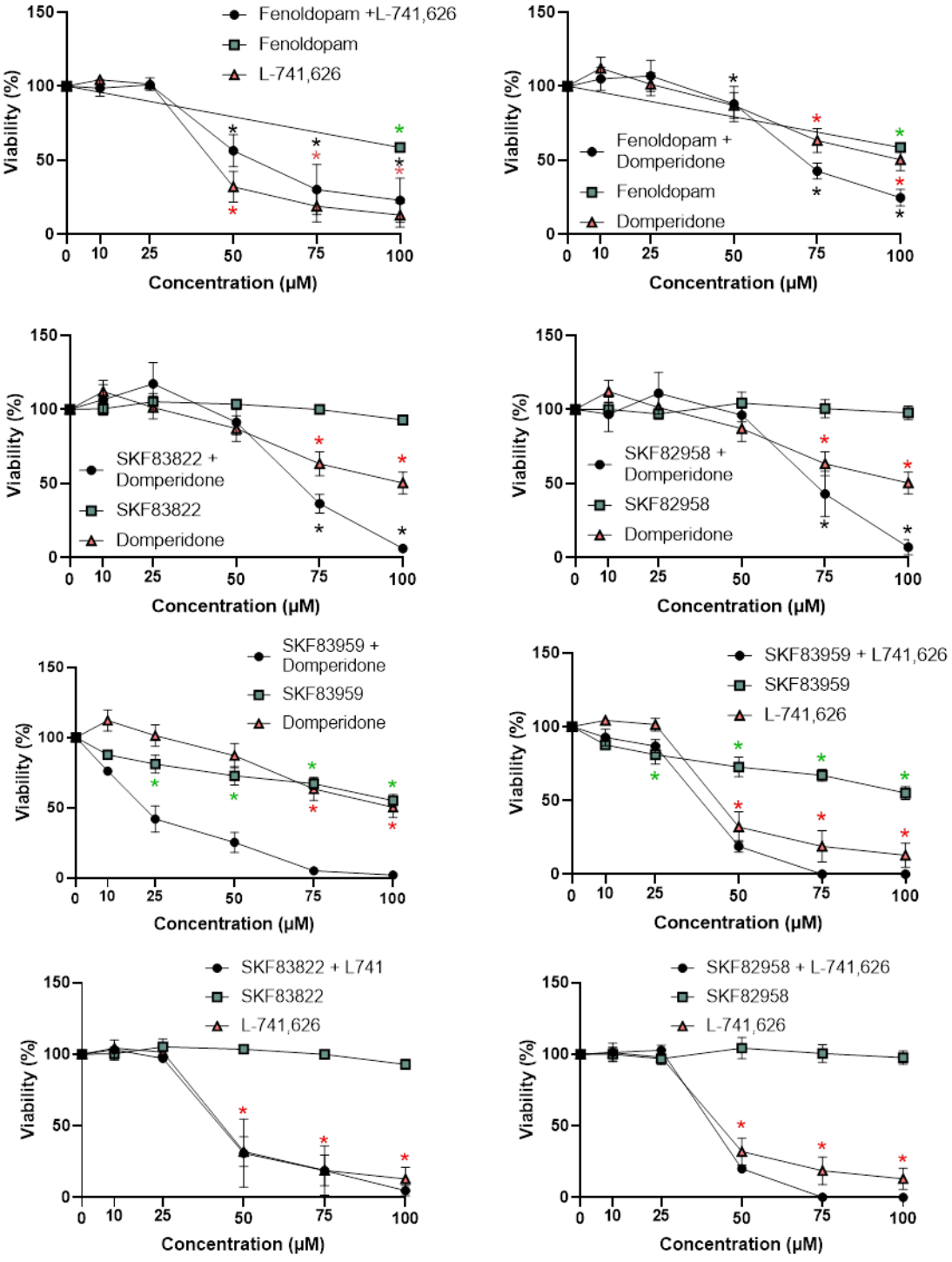

Figure 44. **Effect of dopaminergic agonists and antagonists and its combinations in M2 cell viability**. Data is presented as mean ± SEM. Statistical significance:*p<0.05.

4.2. In depth analysis of the effect of available dopaminergic agonists and antagonists in combination on pancreatic cell proliferation

Next, we sought to study the combined effect of D1 agonism and D2 antagonism. In order to achieve that goal, we used Fenoldopam, SKF83822 and SKF82958 as D1 agonists and Domperidone and L741,626 as D2 antagonists. The selective D1 agonist SKF-83959 was also studied in combination with domperidone and L741,626 in MIA PaCa-2 and M2.

In PANC-1 (Fig. 42) the results show that fenoldopam combined with L741,626 reduces proliferation by 100% at 100µM ($p=0.0001$) but the effect is quite noticeable at 50 µM already where it reaches an 82% reduction ($p=0.0001$), but similar results are achieved with L741,626 as single drug. When combining fenoldopam with domperidone, there are no improvements compared to domperidone administration alone. On the other hand, SKF83822 and SKF82958 in combination with domperidone yielded a 25% difference in proliferation reduction compared to domperidone alone ($p<0.0001$).

In MIA PaCa-2 (Fig. 43), fenoldopam combined with L741,626 reduced significantly cell viability to 0% from 50 µM to 100µM ($p<0.0001$) but these results were also achieved with L741,626 alone. Fenoldopam with domperidone reached almost a 100% reduction in proliferation at 100µM ($p=0.0220$) in comparison to the 85% reduction of domperidone alone. The combination of SKF83822, SKF82958 and SKF-83959 with domperidone yielded similar results, reaching a 100% decrease at 100µM ($p=0.0011$), which is 20% stronger than domperidone administered alone. The combination of SKF83822, SKF82958 and SKF-83959 with L741,626 did not differ from the single use of L741,626.

Finally, fenoldopam combined with L741,626 in M2 cell line (Fig. 44) yielded a mild 10% increase from 50 µM to 100 µM compared to L741,626 alone, reaching a 88% decrease at the highest concentration ($p<0.0001$). The combination of fenoldopam

and domperidone was 25-32% stronger than the single drug administration, reaching a 75% reduction at 100µM (p=0.0131). SKF83822 and SKF82958 with domperidone highly improved the results of the single administration, reaching 94 and 93% reduction respectively (p<0.0001 and p= 0.0004) SKF-83959 with domperidone yielded similar results but the experiment was only performed twice so no statistical analysis was conducted, and the result should be interpreted with caution. SKF83822, SKF82958 and SKF-83959 with L741,626 were similar or slightly better than the single administration of L-741,626, but, as the experiments were performed only twice, no statistical analysis was executed and results should be taken as preliminary.

4.3. Pancreatic cancer spheroid formation and characterization.

To investigate the effects of dopaminergic agonists and antagonists on the pancreatic cancer stem-like cell population, we first developed a robust spheroid formation protocol using anchorage-independent culture of PANC-1, MIA PaCa-2, and M2 cells. This optimization process involved testing three initial seeding densities—500, 1000, and 3000 cells per well—and monitoring spheroid development at 24, 48, and 72 hours post-seeding across the three pancreatic cancer cell lines. The results are represented in Fig. 45, 46 & 47.

These results revealed that higher seeding densities resulted in larger spheroid aggregation, especially in M2 and MIA PaCa-2. However, to ensure consistency, reproducibility, and size across all lines, seeding 1000 cells per well and analyzing spheroids 72 hours post-seeding provided the most reliable conditions. These parameters were thus selected for all subsequent experiments involving cytotoxic evaluation of dopamine drugs in PANC-1, MIA PaCa-2, and M2 derived- spheroids.

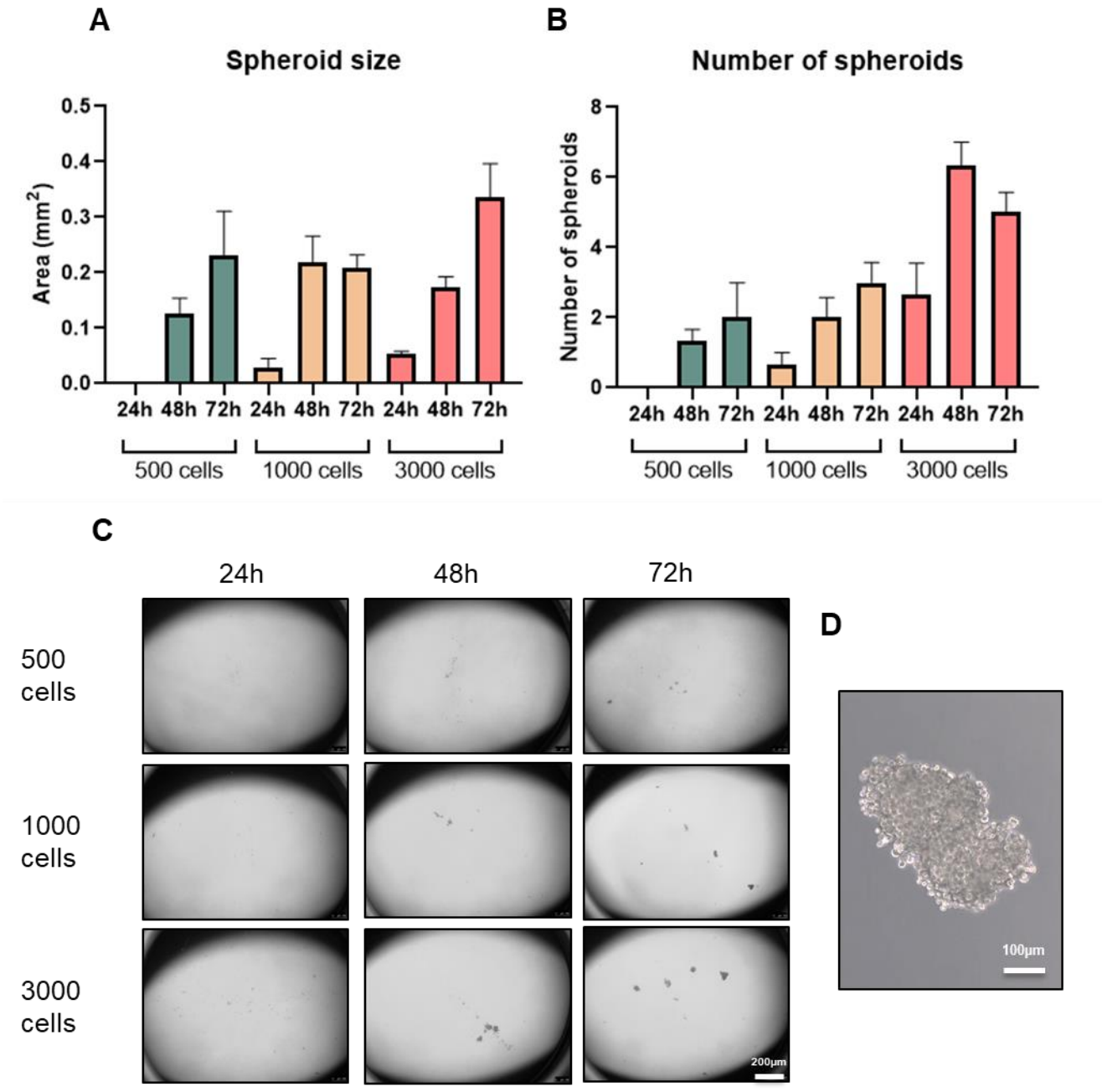

Figure 45. PANC-1 spheroid growth formation at 24, 48 and 72h after seeding 500, 1000 and 3000 cells. A) Spheroid size at specified conditions. B) Number of spheroids at specified conditions. C) Pictures taken at 100x magnification. Scale bar = 200µm D) Picture of a PANC-1 spheroid taken at 200x magnification. Scale bar = 100 µm. Data is represented as mean ± SEM.

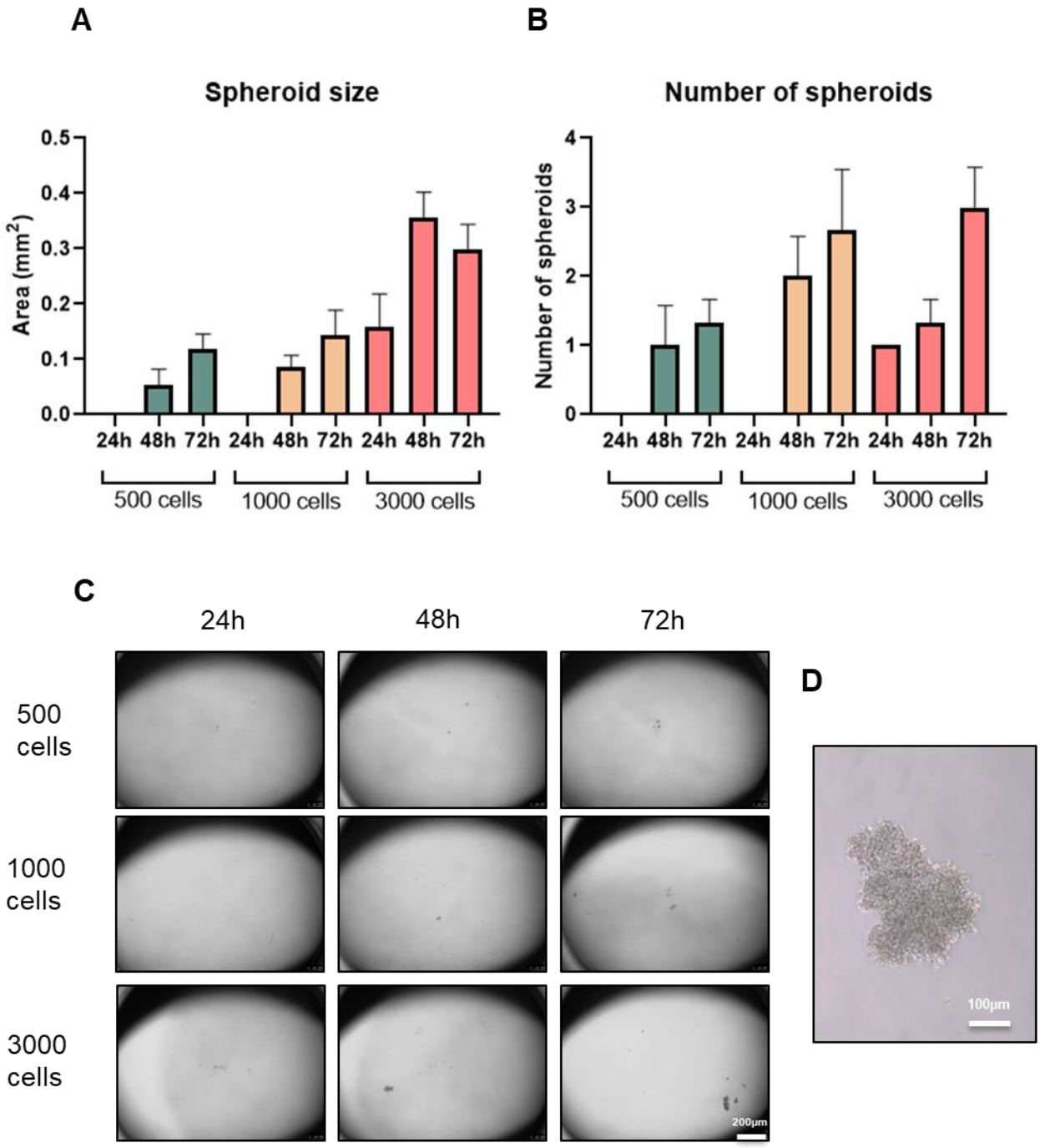

Figure 46. MIA PaCa-2 spheroid growth formation at 24, 48 and 72h after seeding 500, 1000 and 3000 cells. A) Spheroid size at specified conditions. B) Number of spheroids at specified conditions. C) Pictures taken at 100x magnification. Scale bar = 200µm D) Picture of a MIA PaCa-2 spheroid taken at 200x magnification. Scale bar = 100 µm. Data is represented as mean ± SEM.

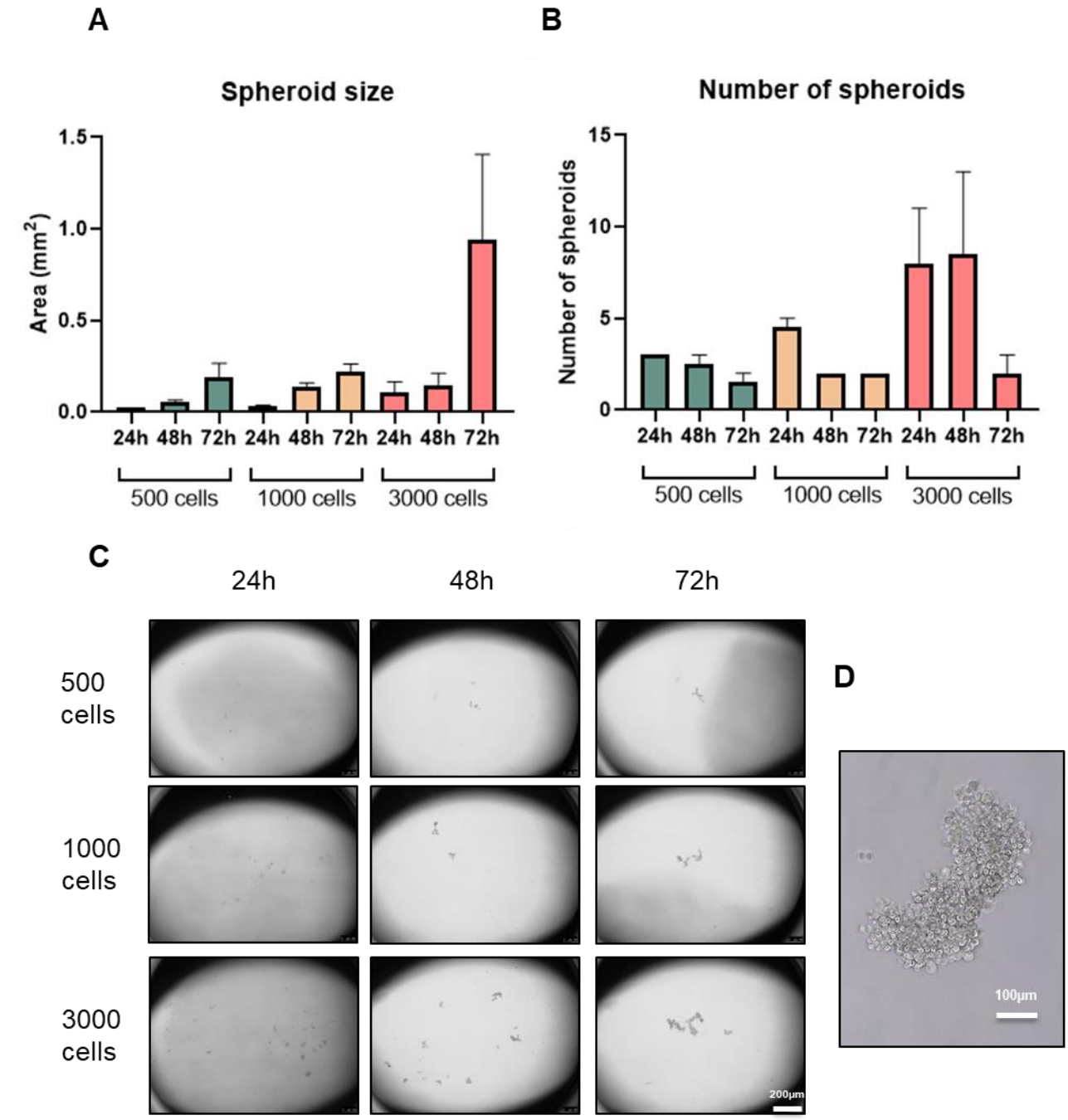

Figure 47. M2 spheroid growth formation at 24, 48 and 72h after seeding 500, 1000 and 3000 cells. A) Spheroid size at specified conditions. B) Number of spheroids at specified conditions. C) Pictures taken at 100x magnification. Scale bar = 200µm D) Picture of a M2 spheroid taken at 200x magnification. Scale bar = 100 µm. Data is represented as mean ± SEM. Statistical significance:*p<0.05.

4.4. Expression of dopamine receptors in PANC1, MIA PaCa-2 and M2 derived spheroids

To study whether the spheroids retained the expression of dopaminergic receptors, we conducted reverse transcription polymerase chain reaction (RT-PCR) using probes specific to each dopaminergic receptor subtype (see Materials and Methods, Section 1.6). The results showed that PANC-1 derived spheroids maintained expression of the mRNA for D1-like receptors but the ratio changed, having D5 double the expression of to D1. MIA PaCa-2 derived spheroids also had a similar increase in D5 receptor expression. On the other hand, M2 and MIA PaCa-2 spheroids exhibited increased expression of the D2 receptor; along with a slight decrease in D1-like receptor expression reaching D2 almost double the expression of D1 in M2 derived spheroids and twice the expression of D5 in MIA PaCa-2. (Fig 48 A) Additionally, we analyzed the protein expression of DRD1, DRD2, and DRD5 using the Western blot technique. All three receptors were detected in the pancreatic cancer spheroids, confirming their presence at the protein level.in all pancreatic cancer spheroids (Fig. 48 B).

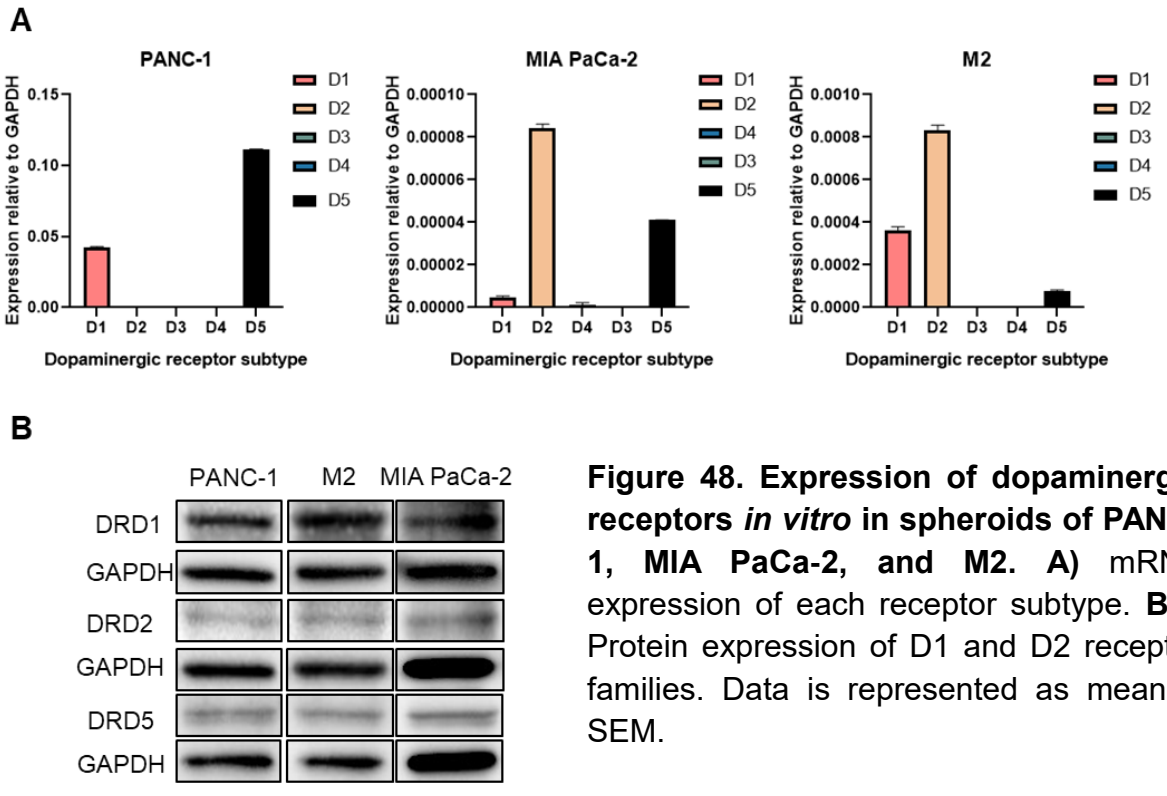

Figure 48. Expression of dopaminergic receptors *in vitro* in spheroids of PANC-1, MIA PaCa-2, and M2. A) mRNA expression of each receptor subtype. **B)** . Protein expression of D1 and D2 receptor families. Data is represented as mean ± SEM.

4.5. Evaluation of the cytotoxic effect of dopaminergic agonists and antagonists on PANC1, MIA PaCa-2 and M2 derived spheroids

Following the optimized experiment, we conducted cytotoxic viability assays on M2 (Fig. 49) ,PANC-1 and MIA PaCa-2 (Fig. 50) and spheroids using a single dose of fenoldopam (87μM) and SKF 83822 (40 μM), selective D1 agonists and domperidone (30 μM) , the D2 blocker and the combination of fenoldopam with domperidone (87/30 μM) .After 48 hours of exposure the results showed that the dopaminergic agonist SKF 83822 reduced the size of the spheroids, reaching 50% in PANC-1 and MIA PaCA-2 and a 60% in M2. Moreover, the number of spheroids was reduced in PANC-1 by a 20%, in M2 by a 33% and in MIAPaCa-2 by a 66% (n=2). Domperidone notably reduced the size in all 3 cell lines, being statistically significant in M2 spheroids (p=0.263), though the effect on spheroid number varied among the cell lines. Fenoldopam treatment reduced the number of spheroids in PANC-1 by 60%, in M2 by 55% and in MIA PaCa-2 by 66% (n=2). The size of the spheroids after fenoldopam treatment was reduced also in PANC-1 by a mild 25%, in M2 by a 52% and in MIA PaCa-2 the reduction was not noticeable (Fig. 50). The effect of the drug combination was quite pronounced as size of the spheroids was drastically reduced reaching a 36% compared to controls in PANC-1, a 50% in MIA PaCa-2 and a statistically significant 10% (p=0.266) in M2 (Fig. 49). The number of spheroids after the combination treatment was reduced by 60% in PANC-1, by 50% in MIA PaCa-2 and by 33% in M2.

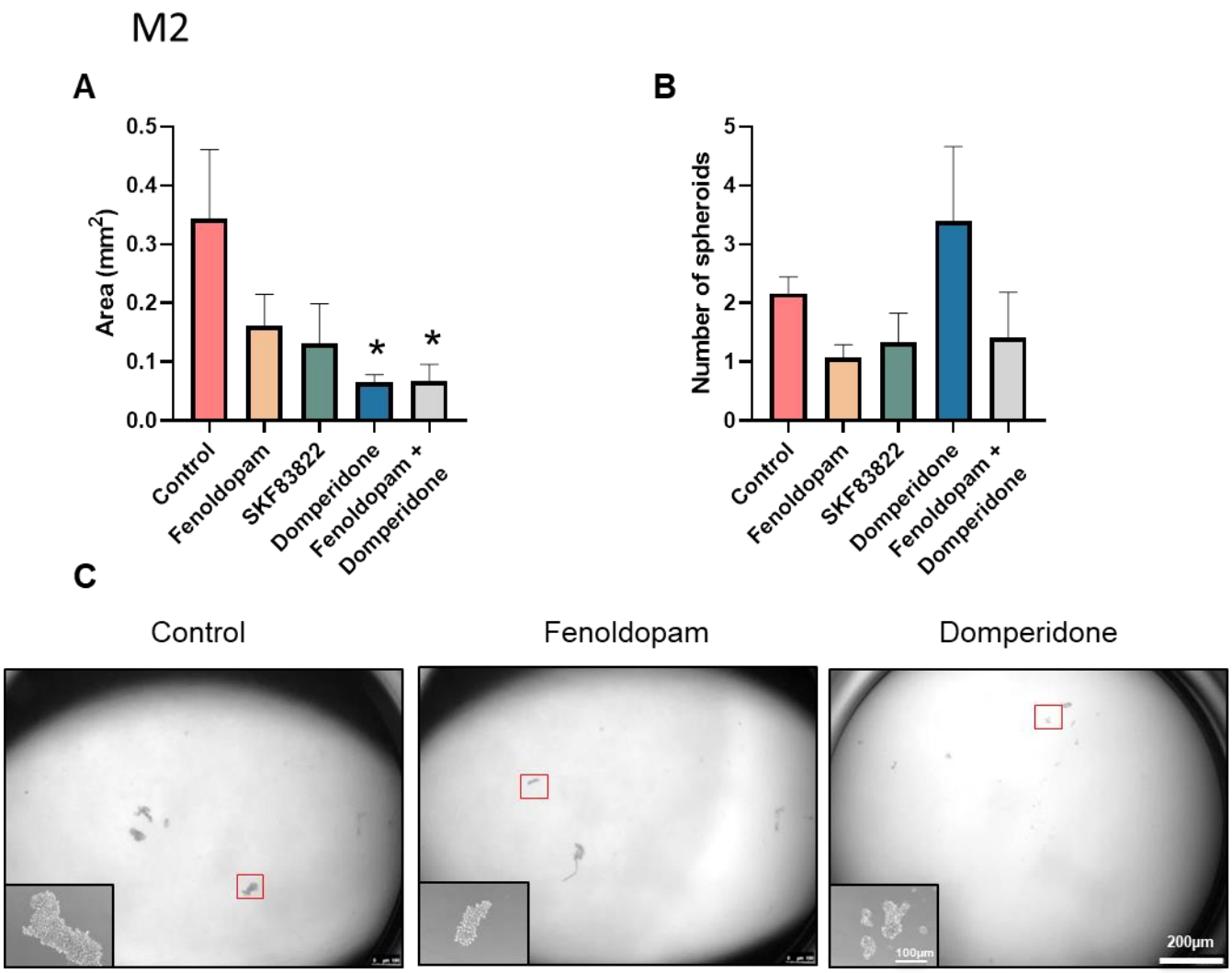

Figure 49. Effect in M2 spheroids after dopaminergic treatments. **A)** Average size of the spheroids after dopaminergic treatments. **B)** Average number of spheroids per well after dopaminergic treatments. **C)** Microscopy images of M2 spheroids after dopaminergic treatments. Scale bar = 200µm. Scale bar of insert= 100 µm. Data is represented as mean ± SEM. Statistical significance:*p<0.05.

A

Cell line	Characteristic	Control	Fenoldopam	SKF83822	Domperidone	Fenoldopam + Domperidone
PANC-1	Spheroid size	0.21±0.08	0.16±0.07	0.09±0.03	0.07±0.01	0.08±0.02
	N of spheroids	6.41±1.34	2.80±1.09	4.80±2.23	3.40±0.91	2.60±0.83
MIA PaCa-2	Spheroid size	0.09±0.04	0.07±0.06	0.04±0.04	0.04±0.02	0.04±0.03
	N of spheroids	4.36±1.53	1.33±1.00	1.67±1.67	4.17±3.83	2.17±1.83

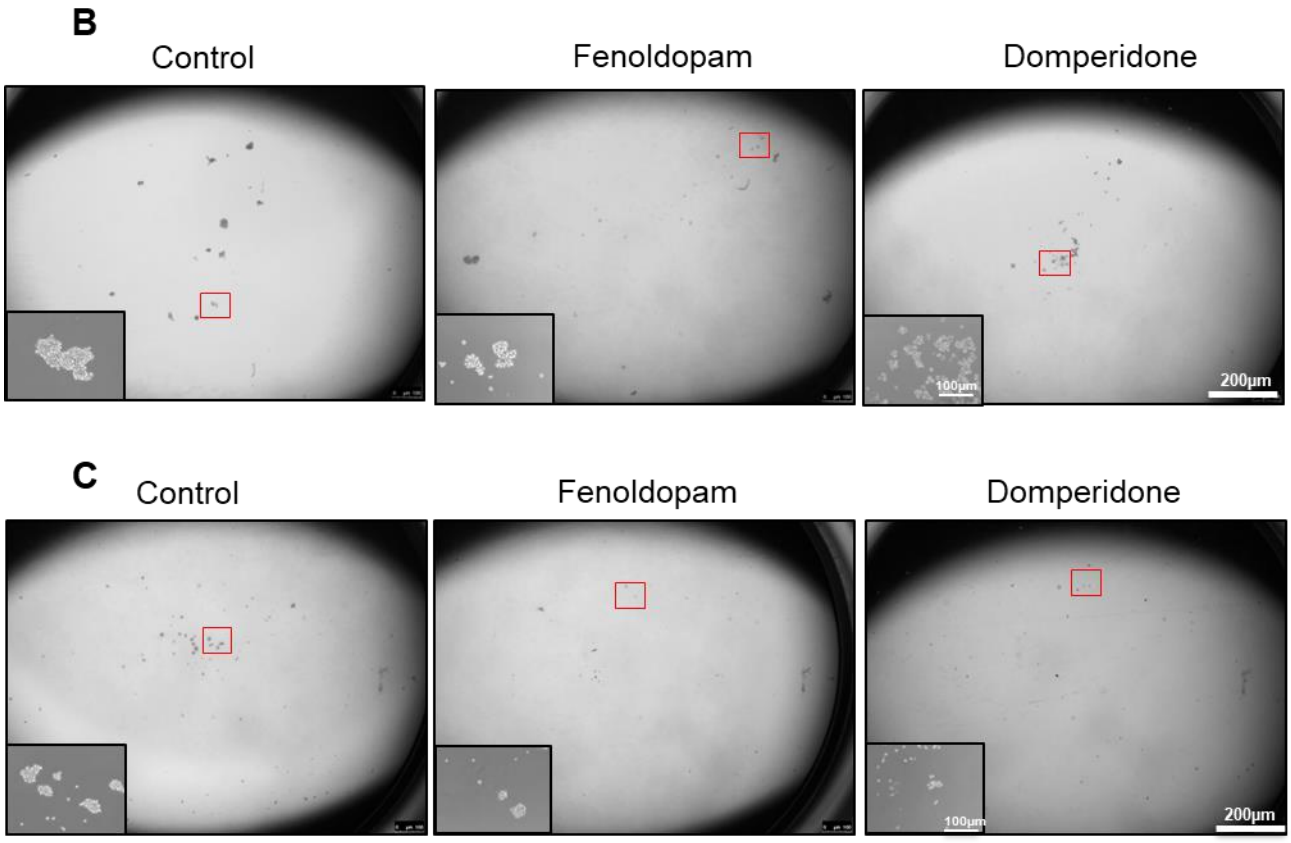

Figure 50. Dopaminergic treatment's effect in PANC-1 and MIA PaCa-2 spheroids. **A)** Table representing the spheroid size and number of spheroids 48h after dopaminergic treatments. Results are presented as mean ±SEM. **B)** Microscopy images of the PANC-1 spheroids after dopaminergic treatments. **C)** Microscopy images of the MIA PaCa-2 spheroids after dopaminergic treatments. Scale bar = 200µm. Scale bar of insert= 100 µm. Data is represented as mean ± SEM.

5. Functional characterization of vault-based nanoparticles and nanobodies in pancreatic cancer cell lines.

To enhance the bioavailability and therapeutic efficacy of dopamine drugs, our group collaborated with Dr. JL Corchero's laboratory. Their team developed vault-based nanoparticles for use as a drug delivery system. We tested, both in pancreatic cancer cell lines and in pancreatic tumor models *in vivo*, various prototypes of these vaults, with or without a tumor-targeting peptide (TPP) and/or a cytotoxic domain (TNR), with the aim of further conjugating with dopaminergic drugs.

5.1. Evaluation of vault-based nanoparticle internalization.

To evaluate the capacity of vault-based nanoparticles for cellular uptake, PANC-1 cells were exposed to GFP-loaded nanoparticles, either with (V-TPP) or without TPP (V), at concentrations of 5 and 10 nM. Two hours after the administration, a flow cytometry assay was carried on and the nanoparticle uptake was evaluated by flow cytometry (Fig. 51 C). The results showed that nanoparticles loaded with TPP were internalized in approximately 10% and 15% of cells at 5 and 10 nM, respectively. In contrast, nanoparticles lacking TPP also entered the cells but at nearly half the rate observed for TPP-functionalized nanovaults. Experiments were only carried twice, so no statistical test was performed.

5.2. Cytotoxic effects of vault-based nanoparticles.

To evaluate whether the empty nanoparticles exerted intrinsic cytotoxic effects and to evaluate their potential as efficient drug delivery vehicles, we also functionalized the nanoparticles with a cytotoxic compound, TNR as preliminary prototype. Proliferation assays were conducted in PANC-1 and MIA PaCa-2 cells (Fig 51 A, 51 B & 52). The conditions tested included nanovaults without TPP (V), nanovaults with TPP (V-TPP), and nanovaults with TPP loaded with TNR (V-TPP-TNR).

The results indicated no statistically significant differences between nanoparticles with and without TPP. When the nanoparticle is loaded with TNR it reduces proliferation to 43% in PANC-1 and 72% in MIA PaCa-2. The comparison between V-TPP and V-TPP-TNR yielded a statistically significant difference in PANC-1 (p= 0.0397) and in MIA PaCa-2 (p = 0.0001) cell lines. This analysis was based on a very limited sample size (n = 2 per group); the results are preliminary and an additional experiment must be conducted to corroborate these positive results.

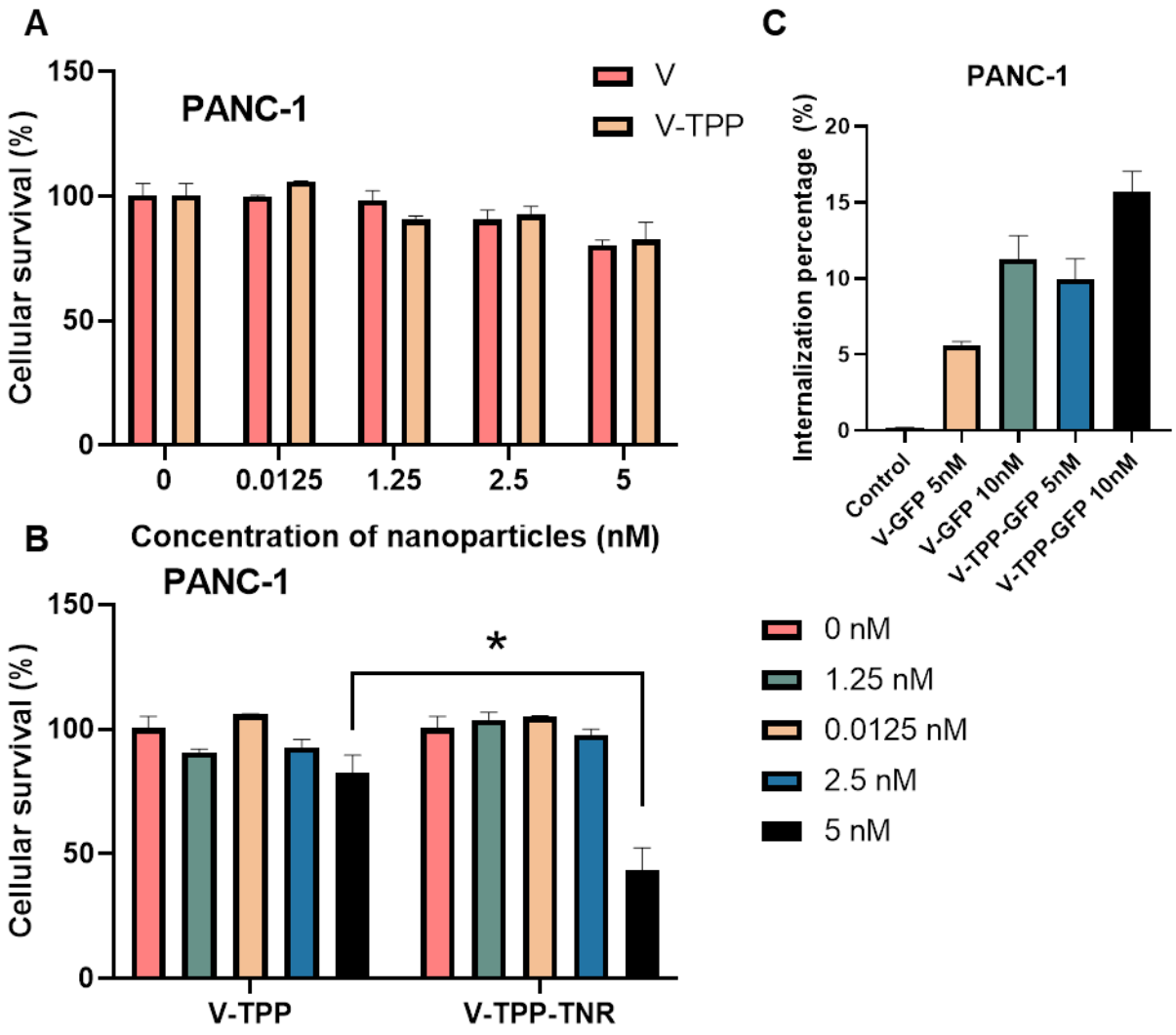

Figure 51. Nanoparticle cytotoxicity and internalization in PANC-1 cell line. (A-B) Cell survival (%) relative to control 48h after administration of nanoparticles at given doses. **A)** Vault and Vault-TPP **B)** Vault TPP vs Vault-TPP-TNR. **C)** Percentage of cells that internalized the nanoparticle at given doses. V= Vault, GFP= green fluorescent protein, TPP= Tumor-penetrating peptide, TNR= cytotoxic compound. Data is presented as mean ± SEM. Statistical significance:*p<0.05.

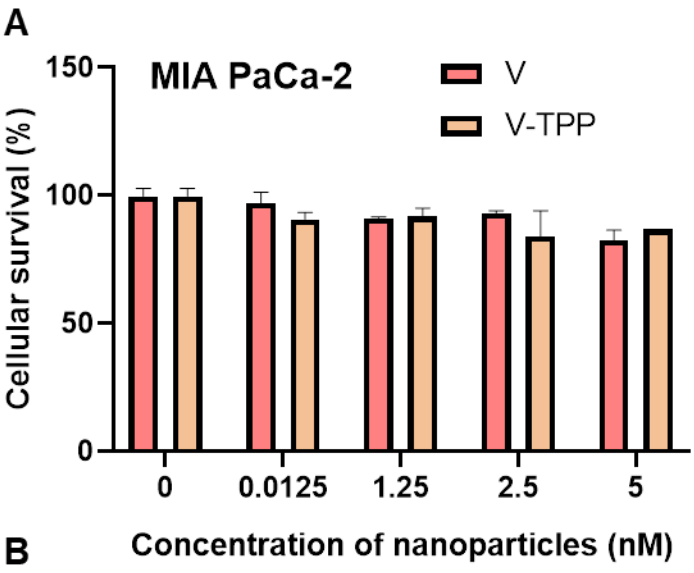

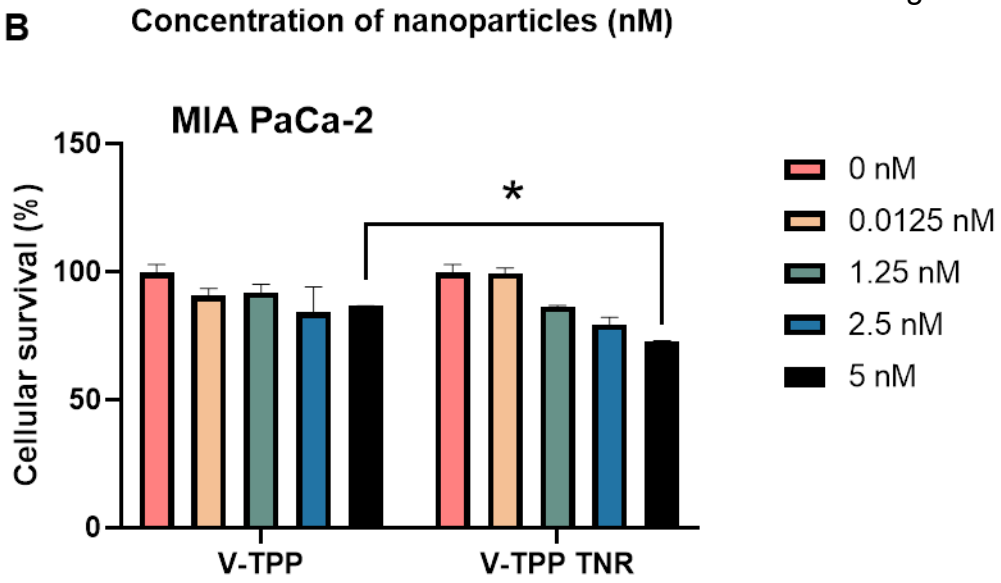

Figure 52. Nanoparticle cytotoxicity and internalization in MIA PaCa-2 cell line. Cell survival (%) relative to control 48h after administration of nanoparticles at given doses. **A)** Vault and Vault-TPP **B)** Vault TPP vs Vault-TPP-TNR.. V= Vault, TPP= Tumor-penetrating peptide, TNR= cytotoxic compound. Data is presented as mean ± SEM. Statistical significance:*p<0.05.

5.3. Vault-based nanoparticle biodistribution in PANC-1 subcutaneous xenograft model.

Another key step in the functional characterization of nanovaults as drug delivery nanocarriers was the analysis of their biodistribution *in vivo*. To enable fluorescence detection, the nanovaults were loaded with GFP. Mice bearing PANC-1 subcutaneous tumors were intravenously administered with vehicle (buffer), V-GFP, or V-GFP-TPP nanoparticles. Tumors and major organs were

collected at 5- and 24-hours post-administration, and fluorescence levels were quantified ex vivo using the IVIS Spectrum 2000 system.

The results indicated nanoparticle accumulation in tumors, with fluorescence intensity being 0.1 times higher at 24 hours compared to 5 hours with or without TPP (Fig. 53). Moreover, tumors treated with V-GFP-TPP nanoparticles exhibited 0.35 times more fluorescence than those treated with V-GFP variants. No accumulation of nanoparticles was detected in any of the analyzed organs (Fig. 54).

Additional experiments are needed to validate these promising findings. We are currently collaborating with Dr. Corchero's laboratory to scale up nanoparticle production and dopaminergic drug conjugation/encapsulation enabling us to produce a larger quantity for analyses and *in vivo* studies to evaluate the therapeutic effects of dopaminergic drug-derived vault nanoparticles.

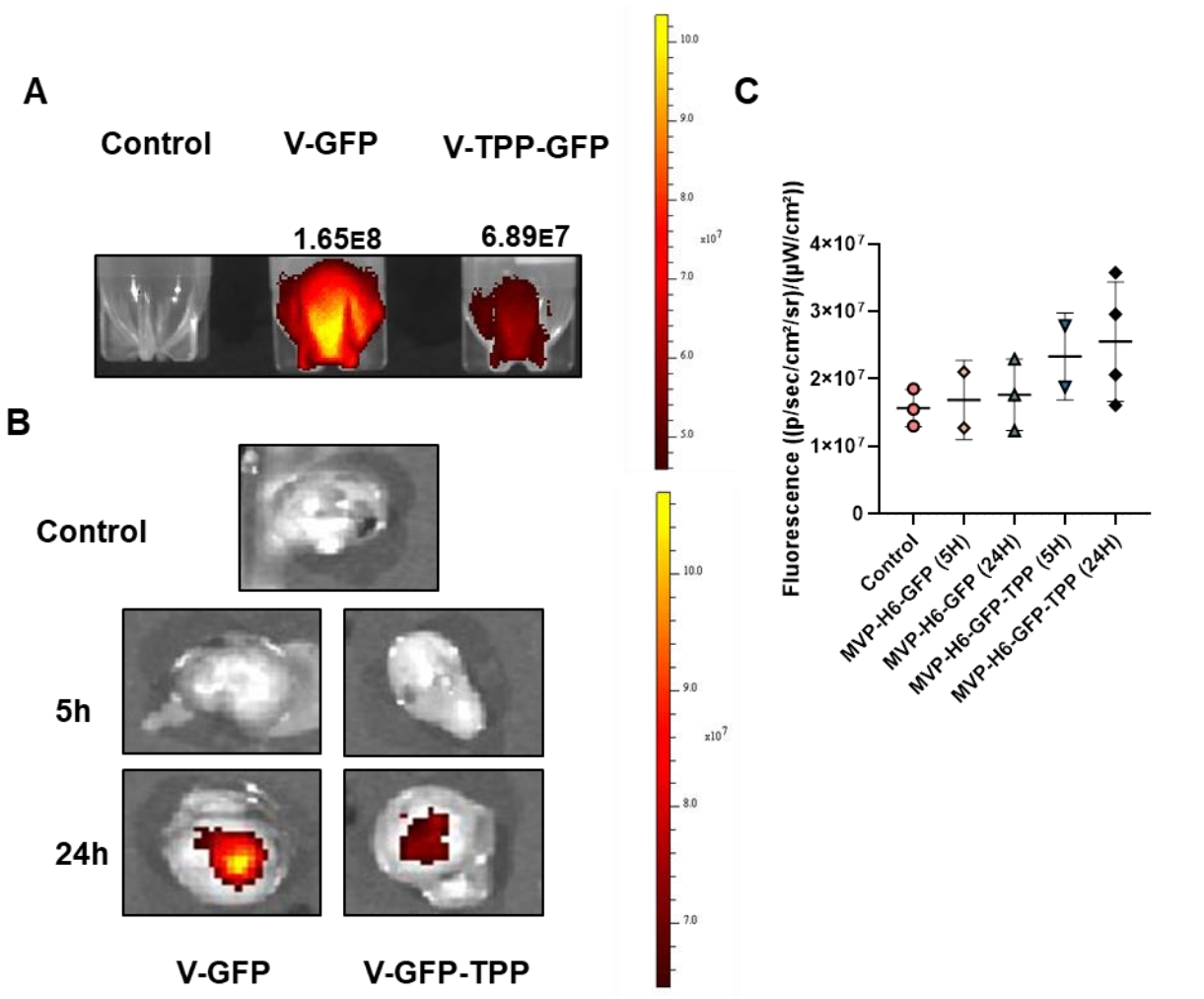

Figure 53. Nanoparticle biodistribution in PANC-1 subcutaneous mouse model. Nanoparticles were loaded with GFP to measure FLI. A) Image of the tumors 5 and 24h after ravenous injection of nanoparticles (400 µg) using In Vivo Imaging Software. **B)** Graphical representation of the fluorescence of PANC-1 subcutaneous tumors 5 and 24h after ravenous injection of nanoparticles (400 µg). V= Vault, GFP= green fluorescent protein, TPP= Tumor-penetrating peptide.

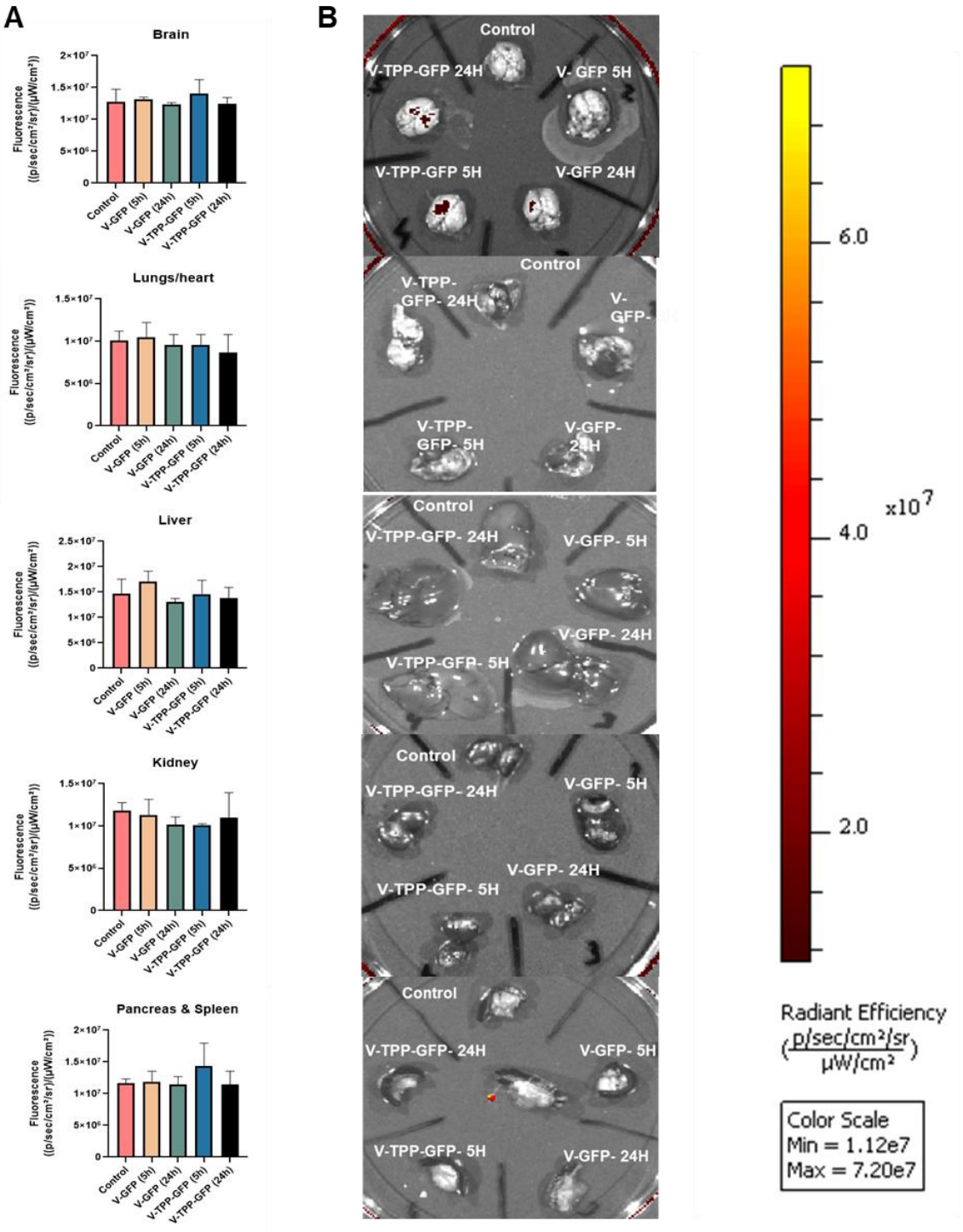

Figure 54. Nanoparticle biodistribution in PANC-1 subcutaneous mouse model. Nanoparticles were loaded with GFP to measure FLI. A) Graphical representation of the fluorescence of mice brains, lungs/heart, liver, kidneys and pancreas/spleen 5 and 24h after intravenous injection of nanoparticles (400 µg) **B)** Image of the brains, lungs/heart, liver, kidneys and pancreas/spleen 5 and 24h after intravenous injection of nanoparticles (400 µg) using In Vivo Imaging Software. V= Vault, GFP= green fluorescent protein, TPP= Tumor-penetrating peptide. Data is presented as mean ± SEM.

5.4. Cytotoxic effects of D1 receptor-targeted nanobodies.

Additionally, we explored an alternative approach to develop selective ligands for the D1 receptor in collaboration with Dr. Corchero's lab. Using phage display technology, we generated two peptides (Nanobody 2 and Nanobody 8). As a preliminary assay, we assessed the cytotoxicity of increasing concentrations (0.01, 0.10, 0.25, 0.50, 0.75, and 1.00 µM) of the two selected clones against this receptor (Fig. 55).

In MIA PaCa-2 cells, no significant cytotoxic effect was observed. However, in PANC-1 cells, both nanobodies induced a 13% reduction in viability at a concentration of 1 µM. In M2 cells, Nanobody 2 led to a 16% reduction in viability, while Nanobody 8 caused a 23% reduction at the same concentration. Additional experiments are required to validate these promising results.

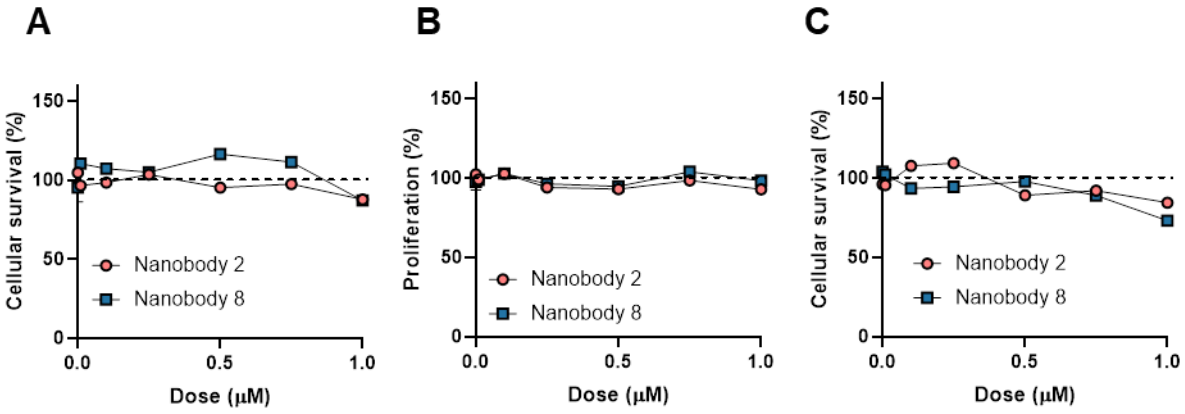

Figure 55. Effect on cell survival on pancreatic cell lines 48h after treatment with nanobodies at 0.01 to 1 µM. A) PANC-1 **B)** MIA PaCa-2 **C)** M2. Data is presented as mean ± SEM. N=2 in duplicates.

V. DISCUSION

Nowadays, being diagnosed with pancreatic cancer is a death sentence. PC is the third leading cause for cancer-related deaths worldwide [1]. **The 5 year-survival rate is around 5-7%**. Moreover, less than **20% of patients survive** after the first year[125]. Research need to focus in improving early diagnose as there are not good protocols or biomarkers yet. On the other hand, current treatments are not sufficient and are usually associated with high toxicity. There is an **urgent emergency** in the development of **new strategies** and drugs to improve therapeutic options and survival of pancreatic patients.

Over the past decade, the significant role of the **nervous system** in the initiation and **progression of cancer** has become increasingly evident. Nerve fibers are integrated in the tumor microenvironment and catecholamines and their neuroreceptors have emerged as one of the mediators in cancer progression.

We hypothesized that neural signaling, which is involved in cell proliferation and migration within our body's stem cell niches may also influence tumor growth, migration, and interact within the tumor microenvironment of pancreatic tumors. Our study focused on exploring novel molecular aspects of pancreatic cancer in relation to **neuromodulation** and new strategies for **pancreatic cancer therapy**.

In this work, we first validated **dopamine receptor signaling** as a novel **therapeutic target** for pancreatic cancer. We utilized both *in vitro* 2D and 3D cultures of established pancreatic cell lines, along with *in vivo* cell line-derived xenograft (CDX) **preclinical models**, to assess the effectiveness of potential **repurposed dopaminergic drugs**. Additionally, as part of our project's objectives, we collaborated with Dr. JL Corchero's team to integrate nanoparticles aimed at **enhancing drug delivery**. This approach not only intends to increase the therapeutic dose but also to **minimize side effects**, thereby facilitating the potential **clinical translation** of this innovative treatment strategy.

1. Antiproliferative effect of the activation of dopaminergic signaling.

Boilly et al. [42] had already described on his work, that tissue regeneration is nerve dependent and Magnon and cols. [126] coined, for the first time the concept of nerve dependence in cancer. Magnon and cols also described that new sympathetic fiber formation (neonerves) were involved in the early stages of tumorigenesis, while the parasympathetic innervation is accomplished in later stages.

Adrenergic signaling has been extensively studied and some beta-adrenergic blockers, such as propanolol, are currently under clinical trials for cancer treatment [127]. Our results in pancreatic cells, consistent with findings in other cancer types, indicate that adrenergic signaling mediated by norepinephrine (NE) and epinephrine (E) significantly impacts cell proliferation, although it varies across cell lines. In contrast, dopamine exhibited an antiproliferative effect in all the tested pancreatic cell lines.

Early evidence of dopamine's role in cancer was provided by Dalton et al. [128] and subsequently Driver et al. [129] reported a reduced incidence of several cancers among patients with schizophrenia or Parkinson’s disease. These observations suggested that dopamine receptors may represent potential targets for the modulation of cancer growth.

Dopamine (DA) is a catecholamine that functions as a neurotransmitter in the brain, but it also acts as both a neurotransmitter and a circulating hormone in the periphery [130]. Peripheral dopamine is sourced from sympathetic nerve fibers, catecholamine-producing cells like adrenal medulla chromaffin cells, and neuroendocrine cells of the APUD system found in the kidney's exocrine and endocrine regions.[131]. Dopamine receptors are expressed in peripheral tissues such as the kidney, gut, and coronary arteries, and their dysregulation has been linked to conditions like hypertension, gastrointestinal motility disorders, and metabolic dysfunction [132].

Emerging research indicates that dopamine plays a role in regulating cell survival and proliferation, which may vary depending on the cell type. In non-transformed cells, dopamine generally supports proliferation and survival, while in tumor cell lines it often shows predominantly antiproliferative properties [133].

In mouse experimental models, chemical sympathectomy (by intraperitoneal injection of the neurotoxin 6- hydroxydopamine) stimulates malignant tumor growth [134] whereas dopamine slows down the growth of xenotransplanted human gastric cancer, an effect attributed to inhibition of angiogenesis [135]. Furthermore, administration of dopamine to mice increases the efficacy of anticancer drugs on breast and colon tumors [136].

Moreover, elevated expression of dopamine receptors in tumors has been associated with poor prognosis across several cancer types, making them potential therapeutic targets. In this context our results add that PANC-1, MIA PaCa-2 and M2 cells expressed both mRNA and proteins of the dopaminergic receptor genes.

Dopamine mediates its effects through two main receptor classes, D1-like (that includes D1 and D5) and D2-like (which includes D2, D3 and D4 receptors). Traditionally, D1-like receptors are known to couple with Gs proteins, stimulating adenylate cyclase (AC), elevating cAMP, and activating protein kinase A (PKA). In contrast, D2-like receptors couple with Gi/o proteins, inhibit AC, reduce cAMP, and suppress PKA activity.

Evaluating conventional dopaminergic agonists including fenoldopam, a highly selective peripheral D1-agonist, and pergolide, a highly selective D2-agonist in pancreatic cells, we confirmed that this effect was specifically mediated by D1-like receptors and that specific D1 agonist are more effective than dopamine at inhibiting tumor cell proliferation.

This aligns with other authors' work, where the dopaminergic pathway activation reduced tumor proliferation in colon, breast, prostate and gastrointestinal cancers [137]–[139]. In their work, these authors describe that dopamine is involved in tumor progression and is able to reduce immunomodulation in cancer. They also

demonstrated that fenoldopam has an antiproliferative effect in vascular smooth muscle cells and in several breast cancer lines. In contrast, there is literature indicating and oncogenic effect of the activation of the pathway [140] in hepatocellular carcinoma.

Fenoldopam (FE) is a derivative of benzazepine and is the first D1 agonist approved for clinical use as an antihypertensive given its vasodilatory and diuretic effects [141]. It has been described that FE induces apoptosis in breast cancer cells, through the DR1/cGMP/PKG pathway [139]. Pergolide and bromocriptine, two D2 agonists, are used as efficient treatments against hyperprolactinemia and Parkinson's disease [142]. There is no evidence regarding pergolide and cancer. In our hands we observed no significant effect in vitro. On the other hand, Fenoldopam and bromocriptine have been studied as potential chemotherapeutic agents, suppressing the growth of breast cancer cells and hepatocellular carcinoma cells in a concentration dependent manner [143], [144]. Bromocriptine was also able to reduce tumor progression in chemoresistant prostate cancer *in vivo* [145].

Other authors describe similar effects of the D1 agonism [137], [139], [146]. Sobczuk et al. summarized in their review how D1 agonists like fenoldopam or A77636 were able to reduce tumor volume in breast cancer and had antineoplastic effect in bone metastasis. Moreover sunitinib (a known anticancer drug) in combination with dopamine exerted a synergistic antitumor effect in breast xenografts.

Going into other specific D1 agonists in this work, SKF82958 was found to have an antitumor effect in ovarian cancer [147] and SKF83959 is able to tumor growth in pituitary tumor and gastric cancer by autophagic cell death through D5 activation [148].

As this is a new approach, not many authors link dopamine to cell death mechanisms. Research on dopamine primarily focus in glioblastoma, when it's been associated to autophagic cell death [149]. Gomez-Santos' lab suggested that

dopamine produces autophagy by generating ROS and activating target proteins. Sobczuk et al., also in their review, pointed that D1 activation induces apoptosis and autophagy in breast cancer [146]. Similarly, in our work, we observed an increase in autophagic markers p62 and LC3-II in pancreatic tumors treated with dopamine and fenoldopam. Additionally, dopamine and D1 activation with fenoldopam also elevated the expression of apoptotic markers, including cleaved PARP and activated caspase 3.

With our microarray analysis we were able to find key genes whose expression was different than the control group. Amongst these genes, we found a couple that are described to be involved in proliferation, migration, cancer stemness and cell death pathways. To name a few, CDC42EP3 was downregulated after dopaminergic agonism with bromocriptine. CDC42EP3 promotes glioma progression of glioblastoma, gastric and colorectal cancer, and is able to regulate cell proliferation, apoptosis and migration [150]–[152]. Fenoldopam treated tumors had HSDL2 downregulated, a gene linked to cancer progression in pancreas, bladder, rectal and lung cancers[153]–[156]. Furthermore genes such as PAICS (a gene involved in DNA building), MRPS23 (protein synthesis), SLC38 (involved in metabolism, growth and signalling), REEP3 (nucleus formation), RPGRIP1L (protein entry and signalling) and ELP3 (involved in transcription) were also downregulated. Moreover the gene USP10 (a gene that mediates apoptosis and autophagy) was upregulated after fenoldopam treatment. In the group treated with both fenoldopam and bromocriptine we found TRIM13 upregulated, a gene described to inhibit lung and clear cell renal carcinoma and progression and induce autophagy and apoptosis [157]–[159] and also CCDC58, a gene involved in cell cycle regulation and energy metabolism, was found downregulated. These findings are the first steps to understand the mechanisms underlying the antitumor response of dopaminergic activation in pancreatic cancer.

Furthermore, the link between catecholamines and migration has been studied; some authors associate adrenergic receptors with increased migration and invasion [160]. Dopamine effect on migration in cancer cells, on the other hand,

has not been studied. Some authors link dopamine and migration of fibroblast *in vitro* [161] and also in the migration of dopaminergic neurons in embryonic mice [162]. In pancreatic cancer we demonstrated that the dopaminergic pathway reduces cell migration, while activating both D1 and D2 receptors separately.

Once the effect of dopaminergic drugs is characterized *in vitro*, animal models are the next step for validating the antitumor and antimetastatic therapy. In our lab, we successfully stablished PDAC subcutaneous and highly metastatic orthotopic models.

Our work follows these previous results and adds that both agonisms are effective in PDAC in the subcutaneous model, and its combination was not toxic for the animals, tested in our orthotopic model. Fenoldopam exerted great effect, reducing tumor growth and the number of metastases, while increasing cell death and apoptotic factors. In the subcutaneous model, bromocriptine effect was subtler. Moreover, we think that the bromocriptine effect might be linked to its inhibitory effect in vascularization, reducing angiogenesis and innervation [44], [163].

2. <u>The inhibition of D2 receptors as a therapeutic target.</u>

As discussed previously, D1 and D2 receptors exert contrary functions in some tissues [95]. Authors like Jandaghi et al. [164] or Weissenrieder JS et al. [97] indicate that DRD2 is overexpressed in pancreatic tumors. In their work they also propose that inhibition of D2 receptors might have an antitumor effect. In our lab, Español. et al. [165] studied the role of catecholaminergic receptors in endometrial cancer. DRD2 expression analysis was significantly associated with serous endometrial cancer, high grade FIGO classification tumors, and worse disease-free and overall survival, being the high expression of DRD2 an independent significant prognostic marker for predicting disease-free survival and overall survival in our patient's cohort [165].

Furthermore, during the recent years many authors have described the antitumor potential of the D2 antagonism. Mu J. et al. [166] studied how thioridazine, a potent D2 antagonist, is able to reduce tumor growth and induce autophagy and

apoptosis. This opens a window for several antipsychotics to be repurposed for cancer treatment.

The recent discoveries place D2 inhibition as promising target for cancer therapy; very recently Sim et al. discovered that domperidone exerts an antitumor effect in colorectal cancer. During their work, Sim described that domperidone at 50µM was able to inhibit proliferation by 90% in HCT116 cells 72h after treatment. On this note Shakya et al. reported that domperidone was able to induce apoptosis in triple-negative breast cancer using a viability assay with similar doses as the ones used in this work [167], [168] . Domperidone is prescribed to treat gastroparesis and reduce nausea and vomiting. Although rapidly absorbed after oral administration, its poor water solubility results in a bioavailability of only 13-17% due to extensive first-pass metabolism in the liver and gut. Furthermore, approximately 91-93% of domperidone binds to plasma proteins, leaving only about 7% freely available in the plasma. Given these solubility and bioavailability challenges, encapsulating domperidone in a nanocarrier is a promising strategy [139].

Earlier this year, L-741,626, another potent D2 antagonist, was reported to inhibit prostate cancer derived stem cells [169], reducing the expression of pluripotency markers. Also L-741,626 was described to inhibit hepatocellular carcinoma's progression through MAPK/ERG signaling pathway [170]. Several authors are finding positive results in other cancer types using D2 inhibitors such as ONC206 and ONC201 by inducing stress responses and activating apoptosis [171]–[174]. In this context our work aligns with these results and adds that D2 antagonism with domperidone and L-741,626 also produce a potent inhibitory effect in tumor growth in pancreatic cell lines.

During the planning of the *in vivo* experiment, domperidone was the D2 antagonist of choice for three main reasons: first, the effect seems dose-dependent; second, it is an already-in-use drug for preventing nausea and vomiting [175] with not many side effects; and third, domperidone does not cross the blood-brain barrier, which is crucial for peripheral treatments.

During this project, we utilized the same subcutaneous PANC-1 model in order to analyze the effect of the D2 antagonism with domperidone. As discussed in this work, the D2 antagonism has been very recently described by some authors to have antitumor effect, yet the discovery is pretty novel. Not many authors have explored domperidone's use against cancer *in vivo*. Sim et al [168] administered domperidone five times a week at 20mg/kg/dose and was able to reduce the tumor volume of treated mice by 50% after 20 days of treatment in colorectal carcinoma with no signs of toxicity. They associate the effect with the generation of ROS species that lead into apoptosis through the inhibition of the ERK/STAT3-mediated pathway. Our work is congruent with these results as we used the same administration regime and got a near 50% reduction in tumor progression, volume and weigh in PDAC xenografts even when our mice lasted for half as long due to the aggressiveness of our model. The effect of the D2 inhibition holds a big potential and needs to be explored. We aim to reproduce this experiment with a bigger sample size, further increasing the doses as no toxicity has been found yet. Moreover, our objective is also to vehicularize domperidone with nanoparticles allowing us to improve the outcomes even more.

3. Combined effect of the activation of DRD1 pathway and inhibition of DRD2.

The combined effect of D1 agonism and D2 antagonism is not described by other groups yet and is novel in the field because the small amount of studies regarding dopamine signaling modulation for cancer treatment are focused on one specific pathway (either D1 activation or D2 inhibition). In vitro studies performed carried in our lab demonstrated that combining DRD1 agonism with DRD2 antagonism significantly reduces cell proliferation in Ishikawa and AN3CA cell lines more effectively than monotherapy, suggesting a promising new combinational therapeutic strategy [165]. In this work we explored the combination of the D1 agonists such as fenoldopam, SFK83822, SKF82958 and SKF83959 with the D2 antagonists domperidone and L741,626. We found that M2 and PANC-1 presented

low sensitivity to the D1 agonism with any SKF drug, but when combined with domperidone the effect was stronger than with domperidone alone. This also happened in MIA PaCa-2 cells but they were responding well to the monotherapy. New *in vivo* experiments are needed for the preclinical validation of this new therapy.

4. Pancreatic cancer stem cells and dopamine modulation.

There is increasing evidence that some tumor cells can survive chemotherapy by activating self-renewal pathways, leading to tumor progression and clinical recurrence. The cancer stem cells (CSCs) can generate the bulk of the tumor using differentiation pathways [176]. These CSCs are a specialized group of cells constituting a small percentage of the tumor mass, display pluripotency, anchorage-independent growth, self-renewal properties, and the ability to trigger tumorigenesis (higher tumor initiating potential) [177]. Due to CSCs resistance to chemotherapy and their ability to initiate and spread tumors, they are clear potential targets for innovative cancer therapies. The CSCs hypothesis is considered a milestone in the understanding of drug resistance and cancer recurrence [178]. Consequently, the development of drugs that can specifically target CSCs, without negative effect on human pluripotent stem cells (hPSCs), seems urgent. In 2012, Sachlos et al. found that dopamine receptors (DR) are specifically expressed in CSCs, while there is limited or no DR expression hPSCs. Thus, it has been hypothesized that signaling through DR could be a potent CSC-specific targetable receptor pathway in humans [179].

During the last decade, researchers have been seeking for new and more reliable models to isolate and cultivate CSCs for drug screening. In this context, spheroids are slowly growing in use [180]–[182] as a model that can correctly replicate some solid tumor characteristics that 2D models are still missing. Notably tumor derived spheroids are grown as floating spheres and have been used as surrogate systems to evaluate the CSC-related characteristics of solid tumors *in vitro*. Our work is novel in this field; signaling through D2 receptor has been described as a modulator of spheroid formation, but no authors have tested D1 agonism and D2

antagonism in this model as an antitumor strategy. Both approaches: the D1 pathway activation and D2 pathway inhibition reduced the size and number of the spheroids and such effects occurred with lower doses than the ones used in 2D models. This thesis also encourages researches to start using spheroids as a solid model for cancer therapeutic research also in PDAC.

Exploring these drugs alone or in combination with the standard chemotherapy may offer an opportunity to overcome the intrinsic chemoresistance of these tumors and prevent recurrence, improving the armamentarium of pancreatic therapy using repurposing. By leveraging existing drugs, the repurposing approach can bypass the lengthy and costly early-stage clinical trials required for new drug development, saving significant time and resources associated with the traditional drug discovery pipeline [183].

5. Nanoparticle as drug delivery system for pancreatic cancer therapy

Dopamine ligands, agonists and antagonists, are usually of low molecular weight, resulting in limited efficacy due to their rapid inactivation in the blood, elimination in the kidney, and crossing of the blood-brain barrier can be detrimental once we move into translational medicine. In this scenario, encapsulation, or conjugation of such small drugs to nanocarriers is a widely explored strategy to improve their therapeutic efficacy, achieving a higher cytotoxic concentration in the tumor and reducing toxicity for the rest of the organism, compared to the free drug [184]. Nanocarriers could protect the drug from degradation, reduce its renal clearance, increase its half-life in the bloodstream, allow control of drug release kinetics, and improve the solubility of insoluble drugs [185], [186]. Angiogenesis in a tumor generates new blood vessels, but these new vessels have greater permeability (enhanced permeability and retention, or EPR effect), which together with the poor lymphatic drainage in the tumor allows the passive accumulation of the nano-vehicles in the tumor tissues, releasing there the chemotherapeutic agent [187], [188]. As a result, nano-sized nanocarriers loaded with antitumor agents can be

targeted to the tumor thanks to the EPR effect [189]. The use of drug delivery Systems (DDS) is an increasingly used strategy in cancer therapy with promising results in pancreatic cancer [49].

With the aim of improving the bioavailability of our treatments, protecting them until they reach the target and allowing us to increase the dose reducing side effects we are collaborating with Dr. JL Corchero's team in the production and set up of nanoparticles. We are producing nanovaults based on the eukaryotic vault complex, a nanoparticle able to encapsulate multiples cargos and act as a vehicle, delivering them to target cells [118]. They can be easily generated and modified/ functionalized through simple genetic engineering techniques, and can be easily produced in different biological systems, like bacterial or eukaryotic cells, as "cell factories" [190]. Multiple authors are modifying its sequence genetically to load different cargos, to direct them towards target cell types or antigens or improve its solubility [119], [120], [191]. Since vaults occur naturally in almost all eukaryotic cells, they do not present toxicity or immunogenicity, resulting in excellent biocompatibility. All these characteristics allow foreseeing new and interesting applications in the controlled delivery of therapeutic compounds for the therapy of various human diseases.

In collaboration with JL Corchero's team we published how these nanoparticles are able to internalize in ovarian cell lines and that the cargo-free nanovaults do not produce cell death in this cancer type [192]. Our experiments in pancreatic cancer cell lines yielded similar results, adding consistency to the statements that they are non-toxic and only a small percentage internalize on a basal level.

JL Corchero's team also described how these eukaryotic nanoparticles bound specifically to cancer cells via the EGF receptors [193]. This finding correlates with our biodistribution experiments *in vivo*. Vault nanoparticles tend to accumulate in the tumor over every other organ in the body which reinforces our hypothesis.

Finally, the design of specific nanobodies -selective new peptides targeting the D1 dopamine receptor- could enhance the potency of inhibition to achieve a strong

antitumor effect as we observed. This approach is unprecedented, and our results, despite being preliminary, position this strategy as a potential new tool to explore in cancer therapy.

Together, these findings provided by us and other authors preclinical evidence that dopaminergic modulation (whether through receptor-specific agonists, antagonists, or combination strategies) represents a promising avenue for targeted therapy in PDAC. However, the clinical application of dopaminergic agents could be currently hindered by rapid inactivation, poor bioavailability, and undesirable penetration of the blood-brain barrier. The use of nanocarriers, such as nanovaults, offers a compelling solution by enhancing drug stability, prolonging circulation time, and facilitating selective delivery to tumor tissues through the EPR effect, thereby minimizing systemic toxicity. This work establishes a proof-of concept for future studies aimed at improving outcomes for pancreatic, which currently lacks effective treatments and limited progress in resistant tumors.

VI. CONCLUSIONS

1) The activation of dopaminergic pathway by DA, but not NE or E, is able to reduce tumor cell proliferation in pancreatic PANC-1, MIA PaCa-2 cells and the patient-derived tumor line M2.

2) The observed cytotoxic effect is mediated through the activation of D1-like receptors and induction of apoptosis and autophagy in the three pancreatic tumor cell lines.

3) Dopamine and more effectively pergolide, a selective D2 receptor (D2R) agonist, inhibit tumor cell migration in PANC-1, MIA PaCa-2 cells, but not in M2 cells.

4) Treatment with fenoldopam, a selective D1 receptor (D1R) agonist, and bromocriptine, a selective D2R agonist, effectively reduces tumor progression in subcutaneous PANC-1 and MIA PACA2 mouse models enhances apoptotic pathways in tumor cells and exhibits an anti-angiogenic effect, without observable toxicity to the mice.

5) In the orthotopic metastatic model, the treatment with fenoldopam and bromocriptine alone or in combination significantly reduced tumor progression and the number of mice with metastasis.

6) The inhibition of the D2-like receptor pathway significantly reduces the proliferation of PANC-1, MIA PaCa-2, and M2 cells *in vitro*. Furthermore, treatment with domperidone, a selective D2R antagonist, effectively reduces tumor progression in subcutaneous PANC-1 mouse models without inducing toxicity.

7) Activation of the D1 or D2 dopaminergic pathways individually reduces the size and number of spheroids derived from PANC-1, MIA PaCa-2, and M2 cells.

Moreover, their combined treatment enhances the antiproliferative effects on pancreatic cancer stem cells and spheroids *in vitro*.

8) Vault-based nanoparticles do not exhibit intrinsic cytotoxicity unless loaded with a cytotoxic cargo. These nanovaults successfully accumulate in PANC-1 tumors within 5 to 24 hours after intravenous administration, while showing minimal accumulation in other major organs in subcutaneous PANC-1 xenograft models.

9) The engineered nanobodies targeting D1 receptors are able to exert a cytotoxic effect at lower doses than the prior agonists in PANC-1, MIA PaCa-2, and M2 cells *in vitro*.

V. BIBLIOGRAPHY

[1] R. L. Siegel, T. B. Kratzer, A. N. Giaquinto, H. Sung, and A. Jemal, “Cancer statistics, 2025,” *Ca*, vol. 75, no. 1, p. 10, Jan. 2025, doi: 10.3322/CAAC.21871.

[2] A. López Serrano, “Factores de riesgo y diagnóstico temprano del cáncer de páncreas,” *Gastroenterol. Hepatol.*, vol. 33, no. 5, pp. 382–390, May 2010, doi: 10.1016/J.GASTROHEP.2009.10.004.

[3] S. Grover and S. Syngal, “Hereditary Pancreatic Cancer,” *Gastroenterology*, vol. 139, no. 4, p. 1076, 2010, doi: 10.1053/J.GASTRO.2010.08.012.

[4] D. Li *et al.*, “DNA repair gene polymorphisms and risk of pancreatic cancer,” *Clin. Cancer Res.*, vol. 15, no. 2, pp. 740–746, Jan. 2009, doi: 10.1158/1078-0432.CCR-08-1607,.

[5] M. F. Bray *et al.*, *Cancer Incidence in Five Continents Volume XII*, vol. 169. 2024.

[6] S. J. Pandol, M. V. Apte, J. S. Wilson, A. S. Gukovskaya, and M. Edderkaoui, “The burning question: Why is smoking a risk factor for pancreatic cancer?,” *Pancreatology*, vol. 12, no. 4, pp. 344–349, 2012, doi: 10.1016/j.pan.2012.06.002.

[7] J. J. Collins, N. A. Esmen, and T. A. Hall, “A review and meta-analysis of formaldehyde exposure and pancreatic cancer,” *Am. J. Ind. Med.*, vol. 39, no. 3, pp. 336–345, 2001, doi: 10.1002/1097-0274(200103)39:3<336::AID-AJIM1022>3.0.CO;2-K,.

[8] M. Capasso *et al.*, “Epidemiology and risk factors of pancreatic cancer,” *Acta Biomed.*, vol. 89, no. 9-S, pp. 141–146, 2018, doi: 10.23750/ABM.V89I9-S.7923,.

[9] R. Huxley, A. Ansary-Moghaddam, A. Berrington De González, F. Barzi, and M. Woodward, “Type-II diabetes and pancreatic cancer: A meta-analysis of 36 studies,” *Br. J. Cancer*, vol. 92, no. 11, pp. 2076–2083, Jun. 2005, doi: 10.1038/SJ.BJC.6602619,.

[10] A. Ekbom *et al.*, “Pancreatitis and pancreatic cancer: A population-based study,” *J. Natl. Cancer Inst.*, vol. 86, no. 8, pp. 625–627, Apr. 1994, doi: 10.1093/JNCI/86.8.625,.

[11] L. R. Teras, A. V. Patel, C. Rodriguez, M. J. Thun, and E. E. Calle, “Parity, other reproductive factors, and risk of pancreatic cancer mortality in a large cohort of U.S. Women (United States),” *Cancer Causes Control*, vol. 16, no. 9, pp. 1035–1040, Nov. 2005, doi: 10.1007/S10552-005-0332-4,.

[12] T. Conroy *et al.*, “Pancreatic cancer: ESMO Clinical Practice Guideline for diagnosis, treatment and follow-up 5 on behalf of the ESMO Guidelines Committee,” *Ann. Oncol.*, vol. 34, pp. 987–1002, 2023, doi: 10.1016/j.annonc.2023.08.009.

[13] J. Toft *et al.*, “Imaging modalities in the diagnosis of pancreatic adenocarcinoma: A systematic review and meta-analysis of sensitivity, specificity and diagnostic accuracy,” *Eur. J. Radiol.*, vol. 92, pp. 17–23, Jul. 2017, doi: 10.1016/j.ejrad.2017.04.009.

[14] G. Karmazanovsky, V. Fedorov, V. Kubyshkin, and A. Kotchatkov, “Pancreatic head cancer: Accuracy of CT in determination of resectability,” *Abdom. Imaging*, vol. 30, no. 4, pp. 488–500, Aug. 2005, doi: 10.1007/S00261-004-0279-Z,.

[15] S. K. Kamarajah, W. R. Burns, T. L. Frankel, C. S. Cho, and H. Nathan, “Validation of the American Joint Commission on Cancer (AJCC) 8th Edition Staging System for Patients with Pancreatic Adenocarcinoma: A Surveillance, Epidemiology and End Results (SEER) Analysis,” *Ann. Surg. Oncol.*, vol. 24, no. 7, pp. 2023–2030, Jul. 2017, doi: 10.1245/S10434-017-5810-X,.

[16] D. Ansari, A. Gustafsson, and R. Andersson, “Update on the management of pancreatic cancer: Surgery is not enough,” *World J. Gastroenterol.*, vol. 21, no. 11, pp. 3157–3165, Mar. 2015, doi: 10.3748/WJG.V21.I11.3157,.

[17] J. D. Birkmeyer, Y. Sun, S. L. Wong, and T. A. Stukel, “Hospital volume and late survival after cancer surgery,” *Ann. Surg.*, vol. 245, no. 5, pp. 777–783, May 2007, doi: 10.1097/01.SLA.0000252402.33814.DD,.

[18] D. Dindo, N. Demartines, and P. A. Clavien, “Classification of surgical complications: A new proposal with evaluation in a cohort of 6336 patients and results of a survey,” *Ann. Surg.*, vol. 240, no. 2, pp. 205–213, Aug. 2004, doi: 10.1097/01.SLA.0000133083.54934.AE,.

[19] L. Zhang, S. Sanagapalli, and A. Stoita, “Challenges in diagnosis of pancreatic cancer,” *World J. Gastroenterol.*, vol. 24, no. 19, pp. 2047–2060, May 2018, doi: 10.3748/WJG.V24.I19.2047,.

[20] P. Sarantis, E. Koustas, A. Papadimitropoulou, A. G. Papavassiliou, and M. V. Karamouzis, “Pancreatic ductal adenocarcinoma: Treatment hurdles, tumor microenvironment and immunotherapy,” *World J. Gastrointest. Oncol.*, vol. 12, no. 2, pp. 173–181, Feb. 2020, doi: 10.4251/WJGO.V12.I2.173,.

[21] K. Yamakawa, J. Ye, Y. Nakano-narusawa, and Y. Matsuda, “Pathological Changes in Pancreatic Carcinogenesis: A Review,” *Cancers 2021, Vol. 13, Page 686*, vol. 13, no. 4, p. 686, Feb. 2021, doi: 10.3390/CANCERS13040686.

[22] O. G. McDonald, “The biology of pancreatic cancer morphology,” *Pathology*, vol. 54, no. 2, pp. 236–247, Mar. 2022, doi: 10.1016/j.pathol.2021.09.012.

[23] R. E. Wilentz *et al.*, “Loss of expression of Dpc4 in pancreatic intraepithelial neoplasia: evidence that DPC4 inactivation occurs late in neoplastic progression,” *Cancer Res.*, vol. 60, no. 7, pp. 2002–2006, Apr. 2000, Accessed: Sep. 09, 2025. [Online]. Available: https://pubmed.ncbi.nlm.nih.gov/10766191/.

[24] D. Sacks *et al.*, “Multisociety Consensus Quality Improvement Revised Consensus Statement for Endovascular Therapy of Acute Ischemic Stroke,” *Int. J. Stroke*, vol. 13, no. 6, pp. 612–632, Aug. 2018, doi: 10.1177/1747493018778713,.

[25] T. J. Grant, K. Hua, and A. Singh, “Molecular Pathogenesis of Pancreatic Cancer,” *Prog. Mol. Biol. Transl. Sci.*, vol. 144, pp. 241–275, 2016, doi: 10.1016/bs.pmbts.2016.09.008.

[26] N. Waddell *et al.*, “Whole genomes redefine the mutational landscape of pancreatic cancer,” *Nature*, vol. 518, no. 7540, pp. 495–501, Feb. 2015, doi: 10.1038/NATURE14169;TECHMETA=45;SUBJMETA=308,692;KWRD=MEDICAL+RESEARCH.

[27] E. A. Collisson *et al.*, “Subtypes of pancreatic ductal adenocarcinoma and their differing responses to therapy,” *Nat. Med.*, vol. 17, no. 4, pp. 500–503, Apr. 2011, doi: 10.1038/NM.2344,.

[28] P. Bailey *et al.*, “Genomic analyses identify molecular subtypes of pancreatic cancer,” *Nature*, vol. 531, no. 7592, pp. 47–52, Mar. 2016, doi: 10.1038/NATURE16965,.

[29] R. A. Moffitt *et al.*, “Virtual microdissection identifies distinct tumor- and stroma-specific subtypes of pancreatic ductal adenocarcinoma,” *Nat. Genet. 2015 4710*, vol. 47, no. 10, pp. 1168–1178, Sep. 2015, doi: 10.1038/ng.3398.

[30] B. J. Raphael *et al.*, “Integrated Genomic Characterization of Pancreatic Ductal Adenocarcinoma,” *Cancer Cell*, vol. 32, no. 2, p. 185, Aug. 2017, doi: 10.1016/J.CCELL.2017.07.007.

[31] M. H. Sherman and G. L. Beatty, “Tumor Microenvironment in Pancreatic Cancer Pathogenesis and Therapeutic Resistance,” *Annu. Rev. Pathol. Mech. Dis.*, vol. 18, pp. 123–148, Jan. 2023, doi: 10.1146/ANNUREV-PATHMECHDIS-031621-024600,.

[32] M. V. Apte *et al.*, “Desmoplastic reaction in pancreatic cancer: Role of pancreatic stellate cells,” *Pancreas*, vol. 29, no. 3, pp. 179–187, Oct. 2004, doi: 10.1097/00006676-200410000-00002,.

[33] M. G. Bachem *et al.*, “Pancreatic carcinoma cells induce fibrosis by stimulating proliferation

and matrix synthesis of stellate cells," *Gastroenterology*, vol. 128, no. 4, pp. 907–921, 2005, doi: 10.1053/j.gastro.2004.12.036.

[34] A. Masamune and T. Shimosegawa, "Signal transduction in pancreatic stellate cells," *J. Gastroenterol.*, vol. 44, no. 4, pp. 249–260, 2009, doi: 10.1007/S00535-009-0013-2,.

[35] V. Pandey and P. Storz, "Targeting the tumor microenvironment in pancreatic ductal adenocarcinoma," *Expert Rev. Anticancer Ther.*, vol. 19, no. 6, pp. 473–482, Jun. 2019, doi: 10.1080/14737140.2019.1622417,.

[36] L. G. Melstrom, M. D. Salazar, and D. J. Diamond, "The pancreatic cancer microenvironment: A true double agent," *J. Surg. Oncol.*, vol. 116, no. 1, pp. 7–15, Jul. 2017, doi: 10.1002/JSO.24643,.

[37] J. Kleeff *et al.*, "Pancreatic cancer microenvironment," *Int. J. Cancer*, vol. 121, no. 4, pp. 699–705, Aug. 2007, doi: 10.1002/IJC.22871,.

[38] G. P. Nagaraju, R. Dontula, B. F. El-rayes, and S. S. Lakka, "Molecular mechanisms underlying the divergent roles of SPARC in human carcinogenesis," *Carcinogenesis*, vol. 35, no. 5, pp. 967–973, 2014, doi: 10.1093/CARCIN/BGU072,.

[39] E. C. Vaquero, M. Edderkaoui, S. J. Pandol, I. Gukovsky, and A. S. Gukovskaya, "Reactive oxygen species produced by NAD(P)H oxidase inhibit apoptosis in pancreatic cancer cells," *J. Biol. Chem.*, vol. 279, no. 33, pp. 34643–34654, Aug. 2004, doi: 10.1074/jbc.M400078200.

[40] M. Monje *et al.*, "Roadmap for the Emerging Field of Cancer Neuroscience," *Cell*, vol. 181, no. 2, pp. 219–222, Apr. 2020, doi: 10.1016/j.cell.2020.03.034.

[41] M. Mancino, E. Ametller, P. Gascón, and V. Almendro, "The neuronal influence on tumor progression," *Biochim. Biophys. Acta - Rev. Cancer*, vol. 1816, no. 2, pp. 105–118, Dec. 2011, doi: 10.1016/J.BBCAN.2011.04.005.

[42] B. Boilly, S. Faulkner, P. Jobling, and H. Hondermarck, "Nerve Dependence: From Regeneration to Cancer," *Cancer Cell*, vol. 31, no. 3, pp. 342–354, Mar. 2017, doi: 10.1016/J.CCELL.2017.02.005.

[43] C. Magnon *et al.*, "Autonomic nerve development contributes to prostate cancer progression," *Science (80-.).*, vol. 341, no. 6142, 2013, doi: 10.1126/SCIENCE.1236361,.

[44] C. Magnon and H. Hondermarck, "The neural addiction of cancer," *Nat. Rev. Cancer*, vol. 23, no. 5, pp. 317–334, May 2023, doi: 10.1038/S41568-023-00556-8,.

[45] M. Del Chiaro, T. Sugawara, S. D. Karam, and W. A. Messersmith, “Advances in the management of pancreatic cancer,” *BMJ*, vol. 383, p. e073995, Dec. 2023, doi: 10.1136/BMJ-2022-073995.

[46] T. Conroy *et al.*, “FOLFIRINOX versus Gemcitabine for Metastatic Pancreatic Cancer,” *N. Engl. J. Med.*, vol. 364, no. 19, pp. 1817–1825, May 2011, doi: 10.1056/NEJMOA1011923,.

[47] D. D. Von Hoff *et al.*, “Increased Survival in Pancreatic Cancer with nab-Paclitaxel plus Gemcitabine,” *N. Engl. J. Med.*, vol. 369, no. 18, pp. 1691–1703, Oct. 2013, doi: 10.1056/NEJMOA1304369,.

[48] M. J. Raphael *et al.*, “The Association of Drug-Funding Reimbursement With Survival Outcomes and Use of NewSystemic Therapies Among Patients With Advanced Pancreatic Cancer,” *JAMA Netw. Open*, vol. 4, no. 11, p. E2133388, Nov. 2021, doi: 10.1001/JAMANETWORKOPEN.2021.33388,.

[49] A. Wang-Gillam *et al.*, “Nanoliposomal irinotecan with fluorouracil and folinic acid in metastatic pancreatic cancer after previous gemcitabine-based therapy (NAPOLI-1): A global, randomised, open-label, phase 3 trial,” *Lancet*, vol. 387, no. 10018, pp. 545–557, Feb. 2016, doi: 10.1016/S0140-6736(15)00986-1,.

[50] A. Carrato *et al.*, “Phase I/II trial of sequential treatment of nab-paclitaxel in combination with gemcitabine followed by modified FOLFOX chemotherapy in patients with untreated metastatic exocrine pancreatic cancer: Phase I results,” *Eur. J. Cancer*, vol. 139, pp. 51–58, Nov. 2020, doi: 10.1016/j.ejca.2020.07.035.

[51] J. P. Neoptolemos *et al.*, “Comparison of adjuvant gemcitabine and capecitabine with gemcitabine monotherapy in patients with resected pancreatic cancer (ESPAC-4): a multicentre, open-label, randomised, phase 3 trial,” *Lancet*, vol. 389, no. 10073, pp. 1011–1024, Mar. 2017, doi: 10.1016/S0140-6736(16)32409-6.

[52] T. Conroy *et al.*, “FOLFIRINOX or Gemcitabine as Adjuvant Therapy for Pancreatic Cancer,” *N. Engl. J. Med.*, vol. 379, no. 25, pp. 2395–2406, Dec. 2018, doi: 10.1056/NEJMOA1809775,.

[53] A. P. Barbour *et al.*, “The AGITG GAP Study: A Phase II Study of Perioperative Gemcitabine and Nab-Paclitaxel for Resectable Pancreas Cancer,” *Ann. Surg. Oncol.*, vol. 27, no. 7, pp. 2506–2515, Jul. 2020, doi: 10.1245/S10434-020-08205-2,.

[54] E. M. O’Reilly *et al.*, “A single-arm, nonrandomized phase II trial of neoadjuvant gemcitabine and oxaliplatin in patients with resectable pancreas adenocarcinoma,” *Ann. Surg.*, vol. 260,

no. 1, pp. 142–148, 2014, doi: 10.1097/SLA.0000000000000251,.

[55] B. Ielpo *et al.*, “Preoperative treatment with gemcitabine plus nab-paclitaxel is a safe and effective chemotherapy for pancreatic adenocarcinoma,” *Eur. J. Surg. Oncol.*, vol. 42, no. 9, pp. 1394–1400, Sep. 2016, doi: 10.1016/j.ejso.2016.01.006.

[56] M. H. Kaiser and S. S. Ellenberg, “Pancreatic Cancer: Adjuvant Combined Radiation and Chemotherapy Following Curative Resection,” *Arch. Surg.*, vol. 120, no. 8, pp. 899–903, 1985, doi: 10.1001/ARCHSURG.1985.01390320023003,.

[57] D. B. Evans *et al.*, “Preoperative gemcitabine-based chemoradiation for patients with resectable adenocarcinoma of the pancreatic head,” *J. Clin. Oncol.*, vol. 26, no. 21, pp. 3496–3502, 2008, doi: 10.1200/JCO.2007.15.8634,.

[58] M. Löhr, G. Klöppel, P. Maisonneuve, A. B. Lowenfels, and J. Lüttges, “Frequency of K-ras mutations in pancreatic intraductal neoplasias associated with pancreatic ductal adenocarcinoma and chronic pancreatitis: A meta-analysis,” *Neoplasia*, vol. 7, no. 1, pp. 17–23, 2005, doi: 10.1593/neo.04445.

[59] M. R. Janes *et al.*, “Targeting KRAS Mutant Cancers with a Covalent G12C-Specific Inhibitor,” *Cell*, vol. 172, no. 3, pp. 578-589.e17, Jan. 2018, doi: 10.1016/j.cell.2018.01.006.

[60] V. H. F. de Jesus, M. C. Mathias-Machado, J. P. F. de Farias, M. P. S. Aruquipa, A. A. Jácome, and R. D. Peixoto, “Targeting KRAS in Pancreatic Ductal Adenocarcinoma: The Long Road to Cure,” *Cancers (Basel).*, vol. 15, no. 20, Oct. 2023, doi: 10.3390/CANCERS15205015,.

[61] G. Bodoky *et al.*, “A phase II open-label randomized study to assess the efficacy and safety of selumetinib (AZD6244 [ARRY-142886]) versus capecitabine in patients with advanced or metastatic pancreatic cancer who have failed first-line gemcitabine therapy,” *Invest. New Drugs*, vol. 30, no. 3, pp. 1216–1223, 2012, doi: 10.1007/S10637-011-9687-4,.

[62] J. R. Infante *et al.*, “A randomised, double-blind, placebo-controlled trial of trametinib, an oral MEK inhibitor, in combination with gemcitabine for patients with untreated metastatic adenocarcinoma of the pancreas,” *Eur. J. Cancer*, vol. 50, no. 12, pp. 2072–2081, 2014, doi: 10.1016/j.ejca.2014.04.024.

[63] P. Pettazzoni *et al.*, “Genetic events that limit the efficacy of MEK and RTK inhibitor therapies in a mouse model of KRAS-driven pancreatic cancer,” *Cancer Res.*, vol. 75, no. 6, pp. 1091–1101, Mar. 2015, doi: 10.1158/0008-5472.CAN-14-1854,.

[64] V. Chung *et al.*, “Effect of selumetinib and MK-2206 vs oxaliplatin and fluorouracil in patients with metastatic pancreatic cancer after prior therapy: SWOG S1115 study randomized clinical trial,” *JAMA Oncol.*, vol. 3, no. 4, pp. 516–522, Apr. 2017, doi: 10.1001/JAMAONCOL.2016.5383,.

[65] A. Drilon *et al.*, “ Efficacy of Larotrectinib in TRK Fusion–Positive Cancers in Adults and Children ,” *N. Engl. J. Med.*, vol. 378, no. 8, pp. 731–739, Feb. 2018, doi: 10.1056/NEJMOA1714448,.

[66] E. S. Christenson, E. Jaffee, and N. S. Azad, “Current and emerging therapies for patients with advanced pancreatic ductal adenocarcinoma: a bright future,” *Lancet Oncol.*, vol. 21, no. 3, pp. e135–e145, Mar. 2020, doi: 10.1016/S1470-2045(19)30795-8,.

[67] T. Einama *et al.*, “Membranous and cytoplasmic expression of epidermal growth factor receptor in metastatic pancreatic ductal adenocarcinoma,” *Exp. Ther. Med.*, vol. 3, no. 6, pp. 931–936, Jun. 2012, doi: 10.3892/ETM.2012.518,.

[68] M. Haas *et al.*, “Afatinib plus gemcitabine versus gemcitabine alone as first-line treatment of metastatic pancreatic cancer: The randomised, open-label phase II ACCEPT study of the Arbeitsgemeinschaft Internistische Onkologie with an integrated analysis of the ‘burden of therapy’ method,” *Eur. J. Cancer*, vol. 146, pp. 95–106, Mar. 2021, doi: 10.1016/j.ejca.2020.12.029.

[69] Y. Seo, H. Baba, T. Fukuda, M. Takashima, and K. Sugimachi, “High expression of vascular endothelial growth factor is associated with liver metastasis and a poor prognosis for patients with ductal pancreatic adenocarcinoma,” *Cancer*, vol. 88, no. 10, pp. 2239–2245, May 2000, doi: 10.1002/(SICI)1097-0142(20000515)88:10<2239::AID-CNCR6>3.0.CO;2-V,.

[70] W. Tian, W. Ding, S. Kim, X. Xu, M. Pan, and S. Chen, “Efficacy and safety profile of combining agents against epidermal growth factor receptor or vascular endothelium growth factor receptor with gemcitabine-based chemotherapy in patients with advanced pancreatic cancer: A meta-analysis,” *Pancreatology*, vol. 13, no. 4, pp. 415–422, 2013, doi: 10.1016/j.pan.2013.04.195.

[71] B. Han *et al.*, “Effect of Anlotinib as a Third-Line or Further Treatment on Overall Survival of Patients with Advanced Non-Small Cell Lung Cancer: The ALTER 0303 Phase 3 Randomized Clinical Trial,” *JAMA Oncol.*, vol. 4, no. 11, pp. 1569–1575, Nov. 2018, doi: 10.1001/JAMAONCOL.2018.3039,.

[72] W. Liu, D. A. Bloom, W. G. Cance, E. V. Kurenova, V. M. Golubovskaya, and S. N. Hochwald, “FAK and IGF-IR interact to provide survival signals in human pancreatic

adenocarcinoma cells," *Carcinogenesis*, vol. 29, no. 6, pp. 1096–1107, Jun. 2008, doi: 10.1093/CARCIN/BGN026,.

[73] J. B. Fitzgerald *et al.*, "MM-141,an IGF-IR-and ErbB3-directed bispecific antibody overcomes network adaptations that limit Activity of IGF-IR Inhibitors," *Mol. Cancer Ther.*, vol. 13, no. 2, pp. 410–425, Feb. 2014, doi: 10.1158/1535-7163.MCT-13-0255,.

[74] H. R. Fei, G. Chen, J. M. Wang, and F. Z. Wang, "Perifosine induces cell cycle arrest and apoptosis in human hepatocellular carcinoma cell lines by blockade of Akt phosphorylation," *Cytotechnology*, vol. 62, no. 5, pp. 449–460, Oct. 2010, doi: 10.1007/S10616-010-9299-4,.

[75] A. Avan *et al.*, "MET As a Potential Target for the Treatment of Upper Gastrointestinal Cancers: Characterization of Novel c-Met Inhibitors from Bench to Bedside," *Curr. Med. Chem.*, vol. 21, no. 8, pp. 975–989, Mar. 2014, doi: 10.2174/09298673113209990231,.

[76] K. E. Sheppard, K. M. Kinross, B. Solomon, R. B. Pearson, and W. A. Phillips, "Targeting PI3 kinase/AKT/mTOR signaling in cancer," *Crit. Rev. Oncog.*, vol. 17, no. 1, pp. 69–95, 2012, doi: 10.1615/CRITREVONCOG.V17.I1.60.

[77] V. J. N. Bykov, S. E. Eriksson, J. Bianchi, and K. G. Wiman, "Targeting mutant p53 for efficient cancer therapy," *Nat. Rev. Cancer*, vol. 18, no. 2, pp. 89–102, Jan. 2018, doi: 10.1038/NRC.2017.109,.

[78] L. T. Vassilev *et al.*, "In Vivo Activation of the p53 Pathway by Small-Molecule Antagonists of MDM2," *Science (80-.).*, vol. 303, no. 5659, pp. 844–848, Feb. 2004, doi: 10.1126/SCIENCE.1092472,.

[79] N. J. Gaspar *et al.*, "Inhibition of transforming growth factor β signaling reduces pancreatic adenocarcinoma growth and invasiveness," *Mol. Pharmacol.*, vol. 72, no. 1, pp. 152–161, Jul. 2007, doi: 10.1124/MOL.106.029025,.

[80] B. Salvador-Barbero *et al.*, "CDK4/6 Inhibitors Impair Recovery from Cytotoxic Chemotherapy in Pancreatic Adenocarcinoma," *Cancer Cell*, vol. 37, no. 3, pp. 340-353.e6, Mar. 2020, doi: 10.1016/j.ccell.2020.01.007.

[81] A. B. Kunnumakkara, S. Guha, S. Krishnan, P. Diagaradjane, J. Gelovani, and B. B. Aggarwal, "Curcumin potentiates antitumor activity of gemcitabine in an orthotopic model of pancreatic cancer through suppression of proliferation, angiogenesis, and inhibition of nuclear factor-κB-regulated gene products," *Cancer Res.*, vol. 67, no. 8, pp. 3853–3861, Apr. 2007, doi: 10.1158/0008-5472.CAN-06-4257,.

[82] T. Uwagawa *et al.*, “Phase II Study of Adjuvant Chemotherapy with Gemcitabine and Nafamostat Mesilate for Pancreatic Cancer,” *Pancreas*, vol. 50, no. 3, pp. 313–316, Mar. 2021, doi: 10.1097/MPA.0000000000001767,.

[83] M. Erkan *et al.*, “The role of stroma in pancreatic cancer: Diagnostic and therapeutic implications,” *Nat. Rev. Gastroenterol. Hepatol.*, vol. 9, no. 8, pp. 454–467, Aug. 2012, doi: 10.1038/NRGASTRO.2012.115,.

[84] J. Bendell *et al.*, “Safety and Efficacy of Andecaliximab (GS-5745) Plus Gemcitabine and Nab-Paclitaxel in Patients with Advanced Pancreatic Adenocarcinoma: Results from a Phase I Study,” *Oncologist*, vol. 25, no. 11, pp. 954–962, Nov. 2020, doi: 10.1634/THEONCOLOGIST.2020-0474,.

[85] V. Picozzi *et al.*, “Gemcitabine/nab-paclitaxel with pamrevlumab: A novel drug combination and trial design for the treatment of locally advanced pancreatic cancer,” *ESMO Open*, vol. 5, no. 4, Aug. 2020, doi: 10.1136/ESMOOPEN-2019-000668,.

[86] S. T. Kim *et al.*, “First-in-human phase I trial of anti-hepatocyte growth factor antibody (YYB101) in refractory solid tumor patients,” *Ther. Adv. Med. Oncol.*, vol. 12, 2020, doi: 10.1177/1758835920926796,.

[87] A. Gurney *et al.*, “Wnt pathway inhibition via the targeting of Frizzled receptors results in decreased growth and tumorigenicity of human tumors,” *Proc. Natl. Acad. Sci. U. S. A.*, vol. 109, no. 29, pp. 11717–11722, Jul. 2012, doi: 10.1073/PNAS.1120068109,.

[88] E. Dotan *et al.*, “Phase Ib study of wnt inhibitor ipafricept with gemcitabine and nab-paclitaxel in patients with previously untreated stage IV pancreatic cancer,” *Clin. Cancer Res.*, vol. 26, no. 20, pp. 5348–5357, Oct. 2020, doi: 10.1158/1078-0432.CCR-20-0489,.

[89] Y. T. Fang, W. W. Yang, Y. R. Niu, and Y. K. Sun, “Recent advances in targeted therapy for pancreatic adenocarcinoma,” *World J. Gastrointest. Oncol.*, vol. 15, no. 4, pp. 571–595, Apr. 2023, doi: 10.4251/WJGO.V15.I4.571,.

[90] M. O. Klein, D. S. Battagello, A. R. Cardoso, D. N. Hauser, J. C. Bittencourt, and R. G. Correa, “Dopamine: Functions, Signaling, and Association with Neurological Diseases,” *Cell. Mol. Neurobiol.*, vol. 39, no. 1, pp. 31–59, Jan. 2019, doi: 10.1007/S10571-018-0632-3,.

[91] Y. PP, L. CY, L. TY, and C. WC, “Hericium erinaceus Mycelium Exerts Neuroprotective Effect in Parkinson’s Disease-in vitro and in vivo Models,” *J. Drug Res. Dev.*, vol. 6, no. 1, 2020, doi: 10.16966/2470-1009.150.

[92] L. Speranza, U. Di Porzio, D. Viggiano, A. de Donato, and F. Volpicelli, “Dopamine: The neuromodulator of long-term synaptic plasticity, reward and movement control,” *Cells*, vol. 10, no. 4, Apr. 2021, doi: 10.3390/CELLS10040735,.

[93] G. Eisenhofer *et al.*, “Substantial production of Dopamine in the human gastrointestinal tract,” *J. Clin. Endocrinol. Metab.*, vol. 82, no. 11, pp. 3864–3871, 1997, doi: 10.1210/JCEM.82.11.4339,.

[94] M. Cosentino *et al.*, “Human CD4+CD25+ regulatory T cells selectively express tyrosine hydroxylase and contain endogenous catecholamines subserving an autocrine/paracrine inhibitory functional loop,” *Blood*, vol. 109, no. 2, pp. 632–642, Jan. 2007, doi: 10.1182/BLOOD-2006-01-028423,.

[95] A. Rosas-Cruz, N. Salinas-Jazmín, and M. A. V. Velázquez, “Dopamine Receptors in Cancer: Are They Valid Therapeutic Targets?,” *Technol. Cancer Res. Treat.*, vol. 20, 2021, doi: 10.1177/15330338211027913,.

[96] C. E. Grant, A. L. Flis, and B. M. Ryan, “Understanding the role of dopamine in cancer: Past, present and future,” *Carcinogenesis*, vol. 43, no. 6, pp. 517–527, Jun. 2022, doi: 10.1093/CARCIN/BGAC045,.

[97] J. S. Weissenrieder, J. D. Neighbors, R. B. Mailman, and R. J. Hohl, “Cancer and the dopamine D2 receptor: A pharmacological perspective,” *J. Pharmacol. Exp. Ther.*, vol. 370, no. 1, pp. 111–126, 2019, doi: 10.1124/jpet.119.256818.

[98] A. J. Haak *et al.*, “Selective YAP/TAZ inhibition in fibroblasts via dopamine receptor D1 agonism reverses fibrosis,” *Sci. Transl. Med.*, vol. 11, no. 516, Oct. 2019, doi: 10.1126/SCITRANSLMED.AAU6296,.

[99] S. Basu *et al.*, “The neurotransmitter dopamine inhibits angiogenesis induced by vascular permeability factor/vascular endothelial growth factor,” *Nat. Med.*, vol. 7, no. 5, pp. 569–574, 2001, doi: 10.1038/87895,.

[100] A. Sagara *et al.*, “New high-throughput screening detects compounds that suppress pancreatic stellate cell activation and attenuate pancreatic cancer growth,” *Pancreatology*, vol. 21, no. 6, pp. 1071–1080, Sep. 2021, doi: 10.1016/j.pan.2021.04.002.

[101] A. Lev *et al.*, “Anti-pancreatic cancer activity of ONC212 involves the unfolded protein response (UPR) and is reduced by IGF1-R and GRP78/BIP,” *Oncotarget*, vol. 8, no. 47, pp. 81776–81793, Sep. 2017, doi: 10.18632/ONCOTARGET.20819.

[102] Q. Liu *et al.*, “Dopamine improves chemotherapeutic efficacy for pancreatic cancer by regulating macrophage-derived inflammations,” *Cancer Immunol. Immunother.*, vol. 70, no. 8, pp. 2165–2177, Aug. 2021, doi: 10.1007/S00262-020-02816-0,.

[103] K. Kong, M. Guo, Y. Liu, and J. Zheng, “Progress in animal models of pancreatic ductal adenocarcinoma,” *J. Cancer*, vol. 11, no. 6, pp. 1555–1567, 2020, doi: 10.7150/JCA.37529,.

[104] S. Bisht and G. Feldmann, “Animal models for modeling pancreatic cancer and novel drug discovery,” *Expert Opin. Drug Discov.*, vol. 14, no. 2, pp. 127–142, Feb. 2019, doi: 10.1080/17460441.2019.1566319,.

[105] U. Schütte, S. Bisht, P. Brossart, and G. Feldmann, “Recent developments of transgenic and xenograft mouse models of pancreatic cancer for translational research,” *Expert Opin. Drug Discov.*, vol. 6, no. 1, pp. 33–48, Jan. 2011, doi: 10.1517/17460441.2011.534453,.

[106] Y. Liu, W. Wu, C. Cai, H. Zhang, H. Shen, and Y. Han, “Patient-derived xenograft models in cancer therapy: technologies and applications,” *Signal Transduct. Target. Ther. 2023 81*, vol. 8, no. 1, pp. 1–24, Apr. 2023, doi: 10.1038/s41392-023-01419-2.

[107] P. L. Garcia, A. L. Miller, and K. J. Yoon, “Patient-Derived Xenograft Models of Pancreatic Cancer: Overview and Comparison with Other Types of Models,” *Cancers 2020, Vol. 12, Page 1327*, vol. 12, no. 5, p. 1327, May 2020, doi: 10.3390/CANCERS12051327.

[108] J. J. Morton, G. Bird, Y. Refaeli, and A. Jimeno, “Humanized mouse xenograft models: Narrowing the tumor-microenvironment gap,” *Cancer Res.*, vol. 76, no. 21, pp. 6153–6158, Nov. 2016, doi: 10.1158/0008-5472.CAN-16-1260,.

[109] H. Agarwal *et al.*, “Theranostic nanoparticles for detection and treatment of pancreatic cancer,” *Wiley Interdiscip. Rev. Nanomedicine Nanobiotechnology*, vol. 16, no. 4, p. e1983, Jul. 2024, doi: 10.1002/WNAN.1983.

[110] R. W. Robey, K. M. Pluchino, M. D. Hall, A. T. Fojo, S. E. Bates, and M. M. Gottesman, “Revisiting the role of ABC transporters in multidrug-resistant cancer,” *Nat. Rev. Cancer*, vol. 18, no. 7, pp. 452–464, Jul. 2018, doi: 10.1038/S41568-018-0005-8,.

[111] R. Álvarez-Gallego *et al.*, “Real-world effectiveness and safety of second- or third-line pegylated liposomal irinotecan plus 5-fluorouracil and folinic acid in pancreatic ductal adenocarcinoma in Spain,” *Ther. Adv. Med. Oncol.*, vol. 17, Jan. 2025, doi: 10.1177/17588359241309828,.

[112] K. Samanta, S. Setua, S. Kumari, M. Jaggi, M. M. Yallapu, and S. C. Chauhan,

"Gemcitabine combination nano therapies for pancreatic cancer," *Pharmaceutics*, vol. 11, no. 11, Nov. 2019, doi: 10.3390/PHARMACEUTICS11110574,.

[113] L. Zhu, C. Staley, D. Kooby, B. El-Rays, H. Mao, and L. Yang, "Current status of biomarker and targeted nanoparticle development: The precision oncology approach for pancreatic cancer therapy," *Cancer Lett.*, vol. 388, pp. 139–148, Mar. 2017, doi: 10.1016/j.canlet.2016.11.030.

[114] F. Yang *et al.*, "Emerging inorganic nanomaterials for pancreatic cancer diagnosis and treatment," *Cancer Treat. Rev.*, vol. 38, no. 6, pp. 566–579, Oct. 2012, doi: 10.1016/J.CTRV.2012.02.003.

[115] P. Mi, "Stimuli-responsive nanocarriers for drug delivery, tumor imaging, therapy and theranostics," *Theranostics*, vol. 10, no. 10, pp. 4557–4588, 2020, doi: 10.7150/THNO.38069,.

[116] S. Habib and M. Singh, "Recent advances in lipid-based nanosystems for gemcitabine and gemcitabine–combination therapy," *Nanomaterials*, vol. 11, no. 3, pp. 1–12, Mar. 2021, doi: 10.3390/NANO11030597,.

[117] Q. Hu, P. S. Katti, and Z. Gu, "Enzyme-responsive nanomaterials for controlled drug delivery," *Nanoscale*, vol. 6, no. 21, pp. 12273–12286, Nov. 2014, doi: 10.1039/C4NR04249B,.

[118] M. González-Álamos, P. Guerra, and N. Verdaguer, "Structure, Dynamics and Functional Implications of the Eukaryotic Vault Complex," *Subcell. Biochem.*, vol. 104, pp. 531–548, 2024, doi: 10.1007/978-3-031-58843-3_20,.

[119] A. Maniatis, D. Rizopoulou, A. N. Shaukat, K. Grafanaki, V. Stamatopoulou, and C. Stathopoulos, "Vault Particles in Cancer Progression, Multidrug Resistance, and Drug Delivery: Current Insights and Future Applications," *Int. J. Mol. Sci.*, vol. 26, no. 4, p. 1562, Feb. 2025, doi: 10.3390/IJMS26041562.

[120] G. Frascotti *et al.*, "The Vault Nanoparticle: A Gigantic Ribonucleoprotein Assembly Involved in Diverse Physiological and Pathological Phenomena and an Ideal Nanovector for Drug Delivery and Therapy," *Cancers 2021, Vol. 13, Page 707*, vol. 13, no. 4, p. 707, Feb. 2021, doi: 10.3390/CANCERS13040707.

[121] M. Lieber, J. Mazzetta, W. Nelson-Rees, M. Kaplan, and G. Todaro, "Establishment of a continuous tumor-cell line (panc-1) from a human carcinoma of the exocrine pancreas," *Int. J. cancer*, vol. 15, no. 5, pp. 741–747, 1975, doi: 10.1002/IJC.2910150505.

[122] R. Gradiz, H. C. Silva, L. Carvalho, M. F. Botelho, and A. Mota-Pinto, “MIA PaCa-2 and PANC-1 - pancreas ductal adenocarcinoma cell lines with neuroendocrine differentiation and somatostatin receptors,” *Sci. Rep.*, vol. 6, Feb. 2016, doi: 10.1038/SREP21648.

[123] A. A. Yunis, G. K. Arimura, and D. J. Russin, “Human pancreatic carcinoma (MIA PaCa-2) in continuous culture: sensitivity to asparaginase,” *Int. J. cancer*, vol. 19, no. 1, pp. 128–135, 1977, doi: 10.1002/IJC.2910190118.

[124] B. Dereje and A. Nardos, “Dopamine 2 agonists for the management of type 2 diabetes: a systematic review and meta-analysis,” *J. Diabetes Metab. Disord.*, vol. 22, no. 2, pp. 931–943, Dec. 2023, doi: 10.1007/S40200-023-01230-4.

[125] A. Adamska, A. Domenichini, and M. Falasca, “Pancreatic Ductal Adenocarcinoma: Current and Evolving Therapies,” *Int. J. Mol. Sci.*, vol. 18, no. 7, p. 1338, Jul. 2017, doi: 10.3390/IJMS18071338.

[126] C. Magnon *et al.*, “Autonomic Nerve Development Cancer Progression,” *Science*, 2013, doi: 10.1038/aja.2013.113.

[127] Z. K. Dong, Y. F. Wang, W. P. Li, and W. L. Jin, “Neurobiology of cancer: Adrenergic signaling and drug repurposing,” *Pharmacol. Ther.*, vol. 264, Dec. 2024, doi: 10.1016/j.pharmthera.2024.108750.

[128] S. O. Dalton, L. Mellemkjær, L. Thomassen, P. B. Mortensen, and C. Johansen, “Risk for cancer in a cohort of patients hospitalized for schizophrenia in Denmark, 1969-1993,” *Schizophr. Res.*, vol. 75, no. 2–3, pp. 315–324, Jun. 2005, doi: 10.1016/j.schres.2004.11.009.

[129] J. A. Driver, G. Logroscino, J. E. Buring, J. M. Gaziano, and T. Kurth, “A prospective cohort study of cancer incidence following the diagnosis of Parkinson’s disease,” *Cancer Epidemiol. Biomarkers Prev.*, vol. 16, no. 6, pp. 1260–1265, Jun. 2007, doi: 10.1158/1055-9965.EPI-07-0038.

[130] B. Rubí and P. Maechler, “Minireview: new roles for peripheral dopamine on metabolic control and tumor growth: let’s seek the balance,” *Endocrinology*, vol. 151, no. 12, pp. 5570–5581, Dec. 2010, doi: 10.1210/EN.2010-0745.

[131] X. Zhang, Q. Liu, Q. Liao, and Y. Zhao, “Potential Roles of Peripheral Dopamine in Tumor Immunity,” *J. Cancer*, vol. 8, no. 15, pp. 2966–2973, 2017, doi: 10.7150/JCA.20850.

[132] J. M. Beaulieu and R. R. Gainetdinov, “The physiology, signaling, and pharmacology of

dopamine receptors," *Pharmacol. Rev.*, vol. 63, no. 1, pp. 182–217, Mar. 2011, doi: 10.1124/pr.110.002642.

[133] D. V. Predescu *et al.*, "G Protein-Coupled Receptors (GPCRs)-Mediated Calcium Signaling in Ovarian Cancer: Focus on GPCRs activated by Neurotransmitters and Inflammation-Associated Molecules," *Int. J. Mol. Sci. 2019, Vol. 20, Page 5568*, vol. 20, no. 22, p. 5568, Nov. 2019, doi: 10.3390/IJMS20225568.

[134] H. Wang *et al.*, "Role of the nervous system in cancers: a review," *Cell death Discov.*, vol. 7, no. 1, Jun. 2021, doi: 10.1038/S41420-021-00450-Y.

[135] X. Wang *et al.*, "The Prospective Value of Dopamine Receptors on Bio-Behavior of Tumor," *J. Cancer*, vol. 10, no. 7, pp. 1622–1632, 2019, doi: 10.7150/JCA.27780.

[136] C. Sarkar, D. Chakroborty, U. R. Chowdhury, P. S. Dasgupta, and S. Basu, "Dopamine increases the efficacy of anticancer drugs in breast and colon cancer preclinical models," *Clin. Cancer Res.*, vol. 14, no. 8, pp. 2502–2510, Apr. 2008, doi: 10.1158/1078-0432.CCR-07-1778.

[137] X. Kou *et al.*, "Dopamine d(1)-like receptors suppress proliferation of vascular smooth muscle cell induced by insulin-like growth factor-1," *Clin. Exp. Hypertens.*, vol. 36, no. 3, pp. 140–147, 2014, doi: 10.3109/10641963.2013.789048.

[138] Y. Z. Di, B. S. Han, J. M. Di, W. Y. Liu, and Q. Tang, "Role of the brain-gut axis in gastrointestinal cancer," *World J. Clin. cases*, vol. 7, no. 13, pp. 1554–1570, Jul. 2019, doi: 10.12998/WJCC.V7.I13.1554.

[139] D. C. Borcherding *et al.*, "Expression and therapeutic targeting of dopamine receptor-1 (D1R) in breast cancer," *Oncogene*, vol. 35, no. 24, pp. 3103–3113, Jun. 2016, doi: 10.1038/ONC.2015.369.

[140] Y. Yan *et al.*, "Increased dopamine and its receptor dopamine receptor D1 promote tumor growth in human hepatocellular carcinoma," *Cancer Commun. (London, England)*, vol. 40, no. 12, pp. 694–710, Dec. 2020, doi: 10.1002/CAC2.12103.

[141] B. A. Berkowitz and E. H. Ohlstein, "Fenoldopam," *Cardiovasc. Drug Rev.*, vol. 5, no. 1, pp. 237–250, 2025, doi: 10.1111/j.1527-3466.1987.tb00511.x.

[142] H. D. Langtry and S. P. Clissold, "Pergolide. A review of its pharmacological properties and therapeutic potential in Parkinson's disease," *Drugs*, vol. 39, no. 3, pp. 491–506, 1990, doi: 10.2165/00003495-199039030-00009.

[143] X. Wang *et al.*, “The Prospective Value of Dopamine Receptors on Bio-Behavior of Tumor,” *J. Cancer*, vol. 10, no. 7, p. 1622, 2019, doi: 10.7150/JCA.27780.

[144] D. C. Borcherding *et al.*, “Expression and Therapeutic Targeting of Dopamine Receptor-1 (D1R) in Breast Cancer,” *Oncogene*, vol. 35, no. 24, p. 3103, Jun. 2015, doi: 10.1038/ONC.2015.369.

[145] L. Bai *et al.*, “Bromocriptine monotherapy overcomes prostate cancer chemoresistance in preclinical models,” *Transl. Oncol.*, vol. 34, p. 101707, Aug. 2023, doi: 10.1016/J.TRANON.2023.101707.

[146] P. Sobczuk, M. Łomiak, and A. Cudnoch-Jędrzejewska, “Dopamine D1 Receptor in Cancer,” *Cancers (Basel).*, vol. 12, no. 11, p. 3232, Nov. 2020, doi: 10.3390/CANCERS12113232.

[147] M. Moreno-Smith *et al.*, “Biologic effects of dopamine on tumor vasculature in ovarian carcinoma,” *Neoplasia*, vol. 15, no. 5, pp. 502–510, 2013, doi: 10.1593/NEO.121412.

[148] Z. G. Leng *et al.*, “Activation of DRD5 (dopamine receptor D5) inhibits tumor growth by autophagic cell death,” *Autophagy*, vol. 13, no. 8, pp. 1404–1419, Aug. 2017, doi: 10.1080/15548627.2017.1328347.

[149] C. Gómez-Santos, I. Ferrer, A. F. Santidrián, M. Barrachina, J. Gil, and S. Ambrosio, “Dopamine induces autophagic cell death and alpha-synuclein increase in human neuroblastoma SH-SY5Y cells,” *J. Neurosci. Res.*, vol. 73, no. 3, pp. 341–350, Aug. 2003, doi: 10.1002/JNR.10663.

[150] Z. Yang *et al.*, “CDC42EP3 promotes glioma progression via regulation of CCND1,” *Cell Death Dis.*, vol. 13, no. 4, Apr. 2022, doi: 10.1038/S41419-022-04733-9.

[151] Q. Feng *et al.*, “CDC42EP3 promotes colorectal cancer through regulating cell proliferation, cell apoptosis and cell migration,” *Cancer Cell Int.*, vol. 21, no. 1, Dec. 2021, doi: 10.1186/S12935-021-01845-8.

[152] W. Chen *et al.*, “CDC42EP3 is a key promoter involved in the development and progression of gastric cancer,” *Carcinogenesis*, vol. 42, no. 9, pp. 1179–1188, Sep. 2021, doi: 10.1093/CARCIN/BGAB048.

[153] A. Han, R. Xu, Y. Liu, X. Yin, Z. Lin, and W. Yang, “HSDL2 Acts as a Promoter in Pancreatic Cancer by Regulating Cell Proliferation and Lipid Metabolism,” *Onco. Targets. Ther.*, vol. 14, pp. 435–444, 2021, doi: 10.2147/OTT.S287722.

[154] Y. Shi *et al.*, “Knockdown of HSDL2 inhibits lung adenocarcinoma progression via down-

regulating AKT2 expression," *Biosci. Rep.*, vol. 40, no. 4, Apr. 2020, doi: 10.1042/BSR20200348.

[155] Y. Cheng *et al.*, "[HSDL2 overexpression promotes rectal cancer progression by regulating cancer cell cycle and promoting cell proliferation]," *Nan Fang Yi Ke Da Xue Xue Bao*, vol. 43, no. 4, pp. 544–551, Apr. 2023, doi: 10.12122/J.ISSN.1673-4254.2023.04.06.

[156] L. H. Jia *et al.*, "HSDL2 Promotes Bladder Cancer Growth In Vitro and In Vivo," *Int. J. Med. Sci.*, vol. 16, no. 5, pp. 654–659, 2019, doi: 10.7150/IJMS.31288.

[157] L. Xu, Q. Wu, X. Zhou, Q. Wu, and M. Fang, "TRIM13 inhibited cell proliferation and induced cell apoptosis by regulating NF-κB pathway in non-small-cell lung carcinoma cells," *Gene*, vol. 715, Oct. 2019, doi: 10.1016/j.gene.2019.144015.

[158] B. Yu, Y. Zhou, and J. He, "TRIM13 inhibits cell proliferation and induces autophagy in lung adenocarcinoma by regulating KEAP1/NRF2 pathway," *Cell Cycle*, vol. 22, no. 12, pp. 1496–1513, 2023, doi: 10.1080/15384101.2023.2216504.

[159] H. Li *et al.*, "TRIM13 inhibits cell migration and invasion in clear-cell renal cell carcinoma," *Nutr. Cancer*, vol. 72, no. 7, pp. 1115–1124, Oct. 2020, doi: 10.1080/01635581.2019.1675721.

[160] J. H. Jeong, H. J. Park, S. H. Park, Y. H. Choi, and G. Y. Chi, "β2-Adrenergic Receptor Signaling Pathway Stimulates the Migration and Invasion of Cancer Cells via Src Activation," *Molecules*, vol. 27, no. 18, Sep. 2022, doi: 10.3390/MOLECULES27185940.

[161] L. van Nie *et al.*, "Dopamine induces in vitro migration of synovial fibroblast from patients with rheumatoid arthritis," *Sci. Rep.*, vol. 10, no. 1, pp. 1–13, Dec. 2020, doi: 10.1038/S41598-020-68836-Z;SUBJMETA.

[162] H. Kawano, K. Ohyama, K. Kawamura, and I. Nagatsu, "Migration of dopaminergic neurons in the embryonic mesencephalon of mice," *Dev. Brain Res.*, vol. 86, no. 1–2, pp. 101–113, May 1995, doi: 10.1016/0165-3806(95)00018-9.

[163] N. Kasica, A. Święch, K. Saładziak, J. Mackiewicz, and M. Osęka, "The Inhibitory Effect of Selected D2 Dopaminergic Receptor Agonists on VEGF-Dependent Neovascularization in Zebrafish Larvae: Potential New Therapy in Ophthalmic Diseases," *Cells*, vol. 11, no. 7, p. 1202, Apr. 2022, doi: 10.3390/CELLS11071202.

[164] P. Jandaghi *et al.*, "Expression of DRD2 Is Increased in Human Pancreatic Ductal Adenocarcinoma and Inhibitors Slow Tumor Growth in Mice," *Gastroenterology*, vol. 151, no.

6, pp. 1218–1231, Dec. 2016, doi: 10.1053/j.gastro.2016.08.040.

[165] P. Español *et al.*, “Dopamine receptors D1 and D2 show prognostic significance and potential therapeutic applications for endometrial cancer patients,” *Gynecol. Oncol.*, vol. 176, pp. 25–35, Sep. 2023, doi: 10.1016/J.YGYNO.2023.06.019.

[166] J. Mu *et al.*, “Thioridazine, an antipsychotic drug, elicits potent antitumor effects in gastric cancer,” *Oncol. Rep.*, vol. 31, no. 5, pp. 2107–2114, 2014, doi: 10.3892/OR.2014.3068.

[167] R. Shakya, M. R. Byun, S. H. Joo, K. S. Chun, and J. S. Choi, “Domperidone Exerts Antitumor Activity in Triple-Negative Breast Cancer Cells by Modulating Reactive Oxygen Species and JAK/STAT3 Signaling,” *Biomol. Ther. (Seoul).*, vol. 31, no. 6, p. 692, 2023, doi: 10.4062/BIOMOLTHER.2023.173.

[168] S. J. Sim, J. H. Jang, J. S. Choi, and K. S. Chun, “Domperidone, a Dopamine Receptor D2 Antagonist, Induces Apoptosis by Inhibiting the ERK/STAT3-Mediated Pathway in Human Colon Cancer HCT116 Cells,” *Biomol. Ther. (Seoul).*, vol. 32, no. 5, pp. 568–576, Sep. 2024, doi: 10.4062/BIOMOLTHER.2024.048.

[169] J. Park *et al.*, “Suppression of dopamine receptor 2 inhibits the formation of human prostate cancer PC-3-derived cancer stem cell-like cells through AMPK inhibition,” *Oncol. Lett.*, vol. 29, no. 3, p. 142, Mar. 2025, doi: 10.3892/OL.2025.14888.

[170] S. Jin *et al.*, “L-741626 inhibits hepatocellular carcinoma progression by targeting Ref-1 to suppress MAPK/ERK signalling pathway activity,” *Biol. Direct*, vol. 20, no. 1, Dec. 2025, doi: 10.1186/S13062-025-00624-Z.

[171] A. Staley *et al.*, “Highly potent dopamine receptor D2 antagonist ONC206 demonstrates anti-tumorigenic activity in endometrial cancer,” *Am. J. Cancer Res.*, vol. 11, no. 11, p. 5374, Oct. 2021, doi: 10.1016/j.ygyno.2020.05.372.

[172] S. R. Pierce *et al.*, “Targeting dopamine receptor D2 as a novel therapeutic strategy in endometrial cancer,” *J. Exp. Clin. Cancer Res.*, vol. 40, no. 1, Dec. 2021, doi: 10.1186/s13046-021-01842-9.

[173] S. E. Paraghamian *et al.*, “A novel dopamine receptor D2 antagonist (ONC206) potentiates the effects of olaparib in endometrial cancer,” *Cancer Biol. Ther.*, vol. 24, no. 1, 2023, doi: 10.1080/15384047.2023.2202104.

[174] V. V. Prabhu *et al.*, “ONC201 and imipridones: Anti-cancer compounds with clinical efficacy,” *Neoplasia (United States)*, vol. 22, no. 12, pp. 725–744, Dec. 2020, doi:

10.1016/j.neo.2020.09.005.

[175] S. C. Reddymasu, I. Soykan, and R. W. McCallum, “Domperidone: review of pharmacology and clinical applications in gastroenterology,” *Am. J. Gastroenterol.*, vol. 102, no. 9, pp. 2036–2045, Sep. 2007, doi: 10.1111/J.1572-0241.2007.01255.X.

[176] W. Manni and W. Min, “Signaling pathways in the regulation of cancer stem cells and associated targeted therapy,” *MedComm*, vol. 3, no. 4, p. e176, Dec. 2022, doi: 10.1002/MCO2.176.

[177] X. Chu *et al.*, “Cancer stem cells: advances in knowledge and implications for cancer therapy,” *Signal Transduct. Target. Ther.*, vol. 9, no. 1, p. 170, Dec. 2024, doi: 10.1038/S41392-024-01851-Y.

[178] V. S. Donnenberg and A. D. Donnenberg, “Multiple drug resistance in cancer revisited: the cancer stem cell hypothesis,” *J. Clin. Pharmacol.*, vol. 45, no. 8, pp. 872–877, Aug. 2005, doi: 10.1177/0091270005276905.

[179] E. Sachlos *et al.*, “Identification of drugs including a dopamine receptor antagonist that selectively target cancer stem cells,” *Cell*, vol. 149, no. 6, pp. 1284–1297, Jun. 2012, doi: 10.1016/j.cell.2012.03.049.

[180] F. Perche and V. P. Torchilin, “Cancer cell spheroids as a model to evaluate chemotherapy protocols,” *Cancer Biol. Ther.*, vol. 13, no. 12, p. 1205, Oct. 2012, doi: 10.4161/CBT.21353.

[181] S. Arora *et al.*, “Spheroids in cancer research: Recent advances and opportunities,” *J. Drug Deliv. Sci. Technol.*, vol. 100, p. 106033, Oct. 2024, doi: 10.1016/J.JDDST.2024.106033.

[182] P. Nayak, V. Bentivoglio, M. Varani, and A. Signore, “Three-Dimensional In Vitro Tumor Spheroid Models for Evaluation of Anticancer Therapy: Recent Updates,” *Cancers (Basel).*, vol. 15, no. 19, p. 4846, Oct. 2023, doi: 10.3390/CANCERS15194846.

[183] R. Rebelo, B. Polónia, L. L. Santos, M. H. Vasconcelos, and C. P. R. Xavier, “Drug Repurposing Opportunities in Pancreatic Ductal Adenocarcinoma,” *Pharmaceuticals*, vol. 14, no. 3, p. 280, Mar. 2021, doi: 10.3390/PH14030280.

[184] F. Danhier, O. Feron, and V. Préat, “To exploit the tumor microenvironment: Passive and active tumor targeting of nanocarriers for anti-cancer drug delivery,” *J. Control. Release*, vol. 148, no. 2, pp. 135–146, Dec. 2010, doi: 10.1016/j.jconrel.2010.08.027.

[185] M. E. Davis, Z. Chen, and D. M. Shin, “Nanoparticle therapeutics: an emerging treatment modality for cancer,” *Nat. Rev. Drug Discov.*, vol. 7, no. 9, pp. 771–782, Sep. 2008, doi:

10.1038/NRD2614.

[186] D. Peer, J. M. Karp, S. Hong, O. C. Farokhzad, R. Margalit, and R. Langer, “Nanocarriers as an emerging platform for cancer therapy,” *Nat. Nanotechnol.*, vol. 2, no. 12, pp. 751–760, Dec. 2007, doi: 10.1038/NNANO.2007.387.

[187] H. Maeda, “The enhanced permeability and retention (EPR) effect in tumor vasculature: The key role of tumor-selective macromolecular drug targeting,” *Adv. Enzyme Regul.*, vol. 41, no. 1, pp. 189–207, 2001, doi: 10.1016/S0065-2571(00)00013-3.

[188] J. Fang, H. Nakamura, and H. Maeda, “The EPR effect: Unique features of tumor blood vessels for drug delivery, factors involved, and limitations and augmentation of the effect,” *Adv. Drug Deliv. Rev.*, vol. 63, no. 3, pp. 136–151, Mar. 2011, doi: 10.1016/j.addr.2010.04.009.

[189] J. Y. C. Edgar and H. Wang, “Introduction for Design of Nanoparticle Based Drug Delivery Systems,” *Curr. Pharm. Des.*, vol. 23, no. 14, Nov. 2017, doi: 10.2174/1381612822666161025154003.

[190] V. A. Kickhoefer *et al.*, “Engineering of vault nanocapsules with enzymatic and fluorescent properties,” *Proc. Natl. Acad. Sci. U. S. A.*, vol. 102, no. 12, pp. 4348–4352, Mar. 2005, doi: 10.1073/PNAS.0500929102.

[191] V. A. Kickhoefer *et al.*, “Targeting Vault Nanoparticles to Specific Cell Surface Receptors,” *ACS Nano*, vol. 3, no. 1, p. 27, Jan. 2009, doi: 10.1021/NN800638X.

[192] F. Martín *et al.*, “All-in-one biofabrication and loading of recombinant vaults in human cells,” *Biofabrication*, vol. 14, no. 2, p. 025018, Mar. 2022, doi: 10.1088/1758-5090/AC584D.

[193] A. Muñoz-Juan, A. Carreño, R. Mendoza, and J. L. Corchero, “pharmaceutics Latest Advances in the Development of Eukaryotic Vaults as Targeted Drug Delivery Systems,” doi: 10.3390/pharmaceutics11070300.

VII. ANNEXES

Control vs Bromocriptine (Upregulated)

Gene Symbol	B Avg (log2)	K Avg (log2)	Fold Change	P-val	FDR P-val	Description
SLC39A8	7.27	6.56	1.64	0.0006	0.9997	Solute carrier family 39 (zinc transporter). member 8
COQ10B	7.08	6.36	1.65	0.0018	0.9997	Coenzyme Q10B
OR2D2	5.45	4.75	1.62	0.0063	0.9997	Olfactory receptor. family 2. subfamily D. member 2
LYPLA1	7.43	6.68	1.69	0.0066	0.9997	Lysophospholipase I
CACYBP	7.59	6.64	1.94	0.0154	0.9997	Calcyclin binding protein
CRNDE	6.06	5.4	1.58	0.0193	0.9997	Colorectal neoplasia differentially expressed (non-protein coding)
ELMOD2	5.79	5.13	1.58	0.0193	0.9997	ELMO/CED-12 domain containing 2
GNS	8.49	7.83	1.58	0.0298	0.9997	Glucosamine (N-acetyl)-6-sulfatase
HSPA4L	8.21	7.26	1.93	0.0373	0.9997	Heat shock 70kDa protein 4-like
HEXB	8.09	7.3	1.73	0.0415	0.9997	Hexosaminidase B (beta polypeptide)

Control vs Bromocriptine (Downregulated)

Gene Symbol	B Avg (log2)	K Avg (log2)	Fold Change	P-val	FDR P-val	Description
CDC42EP3	5.32	5.91	-1.51	0.0103	0.9997	CDC42 effector protein (Rho GTPase binding) 3
DEPDC5	5.53	6.17	-1.55	0.022	0.9997	DEP domain containing 5
MFSD11	5.58	6.23	-1.57	0.0431	0.9997	Major facilitator superfamily domain containing 11

Control vs Fenoldopam (Upregulated)

Gene Symbol	B Avg (log2)	K Avg (log2)	Fold Change	P-val	FDR P-val	Description
NKTR	8.69	7.8	1.86	0.0006	0.802	Natural killer cell triggering receptor
ARFGEF2	10.81	10.03	1.72	0.0024	0.815	ADP-ribosylation factor guanine nucleotide-exchange factor 2 (brefeldin A-inhibited)
PRPSAP2	7.3	6.42	1.84	0.0034	0.815	Phosphoribosyl pyrophosphate synthetase-associated protein 2
HEXB	8.34	7.3	2.06	0.0056	0.815	Hexosaminidase B (beta polypeptide)
PAFAH1B1	7.84	7.07	1.7	0.012	0.856	Platelet-activating factor acetylhydrolase 1b. regulatory subunit 1 (45kDa)
SEC61G	6.81	6.02	1.73	0.0138	0.8573	Sec61 translocon gamma subunit
USP10	8.14	7.2	1.92	0.0163	0.8698	Ubiquitin specific peptidase 10
USP41	6.82	5.26	2.95	0.0178	0.8698	Ubiquitin specific peptidase 41
RPS6KA3	7.08	6	2.11	0.0305	0.8747	Ribosomal protein S6 kinase. 90kDa. polypeptide 3
FAM91A1	7.33	6.03	2.47	0.0457	0.8918	Family with sequence similarity 91. member A1

Control vs Fenoldopam (Downregulated)

Gene Symbol	B Avg (log2)	K Avg (log2)	Fold Change	P-val	FDR P-val	Description
MRPS23	4.72	5.39	-1.59	0.0003	0.802	Mitochondrial ribosomal protein S23
MANEA	6.53	7.24	-1.64	0.0036	0.815	Mannosidase. endo-alpha
NSMCE4A	4.57	5.23	-1.57	0.0037	0.815	NSE4 homolog A. SMC5-SMC6 complex component
PAICS	5.46	6.28	-1.76	0.004	0.815	Phosphoribosylaminoimidazole carboxylase. phosphoribosylaminoimidazole succinocarboxamide synthetase
SLC38A1	8.75	9.41	-1.57	0.0097	0.8506	Solute carrier family 38. member 1
REEP3	6.53	7.28	-1.68	0.0116	0.8542	Receptor accessory protein 3
RPGRIP1L	6.26	6.93	-1.58	0.0328	0.889	RPGRIP1-like
HSDL2	5.35	6.12	-1.7	0.038	0.889	Hydroxysteroid dehydrogenase like 2
ELP3	4.61	5.6	-1.99	0.0425	0.889	Elongator acetyltransferase complex subunit 3
BIRC3	6.96	7.66	-1.62	0.0429	0.889	Baculoviral IAP repeat containing 3

Control vs Fenoldopam + Bromocriptine (Upregulated)

Gene Symbol	B Avg (log2)	K Avg (log2)	Fold Change	P-val	FDR P-val	Description
NCAM1	6.95	6.07	1.84	4E-05	0.7584	Transcript Identified by AceView. Entrez Gene ID(s) 4684
PSD3	6.24	5.48	1.69	0.0003	0.7584	Pleckstrin and Sec7 domain containing 3
PAPOLA	7.42	6.5	1.9	0.0024	0.8363	Poly(A) polymerase alpha
TRIM13; KCNRG	8.55	7.8	1.68	0.0031	0.8363	Tripartite motif containing 13; potassium channel regulator
SF1	6.97	5.13	3.58	0.007	0.8478	Memczak2013 ALT_ACCEPTOR. ALT_DONOR. coding. INTERNAL. intronic best transcript NM_201998
HEXB	8.12	7.3	1.77	0.0117	0.8715	Hexosaminidase B (beta polypeptide)
FUBP1	7.35	6.51	1.78	0.0155	0.8715	Far upstream element (FUSE) binding protein 1
NEB	6.85	5.92	1.91	0.0313	0.8803	Nebulin
CACYBP	7.52	6.64	1.85	0.0461	0.8803	Calcyclin binding protein
YBEY	6.32	5.55	1.7	0.0494	0.8803	YbeY metallopeptidase (putative)

Control vs Fenoldopam + Bromocriptine (Downregulated)

Gene Symbol	B Avg (log2)	K Avg (log2)	Fold Change	P-val	FDR P-val	Description
CCDC58	5.89	6.55	-1.58	0.0006	0.7584	Coiled-coil domain containing 58
MANEA	6.55	7.24	-1.62	0.0086	0.8715	Mannosidase. endo-alpha

Fenoldopam vs Fenoldopam + Bromocriptine (Upregulated)

Gene Symbol	B Avg (log2)	K Avg (log2)	Fold Change	P-val	FDR P-val	Description
NR2C1	5.68	4.92	1.7	0.0009	0.9683	Nuclear receptor subfamily 2. group C. member 1
NCAM1	6.95	6.2	1.68	0.001	0.9998	Transcript Identified by AceView. Entrez Gene ID(s) 4684
POGZ	6.4	5.68	1.65	0.0011	0.9998	Transcript Identified by AceView. Entrez Gene ID(s) 23126
RPS23	8.88	8.15	1.66	0.0069	0.9998	Ribosomal protein S23
PDIA3	7.14	6.41	1.67	0.0075	0.9998	Protein disulfide isomerase family A member 3
NDUFAF6	8.53	7.65	1.83	0.0105	0.9998	NADH dehydrogenase (ubiquinone) complex I. assembly factor 6
CAPRIN1	6.94	5.46	2.8	0.0121	0.9998	Cell cycle associated protein 1
GOSR1	5.98	5.07	1.88	0.0298	0.9998	Golgi SNAP receptor complex member 1
RPL7	8.35	7.55	1.75	0.0345	0.9998	Ribosomal protein L7
MKLN1	7.69	6.71	1.97	0.0439	0.9998	Muskelin 1. intracellular mediator containing kelch motifs

Fenoldopam vs Fenoldopam + Bromocriptine (Downregulated)

Gene Symbol	B Avg (log2)	K Avg (log2)	Fold Change	P-val	FDR P-val	Description
AK5	4.67	5.47	-1.74	0.0003	0.899	Adenylate kinase 5
RBM6	9.49	10.11	-1.54	0.0006	0.899	RNA binding motif protein 6
ATP5O	9.05	8.45	1.51	0.0007	0.899	ATP synthase. H+ transporting. mitochondrial F1 complex. O subunit
INTS4	5.38	6.05	-1.59	0.0063	0.9998	Integrator complex subunit 4
AAED1	4.77	5.71	-1.92	0.0078	0.9998	AhpC/TSA antioxidant enzyme domain containing 1
TMEM165	7.45	8.09	-1.56	0.0078	0.9998	Transmembrane protein 165
PPL	6.4	7.05	-1.57	0.0103	0.9998	Periplakin
MTHFD1L	5.59	6.22	-1.54	0.0146	0.9998	Methylenetetrahydrofolate dehydrogenase (NADP+ dependent) 1-like
RBPMS	6.59	7.43	-1.79	0.0414	0.9998	RNA binding protein with multiple splicing
NKTR	8.05	8.69	-1.56	0.0461	0.9998	Natural killer cell triggering receptor

Shared differential expressions within groups							
Gene Symbol	**ID**	**Fe Avg (log2)**	**K Avg (log2)**	**Fold Change**	**P-val**	**FDR P-val**	**Description**
EIF4A2; SNORA63; SNORD2; SNORA4; SNORA81; MIR1248	K x Fe x Cb	7.26	6.68	1.5	0.0027	0.815	Eukaryotic translation initiation factor 4A2; small nucleolar RNA. H/ACA box 63; small nucleolar RNA. C/D box 2; small nucleolar RNA. H/ACA box 4; small nucleolar RNA. H/ACA box 81; microRNA 1248
PRPSAP2	K x Fe x Cb	7.3	6.42	1.84	0.0034	0.815	Phosphoribosyl pyrophosphate synthetase-associated protein 2
MANEA	K x Fe x Cb	6.53	7.24	-1.64	0.0036	0.815	Mannosidase. endo-alpha
HEXB	K x B x Fe	8.34	7.3	2.06	0.0056	0.815	Hexosaminidase B (beta polypeptide)
PSD3	K x Fe x Cb	6.12	5.48	1.55	0.0117	0.8542	Pleckstrin and Sec7 domain containing 3
PAFAH1B1	K x Fe x Cb	7.84	7.07	1.7	0.012	0.856	Platelet-activating factor acetylhydrolase 1b. regulatory subunit 1 (45kDa)
CRNDE	K x B x Fe	6.16	5.4	1.69	0.0125	0.856	Colorectal neoplasia differentially expressed (non-protein coding)
CACYBP	K x B x Cb	7.52	6.64	1.85	0.0461	0.8803	Calcyclin binding protein

Generalitat de Catalunya
Departament de Territori i Sostenibilitat
Direcció General de Polítiques Ambientals
i Medi Natural
Comissió d'Experimentació Animal
Òrgan Habilitat

Ref. núm. informe: CEA-OH/10234/4

INFORME D'AVALUACIÓ D'UN PROJECTE PER LA COMISSIÓ D'EXPERIMENTACIÓ ANIMAL COM A ÒRGAN HABILITAT PER LA GENERALITAT DE CATALUNYA (Reial Decret 53/2013, d'1 de febrer)
Ref. núm. de projecte: 10234
Títol del projecte: **Evaluación de nanoconjugados para terapia dirigida en modelos murinos de cáncer de páncreas, endometrio y glioblastoma**
Projecte tipus: ☐ I ☐ II ☒ III
Persona responsable del projecte: Maria Virtudes Céspedes Navarro
Data d'admissió de la documentació: 16.07.2018 / 18.10.2018 / 04.02.2019 / 25.02.2019
Data d'avaluació per la CEA com a OH: 12.09.2018 / 07.11.2018 / 30.01.2019 / 20.03.2019

Revisada la documentació presentada, s'informen, d'acord amb la normativa vigent*, els punts següents:

1. Avaluada la informació relativa a la procedència dels animals (art.19 del RD 53/2013 d'1 de febrer i només per a les espècies* incloses a l'annex I del RD 53/2013 d'1 de febrer o a l'annex de la Llei 5/1995, de 21 de juny), s'informa,
(*) la utilització de gossos i gats rodamóns, i els provinents de centres de recollida d'animals abandonats està prohibida a Catalunya (art. 4.1.a de la Llei 5/1995)
☐ No procedeix, atès que l'espècie animal no està inclosa a l'annex I del RD 53/2013, d'1 de febrer.
☒ Favorablement
☐ Desfavorablement, atès que
Observacions/Justificació:

2. Avaluada la informació presentada relativa a la utilització de primats no humans en el projecte, d'acord amb l'art. 21 del RD 53/2013 d'1 de febrer, s'informa,
☒ No procedeix, atès que no s'utilitzen primats no humans.
☐ Favorablement.
☐ Desfavorablement, atès que
Observacions/Justificació:

3. Avaluada la informació relativa a l'ús d'anestèsia durant el projecte (art. 26 del RD 53/2013 d'1 de febrer), s'informa,
☐ No procedeix, atès que el projecte no ho requereix.
☒ Favorablement el protocol d'anestèsia a aplicar.
☐ Favorablement la justificació presentada pel responsable del projecte en relació amb la no utilització de l'anestèsia per ser incompatible amb el projecte o per estar contraindicada.
☐ Desfavorablement, atès que
Observacions/Justificació:

Doctor Roux, 80
08017 Barcelona
Telèfon: 93 567 42 00
FAX: 93 280 33 20

GENERALITAT DE CATALUNYA

Generalitat de Catalunya
Departament de Territori i Sostenibilitat
Direcció General de Polítiques Ambientals
i Medi Natural
Comissió d'Experimentació Animal
Òrgan Habilitat

Ref. núm. informe: CEA-OH/10234/4

4. Avaluada la informació relativa a l'ús d'analgèsia o altres mètodes destinats a eliminar al màxim el dolor, el sofriment durant el projecte (art. 26 del RD 53/2013 d'1 de febrer), s'informa,
☐ No procedeix, atès que el projecte no ho requereix.
☒ Favorablement el protocol d'analgèsia o altres mètodes a aplicar destinats a eliminar al màxim el dolor.
☐ Favorablement la justificació presentada pel responsable del projecte en relació amb la no utilització de l'analgèsia per ser incompatible amb el projecte o per estar contraindicada.
☐ Desfavorablement, atès que
Observacions/Justificació:

5. Avaluada la informació relativa a les condicions d'allotjament, zootècniques i de cura dels animals en el projecte (art. 6 del RD53/2013 d'1 de febrer), s'informa,
☐ No procedeix, atès que el projecte no ho requereix.
☒ Favorablement.
☐ Desfavorablement, atès que
Observacions/Justificació:

6. Mètode d'eutanàsia:
6.1. Avaluada la informació relativa al mètode d'eutanàsia (art. 7 i annex III del RD 53/2013 d'1 de febrer) en finalitzar el projecte, s'informa,
☐ No procedeix, atès que els animals no són eutanasiats
☒ Favorablement
☐ Desfavorablement, atès que
Observacions/Justificació:

6.2. I en relació amb el mètode d'eutanàsia en aplicació a criteris de punt final, s'informa,
☐ No procedeix, atès que el projecte no ho requereix.
☒ Favorablement.
☐ Desfavorablement, atès que
Observacions/Justificació:

7. Avaluades les condicions generals previstes en l'execució del projecte (art. 25.3 del RD 53/2013 d'1 de febrer) s'informa,
☒ Favorablement, atès que el projecte es realitzaria tenint en compte evitar als animals qualsevol dolor, sofriment, angoixa o dany durador innecessari.
☐ Desfavorablement, atès que
Observacions/Justificació:

Doctor Roux, 80
08017 Barcelona
Telèfon: 93 567 42 00
FAX: 93 280 33 20

Generalitat de Catalunya
Departament de Territori i Sostenibilitat
Direcció General de Polítiques Ambientals
i Medi Natural
Comissió d'Experimentació Animal
Òrgan Habilitat

Ref. núm. informe: CEA-OH/10234/4

8. Avaluada la informació presentada en relació amb l'acreditació/capacitació del personal que participa en el projecte (art. 25.5 del RD 53/2013 d'1 de febrer), s'informa,
☒ Favorablement.
☐ Desfavorablement, atès que
Observacions/Justificació:

9. Avaluada la informació relacionada amb el transport dels animals (art. 9.1 del RD 53/2013 d'1 de febrer), s'informa,
☒ No procedeix, atès que els animals no són transportats durant el projecte.
☐ Favorablement.
☐ Desfavorablement, atès que
Observacions/Justificació:

10. Avaluada la informació relativa a la utilització d'animals d'espècies amenaçades (art. 20 del RD 53/2013 d'1 de febrer), s'informa,
☒ No procedeix
☐ Favorablement.
☐ Desfavorablement, atès que
Observacions/Justificació:

11. Avaluada la informació relativa a la utilització d'animals capturats en la natura (art. 22 del RD 53/2013 d'1 de febrer), s'informa,
☒ No procedeix.
☐ Favorablement.
☐ Desfavorablement, atès que
Observacions/Justificació:

12. Avaluada la informació relativa a la reutilització d'animals (utilització d'animals que han esta sotmesos prèviament a un altre projecte) (art. 29 del RD 53/2013 d'1 de febrer), s'informa,
☒ No procedeix.
☐ Favorablement.
☐ Desfavorablement, atès que
Observacions/Justificació:

13. Avaluada la finalitat, els beneficis científics i, si s'escau, el valor docent del projecte (art. 34.2a del RD 53/2013 d'1 de febrer) s'informa,
☒ Favorablement.
☐ Desfavorablement, atès que
Observacions/Justificació:

Doctor Roux, 80
08017 Barcelona
Telèfon: 93 567 42 00
FAX: 93 280 33 20

Generalitat de Catalunya
Departament de Territori i Sostenibilitat
Direcció General de Polítiques Ambientals
i Medi Natural
Comissió d'Experimentació Animal
Òrgan Habilitat

Ref. núm. informe: CEA-OH/10234/4

14. Avaluada la conformitat amb les 3Rs (art.34.2b del RD 53/2013 d'1 de febrer), s'informa,
☒ Favorablement.
☐ Desfavorablement.
Observacions/Justificació:

15. Avaluat el grau de severitat indicat a la memòria del projecte (art.34.2c del RD 53/2013 d'1 de febrer) s'informa,
☒ Favorablement.
☐ Desfavorablement, atès
Observacions/Justificació:

Amb la classificació de:
☐ Sense recuperació ☐ Lleu ☐ Moderat ☒ Sever

16. Balanç ètic: analitzats els danys i beneficis del projecte (art.34.2d del RD 53/2013 d'1 de febrer), s'informa,
☒ Favorablement.
☐ Desfavorablement.
Observacions/Justificació:

17. El projecte requereix un resum no tècnic (art. 33.1 del RD 53/2013 d'1 de febrer).
☒ Sí
☐ No
Atès que és de Tipus III

18. Avaluació retrospectiva del projecte (art. 35.1 del RD 53/2013 d'1 de febrer).
Atès que el projecte,
☐ Utilitza primats.
☐ S'utilitzen primats per a finalitats diferents a les previstes a l'art. 21.2.a del RD 53/2013 d'1 de febrer.
☒ Ha estat classificat com a sever.
☐ El projecte implica un dolor greu i perllongat que no pot ser alleujat.
☐ Altres: Article 33.6 f) del RD 53/2013
Justificació:

S'informa que el projecte,
☐ No requereix avaluació retrospectiva.
☒ Sí, cal realitzar l'avaluació retrospectiva la qual s'ha de presentar al finalitzar el projecte o com a màxim als 5 anys de l'autorització d'aquest.

19. Altres comentaris:

Doctor Roux, 80
08017 Barcelona
Telèfon: 93 567 42 00
FAX: 93 280 33 20

Generalitat de Catalunya
Departament de Territori i Sostenibilitat
Direcció General de Polítiques Ambientals
i Medi Natural
Comissió d'Experimentació Animal
Òrgan Habilitat

Ref. núm. informe: CEA-OH/10234/4

RESULTAT FINAL DE L'INFORME.

Per tant, tenint en compte l'informe de cadascun dels punts anteriors,

☒ S'informa FAVORABLEMENT

☐ S'informa DESFAVORABLEMENT
Justificació:

Sílvia Lleonart
Secretària

Doctor Roux, 80
08017 Barcelona
Telèfon: 93 567 42 00
FAX: 93 280 33 20

Biofabrication

PAPER

All-in-one biofabrication and loading of recombinant vaults in human cells

Fernando Martín[1,7], **Aida Carreño**[1,8], **Rosa Mendoza**[1,2], **Pablo Caruana**[3], **Francisco Rodriguez**[3], **Marlon Bravo**[4,5], **Antoni Benito**[4,5], **Neus Ferrer-Miralles**[1,2,6], **M Virtudes Céspedes**[3,*] and **José Luis Corchero**[1,2,6,*]

[1] Institut de Biotecnologia i de Biomedicina, Universitat Autònoma de Barcelona, Bellaterra, 08193 Barcelona, Spain
[2] CIBER de Bioingeniería, Biomateriales y Nanomedicina (CIBER-BBN), Bellaterra, 08193 Barcelona, Spain
[3] Grup d´Oncologia Ginecològica i Peritoneal. Institut d'Investigacions Biomédiques Sant Pau, Hospital de Santa Creu i Sant Pau, 08041 Barcelona, Spain
[4] Laboratori d'Enginyeria de Proteïnes, Departament de Biologia, Universitat de Girona, 17003 Girona, Spain
[5] Institut d'Investigació Biomèdica de Girona Josep Trueta, (IdIBGi), 17190 Salt, Spain
[6] Departament de Genètica i de Microbiologia, Universitat Autònoma de Barcelona, Bellaterra, 08193 Barcelona, Spain
[7] Present address: Nanobioengineering group, Institute for Bioengineering of Catalonia (IBEC), Helix building, C/ Baldiri Reixac 15-21, Barcelona 08028, Spain.
[8] Present address: Institut de Ciència de Materials de Barcelona, ICMAB-CSIC, Campus UAB, 08193 Bellaterra, Spain.
* Authors to whom any correspondence should be addressed.

E-mail: MCespedes@santpau.cat **and** jlcorchero@ciber-bbn.es

Keywords: vault particles, protein nanocages, drug delivery systems, self-assembling protein nanoparticles, eukaryotic cell factories

OPEN ACCESS

RECEIVED
9 February 2021

REVISED
15 February 2022

ACCEPTED FOR PUBLICATION
24 February 2022

PUBLISHED
9 March 2022

Abstract

One of the most promising approaches in the drug delivery field is the use of naturally occurring self-assembling protein nanoparticles, such as virus-like particles, bacterial microcompartments or vault ribonucleoprotein particles as drug delivery systems (DDSs). Among them, eukaryotic vaults show a promising future due to their structural features, *in vitro* stability and non-immunogenicity. Recombinant vaults are routinely produced in insect cells and purified through several ultracentrifugations, both tedious and time-consuming processes. As an alternative, this work proposes a new approach and protocols for the production of recombinant vaults in human cells by transient gene expression of a His-tagged version of the major vault protein (MVP-H6), the development of new affinity-based purification processes for such recombinant vaults, and the all-in-one biofabrication and encapsulation of a cargo recombinant protein within such vaults by their co-expression in human cells. Protocols proposed here allow the easy and straightforward biofabrication and purification of engineered vaults loaded with virtually any INT-tagged cargo protein, in very short times, paving the way to faster and easier engineering and production of better and more efficient DDS.

1. Introduction

Current therapies based on the administration of recombinant proteins in their native form usually face several drawbacks, such as short *in vivo* half-life, low membrane permeability, rapid elimination from blood stream, and undesired side effects caused by the multiple or high doses administered in order to reach the desirable concentration in the target cell or organ. As a result, these proteins need to be protected, typically by using nanocarriers that, at the same time, can be engineered to improve their targeted delivery to the desired biological site. In this line, a perfect nanocarrier should be able to deliver its cargo at the right moment, place and concentration. Thus, the use of smart drug delivery systems (DDSs), acting as a depot for high therapeutic concentrations and providing a solubilizing and protective environment is a promising strategy [1–3]. Nanoparticles (NPs) have been deeply explored as DDS, either for local release, where they are retained at the site of delivery, or for systemic delivery, increasing the circulation lifetime. NPs with self-assembly properties, good stability and specificity have already been used clinically

Atherosclerosis xxx (xxxx) xxx

Contents lists available at ScienceDirect

Atherosclerosis

journal homepage: www.elsevier.com/locate/atherosclerosis

Targeting LDL aggregation decreases atherosclerotic lipid burden in a humanized mouse model of familial hypercholesterolemia: Crucial role of ApoB100 conformational stabilization

A. Benitez-Amaro [a,b,1], E. Garcia [a,b,c,1], M.T. La Chica Lhoëst [a,b,c,1], A. Martínez [a,b], C. Borràs [d,e], M. Tondo [e,f], M.V. Céspedes [g,h], P. Caruana [g,h], A. Pepe [i], B. Bochicchio [i], A. Cenarro [j,k], F. Civeira [j,k], R. Prades [l], J.C. Escola-Gil [d,e], V. Llorente-Cortés [a,b,k,*]

[a] Institute of Biomedical Research of Barcelona (IIBB)-Spanish National Research Council (CSIC), 08036, Barcelona, Spain
[b] Institut d'Investigacions Biomèdiques IIB Sant Pau, 08041, Barcelona, Spain
[c] Universitat Autònoma de Barcelona, 08193, Bellaterra, Barcelona, Spain
[d] Institut de Recerca de l'Hospital Santa Creu i Sant Pau, Institut d'Investigacions Biomèdiques IIB Sant Pau, 08041, Barcelona, Spain
[e] CIBER de Diabetes y Enfermedades Metabólicas Asociadas (CIBERDEM), 28029, Madrid, Spain
[f] Department of Clinical Biochemistry, Hospital de la Santa Creu i Sant Pau, IIB Sant Pau, 08041, Barcelona, Spain
[g] Grup d'Oncologia Ginecològica i Peritoneal, Institut de Recerca Sant Pau, Hospital de la Santa Creu i Sant Pau, 08041, Barcelona, Spain
[h] Universitat de Barcelona (UB), 08007, Barcelona, Spain
[i] Laboratory of Bioinspired Materials, Department of Science, University of Basilicata, Potenza, Italy
[j] Hospital Universitario Miguel Servet, IIS Aragón, Instituto Aragonés de Ciencias de la Salud, Universidad de Zaragoza, Zaragoza, Spain
[k] CIBER de Enfermedades Cardiovasculares CIBERCV, Institute of Health Carlos III, 28029, Madrid, Spain
[l] Iproteos S.L., Barcelona Science Park (PCB), Barcelona, Spain

ARTICLE INFO

Keywords:
Atherosclerosis
LDL aggregation
LRP1-Based peptides
ApoB100 conformation
Therapeutic peptides

ABSTRACT

Background and aims: Low-density lipoprotein (LDL) aggregation is nowadays considered a therapeutic target in atherosclerosis. DP3, the retro-enantio version of the sequence Gly^{1127}-Cys^{1140} of LRP1, efficiently inhibits LDL aggregation and foam cell *in vitro* formation. Here, we investigate whether DP3 modulates atherosclerosis in a humanized ApoB100, LDL receptor (LDLR) knockout mice (*Ldlr*$^{-/-}$*hApoB*100 Tg) and determine the potential LDL-related underlying mechanisms.

Methods: Tg mice were fed an HFD for 21 days to induce atherosclerosis and then randomized into three groups that received a daily subcutaneous administration (10 mg/kg) of i) vehicle, ii) DP3 peptide, or iii) a non-active peptide (IP321). The *in vivo* biodistribution of a fluorescent-labeled peptide version (TAMRA-DP3), and its colocalization with ApoB100 in the arterial intima, was analyzed by imaging system (IVIS) and confocal microscopy. Heart aortic roots were used for atherosclerosis detection and quantification. LDL functionality was analyzed by biochemical, biophysical, molecular, and cellular studies.

Results: Intimal neutral lipid accumulation in the aortic root was reduced in the DP3-treated group as compared to control groups. ApoB100 in LDLs from the DP3 group exhibited an increased percentage of α-helix secondary structures and decreased immunoreactivity to anti-ApoB100 antibodies. LDL from DP3-treated mice were protected against passive and sphingomyelinase (SMase)-induced aggregation, although they still experienced SMase-induced sphingomyelin phospholysis. In patients with familial hypercholesterolemia (FH), DP3 efficiently inhibited both SMase-induced phospholysis and aggregation.

Conclusions: DP3 peptide administration inhibits atherosclerosis by preserving the α-helix secondary structures of ApoB100 in a humanized ApoB100 murine model that mimicks the hallmark of human hypercholesterolemia.

* Corresponding author. Institute of Biomedical Research of Barcelona (IIBB)-Spanish National Research Council (CSIC), 08036, Barcelona, Spain.
E-mail address: cllorente@santpau.cat (V. Llorente-Cortés).
[1] These authors equally contributed.

https://doi.org/10.1016/j.atherosclerosis.2024.118630
Received 21 February 2024; Received in revised form 30 September 2024; Accepted 15 October 2024
Available online 19 October 2024

Gynecologic Oncology 176 (2023) 25–35

Contents lists available at ScienceDirect

Gynecologic Oncology

journal homepage: www.elsevier.com/locate/ygyno

Dopamine receptors D1 and D2 show prognostic significance and potential therapeutic applications for endometrial cancer patients

Pia Español [a,b,c,*], Ramon Rovira [a,b], Pablo Caruana [a], Rocío Luna-Guibourg [a,b], Cristina Soler [a,b], Natalia Teixeira [a,b], Francisco Rodríguez [a], Alberto Gallardo [d], Maria Edwards [a], Oriol Porta [e], Maria Gámez [f], Olga Sánchez [g,h,j], Elisa Llurba [b,g,h,j], Jose Luis Corchero [i,1], María Virtudes Céspedes [a,h,**,1]

[a] Gynecologic and Oncology Peritoneal group, Biomedical Research Institute Sant Pau (IIB Sant Pau), Hospital de la Santa Creu i Sant Pau, 08041 Barcelona, Spain
[b] Department of Obstetrics and Gynecology, Hospital de la Santa Creu i Sant Pau, Barcelona 08041, Spain
[c] Department of Obstetrics and Gynecology, Hospital Universitari Son Espases, Palma 07120, Spain
[d] Department of Pathology, Hospital de la Santa Creu i Sant Pau, Barcelona 08041, Spain
[e] Department of Obstetrics and Gynecology, University Hospital Mútua Terrassa, Terrassa 08221, Spain
[f] Department of Pharmacy, Hospital de la Santa Creu i Sant Pau, 08041 Barcelona, Spain
[g] Women and Perinatal Health Research group. Department of Obstetrics and Gynecology. Biomedical Research Institute Sant Pau (IIB Sant Pau), Hospital de la Santa Creu i Sant Pau, 08041 Barcelona, Spain
[h] Primary care interventions to prevent maternal and child chronic diseases of Perinatal and developmental origin network (RICORS), Instituto Salud Carlos III, Madrid, Spain
[i] Institut de Biotecnologia i de Biomedicina and Centro de Investigación Biomédica en Red de Bioingeniería, Biomateriales y Nanomedicina, Instituto de Salud Carlos III, Universitat Autònoma de Barcelona, Bellaterra, 08193 Barcelona, Spain
[j] Universitat Autònoma de Barcelona, Barcelona, Spain

HIGHLIGHTS

- ADRβ2 expression was neither associated with clinico-pathological parameters nor prognostic value in the analyzed patients.
- DRD1 expression showed an inverse association with tumor size and stage in our endometrial cancer patient cohort.
- DRD2 expression showed significant positive association with non-endometrioid endometrial cancer, high grade and tumor size.
- High expression of DRD2 is an independent significant prognostic marker for predicting OS and DFS in the patient's cohort.
- DRD1 agonism and DRD2 antagonism combination reduced cellular viability and could have a potential therapeutic benefit.

ARTICLE INFO

Article history:
Received 22 March 2023
Received in revised form 17 June 2023
Accepted 23 June 2023
Available online 11 July 2023

Keywords:
Endometrial cancer
Dopamine receptor
DRD1
DRD2
Prognostic value
Neuromodulation
Targeted therapy
Drug repurposing

ABSTRACT

Objective. Catecholaminergic signaling has been a target for therapy in different type of cancers. In this work, we characterized the ADRβ2, DRD1 and DRD2 expression in healthy tissue and endometrial tumors to evaluate their prognostic significance in endometrial cancer (EC), unraveling their possible application as an antitumor therapy.

Methods. 109 EC patients were included. The expression of the ADRβ2, DRD1 and DRD2 proteins was evaluated by immunohistochemistry and univariate and multivariate analysis to assess their association with clinic-pathological and outcome variables. Finally, HEC1A and AN3CA EC cell lines were exposed to different concentrations of selective dopaminergic agents alone or in combination to study their effects on cellular viability.

Results. ADRβ2 protein expression was not associated with clinico-pathological parameters or prognosis. DRD1 protein expression was reduced in tumors samples but showed a significant inverse association with tumor size and stage. DRD2 protein expression was significantly associated with non-endometrioid EC, high grade tumors, tumor size, worse disease-free survival (HR = 3.47 (95%CI:1.35–8.88)) and overall survival (HR = 2.98 (95%CI:1.40–6.34)). The DRD1 agonist fenoldopam showed a reduction of cellular viability in HEC1A and AN3CA cells. The exposure to domperidone, a DRD2 antagonist, significantly reduced cell viability compared to the control. Finally, DRD1 agonism and DRD2 antagonism combination induced a significant

* Correspondence to: P. Español, Department of Obstetrics and Gynecology, Hospital Universitari Son Espases, Palma 07120, Spain.
** Correspondence to: M.V. Céspedes, Biomedical Research Institute Sant Pau (IIB Sant Pau), Hospital de Santa Creu i Sant Pau, 08041 Barcelona, Spain.
E-mail addresses: mariapia.espanol@ssib.es (P. Español), mcespedes@santpau.cat (M.V. Céspedes).
[1] Co-last author.

https://doi.org/10.1016/j.ygyno.2023.06.019

Review

WOMEN'S HEALTH

Women's Health
Volume 18: 1–13

DOI: 10.1177/17455057221095537
journals.sagepub.com/home/whe
SAGE

Neural plasticity of the uterus: New targets for endometrial cancer?

Pia Español[1,2], Rocio Luna[1,2], Cristina Soler[1,2], Pablo Caruana[1], Amanda Altés-Arranz[1], Francisco Rodríguez[1], Oriol Porta[1,2], Olga Sanchez[3,4], Elisa Llurba[2,3,4], Ramón Rovira[1,2*] and María Virtudes Céspedes[1,5*]

Abstract

Endometrial carcinoma is the most common gynecological malignancy in Western countries and is expected to increase in the following years because of the high index of obesity in the population. Recently, neural signaling has been recognized as part of the tumor microenvironment, playing an active role in tumor progression and invasion of different solid tumor types. The uterus stands out for the physiological plasticity of its peripheral nerves due to cyclic remodeling brought on by estrogen and progesterone hormones throughout the reproductive cycle. Therefore, a precise understanding of nerve-cancer crosstalk and the contribution of the organ-intrinsic neuroplasticity, mediated by estrogen and progesterone, of the uterine is urgently needed. The development of new and innovative medicines for patients with endometrial cancer would increase their quality of life and health. This review compiles information on the architecture and function of autonomous uterine neural innervations and the influence of hormone-dependent nerves in normal uterus and tumor progression. It also explores new therapeutic possibilities for endometrial cancer using these endocrine and neural advantages.

Keywords

autonomic nervous system, endometrial cancer, nerve-cancer, nerve plasticity, neuroreceptor, neurotherapy, neurotransmitter, sex hormones signaling

Date received: 12 November 2021; revised: 28 March 2022; accepted: 1 April 2022

Introduction

Nerve-cancer interaction was first described in the pain process associated with cancer progression[1] and perineural invasion (PNI), which cancer cells use as a track to disseminate.[2] Over recent decades, nerve-cancer crosstalk as a contributor to the tumor microenvironment has come to be seen as an important key-player. It is where activated downstream signaling pathways stimulate cancer cells to grow and migrate.[3]

Tumors interplay with nerves to stimulate and maintain nerve infiltration through a paracrine mechanism involving the secretion of growth factors driving to neurogenesis.[4] Reciprocally, cancer cells use nerves to activate angiogenesis and contribute to immune modulation and to tumor dissemination through the release of catecholamines like noradrenaline, epinephrine, dopamine, acetylcholine, and neurotrophic factors induced by cancer and stromal cells.[5,6]

The active crosstalk between nerves and tumor cells was first demonstrated in prostate[7] and gastric[8] cancers, and

[1]Gynecology and Oncology Peritoneal Group, Institut d'Investigacions Biomèdiques Sant Pau, Hospital de la Santa Creu i Sant Pau, Barcelona, Spain
[2]Department of Obstetrics and Gynecology, Hospital de la Santa Creu i Sant Pau, Barcelona, Spain
[3]Women and Perinatal Health Research Group, Obstetrics and Gynaecology Department, Hospital Sant Pau and Universitat Autònoma de Barcelona, Barcelona, Spain
[4]Maternal and Child Health and Development Network, Instituto Salud Carlos III, Madrid, Spain
[5]CIBER de Bioingeniería, Biomateriales y Nanomedicina (CIBER-BBN), Barcelona, Spain

*Ramón Rovira and María Virtudes Céspedes provided equal co-author contribution.

Corresponding authors:
María Virtudes Céspedes, Gynecology and Oncology Peritoneal Group, Institut d'Investigacions Biomèdiques Sant Pau, Hospital de la Santa Creu i Sant Pau, 08041 Barcelona, Spain.
Email: mcespedes@santpau.cat

Pia Español, Department of Obstetrics and Gynecology, Hospital de la Santa Creu i Sant Pau, 08025 Barcelona, Spain.
Email: pia.espanol.lloret@gmail.com

RESEARCH ARTICLE METASTATIC PANCREATIC CANCER

A New Perspective for Pancreatic Ductal Adenocarcinoma Management: Diagnosis and Therapy Using Nanoparticle-Based Technology

Noa de la Fuente[1]*, Vicenç Artigas[2], Pablo Caruana[3], Francisco Rodríguez[3], María Virtudes Céspedes[3]*

[1]Department of General and Digestive Surgery, HM Rosaleda Hospital, Santiago de Compostela, Galicia, Spain
[2]Department of Surgery, Autonomous University of Barcelona, Barcelona, Cataluña, Spain
[3]Gynecologic & Peritoneal Oncology Group (GOGyP), Sant Pau Biomedical Research Institute (IIB Sant Pau), Barcelona, Cataluña, Spain

ABSTRACT

Pancreatic cancer is the 4th most common cause of cancer-related mortality in the Western world. Pancreatic ductal adenocarcinoma (PDAC) is usually diagnosed at a later stage and mechanisms of growth and progression have yet to be clarified. Treatment fails mostly due to chemo- and radiation resistance. In order to overcome this issue, nanomedicine has become an opportunity for new diagnostic and therapeutic approaches, providing a tool to enhance drug delivery to treat PDAC. It allows the development of a nanoparticle-based drug delivery system (DDS) that combines several chemotherapeutic agents with nanocarriers for PDAC management. In this review, we describe the latest therapies and advances in pharmaceutical nanoformulations for PDAC management.

BACKGROUND

Advances in nanotechnology over the last years provide a new pathway for diagnosis and treatment of cancer disease. Current pancreatic cancer diagnosis and treatment options are suboptimal and it is urgent to look for new strategies. Pharmaceutical nanoformulations could have better site-specificity and diagnostic and therapeutic efficiency. This efficiency could also have an impact on the number of patients rescued for curative surgery, which currently amounts to barely 15% of the patients diagnosed with the resectable disease.

Received September 10th, 2021 - Accepted October 04th, 2021
Keywords Pancreatic cancer; Pancreatic ductal adenocarcinoma; Targeted drug delivery system; Targeted nanocarrier; Nanoparticle based drug delivery system; Chemotherapy
List of abbreviations PDAC Pancreatic Ductal Adenocarcinoma; DDS Drug Delivery System; CAFs Cancer Associated Fibroblasts; PSCs Pancreatic Stellate Cells; MDSCs Myeloid Derived Suppressor Cells; TAMs Tumour Associated Macrophages; CSCs Cancer Stem Cells; PCSc Pancreatic Cancer Stems Cells; Ca Carbohydrate Antigen; CT Computed Tomography; PEG Polyethylene Glycol; IONPs Iron Oxide Nanoparticles; MRI Magnetic Resonance Imaging; PAI Photoacoustic imaging; PLGA Poly (Lactic–Co Glycolic Acid); HER-2 Human Epidermal Growth Factor Receptor 2; MMP-2 Matrix Metalloproteinase-2; siRNA Small Interfering Ribonucleic Acid; SLNs Solid Lipid Nanoparticles; NLCs Nanostructured Lipid Carriers; SMEDDS/SNEDDS Self-Micro/Nano-Emulsifying Drug Delivery Systems; Nab-Paclitaxel Nanoparticle Albumin-Bound Paclitaxel; PHAs Polyhydroxyalkanoates; PCL Poly (Caprolactone); CNTs Carbon Nanotubes; QDs Quantum Dots; NIR Near Infrared;
Correspondence Noa de la Fuente
HM Rosaleda Hospital,
Santiago León de Caracas Street, 1; 15701,
Santiago de Compostela (A Coruña), Spain
Tel 034-652-445-513
María Virtudes Céspedes
Gynecologic & Peritoneal Oncology Group (GOGyP),
Sant Pau Biomedical Research Institute (IIB Sant Pau),
Barcelona, Cataluña, Spain
Tel 034-932919000 (1427)
E-mail noa_fh@hotmail.com; mcespedes@santpau.cat

In our manuscript, we described the characteristics of pancreatic cancer biology, focusing on the latest therapies and advances in pharmaceutical nanoformulations available in pancreatic ductal adenocarcinoma management. We include different types of nanoformulations tested for diagnosis and treatment and explore the latest clinical trials evaluation of nanoparticle-based drug delivery Systems in PDAC.

Introduction

PDAC is the most frequent malignant tumour in the pancreas and the fourth cause of cancer death in Europe [1].

The characteristics of PDAC, such as tumour stroma and cancer stem cells, play an important role in the physiopathology of pancreatic cancer, and they are strongly related to late diagnosis, bad prognosis and chemoresistance [2].

The PDAC stroma forms the tumour microenvironment and about 80% of the tumour's mass. The proliferation of cellular components of the tumour stroma, such as Cancer Associated Fibroblasts (CAFs) and pancreatic stellate cells (PSCs), leads to a desmoplastic reaction, producing extracellular matrix proteins contributing to tumour growth and migration. Other cellular components, such as Myeloid Derived Suppressor Cells (MDSCs) and Tumour Associated Macrophages (TAMs), may promote tumour progression by

biomolecules

MDPI

Review

Nano-Based Approved Pharmaceuticals for Cancer Treatment: Present and Future Challenges

Francisco Rodríguez [1,†], Pablo Caruana [1,†], Noa De la Fuente [2], Pía Español [3], María Gámez [4], Josep Balart [5], Elisa Llurba [3], Ramón Rovira [3], Raúl Ruiz [1], Cristina Martín-Lorente [6], José Luis Corchero [7,*] and María Virtudes Céspedes [1,*]

1 Grup d'Oncologia Ginecològica i Peritoneal, Institut d'Investigacions Biomédiques Sant Pau, Hospital de la Santa Creu i Sant Pau, 08041 Barcelona, Spain; frodriguezl@santpau.cat (F.R.); pcaruana@santpau.cat (P.C.); raulruizpalacios17@gmail.com (R.R.)
2 Servicio de Cirugía General y del Aparato Digestivo, Hospital HM Rosaleda, 15701 Santiago de Compostela, Spain; ndelafuente@hmhospitales.com
3 Department of Obstetrics and Gynecology, Hospital de la Santa Creu i Sant Pau, Universitat Autònoma de Barcelona, 08041 Barcelona, Spain; mespanoll@santpau.cat (P.E.); ellurba@santpau.cat (E.L.); rroviran@santpau.cat (R.R.)
4 Department of Pharmacy, Hospital de la Santa Creu i Sant Pau, 08041 Barcelona, Spain; mgamezl@santpau.cat
5 Department of Radiation Oncology, Hospital de la Santa Creu i Sant Pau, 08041 Barcelona, Spain; jbalart@santpau.cat
6 Department of Medical Oncology, Hospital de la Santa Creu i Sant Pau, 08041 Barcelona, Spain; cmartinl@santpau.cat
7 Institut de Biotecnologia i de Biomedicina and CIBER-BBN, Universitat Autònoma de Barcelona, Bellaterra, 08193 Barcelona, Spain
* Correspondence: jlcorchero@ciber-bbn.es (J.L.C.); mcespedes@santpau.cat (M.V.C.); Tel.: +34-93-5812148 (J.L.C.); +34-93-400000 (ext. 1427) (M.V.C.)
† These authors contributed equally to this work.

Abstract: Cancer is one of the main causes of death worldwide. To date, and despite the advances in conventional treatment options, therapy in cancer is still far from optimal due to the non-specific systemic biodistribution of antitumor agents. The inadequate drug concentrations at the tumor site led to an increased incidence of multiple drug resistance and the appearance of many severe undesirable side effects. Nanotechnology, through the development of nanoscale-based pharmaceuticals, has emerged to provide new and innovative drugs to overcome these limitations. In this review, we provide an overview of the approved nanomedicine for cancer treatment and the rationale behind their designs and applications. We also highlight the new approaches that are currently under investigation and the perspectives and challenges for nanopharmaceuticals, focusing on the tumor microenvironment and tumor disseminate cells as the most attractive and effective strategies for cancer treatments.

Keywords: nanomedicine; cancer therapy; nanotechnology; approved nanopharmaceuticals; targeted therapy

check for updates

Citation: Rodríguez, F.; Caruana, P.; De la Fuente, N.; Español, P.; Gámez, M.; Balart, J.; Llurba, E.; Rovira, R.; Ruiz, R.; Martín-Lorente, C.; et al. Nano-Based Approved Pharmaceuticals for Cancer Treatment: Present and Future Challenges. *Biomolecules* **2022**, *12*, 784. https://doi.org/10.3390/biom12060784

Academic Editor: Bahman Anvari

Received: 10 May 2022
Accepted: 2 June 2022
Published: 4 June 2022

Publisher's Note: MDPI stays neutral with regard to jurisdictional claims in published maps and institutional affiliations.

1. Introduction

More than ten million people are diagnosed with cancer annually [1]. Cancer comprises a wide diversity of diseases, all of them characterized by numerous cellular physiological systems leading to abnormal and non-stop cell growth in a specific tissue location, forming the tumor [2].

After cancer diagnosis, combined therapies are commonly used, applying different modalities such as surgery followed by chemotherapy and/or radiotherapy. Currently, and despite the advances in conventional treatment options, cancer therapy is still far from optimal. Conventional chemotherapeutic drugs are non-selective small molecules

biomolecules

MDPI

Article

Lenvatinib-Loaded Poly(lactic-co-glycolic acid) Nanoparticles with Epidermal Growth Factor Receptor Antibody Conjugation as a Preclinical Approach to Therapeutically Improve Thyroid Cancer with Aggressive Behavior

Giovanna Revilla [1,2,3], Nuseibah Al Qtaish [4,5,6], Pablo Caruana [1], Myriam Sainz-Ramos [4,5,7], Tania Lopez-Mendez [4,5,7], Francisco Rodriguez [1], Verónica Paez-Espinosa [8], Changda Li [1,2,3], Núria Fucui Vallverdú [1], Maria Edwards [1], Antonio Moral [4,9], José Ignacio Pérez [9], Juan Carlos Escolà-Gil [1,2,10], José Luis Pedraz [4,5,7], Idoia Gallego [4,5,7], Rosa Corcoy [1,3,10], María Virtudes Céspedes [1,*], Gustavo Puras [4,5,7] and Eugènia Mato [1,3,4,*]

1 Research Biomedical Institute (IIB) Sant Pau, C/Sant Quintí 77, 08041 Barcelona, Spain; grevilla@santpau.cat (G.R.); pcaruana@santpau.cat (P.C.); pacorl97@outlook.es (F.R.); clix@santpau.cat (C.L.); nuriafvg@gmail.com (N.F.V.); medwards@santpau.cat (M.E.); jescola@santpau.cat (J.C.E.-G.); rcorcoy@santpau.cat (R.C.)
2 Departament of Biochemistry and Molecular Biology, Universitat Autònoma de Barcelona, C/Antoni M. Claret 167, 08025 Barcelona, Spain
3 Department of Endocrinology and Nutrition, Hospital de la Santa Creu i Sant Pau, 08041 Barcelona, Spain
4 Networking Research Centre of Bioengineering, Biomaterials and Nanomedicine (CIBER-BBN), C/Monforte de Lemos 3-5, 28029 Madrid, Spain; nusaiba.qtaish@gmail.com (N.A.Q.); myri.2694@gmail.com (M.S.-R.); tania.lopez@ehu.eus (T.L.-M.); amoral@santpau.cat (A.M.); joseluis.pedraz@ehu.eus (J.L.P.); idoia.gallego@ehu.eus (I.G.); gustavo.puras@ehu.eus (G.P.)
5 NanoBioCel Research Group, Laboratory of Pharmacy and Pharmaceutical Technology, Faculty of Pharmacy, University of the Basque Country (UPV/EHU), Paseo de la Universidad 7, 01006 Vitoria-Gasteiz, Spain
6 Pharmacy Department, College of Pharmacy, Amman Arab University, P.O. Box 2234, Amman 11953, Jordan
7 Bioaraba, NanoBioCel Research Group, 01009 Vitoria-Gasteiz, Spain
8 Department Clinical Biochemistry, School of Medicine, Pontificia Universidad Católica del Ecuador (PUCE), Av. 12 de Octubre 1076 y Roca, Quito 17012184, Pichincha, Ecuador; epaez387@puce.edu.ec
9 Department of General Surgery, Hospital de la Santa Creu i Sant Pau, C/Sant Quintí 89, 08041 Barcelona, Spain; jperezg@santpau.cat
10 CIBER de Diabetes y Enfermedades Metabólicas Asociadas (CIBERDEM), C/Monforte de Lemos 3-5, 28029 Madrid, Spain
* Correspondence: mcespedes@santpau.cat (M.V.C.); emato@santpau.cat (E.M.)

check for updates

Citation: Revilla, G.; Al Qtaish, N.; Caruana, P.; Sainz-Ramos, M.; Lopez-Mendez, T.; Rodriguez, F.; Paez-Espinosa, V.; Li, C.; Vallverdú, N.F.; Edwards, M.; et al. Lenvatinib-Loaded Poly(lactic-co-glycolic acid) Nanoparticles with Epidermal Growth Factor Receptor Antibody Conjugation as a Preclinical Approach to Therapeutically Improve Thyroid Cancer with Aggressive Behavior. *Biomolecules* **2023**, *13*, 1647. https://doi.org/10.3390/biom13111647

Academic Editor: Giuseppe Pappalardo

Received: 28 September 2023
Revised: 6 November 2023
Accepted: 8 November 2023
Published: 13 November 2023

Abstract: Background: Lenvatinib, a tyrosine kinase inhibitor (TKI) approved for the treatment of progressive and radioactive iodine (RAI)-refractory differentiated thyroid cancer (DTC), is associated with significant adverse effects that can be partially mitigated through the development of novel drug formulations. The utilization of nanoparticles presents a viable option, as it allows for targeted drug delivery, reducing certain side effects and enhancing the overall quality of life for patients. This study aimed to produce and assess, both in vitro and in vivo, the cytotoxicity, biodistribution, and therapeutic efficacy of lenvatinib-loaded PLGA nanoparticles (NPs), both with and without decoration using antibody conjugation (cetuximab), as a novel therapeutic approach for managing aggressive thyroid tumors. Methods: Poly(lactic-co-glycolic acid) nanoparticles (NPs), decorated with or without anti-EGFR, were employed as a lenvatinib delivery system. These NPs were characterized for size distribution, surface morphology, surface charge, and drug encapsulation efficiency. Cytotoxicity was evaluated through MTT assays using two cellular models, one representing normal thyroid cells (Nthy-ori 3-1) and the other representing anaplastic thyroid cells (CAL-62). Additionally, an in vivo xenograft mouse model was established to investigate biodistribution and therapeutic efficacy following intragastric administration. Results: The NPs demonstrated success in terms of particle size, polydispersity index (PDI), zeta potential, morphology, encapsulation efficiency, and cetuximab distribution across the surface. In vitro analysis revealed cytotoxicity in both cellular models with both formulations, but only the decorated NPs achieved an ID50 value in CAL-62